Cellulose composite structures – by design

Charles G. Winkworth-Smith

Thesis submitted to the University of Nottingham for the degree of Doctor of Philosophy

Division of Food Sciences
School of Biosciences
University of Nottingham
Loughborough
LE12 5RD

September 2014

The research leading to these results has received funding from Unilever and the Engineering and Physical Sciences Research Council (EPSRC).

Abstract

The aim of the work presented in this thesis was to investigate different mechanical and chemical pre-treatments which can dramatically change the properties of native cellulose and add alternative routes to structure formation. Ball milled cellulose, which had a reduced crystallinity, degree of polymerisation and degradation temperature, was rehydrated in excess water resulting in recrystallisation. Fully amorphous samples recrystallised to the more thermodynamically stable type II polymorphic crystal structure. Flash differential scanning calorimetry (DSC), which allows thermal transitions to be scanned at much higher rates than conventional DSC, was able to register a glass transition temperature for amorphous cellulose. The next stage of the study focussed on the production of freeze dried galactomannan foams. Cellulose fibres provided reinforcement to the foams. The level of reinforcement was related to fibre content, size, crystallinity and surface roughness. Microfibrillated cellulose (MFC) provided the greatest reinforcement due to its much higher surface area and fibrillated structure. Extrusion was found to be a useful alternative to homogenisation for the production of MFC and to create foams using alternative processing to the freeze drying routes.

A novel molten salt hydrate, LiCl/urea/water, was found to swell native cellulose and reduce its crystallinity. A weak gel-like structure was formed at ambient temperature. Micro DSC results showed that this structure was melted out at 60^{o}C but the process was reversible indicating hydrophilic to hydrophobic conformational changes on the surface of the cellulose fibres, although these were likely to be dependent on the celluloses having a low degree of polymerisation. In these solvent conditions starch granules were eroded from the outside rather than being swollen as has been found

for some ionic liquids and underwent total dissolution in LiCl/urea/water. Fenugreek and xyloglucan, which are both highly branched, were found to increase in viscosity in LiCl/urea/water relative to water, possibly due to the breakage of all intramolecular associations whereas the viscosity of konjac which is predominantly unbranched did not change. Locust bean gum (LBG) had a lower viscosity in LiCl/urea/water compared to water due to the disruption of aggregates. Confocal microscopy showed that fenugreek and LBG are able to bind to cellulose in water, however, the conformational change of fenugreek in these solvent conditions inhibited it from binding to cellulose in LiCl/urea/water whereas conformational change allowed xyloglucan to bind to cellulose in LiCl/urea/water whilst it was unable to bind in water. Konjac did not bind to cellulose in either solvent system. The pre-treatments shown in this work will enable the creation of novel cellulose composites.

Acknowledgements

It is a pleasure to thank all the people that have made this doctorate possible. First and foremost, I wish to thank my supervisor, Professor Tim Foster for giving me this opportunity and for his support, supervision and encouragement throughout the course of my PhD.

I am very grateful to the Engineering and Physical Sciences Research Council (EPSRC) and to Unilever for providing the financial support for my PhD research. I would particularly like to thank Dr Eddie Pelan from Unilever for organising the CASE studentship and his support throughout my PhD.

I would also like to thank a number of other people that have supported me during my PhD. I owe an enormous debt to Dr Bill MacNaughton for all his advice, training and encouragement and to Val Street for her technical assistance and tireless travel planning. I also wish to thank Dr Sanyasi Gaddipati for all his help and enthusiasm and Professor John Mitchell for many fascinating and enlightening discussions. I am also very grateful to Dr Wim Thielemans for his guidance and I would like to thank Professor Steve Harding for his help with Hydrodynamics. I would also like to thank Professor Sandra Hill, Dr Betina Wolf, Dr David Gray and Dr Roget Ibbett for their help and support.

I am very grateful to Professor Cheng and his students from the China Agricultural University in Beijing for their generous hospitality during my secondment in 2013. Work during the secondment led to some of the results in Chapter 6.

I would like to thank all my friends from the Division of Food Sciences who have made my time at the University of Nottingham so enjoyable and memorable.

Finally I would like to thank my family for all their kindness, help and support throughout my life. It is to them that I dedicate this thesis.

List of Abbreviations and Symbols

Å	Angstroms
α	Alpha
Ara	Arabinose
AmimCl	1-allyl-3-methylimidazolium chloride
ATR FTIR	Attenuated total reflectance Fourier transform infrared spectroscopy
β	Beta
BM	Ball milled
BM MCC	Ball milled microcrystalline cellulose
BmimCl	1-butyl-3-methylimidazolium chloride
^{o}C	Degrees Celsius
c*	Critical concentration
$Ø_c$	Critical volume fraction
CED	Copper (II) ethylenediamine
CF	Cellulose fibre
CLSM	Confocal laser scanning microscope
cm	Centimetre(s)
CO_2	Carbon dioxide
cP	Centipoise
CP	Cellulose powder
CPMAS	Cross polar magic angle spinning
CWP	Cell wall particles
3D	Three dimensional
dl/g	Decilitre (1 x 10^{-1} litres) per gram
DE	Degree of esterification
DMA	Dynamic mechanical analysis
DMAc	N,N-dimethylacetamide
DMTA	Dynamic mechanical thermal analysis
DP	Degree of polymerisation
DSC	Differential scanning calorimetry
DTA	Differential thermal analysis
dTGA	Differential thermogravimetric analysis
DTGS	Deuterated triglycine sulphate
DVS	Dynamic vapour sorption
Δ	Delta
ΔH	Enthalpy
FTIC	Fluorescein isothiocyanate
FTIR	Fourier transform infrared spectroscopy
Fuc	Fucose
G'	Storage modulus
G''	Loss modulus
Gal	Galactose
GalA	Galacturonic acid
Glc	Glucose
GlcA	Glucuronic acid
GPa	Gigapascal(s)
δ_H	Hansen solubility parameter
HCl	Hydrochloric acid
HGA	Homogalacturonan

HM	High methoxy
HPC	Hydroxypropylcellulose
Hz	Hertz
J/g	Joules per gram
K	Degrees Kelvin
kDA	Kilodalton
kHz	Kilohertz
kJ	Kilojoule
kPa	Kilopascal(s)
kWh	Kilowatt-hour
LBG	Locust bean gum
LiCl	Lithium chloride
LM	Low methoxy
L/w	Length to width ratio
M	Molar
Man	Mannose
MCC	Microcrystalline cellulose
MFC	Microfibrillated cellulose
M:G	Mannose to galactose ratio
mg	Milligram(s) (1×10^{-3} grams)
MHKS	Mark-Houwink-Kuhn-Sakuranda
min	Minute(s)
ml	Millilitres(s) (1×10^{-3} litres)
Mol	Mole
MPa	Megapascals
ms	Microsecond
mN	Millinewtons
NaOH	Sodium hydroxide
NFC	Nanofibrillated cellulose
nm	Nanometer(s) (1×10^{-9} meters)
NMMO	N-methylmorpholine-N-oxide
NMR	Nuclear magnetic resonance
Pa	Pascal
PLA	Polylactic acid
ppm	Parts per million
PVA	Polyvinyl alcohol
PVC	Polyvinyl chloride
µm	Micrometer(s) (1×10^{-6} meters)
RER	Radial expansion ratio
R_{coil}	Coil radius
RH	Relative humidity
Rha	Rhamnose
rpm	Revolutions per minute
R_g	Radius of gyration
RG-I	Rhamnogalacturonan one
RG-II	Rhamnogalacturonan two
RVA	Rapid visco analyser
SEC MALS	Size exclusion chromatography multi-angle laser light scattering
SEM	Scanning electron microscopy
SME	Specific mechanical energy
TEM	Transmission electron microscope

T_g	Glass transition temperature
TGA	Thermogravimetric analysis
TPS	Thermoplastic starch
UV	Ultraviolet
η	Viscosity
η_{rel}	Relative viscosity
η_{sp}	Specific viscosity
[η]	Intrinsic viscosity
V_{coil}	Coil radius
WAXD	Wide angle X-ray diffraction
wt%	Weight percentage
Xyl	Xylose
XRD	X-ray diffraction

Table of Contents

List of Figures

List of Tables

List of Publications

Publications

Zhou, Y., Dan, Z., Winkworth-Smith, C. G. & Foster, T. J. Nirasawa, S., Tatsumi, E. & Cheng, Y. Effect of a small amount of sodium carbonate on konjac glucomannan-induced changes in wheat starch gel. *Carbohydrate Polymers,* In Press.

Winkworth-Smith, C. G. & Foster, T. J. 2013. General overview of biopolymers: Structure, properties and applications. *In:* Thomas, S., Durand, D., Chassenieux, C. & Jyotishkumar, P. (eds.) *Handbook of Biopolymer-Based Materials.* Wiley-VCH.

Manuscripts under preparation

Winkworth-Smith, C. G., Gaddipati S. R., MacNaughton W., Mitchell, J. R. & Foster, T. J. The recrystallisation in excess water of ball milled cellulose.

Winkworth-Smith, C. G., Gaddipati S. R., MacNaughton W., Mitchell, J. R. & Foster, T. J. The application of Flash DSC to carbohydrates.

Winkworth-Smith, C. G., MacNaughton W., Thielemans, W. & Foster, T. J. Conformational changes of branched polysaccharides in LiCl/urea/water.

Winkworth-Smith, C. G., MacNaughton W., Thielemans, W. & Foster, T. J. Native celluloses in a LiCl/urea/water swelling solution.

Presentations

Winkworth-Smith, C. G., Pelan, E., Thielemans, W. & Foster, T. J. Cellulose composite structures. 245th National meeting of the American Chemical Society (ACS), April 7-11 2013. New Orleans, USA (Oral presentation).

Winkworth-Smith, C. G., Thielemans, W. & Foster, T. J. Plant polysaccharides in a novel swelling solution. Naro.tech Congress, September 5-6 2012. Erfurt, Germany (Poster presentation).

Winkworth-Smith, C. G. & Foster, T. J. Propeties of plant polysaccharides in a novel swelling solution. 11th International Hydrocolloids Conference, May 14-18 2012. Purdue, USA (Oral presentation).

Winkworth-Smith, C. G. & Foster, T. J. Viscosifying effects of cellulose swollen in LiCl/urea/water. Royal Society of Chemistry Discussion Meeting: Stability and degradation of complex carbohydrate structures September 5 2011. London, UK (Poster presentation).

Chapter 1. Introduction

1.1 Introduction

Cellulose is the main building block of the plant cell wall. Cellulose fibres have been used for millennia to make rope, textiles and reinforce mud bricks. Cellulose has found a renewed interest in 'green' composite materials. It is considered to be an almost inexhaustible source of raw material with a total annual biomass production of about 1.5 x 10^{12} tons (Klemm *et al.*, 2005).

Composites are a combination of a strong reinforcing, load carrying material embedded in a matrix which acts as a binder and maintains the position and orientation of the reinforcement material. While both components retain their own chemical and physical properties, together they produce a material with unique qualities they would be unable to produce on their own. There are many natural composites including wood, bone and teeth (Fratzl and Weinkamer, 2007). There are many historical examples of composites such as reinforced mud walls, concrete and combinations of wood, bone and animal glue. The first major industrial composites were glass fibre reinforced resins, invented in the 1930s. This provided a strong, light weight alternative to wood and metal to build boats and aircraft. By the 1970s, as better plastic resins and stronger reinforcing fibres, including aramid fibre (better known as Kevlar, developed by DuPont) and carbon fibre were developed, new composites were invented. Recently, the push towards more environmentally friendly materials and processes has resulted in a large increase into the research of bio-based composites.

One of the main focuses of bio-based composites is natural fibres. Cells of higher plants are able to withstand an internal osmotic pressure of between 0.1 and 3.0 MPa (1MPa = 145 pounds per square inch) (Somerville *et al.*, 2004). The pressure rigidifies the cells by creating tension in the walls. Despite the large variety in cell wall

structure among all types of plants, a high cellulose content is common to all. Typically 35-50% of plant dry weight is cellulose. Cellulose is normally embedded in a matrix primarily composed of hemicelluloses and lignin which comprise 20-35% and 5-30% respectively of plant dry weight (Lynd *et al.*, 2002). In a few cases such as cotton bolls, cellulose is present in a nearly pure state. Hemicelluloses are comprised of several different polysaccharides such as xylans, xyloglucans, glucomannans, galactomannans and galactoglucomannans. (Spencer and Maclachl, 1972, Herth and Meyer, 1977). Lignin is a complex amorphous polymer consisting mainly of aromatic units such as guaiacyl, syringyl and phenylpropane (Moran *et al.*, 2008). Plant cell walls are comprised of the middle lamella and the primary and secondary cell walls. The primary cell wall is formed while the cell is growing. It defines not only the rate of growth of the plant cells but also its size and shape. The primary cell wall is comprised of 90% polysaccharide and 10% proteins (glycoproteins) (McNeil *et al.*, 1984). The secondary cell wall is formed after the cell is fully grown and is much thicker, more rigid and stronger than the primary cell wall. The middle lamella is the outermost layer, comprised mainly of pectins which glue the adjacent plant cells together. The degree of polymerisation (DP) (Spencer and Maclachl, 1972) and the degree of crystallinity of cellulose are also higher in the secondary cell wall.

As well as solid composites such as films and foams there is also a growing interest in using plant cell wall material to create soft solid structures, particularly in the food, cosmetics and pharmaceutical industries driven by their low cost, sustainability and inferred naturalness (Foster, 2011). There are also many health benefits; a high intake of dietary fibre, traditionally defined as the portions of plant foods that are resistant to digestion by human digestive enzymes (i.e. polysaccharides and lignin), appears to significantly lower the risk of developing coronary heart disease, stroke, hypertension, diabetes, obesity and certain gastrointestinal diseases (Anderson *et al.*,

2009). Recommended intakes for healthy adults are between 20-35 g/day (Marlett *et al.*, 2002). However many people consume very low levels, for instance the majority of people in the United States consume less than half the recommended levels of dietary fibre daily (Park *et al.*, 2005). It would therefore be beneficial to increase the use of cellulose and other cell wall polysaccharides in food systems.

1.2 Plant Cell Wall Polysaccharides

1.2.1 Cellulose

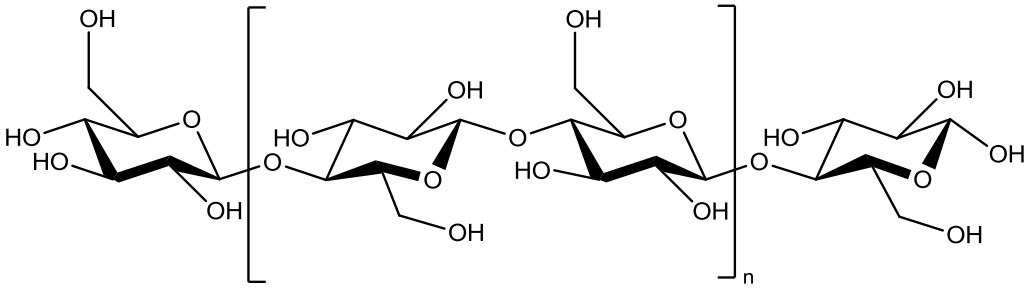

Figure 1.1 Chemical structure of cellulose.

The French chemist Anselm Payen in 1838 first described cellulose as a resistant fibrous solid that remains behind after treatment of various plant tissues with acids and ammonia. He determined the molecular formula to be $C_6H_{10}O_5$, an isomer of starch. Cellulose has since been established to be a high molecular weight homopolymer of β-1,4-linked anhydro-D-glucose units. Due to the bond angles of the acetyl oxygen bridges, every second anhydroglucose ring is rotated 180^o in the plane. This means that the repeating unit of cellulose is a dimer of glucose, cellobiose (Figure 1.1). The structure is stabilised by an intramolecular hydrogen bond network. This network makes cellulose a relatively stable polymer, which does not readily dissolve in aqueous solvents and has no measurable melting point (Kroonbatenburg *et al.*, 1986). Each chain possesses directional asymmetry with one end having a reducing functional group and the other end non reducing (Habibi *et al.*, 2010).

The size of the cellulose molecule is often described by its DP. The DP strongly depends on the source of the cellulose (Collinson and Thielemans, 2010). The degree of polymerization is also dependant on the processing and extraction method. Naturally, cellulose does not occur as an isolated molecule but is found in the form of fibrils. Cellulose is synthesised in the cell as individual molecules which undergo self-assembly at the site of biosynthesis (Brown and Saxena, 2000). Approximately 36 molecules are then assembled into larger units known as elementary fibrils (protofibrils) (Habibi *et al.*, 2010). These are then packed into larger units known as microfibrils, which are further assembled into the large macroscopic cellulose fibres (Figure 1.2). Microfibrils have cross sectional dimensions ranging from 2 to 20 nm depending on the source of cellulose. An important feature of cellulose is its crystalline nature, which means the cellulose chains have a structured order. The component molecules of each individual microfibril are packed so tightly that it prevents penetration by enzymes and even small molecules such as water. The supramolecular structure of the cellulose fibre is crystalline but there are some regions that are amorphous as well as some irregularities such as kinks and twists of the microfibrils and voids such as surface micropores. The effect of structural heterogeneity is that the macroscopic fibres are at least partially hydrated by water and there is some penetration by larger molecules such as enzymes (Stone *et al.*, 1969).

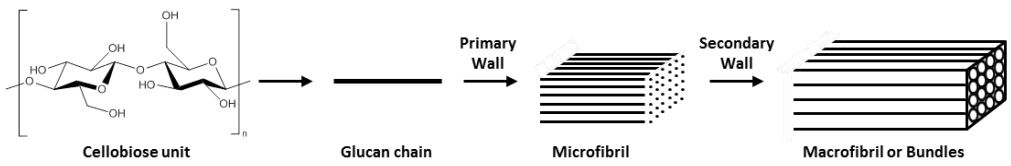

Figure 1.2 Steps in the assembly of native cellulose. Adapted from Delmer and Amor (1995).

In the ordered crystalline regions the cellulose chains are tightly packed together and held in place by strong hydrogen bonding (in-plane) and Van der Waals interactions (between planes). The molecular orientation in the cellulose chains, and therefore their packing arrangement, can vary widely depending on the source, method of extraction or treatment of the cellulose, resulting in a variety of crystal structures or allomorphs. The allomorph most commonly found in nature is cellulose I. Native cellulose is composed of two sub-allomorphs Iα and Iβ. Cellulose Iα has a one chain triclinic structure and is predominant in primitive organisms. Iβ has monoclinic unit cells and is predominant in higher plants (Collinson and Thielemans, 2010). Native cellulose has parallel chain alignment. This refers to the chain direction as regards to the reducing and non-reducing ends of the polymer. Regenerated or mercerised cellulose II has anti-parallel chains (Langan *et al.*, 1999) in a two chain unit cell. Cellulose III can be generated by adding liquid ammonia to cellulose I or cellulose II producing cellulose III_1 and III_2 respectively. Heat treatment of cellulose III_1 and III_2 leads to cellulose IV_1 and IV_2 (Zugenmaier, 2001). These can then be reverted back to their original cellulose. Whilst cellulose I is the most commonly found form in nature it is the least thermodynamically stable, with cellulose III being the most stable form (Collinson and Thielemans, 2010).

1.2.1.1 Cellulose extraction

Cellulose extraction is generally difficult as it does not melt and is not soluble in either water or common organic solvents. This is due to the hydrogen bond network and its partially crystalline structure. Currently the most important industrial scale extraction process of cellulose is the viscose process, which is more than 100 years old. Cellulose, often from wood pulp or cotton linters is treated with sodium hydroxide and then carbon disulfide. The resulting product, dissolved in sodium hydroxide, is cellulose xanthogenate forming a thick solution called viscose. The

viscose is then forced through very small openings into an acid bath which coagulates the regenerated cellulose. Depending on the size of the openings, fibres (rayon) or films (cellophane) can be produced. The viscose process has some environmental concerns due to the hazardous by-products such as CS_2, H_2S and heavy metals. The cuprammonia process is another route for producing regenerated cellulose but also has environmental problems (Fink *et al.*, 2001) and is no longer widely used.

An alternative to the viscose method is the Lyocell process. Lyocell was first manufactured in 1987 and has been produced commercially since 1991. It is a much more environmentally friendly process (Fink *et al.*, 2001):

- Preparation of a homogenous concentrated solution (dope) of the starting cellulose (dissolving pulp) in an *N*-methylmorpholine-*N*-oxide (NMMO) - water mixture,
- Extrusion of the highly viscous spinning dope at elevated temperatures through an air gap into a precipitation bath (dry jet-wet spinning process),
- Coagulation of the cellulose fibre in the precipitation bath,
- Washing, drying and post treatment of the cellulose fibre,
- Recovery of the NMMO from the precipitation and washing baths.

A major benefit of the Lyocell process is that it is capable of dissolving cellulose without derivitisation, complexation or special activation (Franks, 1980).

Research into Ionic liquids has seen enormous growth recently due to the increased interest in green chemistry. Ionic liquids are often referred to as 'green' solvents (El Seoud *et al.*, 2007). They are organic salts that exist as liquids at relatively low temperatures (<100 ^{o}C) (Seddon, 1997). Ionic liquids are also known as ionic fluids, molten salts, fused salts, or neoteric solvents. Some studies have shown that Ionic

liquids such as 1-butyl-3-methylimidazolium chloride (BMIMCl or [C4mim]Cl) and 1-allyl-3-methylimidazolium chloride (AMIMCl) can dissolve cellulose, whether it is refined or natural, without causing derivation (Zhu *et al.*, 2006). Microwave heating can significantly accelerate its dissolution (Varma and Namboodiri, 2001). Solutions containing up to 25% cellulose can be obtained by using [C4mim]Cl as the solvent at 70^{o}C (heated by microwave pulses), although compositions between 5 and 10% are more readily prepared (Swatloski *et al.*, 2002). Cellulose can then be precipitated from the Ionic liquid by adding water, ethanol or acetone.

Recently, Tatarova *et al.* (2010) have shown that mixed solutions of LiCl, urea and water, exert a swelling effect on regenerated cellulosics due to the propensity for formation of Li-cellulose coordination complexes where urea acts as a co-solvent for the LiCl. This may prove a useful alternative to alkali swelling treatments.

1.2.1.2 Nano Cellulose

Within the last 15 years there has been a growing interest in nano cellulose. There are two major classes of nano cellulose; micro (or nano) fibrillated cellulose and cellulose nanowhiskers (nanocrystals) although there are many differing terminologies which can lead to confusion. Both have at least one dimension in the nano scale (1-100nm). The two classes of nano cellulose are distinguished by their method of preparation. Cellulose nanowhiskers are prepared using strong acid while nanofibrillated cellulose is mainly prepared by mechanical homogenisation.

1.2.1.3 Microfibrillated cellulose

Microfibrillated cellulose (MFC) (also termed nanofibrillated cellulose or NFC) can be extracted from cellulose fibrils using a variety of mechanical processes including high-pressure homogenisers, grinders/refiners, cryocrushing, high intensity ultrasonic treatments and microfluidisation (Moon *et al.*, 2011). These processes generate high

shear which cleaves the cellulose fibrils along their longitudinal axes resulting in a greatly increased surface area. The long, flexible fibrils have lateral dimensions between 10-100 nm and length generally in the micrometre scale and consist of both the crystalline and amorphous domains (Andresen *et al.*, 2006). The long fibrils result in a web like structure (Siqueira *et al.*, 2009). The elastic modulus of single microfibrils from tunicate (a marine invertebrate) has recently been measured using atomic force microscopy with values between 145-150 GPa (Iwamoto *et al.*, 2009).

MFC was first extracted from wood by Turbak *et al.* (1983) and Herrick *et al.* (1983). The high energy requirements, however, meant that there was no large scale production of MFC. The energy required to produce MFC in the early 1980s was as high as 30,000 kWh/tonne. Using different pre-treatment methods this has been reduced by as much as 98% to 500 kWh/tonne (Aulin *et al.*, 2011). Pre-treatments that have been developed include acid hydrolysis, enzymatic hydrolysis, pre-beating/grinding, TEMPO oxidation and carboxymethylation (Klemm *et al.*, 2011, Paakko *et al.*, 2007, Spence *et al.*, 2011).

Due to cellulose's hygroscopic nature, one of the major problems encountered with MFC is hornification (agglomeration upon drying). This results in the MFC having to either be used in a never dried state or chemically modified. The use of never dried suspensions is ultimately undesirable due to high shipping costs, the need for large storage facilities and its propensity for bacterial spoilage (Eyholzer *et al.*, 2010a). Different routes that have been investigated to produce a re-dispersible powdered MFC include carboxymethylation, grafting of acetyl moieties or silylation (which also improves compatibilisation with hydrophobic matrices) (Eyholzer *et al.*, 2010b). All these methods attempt to limit hydrogen bonding between fibrils by introducing steric hindrance or electrostatic groups. The original MFC structure may also be

preserved using a variety of cryo techniques such as high pressure freezing (vitrification), freeze fracturing or freeze etching (Eyholzer *et al.*, 2010c).

1.2.1.4 Cellulose Nanowhiskers

Cellulose nanowhiskers have many appealing intrinsic properties such as their nano-scale dimensions, high surface area, unique morphology, low density and high mechanical strength (the axial Young's modulus is theoretically stronger than steel and similar to that of Kevlar (Tashiro and Kobayashi, 1991)). Cellulose whiskers also have the concomitant benefit of being easily chemically modified. Cellulose whiskers have many potential applications such as tablet binders, texturising agents, fat replacers, additives in paper (e.g. security paper) and in nanocomposites.

Cellulose nanowhiskers are isolated from cellulose microfibrils by the treatment with an acid. The microfibrils consist of crystalline regions surrounded by disordered amorphous regions. The acid hydrolyses the non-crystalline regions faster than the crystalline areas which have a higher resistance to hydrolysis (Favier *et al.*, 1995). Needle shaped particles remain as a residue; the resulting suspension is then diluted with water and washed with successive centrifugations. The remaining suspension is then dialysed against distilled water to remove any free acid molecules from the dispersion. Additional steps such as filtration, differential centrifugation and ultracentrifugation can also be used (Elazzouzi-Hafraoui *et al.*, 2008, Bai *et al.*, 2009). Generally, the longer the hydrolysis the shorter the nanowhisker and the narrower the size polydispersity (Beck-Candanedo *et al.*, 2005).

The type of acid used will impart different properties to the whiskers. The two most commonly used are sulphuric and hydrochloric acid. Phosphoric and hydrobromic acid have also been used (Kim *et al.*, 1999). The concentration of sulphuric acid is typically about 65 wt% used at between room temperature and 70^{o}C. The hydrolysis

time can be as little as 30 minutes up to leaving it overnight, dependant on the temperature used (Habibi *et al.*, 2010). Hydrolysis using hydrochloric acid generally uses an acid concentration of 2.5-4 N at reflux temperature and for a variable time dependant on the source of the cellulose. Sulphuric acid produces negatively charged whiskers which are more stable in aqueous solution than whiskers from hydrochloric acid which have no charge (Araki *et al.*, 1998). Dependant on the acid used, the whiskers are able to self-assemble into nematic liquid crystalline structures at high concentrations (Revol *et al.*, 1992). The chiral nematic structure can even be preserved after total water removal, making it possible to form iridescent films of the nanowhiskers increasing the range of potential applications (Revol *et al.*, 1995).

Cellulose whiskers can be made from a variety of sources such as valonia, cotton, wood pulp, sugar beet pulp, tunicin and bacterial cellulose. Table 1.1 shows the range of sizes of whiskers from different sources. The aspect ratio of cellulose is its length-to-width (*L/w*) ratio.

Table 1.1 Examples of the Length (L) and Width (w) of cellulose nanowhiskers from various sources obtained by transmission electron microscopy. Adapted from (Habibi *et al*., 2010).

Source	L (nm)	W (nm)
Bacterial	100-1000	10-50
Cotton	100-150	5-10
Cotton linters	25-320	6-70
MCC	35-265	3-48
Ramie	150-250	6-8
Sisal	100-500	3-5
Tunicate	1000-3000	15-30

1.2.2 Hemicelluloses

Most hemicelluloses are characterized by a β-1,4-linked backbone with an equatorial configuration at C1 and C4 (Scheller and Ulvskov, 2010). Hemicelluloses have a tendency to hydrogen bond with cellulose chains due to their cellulose-like conformation but can usually be extracted with alkaline treatment. Hemicelluloses

cover a broad range of structurally and physiochemically different polysaccharides. Polysaccharides often grouped together as hemicelluloses include xylans, mannans and xyloglucans. Hemicelluloses are more abundant in the secondary cell wall than primary cell walls (Caffall and Mohnen, 2009).

1.2.2.1 Galactomannans

Galactomannans are a group of polysaccharides that have a β-1,4-linked mannan backbone with different levels of galactose substitution. Galactomannans are structurally important components of the cell wall as well as an important source of storage polysaccharides. They are typically obtained from the endosperms of the seeds of leguminous plants. Table 1.2 shows the mannose to galactose ratio (M:G) of some typical galactomannans.

Table 1.2 The mannose to galactose ratio of some typical galactomannans.

Galacotmannan	Mannose:Galactose ratio
Fenugreek gum	1:1
Guar gum	2:1
Tara gum	3:1
Locust bean gum	4:1

Galactomannan solubility is due to the presence of the galactose side units which prevent the mannan backbone from forming aggregates (Garti *et al.*, 1997). The mannose chains must have at least 12% galactose substitution to be water soluble. Ivory nut mannan contains about 95% mannose with few galactose side units and is therefore insoluble in water (Marchessault *et al.*, 1990).

Galactomannans are non-ionic so are unaffected by ionic strength or pH but will degrade at extreme pH.

1.2.2.1.1 LBG

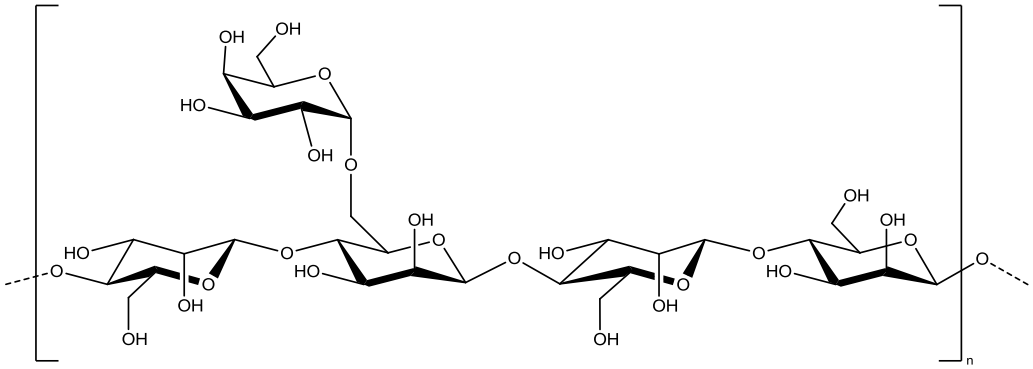

Figure 1.3 Chemical structure of Locust bean gum.

Locust bean gum (LBG), also known as carob bean gum, is extracted from the seeds of the carob tree (*Ceratonia siliqua*), found mostly in Mediterranean regions. It has β-1,4-linked mannose backbone. Approximately every fourth mannose unit is substituted with a 1,6-linked α-galactose residue (Figure 1.3). The galactose side chains are unevenly distributed resulting in there being smooth regions of the mannose backbone which are able to self-associate with other LBG molecules (McCleary *et al.*, 1985, Dea *et al.*, 1986). LBG therefore needs heating to 60-90^{o}C to break the network of self-associations. This can make the determination of molecular weight problematic. A reduction in water activity or solution temperature can increase the amount of aggregation which results in the formation of a 3D network. This is particularly useful in ice cream production (Patmore *et al.*, 2003, Regand and Goff, 2003). The weak gel structure can help impart excellent meltdown resistance in ice cream with a smooth texture without giving a slimy mouthfeel. Ice creams stabilised with LBG contain significantly smaller ice crystals than ice creams produced without stabilisers. LBG is also used in cream cheese to bind water and produce a spreadable texture without imparting sliminess.

LBG and kappa carrageenan gels are used as alternative to gelatin gels. They have higher melting points than gelatin which can be advantageous in hot countries. LBG

also acts synergistically with xanthan gum which interacts with the unsubstituted regions of the mannan backbone. At low concentrations there is a synergistic increase in viscosity. At higher concentrations soft, elastic gels are formed (Phillips and Williams, 2000).

1.2.2.1.2 Guar

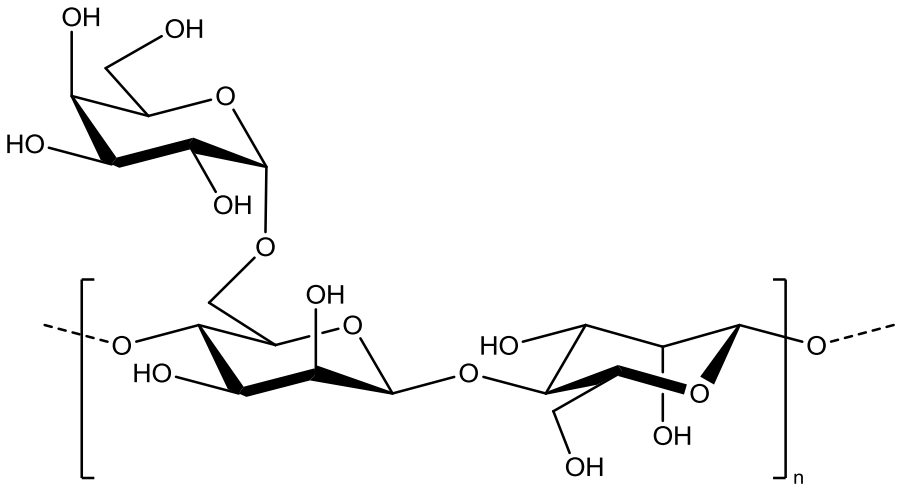

Figure 1.4 Chemical structure of Guar.

Guar gum is derived from guar beans (*Cyamopsis tetragonolobus*). India is the major producer, accounting for 80% of the world's total production. Guar has a β-1,4-linked mannose backbone with a galactose side chain approximately every two mannose units (Figure 1.4). Guar is able to fully hydrate in cold water. It does not form gels but does show good stability to freeze-thaw cycles and retards ice crystal growth.

Guar produces high viscosity solutions making it useful as a thickener. Only small amounts are needed making it a very cost effective alternative to corn-starch. Guar is also used in baked goods to increase dough yield, improve texture and prevent syneresis. As well as the food industry, guar is used in textiles, pharmaceuticals and cosmetics. Recently, guar has found a new use as an additive to the fluids used in fracking gas (hydraulic fracturing, a technique used to force liquids at high pressure into shale rock to release natural gas).

1.2.2.1.3 Fenugreek

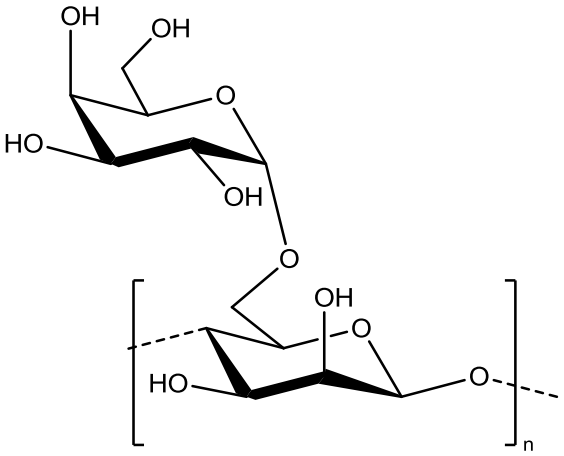

Figure 1.5 Chemical structure of Fenugreek.

India is the largest producer of fenugreek gum (*Trigonella foenum-graecum*), also known as '*Methi*' in Hindi. The galactomannan is found in the endosperm of the fenugreek seeds. Fenugreek gum has only been used industrially since 1990. It has a β-1,4-linked mannose backbone that is fully substituted with galactose residues (Figure 1.5). Due the high galactose content, fenugreek is the most water soluble galactomannan.

Fenugreek is currently used mainly as a health additive to lower blood sugar and reduce cholesterol levels (Sharma, 1986, Sharma *et al.*, 1990).

1.2.2.2 Konjac Glucomannan

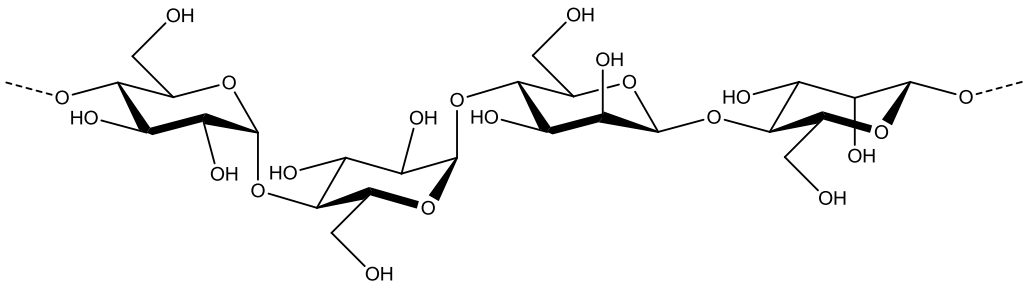

Figure 1.6 Chemical structure of Konjac glucomannan. The acetyl group is not shown.

Konjac glucomannan is the major storage polysaccharide from the tubers of *Amorphophallus konjac* which grows in eastern tropical regions. It has a of β-1,4-linked mannose and glucose backbone in a ratio of 1.6:1 (Figure 1.6) with an acetyl group about every 19 glucose residues (Williams *et al.*, 2000). Konjac readily dissolves in water producing a highly viscous pseudo-plastic liquid. The polymer remains in solution due to the presence of the acetyl groups. If konjac is treated with alkali, the acetyl groups will be removed resulting in konjac becoming water insoluble. Konjac is a non-ionic polymer so is acid stable and tolerant to high levels of salt. Konjac produces synergistic gels with xanthan and kappa carrageenan. Some applications for konjac include healthy/slim foods, noodles, fruit jellies, thickeners and edible films.

1.2.2.3 Xylan

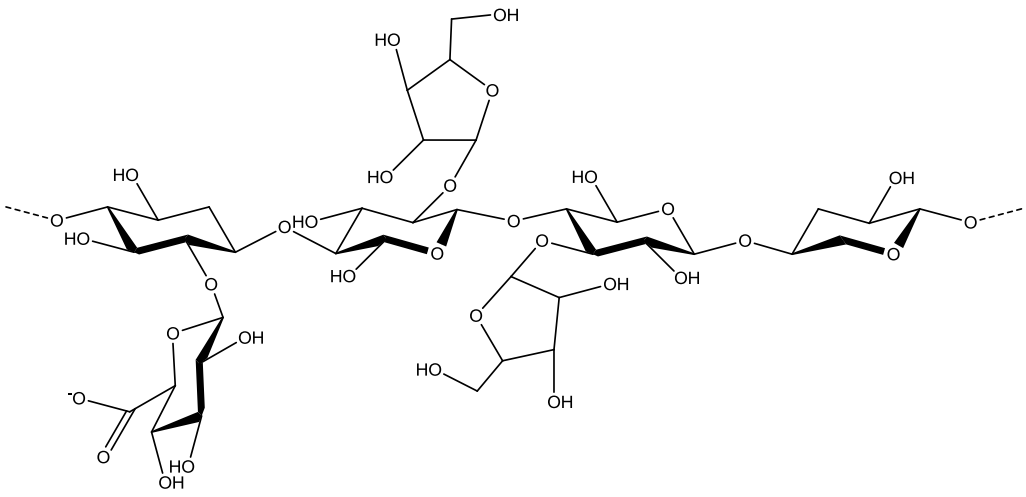

Figure 1.7 Chemical structure of Glucuronoarabinoxylan substituted by glucuronic acid at the O-2 and by arabinose at the O-2 and O-3.

Xylans have β-1,4-linked xylose backbone. Xylans may be substituted with α-1,2-linked glucuronosyl and 4-O-methyl glucuronosyl residues and are often referred to as glucuronoxylans (Figure 1.7). Xylans do not have a repeated structure (Scheller and Ulvskov, 2010). They are the dominant hemicellulose in the secondary walls of dicotyledons. Xylans may also contain arabinose residues attached to the xylose

backbone. Arabinoxylans are the primary non-cellulosic polysaccharide in the primary cell walls of monocotyledons (e.g. grasses). Xylans are predominantly found in softwoods (10-15%), hardwoods (10-35%) and annual plants such as oat spelts (35-40%) (Hettrich *et al.*, 2006).

1.2.2.4 Xyloglucan

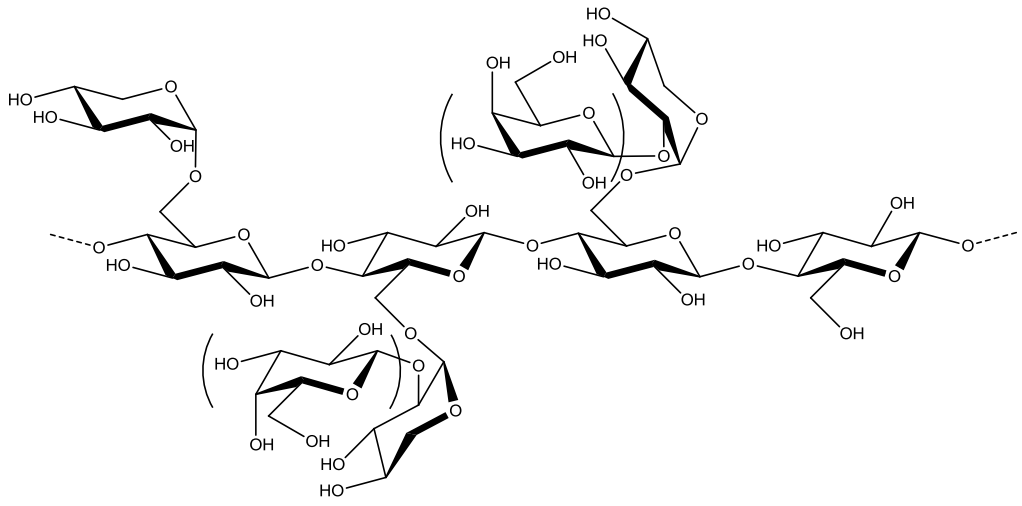

Figure 1.8 Chemical structure of Xyloglucan with an XLLG configuration.

Xyloglucans are a family of hemicelluloses with a cellulose-like β-1,4-linked glucan backbone highly substituted with α-D-linked xylospyranosyl residues attached at O-6 (Figure 1.8). Some xylose branches are further substituted at O-2 by combinations of galactopyranose, fucopyranose, arabinofuranose and O-acetyl residues. Xyloglucans are made of repetitive units, generally described using a one-letter code denoting the different side chains (Scheller and Ulvskov, 2010).

- G – Unbranched glucose residue
- X – α-D-Xyl-(1-6)-Glc
- L – Xylose residue substituted with β-Gal
- S – Xylose residue substituted with α-L-Ara*f*
- F – A Gal residue substituted at O-2 with *α*-L-Fuc

The most common core repeating units are XXGG and XXXG. The most widely studied xyloglucan is from tamarind seed and has a repeating unit of XXXG.

X-ray fibre diffraction indicates that the main chain has a flat ribbon like conformation, similar to that of crystalline cellulose chains (Levy *et al.*, 1991). The side chains fold tightly onto the main chain surface. In aqueous solution the main chain has a twisted conformation so the side chains are unable to fold as tightly onto the main chain (Umemura and Yuguchi, 2005).

In the plant cell wall, xyloglucan coats the cellulose microfibrils, limits their aggregation and connects them via cross-links. These cross-links can directly influence the mechanical properties of the cell wall (Ebringerova, 2006). Xyloglucan *endo*-transcglycosylase (XET) has been implicated in both wall-loosening and wall-strengthening roles (Eklof and Brumer, 2010).

Xyloglucan (extracted from tamarind kernel powder) is currently used as a sizing agent in textiles, especially in Asia. It improves yarn strength during weaving and imparts smoothness and stiffness to fabrics (Zhou *et al.*, 2007). It is also used as a replacement for starch and galactomannans in papermaking but is not widely implemented (Shankaracharya, 1998). The xyloglucan helps paper formation and strength as well as reducing fibre flocculation (Christiernin *et al.*, 2003, Lima *et al.*, 2003, Yan *et al.*, 2006).

1.2.3 Pectins

Along with hemicelluloses, pectins help form part of the cell wall matrix. Pectins are present in the primary cell wall and the middle lamella where it binds cells together. Pectins are a group of polysaccharides that are rich in galacturonic acid (GalA). There are three major structural domains of pectin, homogalacturonan (HGA), rhamnogalacturonan-I (RG-I) and rhamnogalacturonan-II (RG-II). These can be linked

to form a pectin network throughout the primary cell wall matrix and the middle lamella.

HGA is a linear homopolymer of α-1,4-linked-D-galacturonic acid and is thought to contain about 100-200 GalA residues (Zhan *et al.*, 1998); the GalA residues can be methylesterified and *O*-acetylated. Sugar beet root and potato tubers have a particularly large amount of acylated GalA (Pauly and Scheller, 2000). The GalA residues may be substituted with xylose to form xylogalacturonan (XGA) (Willats *et al.*, 2001). HGA tends to be insoluble, so is hard to extract (McNeil *et al.*, 1984).

RG-I consists of as many as 100 repeats of the disaccharide 1,2-α-L-rhamnose-1,4-α-D-galacturonic acid (Albersheim *et al.*, 1996). RG-I is abundant and heterogenous and generally thought to be glycosidically bonded to HGA domains. Many of the rhamnose residues have side chains. The side chains can range from one glycosyl residue up to 50 or more. The predominant side chains contain linear and branched α-L-arabinofuranosyl (Ara*f*), and/or β-D-galactopyranosyl (Gal*p*) residues, although their relative proportions and chain lengths may differ depending on the plant source (Lerouge *et al.*, 1993, Ralet *et al.*, 2009). The highly branched nature of RG-I has led to it being known as the hairy region of pectin, in contrast to HGA domains which are known as the smooth region (Willats *et al.*, 2001).

RG-II is not structurally related to RG-I; it has an HGA backbone, nine or more residues long and has side chains composed of eleven different sugars (Willats *et al.*, 2001). RG-II is the only boron containing polysaccharide that can be isolated from a biological source (Kobayashi *et al.*, 1996). Boron is an essential microelement for plant growth and its deficiency can lead to disorganised cell expansion and cell walls with abnormal morphology (O'Neill *et al.*, 1996). O'Neill *et al*. propose that dRG-II-B (a borate ester cross-linked dimer of RG-II) is an essential component of the cross-

linked pectin matrix. The covalent cross links of the primary cell wall may result in the formation of a macromolecular complex composed of RG-II, RG-I and HGA, linked by glycosidic bonds. This matrix may participate in regulating the rate of cell growth and may create wall domains that control the rate at which enzymes, polysaccharides, biologically active oligosaccharides and even lower molecular weight compounds pass through the wall (Baronepel *et al.*, 1988).

Many of the galacturonic acid groups along the main chain are esterified with methoxy groups. The percentage of galacturonic acids that are esterified is referred to as the degree of esterification (DE). The pattern of the distribution of methoxy groups is also important and is often described as blockiness (Daas *et al.*, 1999, Winning *et al.*, 2007). Commercially, pectins are generally categorised according to their methoxy content:

- High methoxy (HM) pectin – DE higher than 50
- Low methoxy(LM) pectin – DE lower than 50

HM pectin forms gels under conditions of low pH (below 3.5) and high solids content (above 55 wt%) and is typically used for jam making (Pilgrim *et al.*, 1991). The number of methoxy groups determines the speed at which the gels will set. The rate of gelation is decreased as more methoxy groups are removed. As the pH is reduced, gel strength and setting temperature will decrease (Phillips and Williams, 2000). If the pH is reduced to a point where the setting temperature and preparation temperature are similar the pectin tends to pre-gel. This results in a non-homogenous weaker gel which is therefore more susceptible to syneresis. This can be solved by preparing pectin mixtures at higher pH and then acidifying when ready.

LM pectin forms gels in the presence of divalent cations, most commonly calcium; the reactivity to calcium increases with decreasing DE. LM pectins are often used to

produce low sugar jams. They are also often used in milk products where they utilise the calcium present to enhance viscosity and stabilise emulsions (Glahn, 1982, BenZion and Nussinovitch, 1997). If HM pectins are reacted with ammonia, normally in an aqueous alcohol slurry at ambient temperature, an LM amidated pectin can be produced. Amidated pectin requires less calcium to gel than conventional LM pectins.

Pectin is present in nearly all terrestrial plants but is most abundant in vegetables and fruits. The major source is from the rind of citrus fruit. Apple pomace and sugar beet pulp are also widely used as sources of pectin. This is often waste material from another industry, for example, apple pomace from cider production. Pectin is generally extracted from plant material using hot aqueous mineral acid. The pectin is then isolated from the solution. One of the main challenges for producers is to retain a high molecular weight as pectin is very susceptible to degradation either by enzymes already present in the plant material or heat during drying and subsequent processing (Phillips and Williams, 2000).

Jams have been made for centuries by adding fruit containing high levels of pectin. Pectin has been industrially produced since the early 20th century. Pectin is now also used in other food and personal care products as a thickener, stabiliser and gelling agent. Pectin also forms excellent films.

1.2.4 Starch

1.2.4.1 Starch Structure

Starch is one of the main energy reserves in nature and is a staple food in most human diets. Starch also has many non-food uses, for instance in papermaking, adhesives or as a gum in the textile industry. It is also used as a feedstock for the production of chemicals such as ethanol and acetone or polymers such as polylactic

acid (PLA). There is now growing interest in the use of starch as a plastic material that could be a possible replacement to oil based materials (Laycock and Halley, 2014).

Starch granules are produced by plants as a carbohydrate storage. Depending on botanical source, the size of the starch granule can vary from as small as 2µm (e.g. rice) up to 80-100µm (e.g. tubers).

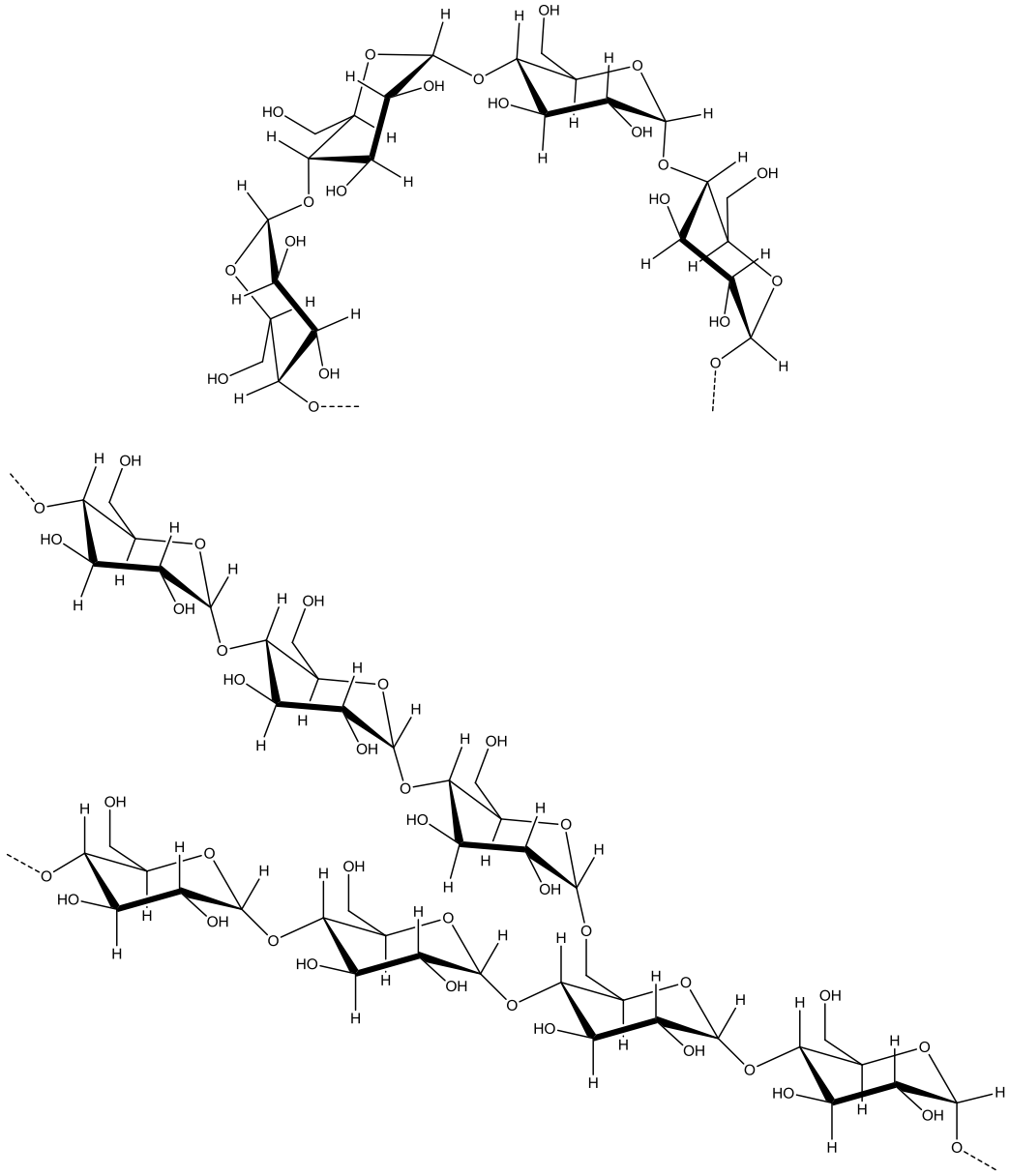

Figure 1.9 Chemical structure of amylose (top) and amylopectin (bottom).

Starch is comprised of linear chains of α-1,4-linked anhydro-D-glucose with some branching with α-1,6 linkages. Native starch has two macromolecular components, amylose (mainly linear) and amylopectin (highly branched) (Figure 1.9). Amylopectin branches approximately every 20 units (Cheetham and Tao, 1998). Due to the α glycosidic linkage a natural twist is imparted to the molecule (Zobel, 1988). The ratio of amylose and amylopectin is dependent on the botanical species. Some starch granules naturally occur with low amounts of amylose and are typically referred to as waxy starches.

1.2.4.2 Starch Crystallinity

Starch granules have alternating crystalline and amorphous regions due to the branched amylopectin structure. This results in spherical rings (Figure 1.10) with diameters ranging from 20 to 500nm (Gallant *et al.*, 1997). Starch granules exhibit two crystalline polymorphic forms depending on their amylose/amylopectin ratio and amylopectin branch length, the A-type, found predominantly in cereals and the B-type which is found mainly in tubers as well as maize starches with more than 30-40% amylose (Blanshard, 1987). A third polymorph, the C-type is a combination of the A and B-types and is usually found in pea and bean starches (Lopez-Rubio *et al.*, 2008). The A-type crystal structure consists of left handed parallel stranded double helices packed in monoclinic units cells while the B-type has hexagonal unit cells (Imberty *et al.*, 1988, Imberty and Perez, 1988). When lipids are present (particularly in cereal starches) another crystal polymorph may be observed. The V-type crystal form consists of left handed single amylose helices with six residues per turn enclosing the aliphatic tail of a lipid in its centre (Tester and Morrison, 1990, Morrison *et al.*, 1993). The amylose-lipid complexes restrict the swelling capacity of starch (Zuluaga *et al.*, 2007, Nuwamanya *et al.*, 2011).

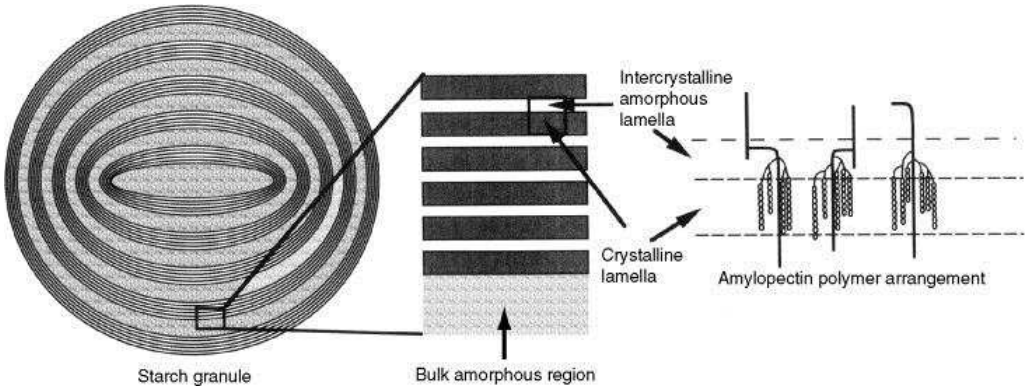

Figure 1.10 Schematic diagram of the starch granule structure (Ratnayake and Jackson, 2008).

1.2.4.3 Starch Gelatinisation

Native starch granules are insoluble in cold water and do not absorb much water. When heated in excess water or another solvent able to form hydrogen bonds, (e.g. liquid ammonia) starch undergoes significant irreversible physical changes known as gelatinisation (**Error! Reference source not found.**). Above the gelatinisation emperature water penetrates and swells the granule. The starch crystals melt and amylose progressively leeches out. The gelatinisation temperature is dependent on the starch-water ratio, pH, salt or sugar concentration and fat or protein content. Upon gelatinisation there is often a large increase in viscosity which is the major reason for its ubiquity in food. Native starch generally gelatinises at temperatures between 55-80^{o}C although high amylose starch may require higher temperatures to fully gelatinise.

After gelatinisation the linear portions of the amylose and amylopectin chains recrystallise in a process often referred to as retrogradation (Figure 1.11). Long amylose chains are able to recrystallise rapidly whereas amylopectin retrogradation occurs at a slower rate, depending on chain length, temperature and moisture content.

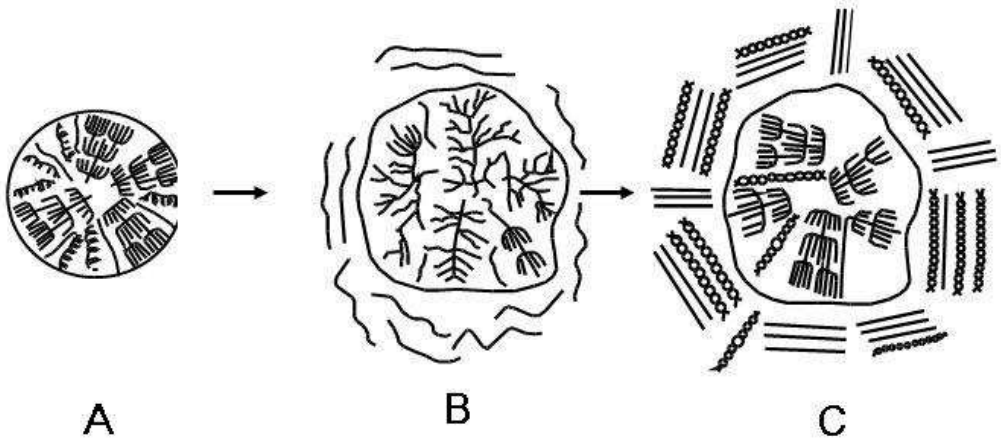

Figure 1.11 Gelationisation and retrogradation of starch. (A) native starch (B) gelatinised starch and (C) retrogradated starch (http://www.food-info.net/uk/carbs/starch.htm date accessed 15.03.2014).

1.3 BioComposites

1.3.1 Natural Fibre Composites

Natural fibres such as jute, flax and sisal have many benefits as they are strong, biodegradable, renewable, low cost, low density and abundantly available. They are also much less abrasive than many fibres currently used in composites.

There are major difficulties in using natural fibres as reinforcing fillers. Natural fibres start degrading at about 240^{o}C so cannot be processed at high temperature. The fibres also absorb moisture and may have a moisture content of between 5-10 wt% (Riccieri *et al.*, 1999) which can lead to poor processability. The fibres can also be biodegraded by microorganisms and are susceptible to UV light (Saheb and Jog, 1999). Natural fibres may also not function well as a reinforcing component due to poor adhesion at the fibre-matrix interface. They also aggregate in a hydrophobic polymer matrix. This can be counteracted by appropriate pre-treatments with suitable additives such as stearic acid, mineral oil or maleated ethylene (generally at a concentration of about 1 wt%) which will reduce fibre-fibre interaction (Saheb and Jog, 1999). To improve adhesion between the fibres and matrix polymers, compatibilisers or coupling agents may also be used, such as silane, zirconate or

titanate. Sodium alginate and sodium hydroxide have also been used with banana and coir fibres to increase adhesive bonding and thus improve their ultimate tensile strength (Mani and Satyanarayana, 1990). Chemical grafting is another route to improving the physical properties of fibres by attaching suitable additives such as vinyl monomers to the surface of the fibre which will improve the bonding between fibre and matrix (Ellis and O'Dell, 1999).

Many different parameters influence the strength of composites, including, the volume fraction of fibres, fibre aspect ratio, fibre-matrix adhesion, stress transfer at the interface and orientation (Saheb and Jog, 1999).

Natural fibre composites have been produced with a variety of matrix materials. Many that are in use now, for instance in the automotive industry, rely on oil based matrix resins such as polypropylene, polyethylene and poly vinyl chloride (PVC) (Keener *et al.*, 2004, Abdelmouleh *et al.*, 2007, Zheng *et al.*, 2007, Mohanty *et al.*, 2002). In the pursuit of completely renewable and biodegradable composites, other matrix materials are currently being researched. Those of interest include, polylactic acid, cellulose esters, poly hydroxy butyrate, starch and lignin based plastics (Oksman *et al.*, 2003). Few are commercially available so are often high cost, as well as having poor processability and, as with most polymers from natural sources, a low moisture stability. Polylactic acid (PLA), which is derived from starch by fermentation, is perhaps one of the most promising renewable polymers (Graupner *et al.*, 2009). Bodros *et al.* (2007) have shown that PLA/flax composites have a specific tensile strength and Young's modulus close to that of fibre glass polyester composites and have a greater tensile strength and modulus than that of similar polypropylene/flax composites.

One answer to achieving improved compatibility between fibre and matrix is to utilise cellulose as the matrix material itself. All-cellulose composites were initially developed by Nishino *et al.* (2004), where the cellulose pulp was dissolved in lithium chloride/N,N-dimethylacetamide (LiCl/DMAc). The cellulose solution then formed the surrounding matrix for aligned ramie fibres. The solution was then coagulated with methanol and dried and the composite had longitudinal strength as high as 480 MPa as well as extremely good thermal stability. One of the major difficulties in producing all-cellulose composites is the high viscosity of concentrated cellulose solutions. An alternative to using a cellulose solution as the matrix material is to only partially dissolve fibres such as flax or ramie (Gindl and Keckes, 2005).

An alternative to using natural fibres is to use purified primary cell wall fragments. This would have the advantage that cheap waste sources of cellulosic material such as sugar beet pulp or vegetable waste could be used for composite manufacture. Hepworth and Bruce (2000a) used Swede root as the source of cell wall material which was ground into a fine paste. Lipid membranes were destroyed with 1 wt% detergent and some of the pectins were removed with 0.5M HCl to break up the cells. The cell wall fragments were then bound together in a matrix of polyvinyl alcohol (PVA). The composite had a tensile stiffness of 5.4GPa and a strength of 70MPa which compares favourably to epoxy and phenolic composites reinforced with randomly orientated vegetable fibres. They did however comment that if the cellulose microfibrils were completely extracted and aligned then a higher strength could probably be achieved. This was later done using chemical extraction of the non-cellulosic components of the cell wall with 2 wt% sodium hydroxide (Hepworth and Bruce, 2000b, Bruce *et al.*, 2005). The purified cellulose suspension was then passed through a homogeniser to separate the microfibrils. They used four different matrix materials; PVA, acrylic polymer, epoxy and hemicellulose which was chosen to

be LBG. Composites made with LBG showed higher tensile strength and stiffness than pure LBG. The LBG composites had a lower stiffness compared to PVA or epoxy but had a higher strength and stiffness compared to flax/epoxy composites.

1.3.2 Cellulose Composites

Despite the many attractive properties of natural fibres there are still major draw backs. The non-cellulosic components of natural fibres often impart some of the most undesirable aspects. It is often useful therefore to create composites with pure cellulose. Lignin is first removed with alkali (usually NaOH) and the fibres are then treated with acid to remove any hemicellulose and pectin (Moon *et al.*, 2011). The cellulose is also often bleached to remove any colour.

Both cellulose nanowhiskers and MFC are prepared in water. To create nanocomposite films the suspensions are mixed with a polymer that has been previously dissolved in water and then the liquid is evaporated. Due to the inherently high sensitivity of these polymers to humidity, storage is difficult (Siqueira *et al.*, 2009). Water also induces a strong plasticising effect and greatly affects the properties of the film (de Rodriguez *et al.*, 2006).

To investigate the effect of moisture on the dynamical mechanical properties of cellulose composites Dammstrom *et al.* (2005) produced composite films with bacterial cellulose and glucuronoxylan from Aspen wood chips. Humidity scans using dynamic mechanical analysis (DMA) showed no softening for the pure bacterial cellulose sample but there was a pronounced softening at 85% relative humidity (RH) for pure glucuronoxylan. The composite of the two polymers also showed a decrease in modulus but at a slightly lower RH as compared to pure glucuronoxylan. The glucuronoxylan acts as a plasticiser but also changes the spatial organisation of the

cellulose fibres although there are no clear interactions between the cellulose and hemicellulose.

The use of cellulose nanowhiskers may improve the water transmission properties of xylan films. Saxena and Ragauskas (2009) have shown that xylan films reinforced with 10 wt% sulphuric nanowhiskers had a 74% reduction in specific water transmission properties compared to control xylan films. There was also a 362% improvement with respect to xylan reinforced with 10 wt% softwood Kraft pulps. The high crystallinity of the nanowhiskers and the dense composite structure formed due to a rigid hydrogen bonded network leads to a film that has reduce moisture transmission properties (Saxena *et al.*, 2011). Nanowhisker reinforced xylan films also have excellent tensile strength (Saxena *et al.*, 2009). The use of plasticisers such as xylitol or sorbitol improves the mechanical properties of the films by conferring flexibility and workability (Peng *et al.*, 2011).

Nanowhisker reinforced hemicellulose films have also been produced using konjac glucomannan (Mikkonen *et al.*, 2010). The addition of nanowhiskers to konjac, plasticised by glycerol, induced the formation of fibre-like structures with lengths of several millimetres although the differences in film structure did not appear to be related to the thermal properties of the films.

Recently Azeredo *et al.* (2009) have used nanowhiskers to reinforce mango puree to produce edible films. The nanowhiskers increased the tensile strength and Young's modulus in respect to pure puree films as well as improving the water barrier properties of the films.

1.3.3 Cellulose/Polymer interactions

Both hemicelluloses and pectins are likely to bind to cellulose in the plant cell wall but there is as yet no complete consensus as to what the binding mechanisms are.

Xyloglucan is known to bind to cellulose but there is some debate as to whether it is dependent on molecular weight or side chain composition. The presence of fucose was suggested by Levy *et al.* (1991) to create a flat conformation which enabled xyloglucan to bind to cellulose. This was further confirmed by binding experiments with fucosylated (pea) and non-fucosylated (tamarind seed) xyloglucans (Levy *et al.*, 1991, Hayashi *et al.*, 1994). However, the role of fucose in facilitating xyloglucan-cellulose interactions was later cast into doubt by Vanzin *et al.* (2002) by using the *Arabidopsis* mutant *mur2* which eliminates xyloglucan fucosylation in all major plant organs. Despite the lack of fucose the *mur2* plants showed a normal growth habit and wall strength. Lima *et al.* (2004) have since shown with *in vitro* experiments that the binding capacity of xyloglucan is improved when the molecular weight of the polymer is decreased by enzymatic hydrolysis and that the branching with fucose seems not to be a key factor in binding. Fucose though may still have some role in strengthening the cell wall structure.

Whitney *et al.* (1995) first developed the method of modelling plant cell wall interactions using the Gram negative bacterium *Acetobacter aceti* ssp. *xylinum* which synthesises pure, highly crystalline cellulose I as an extracellular polysaccharide. The cellulose forms a thick pellicle which floats on the surface of the medium. Viewed using deep etch freeze fracture transmission electron microscopy (TEM), the cellulose ribbons appear to form a randomly orientated network. Different polysaccharides can be added to the medium. In the presence of tamarind xyloglucan, the bacterial cellulose also forms a network similar in structure to that of plant cell walls (Whitney *et al.*, 2000). Whitney *et al.* (2006) found that galactose depleted xyloglucan is likely to self-associate, leading to phase separation into xyloglucan-rich and cellulose-rich phases with limited direct binding between the two polymer types. This led them to conclude that galactose content has a greater effect

on composites than other xyloglucan variants with fucose substitution only acting as a secondary modulator. These results are consistent with the work done on Arabidopsis mutants.

The *A xylinum* system has also been used for other cell wall polysaccharides such as mannans. In the presence of konjac glucomannan a structure is formed which shows considerable heterogeneity (Whitney *et al.*, 1998). Micrographs show regions of apparent cross-linking of cellulose ribbons by glucomannan and areas of glucomannan network within a cellulose network. The cellulose acts as a template where the mannan residues along the polymer chains adopt a cellulosic conformation. Konjac, as well as low galactose galactomannans, dramatically reduces the cellulose crystallinity. Mannans with a low galactose content are also more effective at disrupting cellulose organisation. This suggests that the galactose side chains present a significant barrier to incorporation within cellulose fibrils. Due to the much more polydisperse fine structure of galactomannans, as opposed to xyloglucan, the long range alignment of fibrils is not as pronounced. In secondary cell walls both gluco- and galactomannans are significant components. The mannan based polymers are able to help the coalescence/densification of cellulose and thus provide a stronger composite compared to xyloglucan in the primary cell wall where flexibility is the major requirement.

Many of the models of cell wall organisation suggest that the cellulose-hemicellulose network is independent from the one formed by pectins (Cosgrove, 2000). However, Zykwinska *et al.* (2005) have demonstrated that pectin is able to bind *in vitro* to cellulose microfibrils. The neutral pectin side chains are likely to enable non-covalent cellulose binding rather than the pectin backbone domains (Zykwinska *et al.*, 2007).

Commercial citrus pectins which have a very low number of neutral side chains, due to their harsh acidic extraction, do not bind to cellulose (Chanliaud and Gidley, 1999).

1.3.4 Semi Solid Composites

There are many semi-solid composites particularly in food systems where a gel network is embedded with a filler. The filler enhances the rheological properties and textural characteristics of the system. Common fillers in the food industry include meat fibres, starch granules or emulsified oil droplets (Mavrakis and Kiosseoglou, 2008). Inorganic fillers such as glass fibre or hydroxyapatite clay may be used in non-food applications. The size, shape, strength and phase volume of the filler will all influence its reinforcing effect (Fu *et al.*, 2008, Ahmed and Jones, 1990, Fiedler *et al.*, 2006). When suitably incorporated the filler should improve the mechanical properties of the system due to load transfer from the matrix to the filler particle. One of the most common fillers in the food industry is microcrystalline cellulose (MCC). MCC has been shown to improve gelatin gel strength (Kasapis, 1999, Koh and Kasapis, 2011). By applying torque to the setting gels Koh and Kasapis (2011) found they could highly orientate the MCC fibres resulting in a higher storage modulus of 1.5 wt% gelatin gels due to an enhancement in network strength.

Microfibrillated cellulose (MFC) has outstanding rheological properties. MFC suspensions possess a classical pseudoplastic (shear thinning) behaviour that is common to many polymer solutions (Paakko *et al.*, 2007) and have a solid like viscoelastic behaviour. The rheological properties are not effected by either temperature or pH although an increase in ionic strength does increase both the storage modulus (G') and loss modulus (G'') moduli of MFC suspensions (Agoda-Tandjawa *et al.*, 2010). MFC may also be able to increase viscosity or gel strength of low methoxy (LM) pectin. Agoda-Tandjawa *et al.* (2012) added LM pectin to a

suspensions of MFC which had a synergistic effect on the rheological properties of the composites. Addition of calcium to the mixtures induced gelation which was enhanced by the presence of sodium resulting in the formation of a stronger cellulose/ LM pectin gel.

Since the early 1990s MCC has been used as a fat replacer. The MCC is first subjected to severe mechanical attrition such as high pressure homogenisation which breaks it down into colloidal crystalline aggregates. It can then be co-dried with a hydrocolloid such as carboxymethylcellulose which aids later re-dispersion and forms a network which evenly distributes the particles (Lucca and Tepper, 1994). When added to an aqueous medium (generally above 5 wt% solids content) the insoluble sub-micron sized crystals disperse to create a stable thixotropic gel which has a creamy mouth feel, opacity and body (Samir *et al.*, 2005). MCC also enhances the gelling properties of galactomannans (Newman and Hemmingson, 1998).

Ang (1991) and Ang and Miller (1991) first reported the effect of powdered cellulose on the viscosity of polymer solutions. Powdered cellulose was able to increase the viscosity of guar, carboxymethylcellulose and xanthan solutions of between 0.1 and 0.3 wt%. Recently Day *et al.* (2010) added xanthan to rehydrated carrot cell wall particles (CWP). The addition of xanthan to CWP at concentrations lower than 1 wt% influenced the rheological behaviour of the CWP dispersions due to the increase in the viscoelastic properties of the continuous phase but this was not the case for concentrations higher than 3 wt% as the viscoelastic behaviour of the mixtures was dominated by the CWP particle network. There have been several other studies using cell wall dispersions from a variety of horticultural sources such as tomato, apple and carrot which have all demonstrated the importance of interactions between the solid particles and the deformability of the fully packed particles (Kabbert *et al.*, 1997,

Kotcharian *et al.*, 2004, Kunzek *et al.*, 1999, Kunzek *et al.*, 2002, Pickardt *et al.*, 2004, Vetter and Kunzek, 2002).

1.4 A brief introduction to the thesis

With growing environmental concerns as well as food shortages, cellulosic research is increasingly important. Cellulose, the most abundant natural polymer on earth, is the major component of plant cell walls, but due to its poor water solubility it has seen little use in the promotion of structures in manufactured products in its native state. Traditional methods of utilising cellulose involve harsh chemical treatments. Recent research has focussed on 'green' solvents such as ionic liquids and molten salt hydrates which have a much lower environmental footprint or using different mechanical pre-treatments such as ball milling and homogenisation which dramatically change the properties of native cellulose and add alternative routes to structure formation.

Recently, Tatarova *et al.*, (2010) have developed a novel swelling solution (LiCl/urea/water) for the treatment of regenerated cellulose fibres during textile processing. Fibres were shown to swell to the same extent as found in traditional alkali swelling treatments. The LiCl/urea/water system has the advantage of being noncorrosive, so reverse osmosis can be used to recycle the LiCl and urea. The swelling system provides the opportunity to change the structure of cellulose without complete dissolution. Other plant polysaccharides can also be co-processed with cellulose in the swelling solution (Eichhorn *et al.*, 2001).

There has also been a growing interest in amorphous cellulose. By completely disrupting the crystal structure there is a possibility that cellulose can be thermoformed to produce renewable bioplastics, however, there are serious limitations due to cellulose degrading before it melts. However, as well as reducing the crystallinity of cellulose (Paes *et al.*, 2010), ball milling also decreases the degree

of polymerisation (Csiszar and Fekete, 2011) which may help overcome the issues involved in thermoforming (Zhang *et al.*, 2012).

Cellulose can also be used in its native form as a reinforcement material in polymer composites, for example, there are already applications in wound dressings, bone scaffolds, automotive parts and packaging. There is a particular interest in renewable foams which could be used as insulation, packaging and cushioning materials, however, many of the matrix polymers used are hydrophobic leading to poor interactions with natural fibres so there needs to be further work to identify other natural matrix polymers.

By understanding the structural changes that cellulose and hemicelluloses undergo during different pre-treatments novel structures can be formed which will help reduce the dependency on oil based materials.

1.5 Objectives and structure of the Thesis

1.5.1 Objectives

The main aim of the work was to find novel ways of utilising native cellulose, for example, in the production of bioplastics, aerogels or thickeners, using either mechanical or chemical pre-treatments. A greater understanding of the structural changes that occur during various pre-treatments will enable the creation of novel, renewable and biodegradable structures from cellulose or cellulose-polymer composites. Within this framework the objectives of this work were:

- To further understand the effect of ball milling on different types of cellulose and study its recrystallisation in excess water.
- To investigate the possibility of thermoforming amorphous cellulose
- To produce cellulose-polymer composites
- To investigate the effect of a novel swelling solution on cellulose and different plant polysaccharides.
- To investigate any interactions between cellulose and plant polysaccharides in different solvent systems.

1.5.2 Structure of Thesis

A general literature review has been presented in Chapter 1 which is now followed by a description of the main techniques used throughout the thesis in Chapter 2. Within each results chapter there is also a specific literature review and materials and methods section.

The work in Chapter 3 focussed on the effect of ball milling on two different types of cellulose and in particular their change in degree of polymerisation, crystallinity and degradation temperature with increased milling time. The ball milled celluloses were then rehydrated in excess water and any changes due to recrystallisation were investigated. Flash differential scanning calorimetry (DSC) was used for the first time to measure a glass transition temperature for amorphous cellulose.

The work presented in Chapter 4 investigates different ways of utilising cellulose in the construction of biofoams. Three different celluloses were added to locust bean gum or fenugreek freeze dried foams. Their effect on mechanical properties, morphology and water absorption were monitored. Further work was carried out to produce biofoams using through extrusion which is a less time consuming and less energy intensive process than homogenisation.

In Chapter 5, the effect of a novel swelling solution (LiCl/urea/water) on the crystallinity, morphology and rheological properties of different celluloses was studied. To further understand the system, two starches were compared in either water or LiCl/urea/water.

In Chapter 6, the solution properties of four different plant polysaccharides in two solvent systems, water or LiCl/urea/water, were investigated to identify any conformational changes. These changes were further studied after the solvents were removed. Having gained an understanding of the effect of LiCl/urea/water on

cellulose or hemicelluloses alone, the polysaccharides were co-processed to identify any changes in interactions between cellulose and hemicelluloses in different solvent systems.

In Chapter 7 general conclusions of this work are presented along with suggestions for future studies.

Chapter 2. Techniques

2.1 Nuclear magnetic resonance (NMR)

NMR spectroscopy makes use of nuclei with an uneven number of subatomic particles in the nucleus (often ^{1}H or ^{13}C). These nuclei spin on their axis either clockwise or counter clockwise (spin states of +1/2 or -1/2) (Figure 2.1). The spin makes the nuclei act like magnets. The resulting spin-magnet has a magnetic moment proportional to the spin. When an external magnetic field is applied these nuclei will align in their low energy state (+1/2). For the two states to be significantly different a very powerful magnet is required.

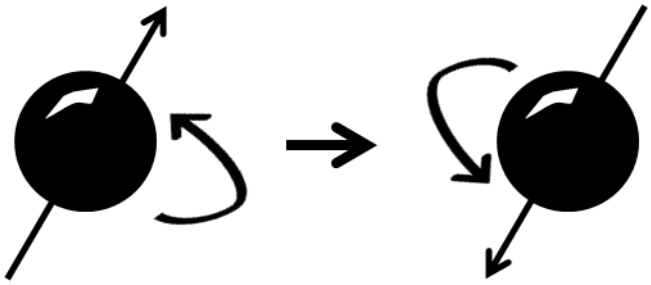

Figure 2.1 Spinning nuclei.

When radiation (radio waves) hits the nuclei at a certain wavelength which corresponds exactly to the spin state separation energy it will flip to a higher energy. When the spin returns to its base level, energy is emitted at the same frequency. This signal can then be measured.

All nuclei will flip at different wavelengths of radiation levels dependant on their chemical environment (i.e. where the electrons surrounding the nuclei are positioned). The electrons will generate a secondary magnetic field which shields the nucleus from the applied external magnetic field.

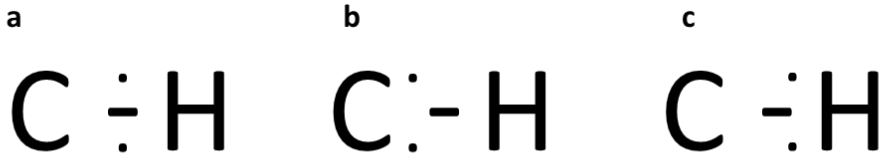

Figure 2.2 A carbon-hydrogen bond showing its shared pair of electrons where (a) electrons are shared equally (b) the electron pair is drawn towards the carbon nucleus and (c) the electron pair is drawn towards the hydrogen nucleus.

Electronegativity is the power of an atom in a molecule to attract electrons to itself. The Pauling scale is a scale of electronegativity which ranges from Fluorine (the most electronegative element) which has a value of 4.0, to Francium (the least electronegative element) which has a value of 0.7. Figure 2.2a shows a simple carbon-hydrogen bond. If the carbon is attached to something that is electron withdrawing (for instance a benzene ring) then it will pull the pair of electrons away from the hydrogen giving it less shielding (Figure 2.2b). Conversely if the carbon is attached to something less electronegative than itself (for instance Si, which has a value of 1.90 on the Pauling scale, compared to carbon and hydrogen which have values of 2.55 and 2.20 respectively) then the hydrogen will draw the shared electrons closer to itself increasing the level of shielding (Figure 2.2c). The wavelength of radiation required to make each of these protons flip will therefore vary. The more the proton is shielded the less energy is required to flip the proton. The precise resonant frequency of the energy transition is described as a chemical shift (ppm). The effective magnetic field is also affected by neighbouring nuclei in an effect known as spin-spin coupling.

^{13}C NMR uses the nuclei of an isotope of carbon (which has a natural abundance of 1.1%) instead of protons. It is much less sensitive than ^{1}H NMR but can show a single peak for each non-equivalent carbon atom (as couplings between carbon atoms can

be ignored due to the scarcity of the ^{13}C isotope). Figure 2.3 shows the NMR spectra of native cellulose with each carbon in the glucose molecule labelled.

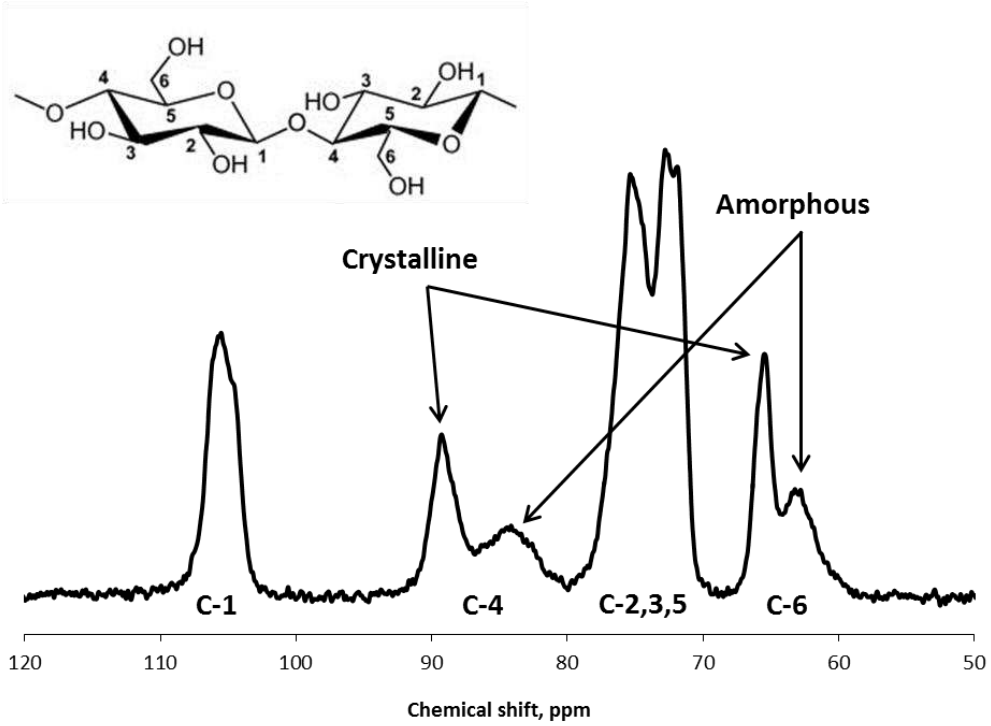

Figure 2.3 Solid state ^{13}C NMR spectra of microcrystalline cellulose showing the assignment of peaks to the carbons in a glucopyranose repeat unit (adapted from Park *et al.* (2010)).

2.2 X-Ray Diffraction (XRD)

An X-ray is electromagnetic radiation that has a wavelength of between 0.1Å and 100Å which is similar to the interatomic distances in a crystal. To produce X-rays, a tungsten filament is heated inside a vacuum tube. Electrons are emitted and accelerated by an electric potential and impact on a metal target (often copper). These electrons will disturb the metal atom's inner electrons. When the outer electrons fall to a lower orbital to take their place X-rays are emitted.

In an amorphous material, atoms have no order. When the atoms are hit by X-ray beams, the surrounding electrons will oscillate at the same frequency as the beam. Due to the lack of order, the x-ray beams will be reflected at all angles resulting in destructive interference as the waves are out of phase of one another. However,

crystals have an ordered structure. Due to the regular patterns in the crystal when X-ray beams hit the atoms, in some directions, the waves will be in phase which will cause constructive interference that can be measured by the detector (Figure 2.4).

The smallest repeating part is the unit cell which has a fixed arrangement. It reflects X-ray beams at certain angles of incidence (θ). This angle is dependent on the distance (d) between atomic layers and the wavelength of the incident X-ray beam (λ). This relationship is defined by Bragg's Law:

$$n\lambda = 2d \sin\theta \tag{2.1}$$

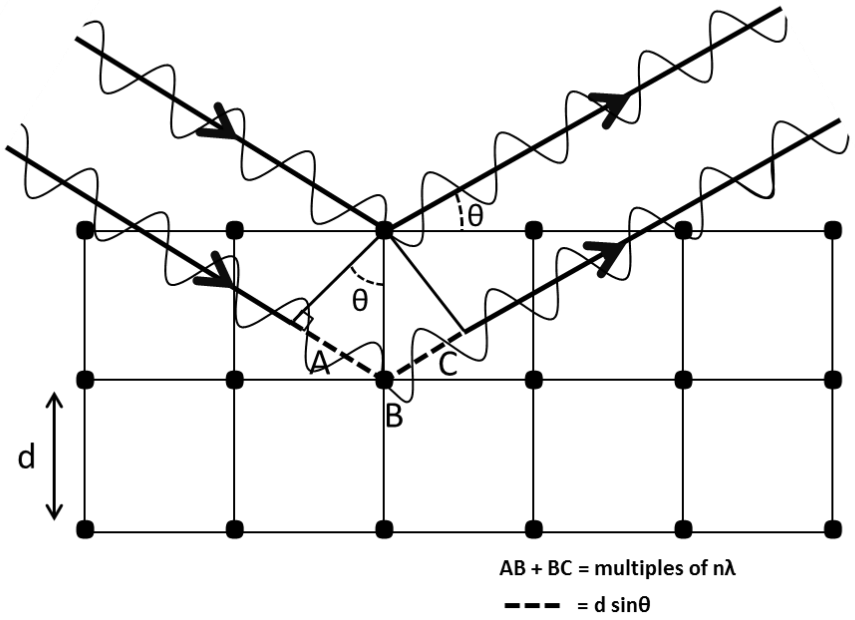

Figure 2.4 Bragg diffraction in a crystal showing constructive interference of reflected waves.

Miller indices are used to describe the orientation of a plane within a lattice in relation to the unit cell (Figure 2.5). The "overbar" denotes a negative index.

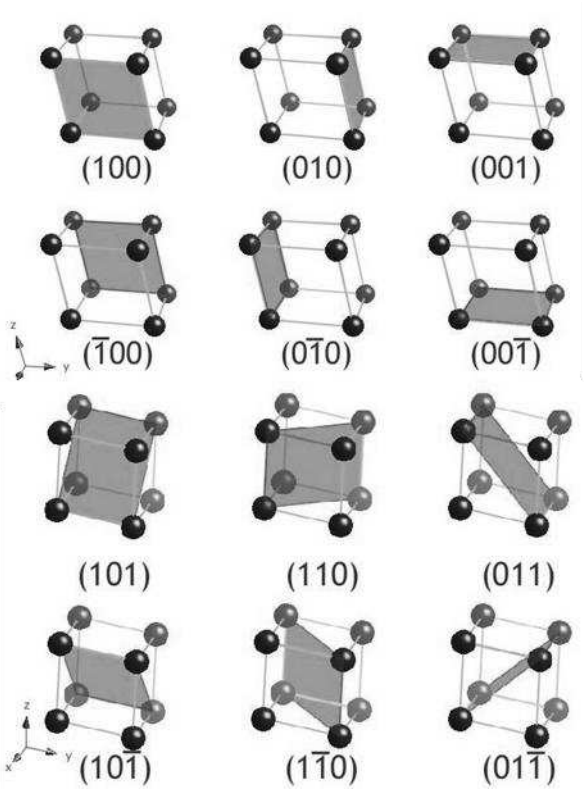

Figure 2.5 Example of Miller indices (http://www.doitpoms.ac.uk/tlplib/miller_indices/printall.php date accessed 18.03.2014)

One of the most common ways of measuring crystallinity is using powder diffraction. The powder must be randomly packed so the crystals are in all directions. This will mean all the possible diffraction directions of the lattice are attained. Figure 2.6 and 2.7 show the typical spectra of type I and type II celluloses respectively.

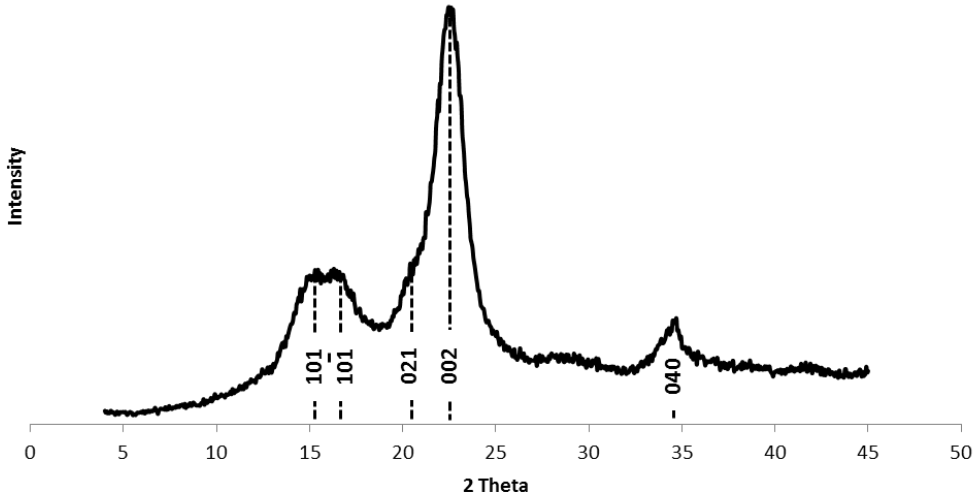

Figure 2.6 X ray diffraction spectra of type I microcrystalline cellulose showing Miller indices.

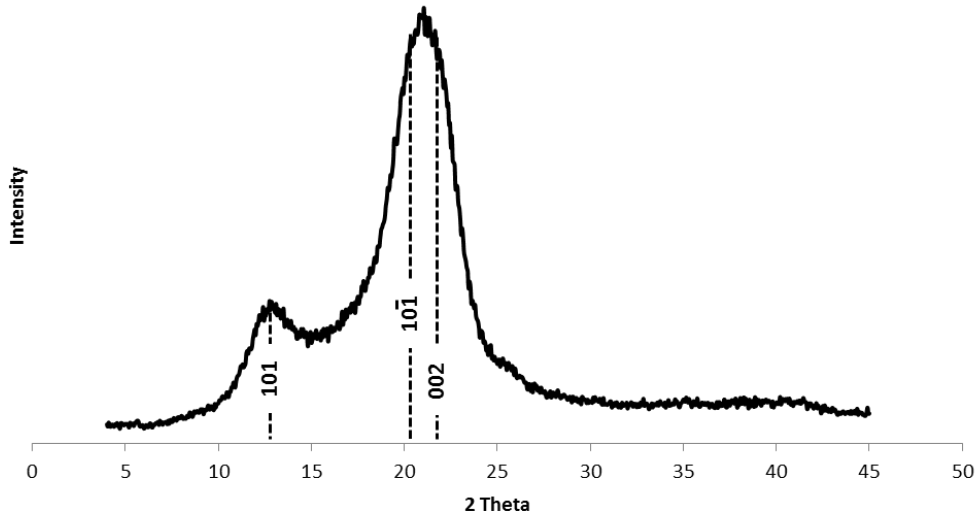

Figure 2.7 X ray diffraction spectra of type II regenerated cellulose (Lyocell) showing Miller indices.

2.3 Thermogravimetric Analysis (TGA)

Thermogravimetric analysis is a quick method to determine moisture content and degradation temperature of a sample. A sample is loaded onto a very sensitive balance with a robotic arm (Figure 2.8). The sample is then heated up at a constant rate in a furnace in either an inert atmosphere (nitrogen) or an oxidising atmosphere (oxygen and nitrogen). The weight of the sample will decrease as the temperature rises, first through moisture loss, and then vaporisation due to decomposition.

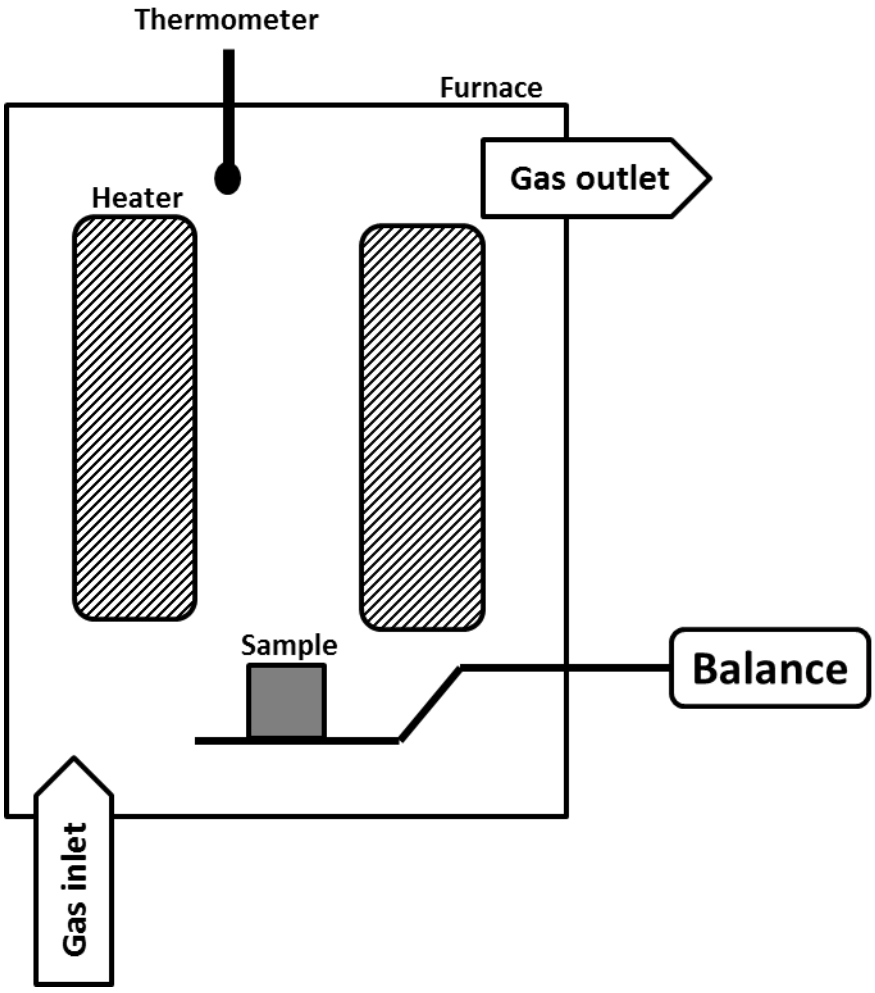

Figure 2.8 A simplified diagram of a thermogravimetric analysis system.

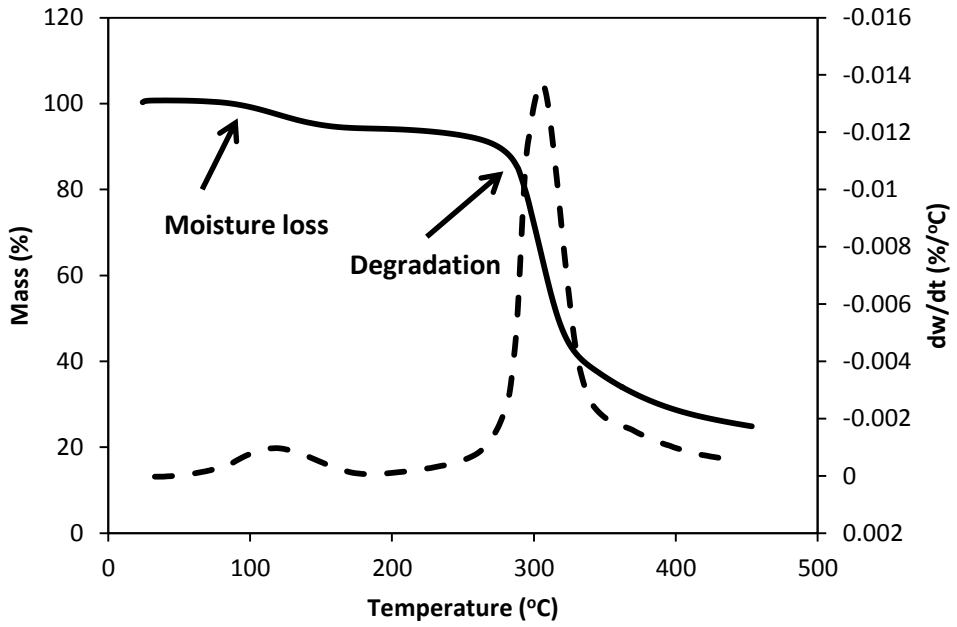

Figure 2.9 Thermogravimetric analysis (solid line) and differential thermal analysis (dotted line) plots of microcrystalline cellulose showing where moisture loss and degradation occur.

TGA results provide the mass over the temperature range. Often the differential thermal analysis (DTA) of the raw data provides a clearer picture (Figure 2.9).

2.4 Dynamic Vapour Sorption (DVS)

DVS measures how quickly a solvent (often water) can be absorbed by a sample. A reference and a sample holder are attached to a very sensitive microbalance (Figure 2.10). These are initially dried in pure nitrogen. When the weight has stabilised the relative humidity (RH) is raised in steps of 10%. When the weight has stabilised the RH will be raised another step up to 95% RH and then back to 0%. Samples are considered equilibrated when the change in mass per unit time is less than 0.0005 mg min^{-1} or the equilibration time has reached 1500 min.

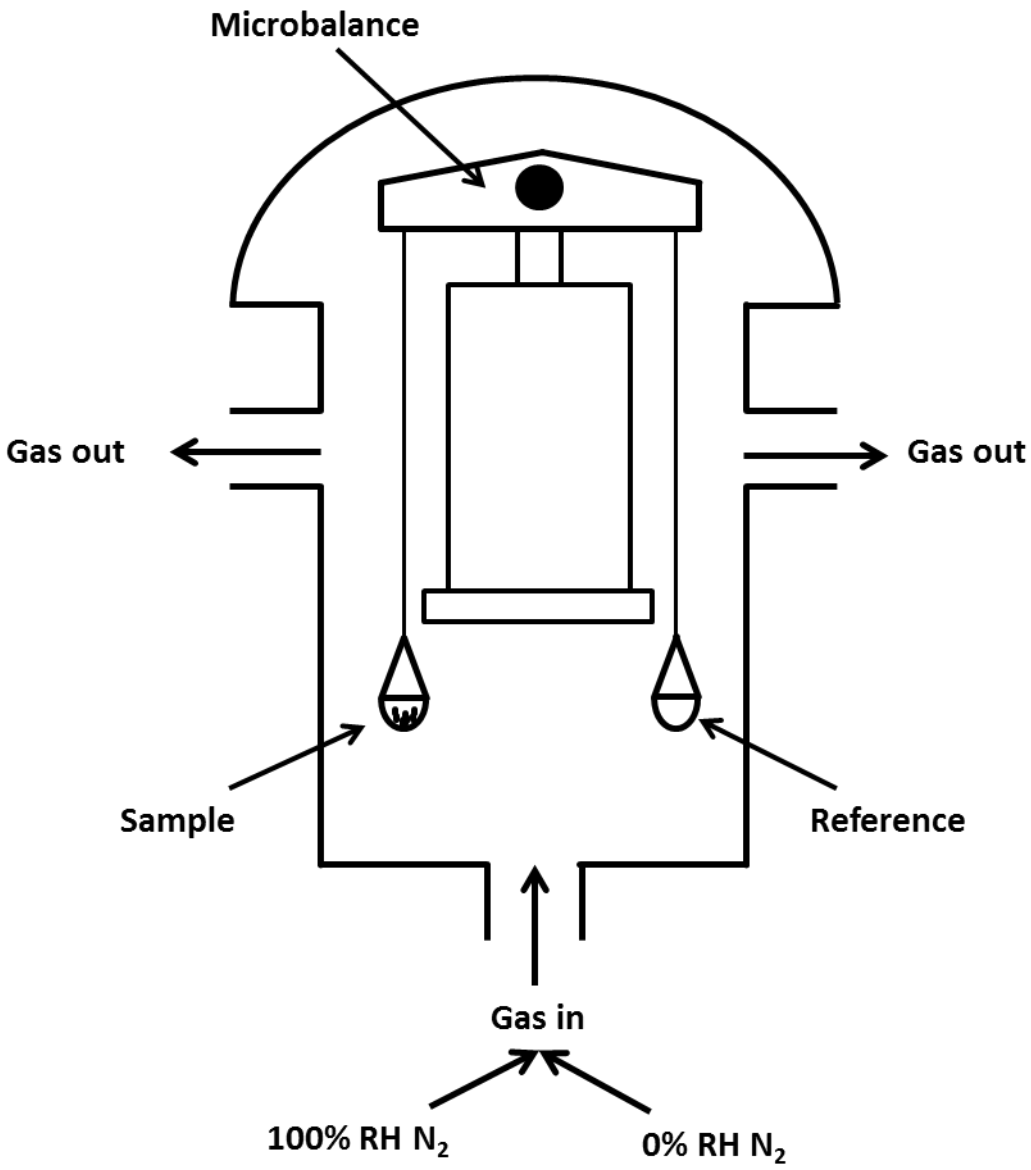

Figure 2.10 A Simplified diagram of a dynamic vapour sorption system.

2.5 Differential Scanning Calorimetry (DSC)

DSC measures the heat required to increase the temperature of a reference and a sample. Any differences between the heat required for the reference and sample will indicate some sort of physical transition, such as a glass transition. The event will be either exothermic or endothermic. When the temperature of some amorphous materials is raised the polymer molecules will gain sufficient translational and torsional energy to reorganise into a crystalline structure which is a lower entropic

state and therefore energy will be released which can be seen on the DSC as an exothermic transition. Due to the small sample size some transitions cannot be seen with traditional DSC. One option is Micro DSC which has a much larger sample volume of 0.8g and can be run at much slower rates. A second option is Flash DSC, in which a very small amount of the sample is loaded onto a chip with a heating element. The sample is then heated and cooled at an incredibly fast rate (10,000^{o}C/s). This then enables the sample to be heated above its degradation temperature and cooled down before it is able to degrade. Flash DSC is therefore much more sensitive than standard DSC.

2.6 Rheology

Rheology is the study of the flow and deformation of materials under applied forces. Viscosity is the resistance of a fluid to flow and is often measured using a rotational rheometer. One of the most commonly used geometries for a rotational rheometer is the cone and plate (Figure 2.11a) which is often referred to by its diameter and the angle of the cone however it is important that the gap size (the distance between the base plate and the cone) is correctly positioned. For this reason, systems containing particulate material must be measured using a parallel plate geometry (Figure 2.11b) which allows for a bigger gap size. The gap size must be about ten times the mean particle diameter. However, due to the larger gap size the parallel plate geometry is not as sensitive as the cone and plate as the shear rate produced varies across the sample (although software normally takes this into account) and there may be a temperature gradient across the sample. For samples of lower viscosity, a double gap geometry (Figure 2.11c) can be used which has a much greater sensitivity due to its large surface area, however much larger sample volumes are required.

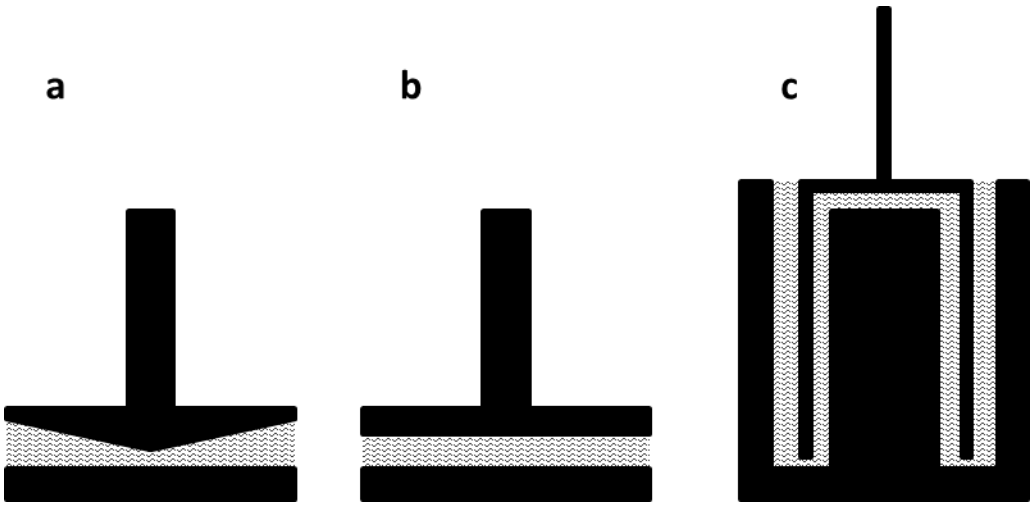

Figure 2.11 Different types of rheometer geometries; (a) cone and plate (b) parallel plate and (c) double gap.

2.7 Capillary viscometry

For liquids of very low viscosity a capillary viscometer can be used, the simplest version being an Ostwald (U-tube) viscometer (Figure 2.12). The viscometer is held vertically in a temperature controlled water bath and the bottom bulb is filled with the sample. The liquid is then drawn into the upper bulb and above the upper mark (Figure 2.12a). The liquid is then allowed to freely flow and the time is measured for the sample to flow from the upper to lower mark.

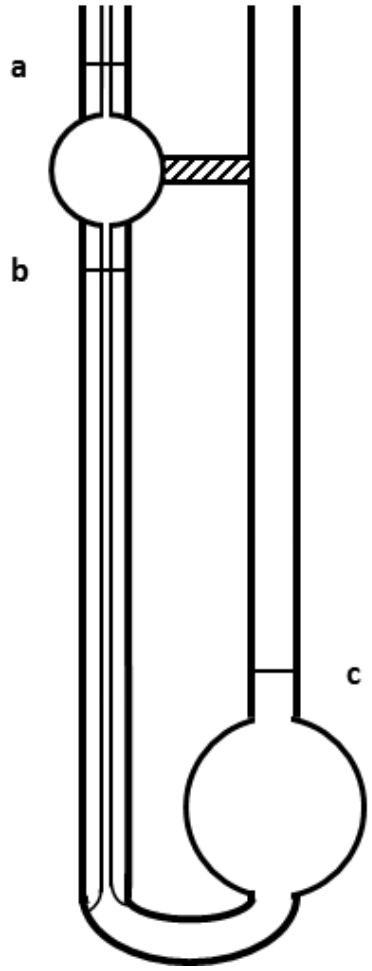

Figure 2.12 Diagram of an Ostwald U-tube viscometer where (a) is the upper mark (b) is the lower mark and (c) is the sample mark.

2.8 Rapid Visco Analyser (RVA)

The RVA is a useful tool to measure the viscosity of a system while under shear. It was originally developed for starch pasting analysis. Temperature and rpm can be controlled.

Chapter 3. Ball milled cellulose

3.1 Introduction

Ball milling is used extensively as a pre-treatment for biofuel production to enhance enzymatic hydrolysis of cellulosic and lignocellulosic material such as corn stover (Lin *et al.*, 2010), bleached pine pulp (Hu *et al.*, 2014), corncob (Luo *et al.*, 2013) and wheat straw (Silva *et al.*, 2012) as well as being used in combination with other pre-treatments such as microwave irradiation (Peng *et al.*, 2013), hot compressed water (Inoue *et al.*, 2008), non-thermal atmospheric plasma (Benoit *et al.*, 2012) and extrusion (Lee *et al.*, 2010). All of these studies have found that a decrease in the crystallinity increased the rate of enzymatic hydrolysis. Ball milling is also used to grind fibres such as flax to optimize the interaction between fibre and matrix in polymer composites (Csiszar and Fekete, 2011, Csiszar *et al.*, 2013, Ghozali and Haryono, 2013, Baheti and Militky, 2013, Huang *et al.*, 2012, Qua *et al.*, 2009). The physical stability of para-crystalline cellulose is also of importance in tableting pharmaceuticals (Bates *et al.*, 2006). It is therefore useful to have a better understanding of the structural changes caused by ball milling.

Ball milling cellulose leads to a decreased crystallinity, particle size and degree of polymerisation (DP), the levels of which depend on the speed (rpm) and milling time (Howsmon and Marchessault, 1959) as well as the material that the balls and cups are made of, such as either ceramic (zirconium oxide) or metal (aluminium). Cellulose crystallinity is caused by the large number of intermolecular hydrogen bonds in the β-1,4 linked glucose chains (Nishiyama *et al.*, 2002, Delmer and Amor, 1995, Matsuda *et al.*, 1992). In the presence of water, amorphous cellulose can recrystallise. Iyer *et al*., (1984) have shown that for amorphous cellulose to recrystallise back to cellulose I, the presence of the type I nuclei is required (to act as seed crystals), or it will recrystallise to the more thermodynamically stable type II cellulose (antiparallel packing) if the amorphous content is above 75%. Heat has also been found to

increase cellulose crystallinity (Bhuiyan *et al.*, 2000). Abbaszadeh *et al*., (2014) found that after ball milling, type I cellulose that had been newly recrystallised gradually converted to type II at a relative humidity (RH) of 97% and ambient temperature over 7 days.

Avolio *et al*., (2012) performed a comprehensive analysis on the effect of ball milling cellulose fibres for up to 60 minutes. A combination of wide angle X-ray diffraction (WAXD), solid state ^{13}C NMR and attenuated total reflectance Fourier transform infrared spectroscopy (ATR FTIR) showed that the crystal structure was completely destroyed after 60 minutes. Thermogravimetric analysis (TGA) analysis also revealed that the amount of absorbed water increased with higher milling time due to the increase in the amorphous fraction which is more accessible to water molecules than the crystalline fraction. They also showed that the fibre structure was completely lost after 60 minutes. Using sorption calorimetry Kocherbitov *et al*., (2008) showed that at an RH of above 90% amorphous cellulose will recrystallise which leads to a loss of adsorbed water.

A glass transition is the reversible transition that amorphous and semi-crystalline materials go through from a hard/ brittle (glassy) state to a rubbery (elastic) state. The glass transition temperature (T_g) of polymers is the temperature below which the physical properties of amorphous materials are similar to those of a solid, and above which amorphous materials have liquid characteristics (Paes *et al.*, 2010). The T_g of biopolymers is known to decrease with the absorption of water (Szczesniak *et al.*, 2008) but is difficult to measure for cellulose due to the main relaxation being close to the degradation temperature as well as the small change in heat capacity although the T_g has been reported as 221^{o}C (Batzer and Kreibich, 1981) and 235^{o}C (Salmen and Back, 1980). Vittadine *et al.,* (2001) were unable to find a glass transition

temperature for cellulose with a moisture range of 0-19 wt% (dry basis) using differential scanning calorimetry (DSC). Paes *et al*., (2010) investigated the glass transition of ball milled cellulose using dynamic mechanical thermal analysis (DMTA) which showed an underlying glass transition between 47-107^{o}C which was dependant on water content and a second transition at around 117^{o}C which was only weakly water dependant (which may have been due to evaporation at high temperature and low scan rate). By using differential thermal analysis (DTA), Ciolacu and Popa (2006) found that a reduction in cellulose crystallinity lead to a reduced thermal stability. Nada and Hassan (2000) found bleached viscose pulp has an initial decomposition temperature of 266^{o}C and a charring temperature of 315^{o}C. Huang (2012) have shown that the temperature at the maximum rate of degradation for microcrystalline cellulose (MCC) (viscosity average DP=235) is 344.6^{o}C.

Alternative fast heating methods have been used to identify thermal changes in cellulose. A glass transition temperature of about 210^{o}C was reported by Back *et al*., (1967) using ultrasonic pulse velocity measurements. Although the heating times were very short (2.5 to 3 seconds) there was some auto-crosslinking at 240^{o}C which was followed by thermal hardening between 240-300^{o}C.

Due to the large number of hydrogen bonds within the cellulose structure, the level of thermal energy required to break a sufficient number in order to melt cellulose is higher than the temperature at which intramolecular bonds are broken, resulting in degradation and incineration (Calahorra *et al.*, 1989). Nordin *et al*., (1973) first theorised the possibility of melting cellulose by rapid heating and cooling so as to avoid significant degradation. They used a carbon dioxide laser beam to heat cellulose samples rapidly (within 0.1 ms to 500^{o}C) so that chemical reactions were kept to a minimum. The samples were then cooled immediately using liquid nitrogen.

The laser cut holes through the cellulose paper, but, surrounding the holes there were fibres that had developed bubbles with diameters of a few micrometres where the fibrillar structure of the cellulose had been lost. The authors suggested that in these areas the cellulose had melted. They also found there was a concomitant decrease in the crystallinity of the samples which they attributed to melting rather than degradation (Nordin *et al.*, 1974).

Boutin *et al*., (1999) used brief flashes of concentrated radiation at the focus of an image furnace and showed that short life time liquid intermediates were formed for flash durations lower than 1 second. These products were stable and soluble in water indicating the cellulose had been considerably degraded. They predicted that the reaction temperature was close to 467^{o}C. Later, Boutin *et al*., (2002) found that cellulose goes through an intermediate liquid phase followed by condensable vapours and char during thermal decomposition. In fast heating conditions levoglucosan and cellobiosan were minority components and 84% of the species had a weight average DP ranging from 3 to 7, measured using a mass spectrometer (Lede *et al.*, 2002, Lede and Boutin, 1999).

Dauenhauer *et al*., (2009) used high speed photography (1000 frames per second) to show that MCC passed through a liquid intermediate phase during pyrolysis when heated on a catalytic surface (700-800^{o}C) where vapours (volatile organic compounds) were seen and droplets were formed when in direct contact with the surface. After 176 ms the cellulose completely vaporised and no char was left on the surface.

While there are many papers that show some sort of cellulose liquid intermediary during pyrolysis there is much less evidence that there is in fact melting before degradation (Lede, 2012). The liquid intermediary is often soluble in water and has a

lower weight average DP than the initial cellulose. However, Schroeter and Felix (2005) did report some level of success. The energy level required to open intermolecular hydrogen bonds is reported to be above 20 kJ/mol (Fengel and Wegener, 1984) which is equivalent to $3.3x10^{-20}$ J per bond. Schroeter and Felix (2005) used an infrared laser with an equivalent photon energy (wavelength of 6 μm) to open the hydrogen bonds. The authors reported they had managed to plasticise cellulose as although there was no severe difference in the IR spectra of the treated and untreated samples (i.e. no chemical modification) there was a significant change in the structure from fibrous to a continuous solid as well as a change in the optical properties from opaque to transparent and from dull to glossy on the surface. A combination of uniaxial pressure, shear and laser radiation were necessary for this transformation. However, the authors were unable to perform structural analysis such as crystallinity due to the small amount of sample produced.

Whilst there have been a few studies on the effect of ball milling cellulose (Hu *et al.*, 2014, Wormald *et al.*, 1996, Kocherbitov *et al.*, 2008, Paes *et al.*, 2010, Hajji *et al.*, 2011, Abbaszadeh *et al.*, 2014), thus far there have been none which directly compare two different celluloses or the use of flash DSC.

3.2 Materials and methods

3.2.1 Materials

The celluloses used in this work are cellulose fibre (CF) (Solka 900FCC, International Fibre Corporation, USA) and Avicel MCC type PH-101 Ph Eur (Sigma Aldrich, UK).

Maltose monohydrate was purchased from Sigma Aldrich.

3.2.2 Ball milling

The celluloses were milled using a Planetary Micro Mill Pulverisette 7 (Fritsch GmbH, Germany) at 600 rpm with 10 minutes milling followed by a 10 minute pause to allow heat to dissipate. Each zirconium oxide pot was filled with 0.5g of cellulose and contained six zirconium oxide balls (10 mm Ø). This is the same speed used by Paes *et al.* (2010) but with more frequent pauses (every 10 minutes rather than 30 minutes) as the pots were found to heat up significantly after 10 minutes. All samples had 3 replicates.

3.2.3 Rehydration of ball milled cellulose

Samples were rehydrated by dispersing the celluloses in excess water (50 ml per 1g of cellulose) and storing for 24 hours at 4^{o}C. The samples were then filtered using Whatman filter paper and dried in an oven overnight at 60^{o}C.

3.2.4 Light microscopy

Samples were mounted on a glass slide and images were taken using a Leitz Diaplan microscope (Leica, Heidelberg, Germany) and a Pixelink PL-A600 (Ottawa, Canada) recording camera at magnifications of 20X and 50X.

3.2.5 Scanning electron microscopy (SEM)

Samples were mounted on aluminium stubs and coated with gold to about 25nm thickness using a sputter coater (Leica EM SCD005 Sputter Coater – Ion). Images were taken using a Quanta 200 (FEI, USA) and captured using the automatic software system at different magnifications.

3.2.6 Wide angle X-ray diffraction

Plastic holders were filled with randomly orientated powders. Some samples had to be ground with a pestle and mortar before use to give a free flowing and compactable powder. X-Ray measurements were carried out using a Bruker D5005

diffractometer (Bruker AXS, UK) using copper K alpha (CuKα) radiation of wavelength 1.5418 Å. Slit focus geometry was used. Total acquisition time for each sample was 40 minutes.

To determine crystallinity, a linear background was first applied over the main diffraction features (5 – 35 2θ). The diffraction peaks were then simulated as a series of pure Gaussian functions, for example at the 110, 110, 021 and 200 crystallographic planes for cellulose I and at the 110, 110 and 020 planes for cellulose II. For the amorphous component one broad Gaussian curve was used (Ozturk *et al.*, 2010). Slight variations in position were due to small errors in the height of samples. To estimate the crystallinity, data manipulation was carried out using intensity vs 2θ data in the Microsoft Excel software package with the Solver add in.

3.2.7 ^{13}C Cross Polarization Magic Angle Spinning Nuclear Magnetic Resonance (CPMAS NMR)

^{13}C CPMAS NMR spectra were recorded on a Bruker (Karlsruhe Germany) AVANCE 600 NMR Spectrometer with narrow bore magnet and 4mm triple resonance probe. The parameters used in CPMAS experiments were as follows. The Proton 90^{o} pulse length was 3 µs. Field strength of the proton and spin locking fields during the contact period was 83 kHz. Samples were packed into 4 mm rotors and spun at 10 kHz. ppm scales were referenced to the high field peak of adamantane (29.5 ppm) run as an external standard under identical conditions to the samples.

Proton decoupling was provided by a Spinal64 sequence and the proton power levels during the contact time and decoupling stage could be varied independently to provide optimum signal to noise levels. The highest intensity signal for all types of bonded carbons in these carbohydrate materials lay between a contact time of 1 and 2 milliseconds hence for all CPMAS experiments a value of 2 milliseconds was used.

3.2.8 Dynamic vapour sorption (DVS)

A dynamic vapour sorption analyser (Surface Measurement Systems Ltd, London, UK) equipped with a Cahn D200 microbalance was used to measure the water sorption isotherms of the cellulose samples. The experiments were carried out at a temperature of 25^{o}C and relative humidities from 0 to 95%. The initial weight of the samples was approximately 20 mg. Samples were pre-dried in the DVS by passing dry air over the powder until equilibration. The dry samples were subsequently hydrated in RH steps of 10%. Samples were considered equilibrated when the change in mass per unit time was less than 0.0005 mg min^{-1} or the equilibration time had reached 1500 min.

3.2.9 Capillary viscometry measurements

Samples were dried overnight at 105^{o}C. 10mg of the dried samples were dispersed with a few pieces of copper wire in a plastic bottle with 5ml of distilled water. The cellulose suspension was then dissolved by adding 5ml of 1M Copper (II) ethylenediamine (CED) solution and placing on a roller bed for 2 hours (ISO, 2009).

Viscosity measurements were carried out with a U-tube viscometer in an accurate temperature regulated water bath. The temperature was kept constant at 25^{o}C throughout. 2ml of each solution was injected into the viscometer and the flow time (t) determined using an automatic timer.

The relative, (η_{rel}), and specific (η_{sp}) viscosities were calculated from the following equations:

$$\frac{\eta}{\eta_0} = \frac{t}{t_0} = \eta_{rel} \tag{3.1}$$

The specific viscosity (η_{sp}) can therefore be determined:

$$\eta_{sp} = \eta_{rel} - 1 \tag{3.2}$$

The intrinsic viscosity can then be calculated using the Solomon – Ciuta equation (Solomon and Ciută, 1962):

$$[\eta] = \frac{1}{c}\sqrt{2\left(\eta_{sp} - \ln \eta_{rel}\right)} \tag{3.3}$$

The viscosity average degree of polymerisation (DP) was then calculated using the Mark – Houwink – Kuhn – Sakurada (MHKS) equation (Evans and Wallis, 1989):

$$[\eta] = K.DP^{a} \tag{3.4}$$

Where K and a are the MHKS coefficients which are taken from the literature for the values of cellulose at 25°C in 0.5M CED (Table 3.1).

Table 3.1 Mark-Houwink coefficients for Eq. (4)

K (cm^3/g)	a	Source
1.37	0.905	Immergut and Eirich (1953)
0.42	1	Marxfigini (1978)
2.28	0.76	Gruber and Gruber (1981)
0.91	0.85	Evans and Wallis (1989)
1.87	0.771	Lojewski *et al.*, (2010)

3.2.10 Thermogravimetric analyser (TGA)

A steel pan loaded with 5 mg of sample was placed inside a TGA 851e thermogravimetric analyser (Mettler Toledo, Switzerland) where the weight of the sample was constantly measured. The samples were heated from ambient to 450°C at a rate of 10°C min^{-1} in a nitrogen atmosphere.

3.2.11 Differential scanning calorimetry (DSC)

Thermal transitions were monitored using a heat flux DSC 823e (Mettler Toledo, UK) with auto sampler and liquid cooling attachment. Samples were placed in gold pans, sealed and run from -80 to 300^{o}C at scan rates of 10^{o}C min^{-1}.

3.2.12 Flash DSC

A very small amount of sample was placed on the chip sensor of a Flash DSC 1 (Mettler Toledo, UK) which had first been conditioned and calibrated using the provided software. Maltose was cured at 100^{o}C for different times and heated and cooled at 200^{o}C s^{-1}. Cellulose samples were heated five times from 25-460^{o}C at 500^{o}C s^{-1} with a cooling rate of 200^{o}C s^{-1}.

3.2.13 Hot press

23g of dry cellulose powder was loaded into a rectangular mould. The mould was then heated for 15 minutes at 200^{o}C and compressed using a Daniels 160 Ton down stroke press at 90 bar. The mould was then transferred to a Macey Bowley 100 ton upstroke press to cool at 90 bar. The compressed cellulose was then carefully pushed out of the mould.

3.3 Results and Discussion

Two types of cellulose were used in this work, cellulose fibre (CF) which is sourced from wood and microcrystalline cellulose (MCC) which (also from wood) is produced by acid hydrolysis, which removes the majority of amorphous regions, due to their lower density (Dufresne, 2012), resulting in high crystallinity and a reduced particle size. CF has a much larger aspect ratio (length to width ratio) than MCC as seen in Figure 3.1. The celluloses were ball milled for between 2 to 610 minutes. Within the first 10 minutes the fibrous structure is completely destroyed (Figure 3.1) and the particles appear to aggregate together (Figure 3.2). This occurs much earlier than was

reported by Avolio *et al.* (2012), although they do not state at what speed they ball milled their samples, suggesting that their work was at a much lower energy.

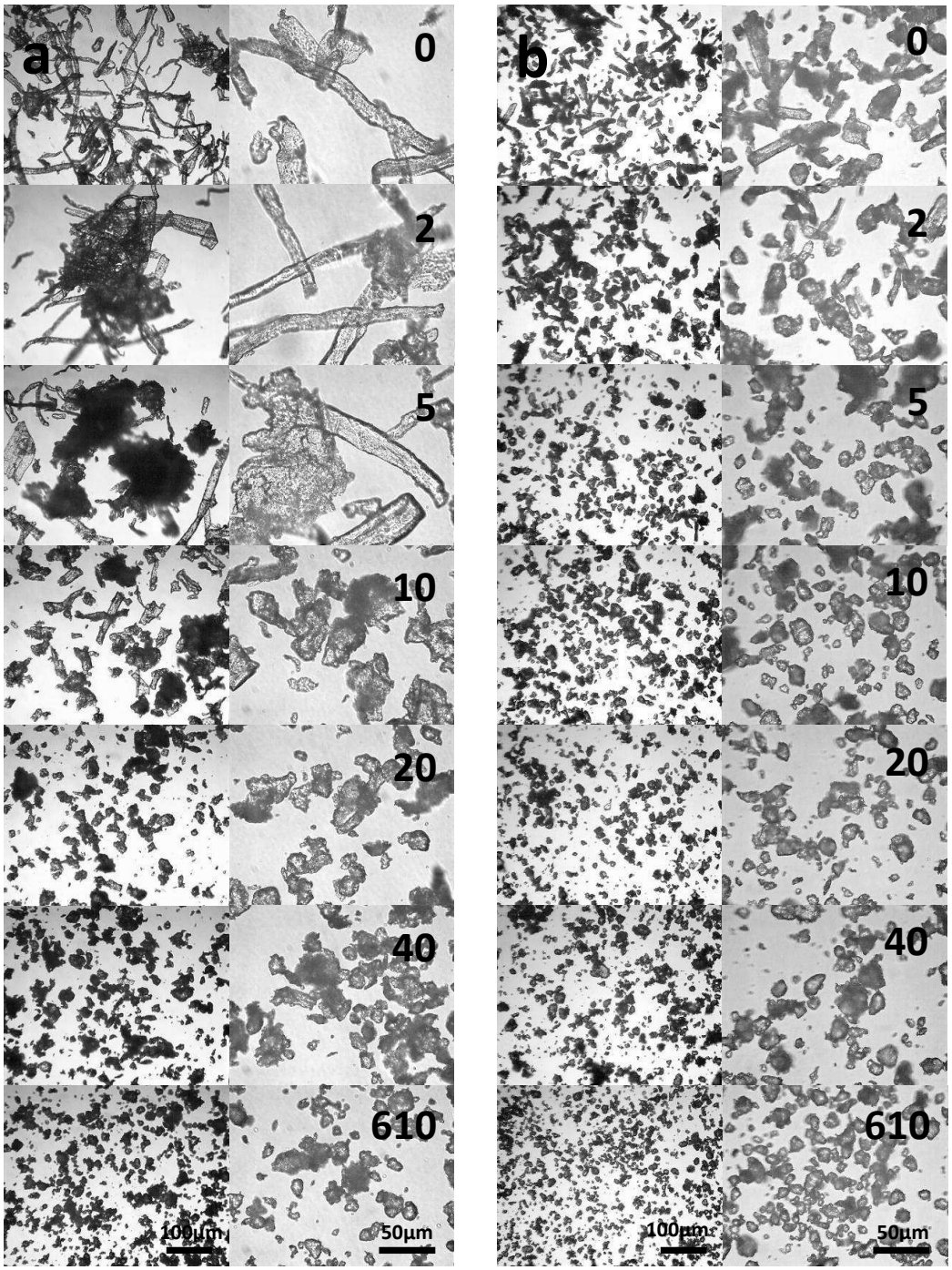

Figure 3.1 Light micrographs of (a) CF and (b) MCC at different ball milling times (minutes). Scale bars are 100 µm (left column) and 50 µm (right column).

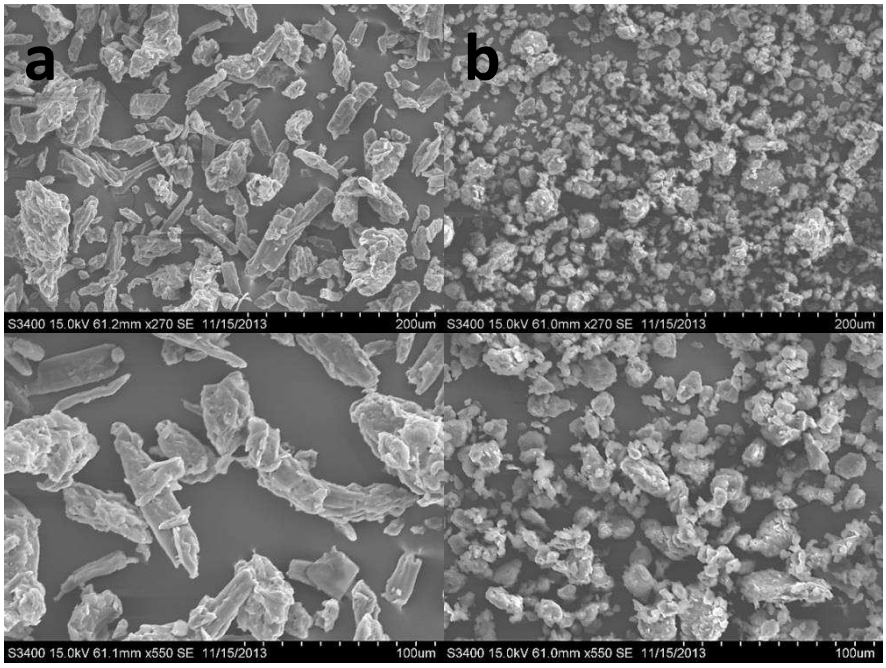

Figure 3.2 SEM micrographs of (a) MCC and (b) MCC ball milled for 610 minutes. Scale bars are shown on the bottom right corner of each micrograph.

Capillary viscometry is a useful way of determining the viscosity average degree of polymerisation (DP). Cellulose is dissolved in copper (II) ethylenediamine (CED) solution and the intrinsic viscosity can then be calculated. However, to calculate the DP, Mark-Houwink coefficients must be used of which there are several different values in the literature. Table 3.2 shows the viscosity average DP of MCC calculated using the Mark-Houwink coefficients from different literature sources (from herein all DPs refer to viscosity average DP). The value of the DP for MCC in the product specification is 350. Lojewski *et al.* (2010) provide the closest value with a DP of 370, therefore, these coefficients are used for the rest of this chapter to determine sample DP.

Table 3.2 Viscosity average DP of MCC calculated using different K and a values; the average of three repeats.

Source	Viscosity average degree of polymerisation
Evans and Wallis (1989)	498
Marxfigini (1978)	424
Lojewski *et al*. (2010)	370
Gruber and Gruber (1981)	311
Immergut and Eirich (1953)	217

Ball milling has previously been shown to decrease DP (Hu *et al.*, 2014, Csiszar and Fekete, 2011). The DP of CF reduced rapidly with ball milling, with the rate of DP loss reducing after 250 minutes (Figure 3.3). MCC has a much smaller starting DP of 370, which is in agreement with the product specifications but after 250 minutes the DP plateaus at 190. With 610 minutes of ball milling CF reached a DP of 247 with the slope of the curve indicating it would also plateau at a similar DP to MCC with longer ball milling time. It is possible that this is the lowest limit to which this method is able to determine DP and in fact the DP continues to fall (Domvoglou *et al.*, 2010) or that this is the value reached due to the ball milling energy constraints. With much longer ball milling times sharp peaks have been shown in WAXD spectra which may indicate the cellulose structure has been largely destroyed leaving only small glucose oligomers (Hajji, 2014).

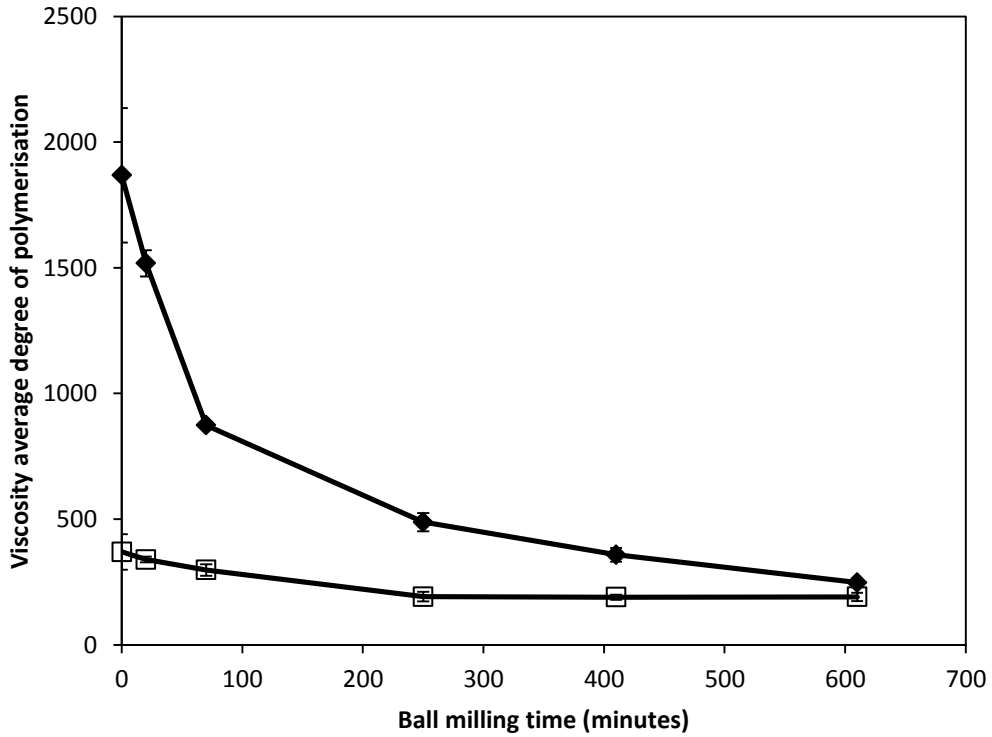

Figure 3.3 Viscosity average degree of polymerisation of CF (diamonds) and MCC (squares) at different ball milling times.

A commonly used method of determining cellulose crystallinity is to use X-ray diffraction (XRD). There are multiple ways of quantifying the data, which can lead to large differences in stated literature values for the same cellulose. Table 3.3 shows this disparity for lyocell (a commercially produced cellulose made by dissolving pulp in N-Methylmorpholine N-oxide (NMMO) and regenerating in water) using different methods to calculate crystallinity. Following the procedure used by Ozturk *et al.* (2010), a multi-peak deconvolution method has been used in this work to estimate the amount of type I and II crystallinity (c.f. Figures 2.6 and 2.7). Figure 3.4 shows an example of the multi-peak deconvolution method which has been used to determine all of the crystallinities of the cellulose samples shown in Figures 3.5-3.8. The results of the multi-peak deconvolution are shown in Figure 3.9 with the averages of three replicates for each sample.

Table 3.3 Selected literature values for regenerated cellulose (lyocell) crystallinity using different methods to calculate cellulose crystallinity.

Method	**Crystallinity (%)**	**Source**
WAXD Amorphous Subtraction	70	Smole *et al.* (2003)
WAXD Peak height	62	Cheng *et al.* (2006)
WAXD Peak deconvolution	50.5	Ozturk *et al.* (2010)
WAXD Peak height	44	Kreze *et al.* (2002)

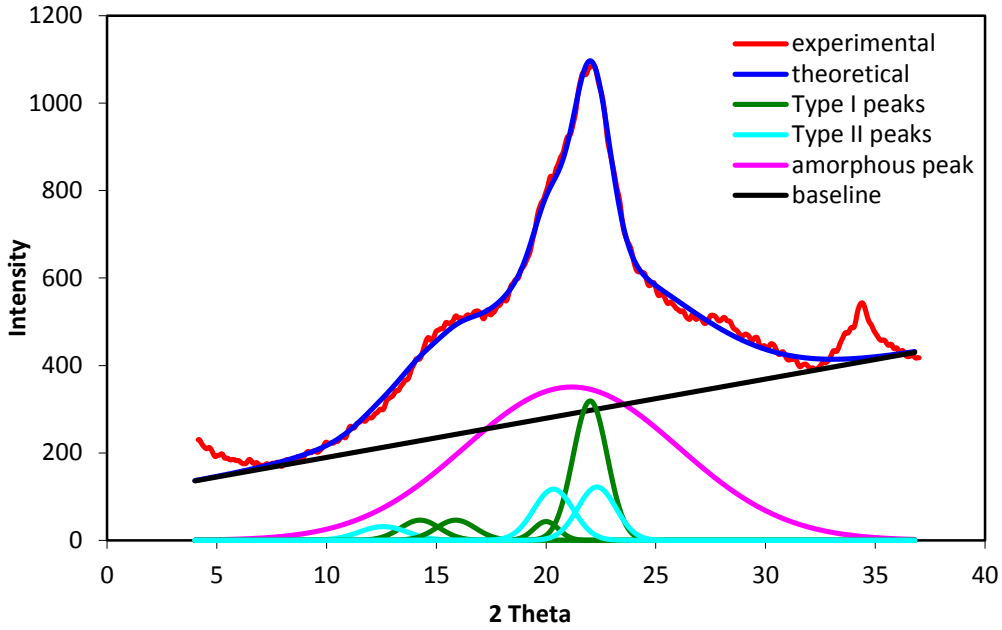

Figure 3.4 The wide angle X-ray diffraction pattern of MCC ball milled for 20 minutes and subsequently rehydrated, showing the Gaussian peaks used to fit the cellulose type I and II cellulose peaks. The percentages of crystallinity based purely on area for type I and II were 15.4 and 10.6 respectively.

The loss in crystallinity due to ball milling is shown in the XRD spectra of CF (Figure 3.5). After the ball milled CF has been rehydrated and subsequently dried it moves from a completely type I crystal structure (0 minutes) to a completely type II structure (610 minutes) (Figures 3.6 and 3.9). For intermediate milling time (5-70 minutes) there is a mixture of both type I and II. MCC shows a similar trend (Figures 3.7 and 3.8).

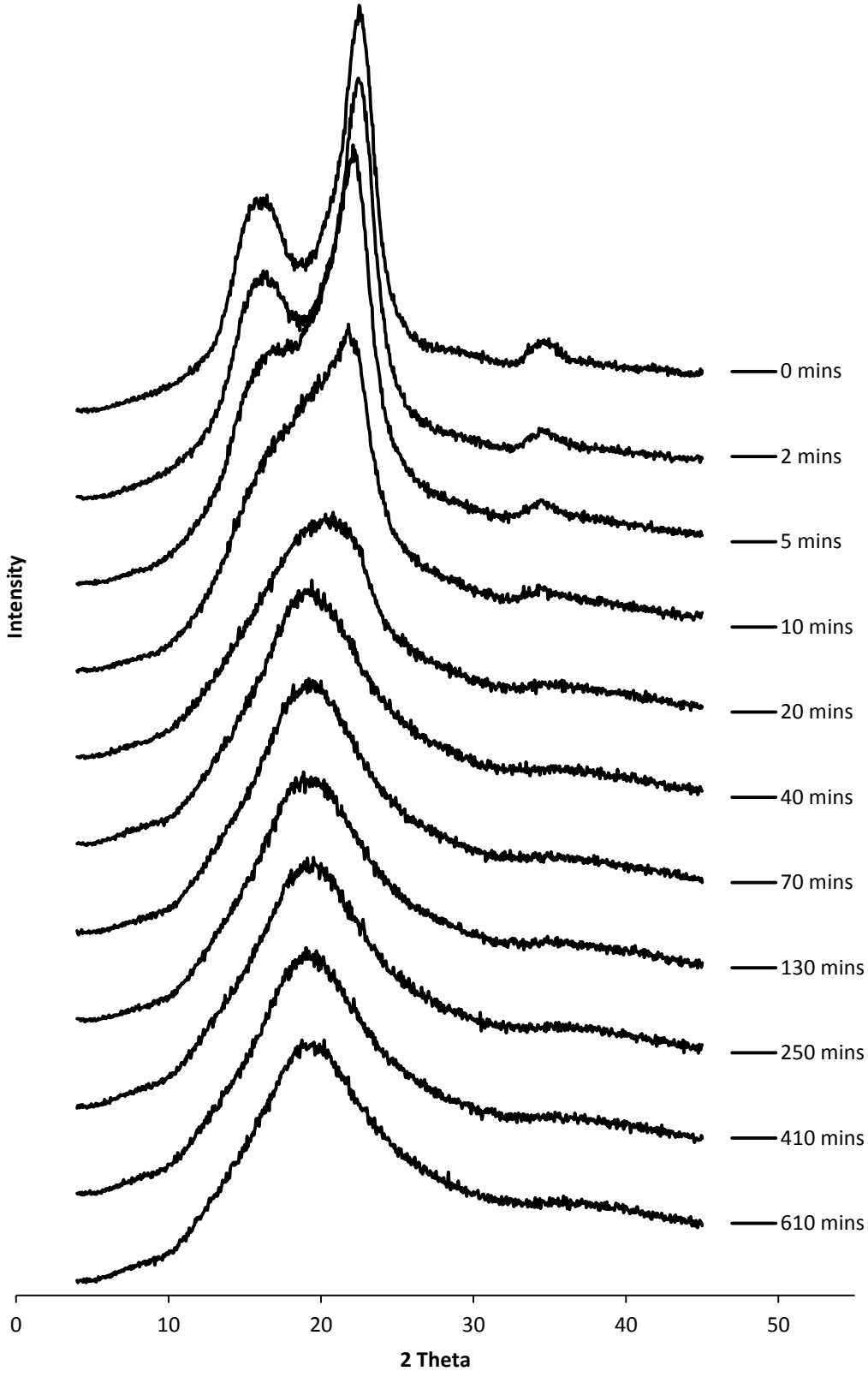

Figure 3.5 Wide angle X-ray diffraction spectra of CF which has been ball milled for different times (length of ball milling is shown to the right of each diffraction pattern).

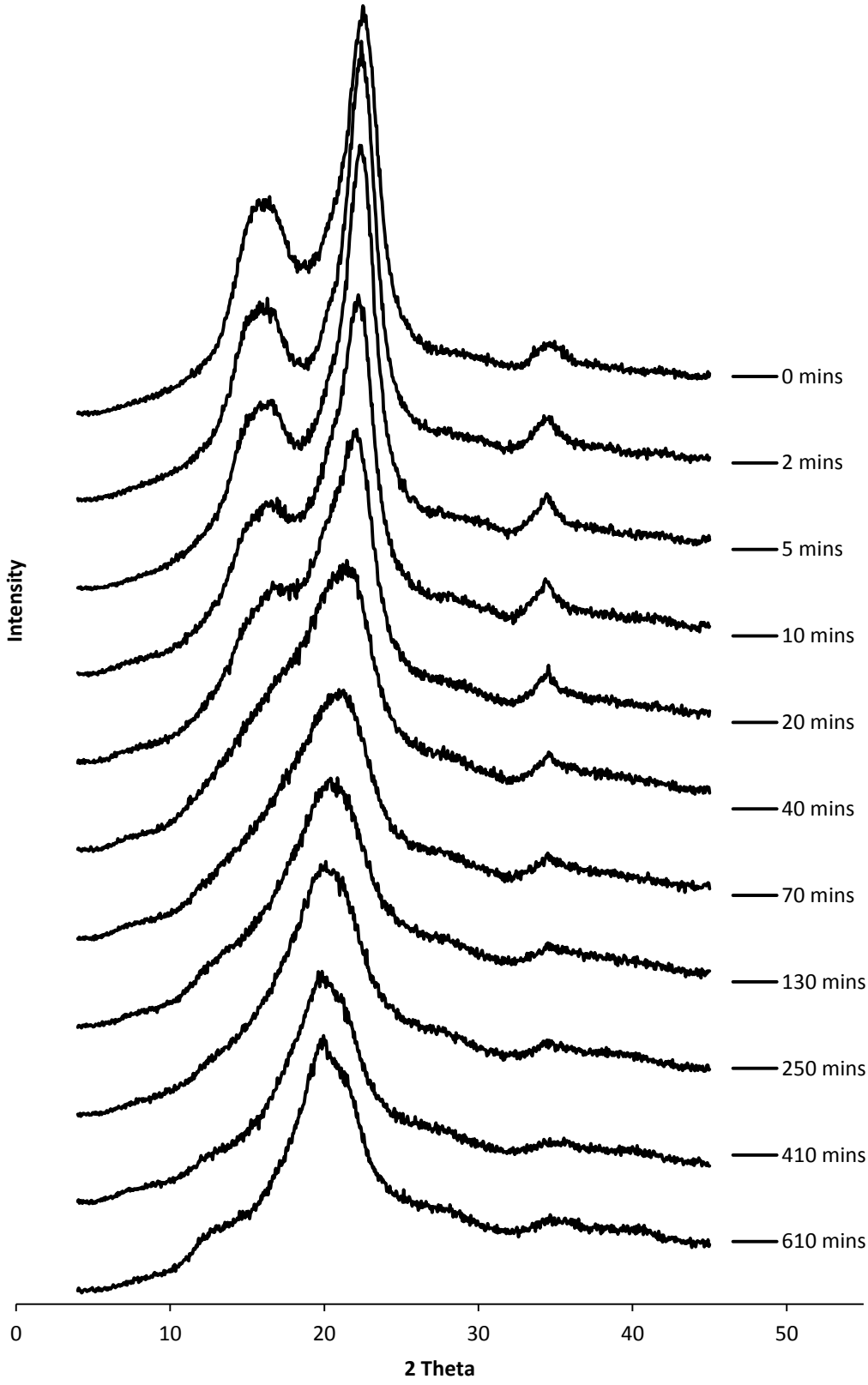

Figure 3.6 Wide angle X-ray diffraction spectra of CF which has been ball milled for different times (length of ball milling is shown to the right of each diffraction pattern), rehydrated in excess water and subsequently dried at 60°C for 24 hours.

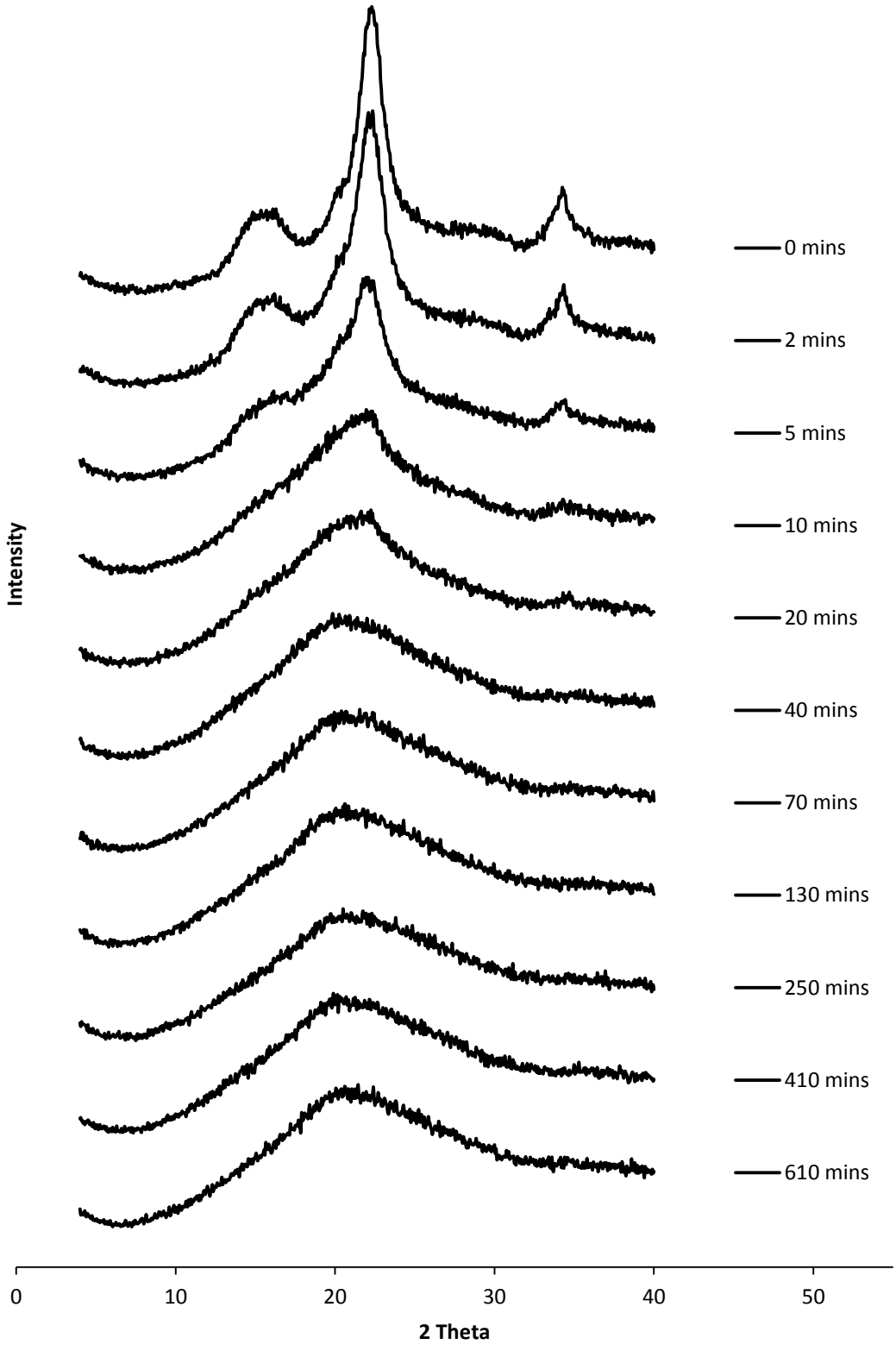

Figure 3.7 Wide angle X-ray diffraction spectra of MCC which has been ball milled for different times (length of ball milling is shown to the right of each diffraction pattern).

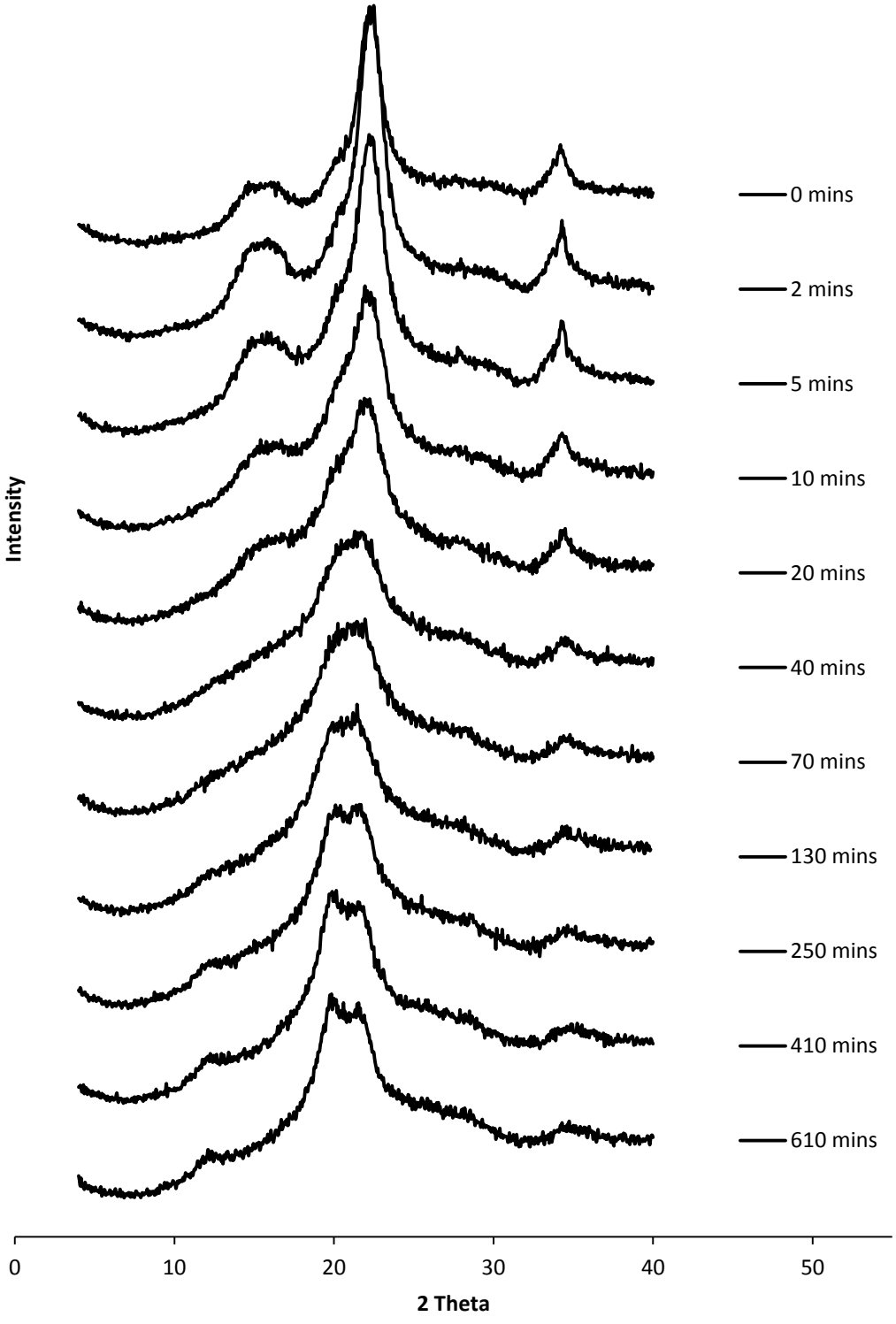

Figure 3.8 Wide angle X-ray diffraction spectra of MCC which has been ball milled for different times (length of ball milling is shown to the right of each diffraction pattern), rehydrated in excess water and subsequently dried at 60^{o}C for 24 hours.

Figure 3.9 shows the numerical values of the crystallinities for both celluloses. Time is plotted on a log scale as there are substantial changes at short milling times. From the XRD data, both celluloses are completely amorphous by 40 minutes of ball milling (Figure 3.9a).

When amorphous cellulose is rehydrated in excess water, the fibrils are able to realign and crystallise in the more thermodynamically stable type II lattice structure (Kocherbitov *et al.*, 2008) (Figure 3.9b). In this work, for samples which have been ball milled up to 70 minutes, both CF and MCC partially recrystallise back to type I, due to a seeding effect of the intact type I crystalline regions (Figures 3.9c and 3.9d). There must then be a small amount of intact type I crystallinity up to 70 minutes even though this level is too low for XRD to detect.

After 70 minutes of ball milling time the crystallinity of rehydrated MCC starts to increase whereas this only occurs for CF after 250 minutes. This may be due to an increased rate of recrystalisation due to the lower DP of MCC. β-glucans have been found to gel faster and produce gels with greater storage modulus (G') values as their molecular weight decrease (Brummer *et al.*, 2014). As seen in Figure 4.3 the DP of CF after 70 minutes is still much greater than that of MCC. After 610 minutes CF still has a lower crystallinity than MCC. This may be due to its slightly higher DP.

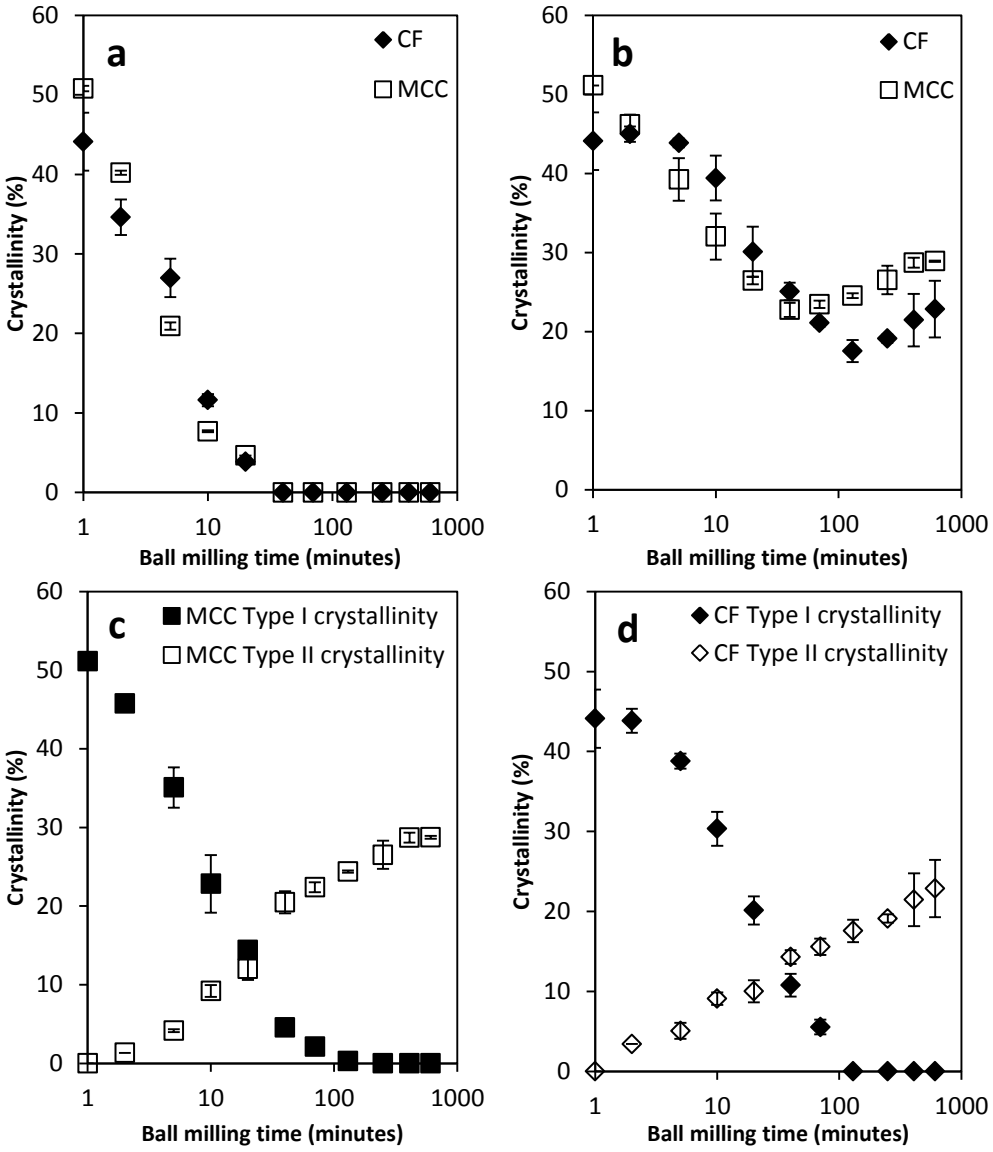

Figure 3.9 The percentage crystallinity of (a) dry ball milled cellulose (b) rehydrated cellulose (c) MCC type I and II and (d) CF type I and II. The crystallinities were calculated using the peak deconvolution method shown in Figure 3.4 which was applied to all the X-ray diffraction spectra, examples of which are shown in Figures 3.5-3.8. Results are the average of three replicates and the error bars show the standard deviation.

The loss of crystal structure is confirmed by NMR as the crystalline areas in the C-4 (88-92 ppm) and C-6 (64-68 ppm) regions are reduced whilst the amorphous areas increase (60-64 and 80-86 ppm) (Figures 3.10 and 3.11) (Park *et al.*, 2010, Ibbett *et al.*, 2007). A small peak at 97 ppm appears (arrow) with longer ball milling which Wormald *et al.* (1996) attributed to an increase in the number of reducing ends caused by depolymerisation. However, it can be seen in Figure 3.11 that this peak

decreases for the recrystallised sample, suggesting that it may not be due to an increase in the number of reducing ends.

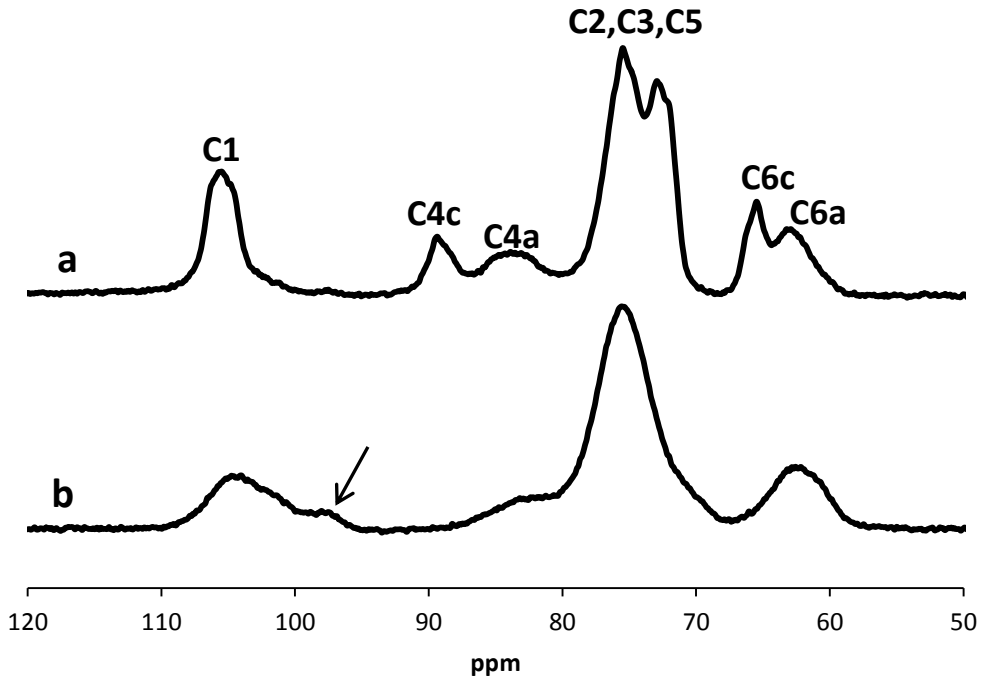

Figure 3.10 ^{13}C CPMAS NMR spectra of CF (a) before and (b) after ball milling for 610 minutes. The six carbons of glucose are shown as well as the crystalline, c; and amorphous, a; regions. Arrow indicates an amorphous peak at 97 ppm.

Dynamic vapour sorption (DVS) is a method used to assess solvent uptake of a sample, by measuring the change in weight of a sample against a reference. The sample is first dried in 0% relative humidity (RH) nitrogen. The RH is then increased in steps of 10% to 95% RH and then decreased in steps of 10% to 0% RH. The weight of the ball milled MCC increased steadily until 95% RH whereupon the weight decreased (Figure 3.12a). When the stepped increase and decrease in RH is repeated the results clearly show a reduced moisture (weight) uptake in the second cycle (Figure 3.12b). This is likely to be due to the recrystallisation of the cellulose during the first rehydration steps where water mobilises amorphous regions initiating recrystallisation, which subsequently is forced out by the closer packing of the crystalline areas (Kocherbitov *et al.*, 2008). Kocherbitov *et al.* (2008) found that the

enthalpy of hydration for MCC, amorphous and rehydrated cellulose is the same; 18 kJ/mol at zero water content. After the initial hydration, there is no weight loss at 95% RH on the second run as the cellulose becomes recrystallised to the extent determined by the relative rates and levels of rehydration used in the experiment. The level of recrystallisation may then be different to that achieved in the excess water experiments.

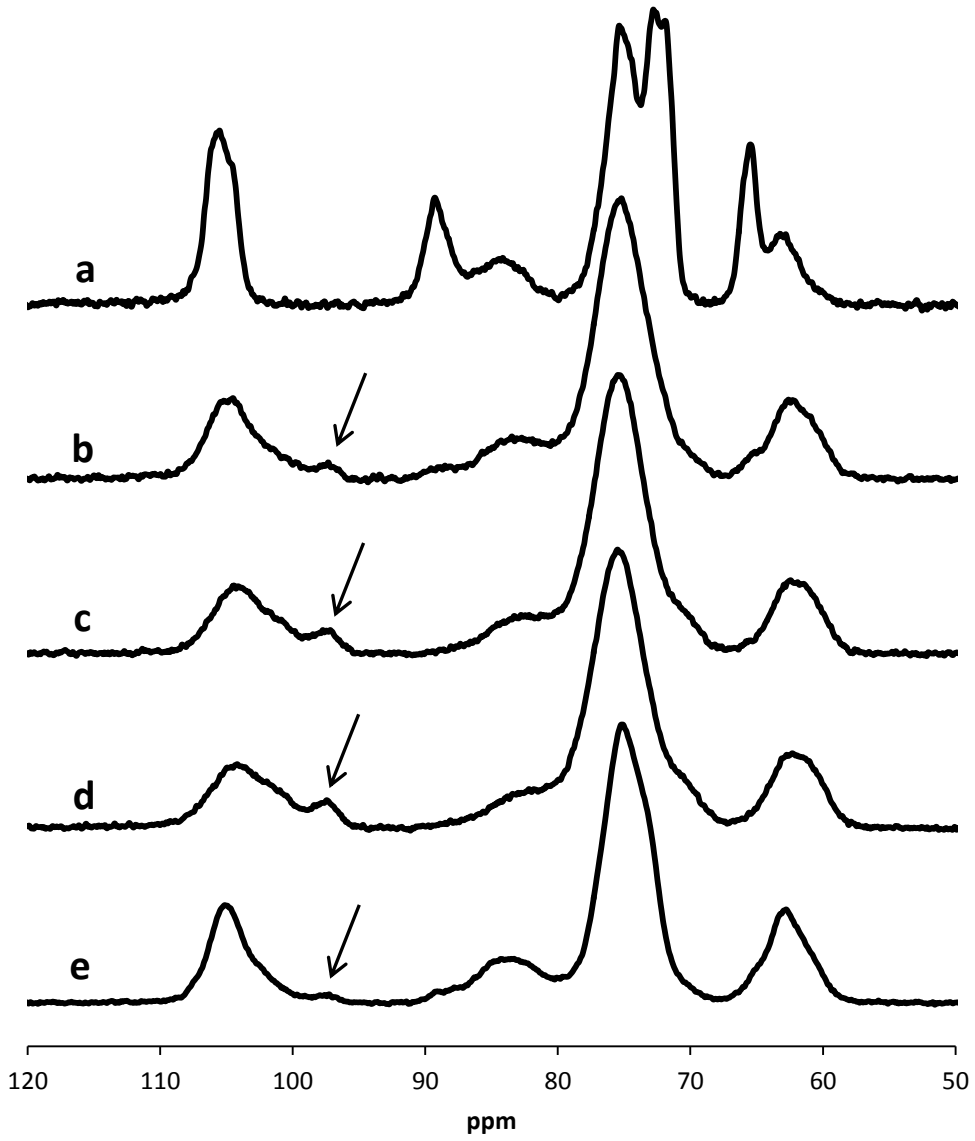

Figure 3.11 ^{13}C CPMAS NMR spectra of MCC with (a) 0 minutes (b) 20 minutes (c) 130 minutes (d) 610 minutes ball milling and (e) rehydrated after 610 minutes ball milling. Arrows indicates an amorphous peak at 97 ppm.

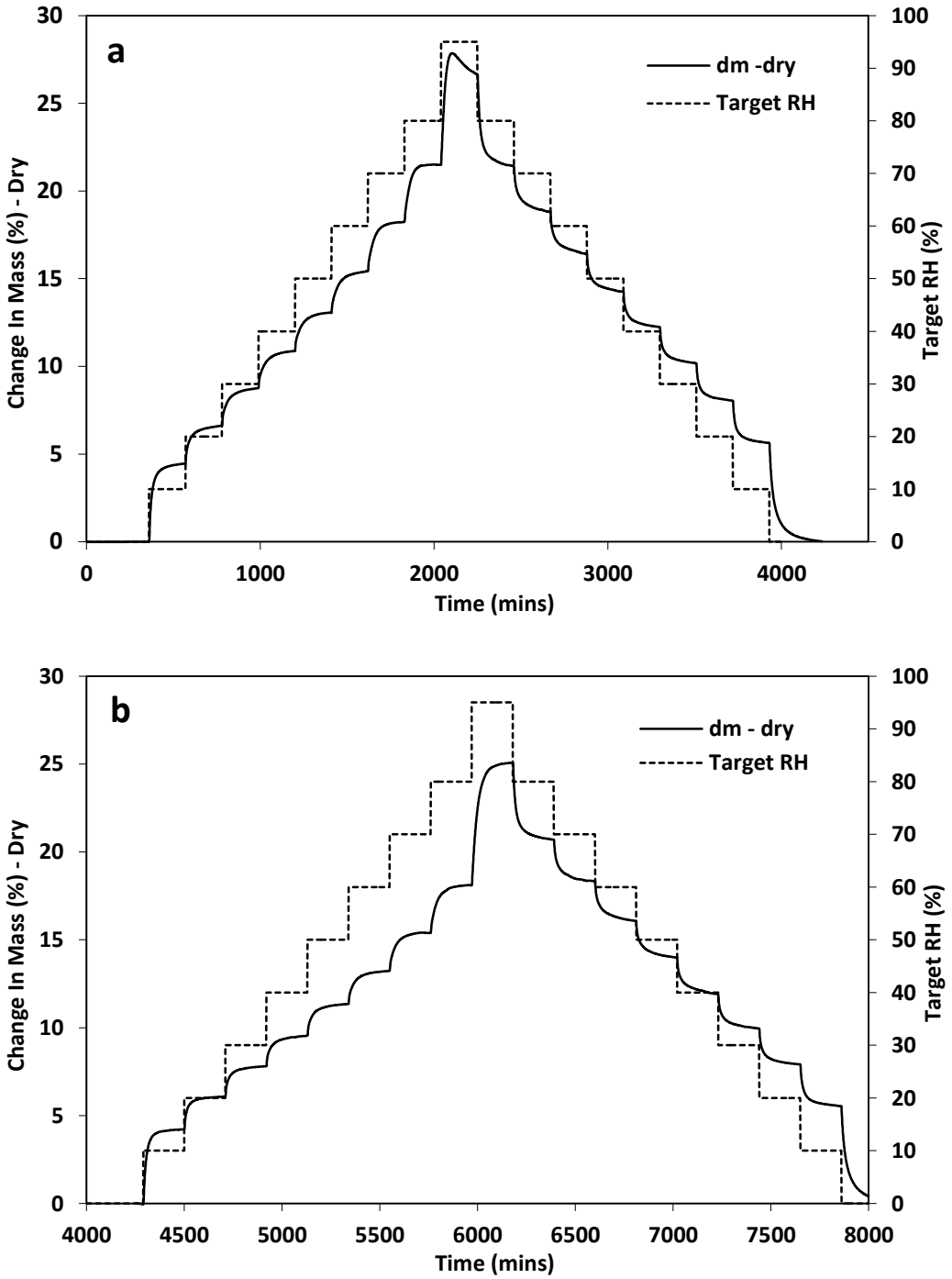

Figure 3.12 DVS water sorption and desorption cycle of CF ball milled for 610 minutes (a) first cycle (b) second cycle at 25°C with steps of 5% relative humidity.

Thermogravimetric analysis (TGA) provides two useful pieces of information, firstly moisture loss and secondly the temperature at which a sample degrades. Samples were not equilibrated to a RH before TGA; however, for both MCC and CF the 610 min ball milled samples have higher moisture contents than the non-ball milled cellulose (Figures 3.13 and 3.14) due to the more open structure and higher surface

area of the fully amorphous celluloses (Mihranyan *et al.*, 2004, Stubberud *et al.*, 1996). This is in agreement with DVS results which show that as the cellulose recrystallises, water is forced out (Figure 4.12). Avolio *et al.* (2012) have previously shown that the amount of water absorbed by cellulose increases with milling time as the amorphous regions are more accessible to water than the crystalline domains, i.e. there are more sorption sites (hydroxyl groups) available (Kocherbitov *et al.*, 2008, Mihranyan and Strømme, 2004). Using DSC, Bertran and Dale (1986) showed there was a large endothermic peak between 110-160^{o}C which was due to the loss of absorbed water and found there was a direct relationship between the area of the peak and the crystallinity of the sample. MCC has previously been shown to absorb up to 3 wt% of water into its internal structure (Khan *et al.*, 1988, Sun, 2008).

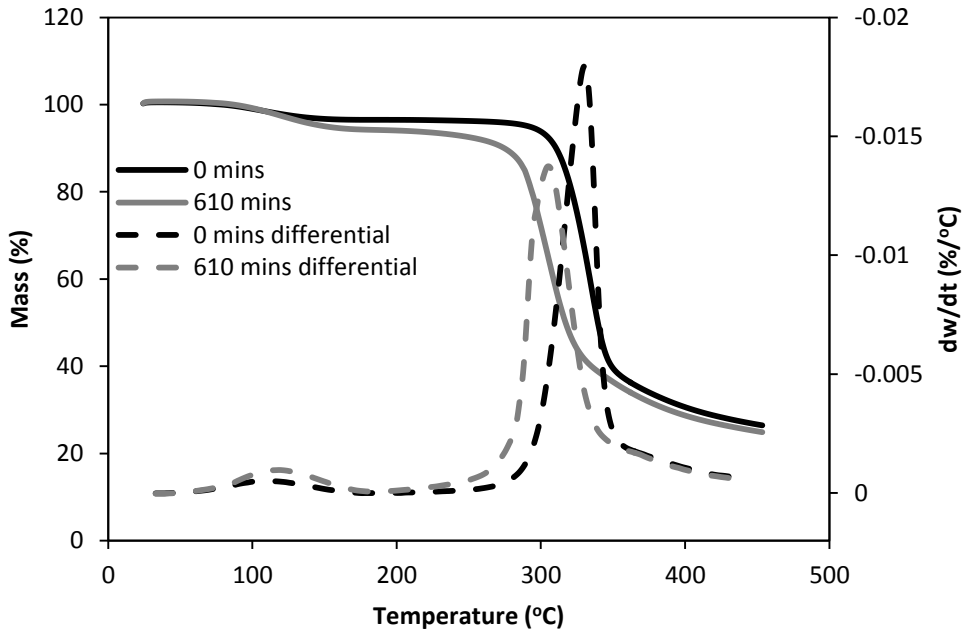

Figure 3.13 TGA plots (solid lines) and their respective differential thermal analysis (dashed lines) for MCC (black lines) and MCC ball milled for 610 minutes (grey lines).

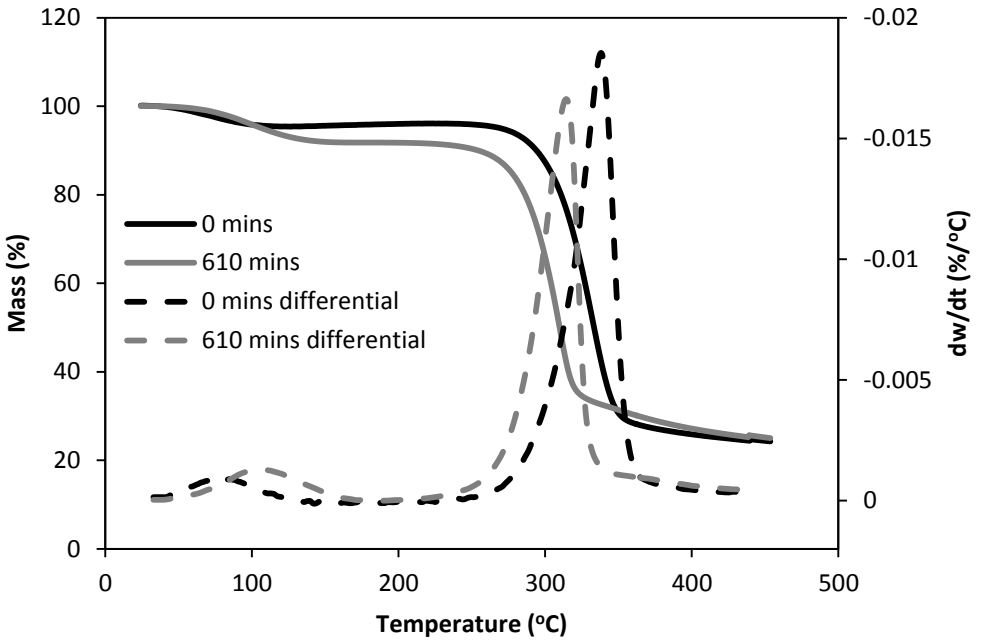

Figure 3.14 TGA plots (solid lines) and their respective differential thermal analysis (dashed lines) for CF (black lines) and CF ball milled for 610 minutes (grey lines).

During the pyrolytic degradation of cellulose several compounds are formed including water vapour, carbon dioxide, carbon monoxide and various hydrocarbon derivatives such as alkanes, alkenes, ketones and aldehydes (Soudais *et al.*, 2007). TGA reveals some differences between the two types of cellulose. CF has a higher peak degradation temperature than MCC, (Figures 3.15 and 3.16) even though it has a lower crystallinity, possibly because of its larger fibre size and higher DP. The degradation temperature of CF decreases with increasing ball milling time but begins to plateau at higher milling times. This correlates with the decrease in DP which also begins to plateau at high milling times. Calahorra *et al.* (1989) have previously shown that thermal stability decreases as molecular weight decreases. There is little difference between the dry and rehydrated samples which indicates that DP rather than crystallinity is the influencing factor in the degradation temperature of CF.

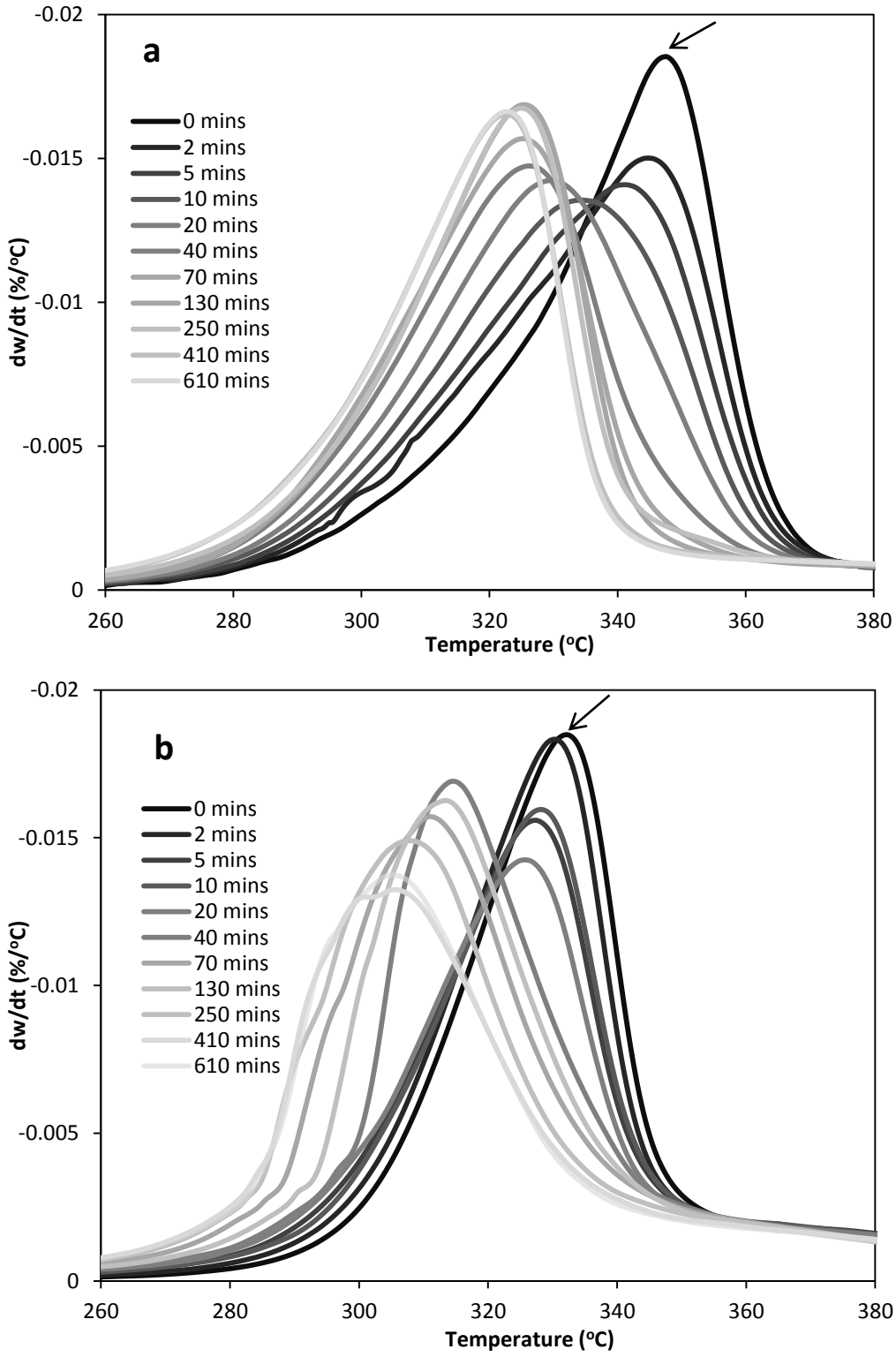

Figure 3.15 Differential thermal analysis of TGA data for (a) CF and (b) MCC ball milled for different times. Arrows show the peak degradation temperature for cellulose that has not been ball milled (0 mins), measured as the maximum height for each differential peak.

The degradation temperature of MCC also decreases with increased milling time; however, there is a large jump of over 10°C between 20 and 40 minutes. This is the

time at which MCC becomes completely amorphous indicating that it is the loss of crystallinity (i.e. a tightly bound structure) which lowers the degradation temperature. The increase in mobility, which may be shown in the increased ability of the amorphous cellulose to absorb water (Figures 3.13 and 3.14), leads to a lower degradation temperature. For the rehydrated samples there is no jump but instead a steady decrease in the degradation temperature. These values are higher than the dry samples indicating that the more ordered crystalline structure is harder to degrade as more energy is required to disrupt the crystalline domains (Avella *et al.*, 2010, Pedersoli, 2000). For MCC then it is likely that both the decrease in DP and crystallinity impact the temperature at which the cellulose degrades.

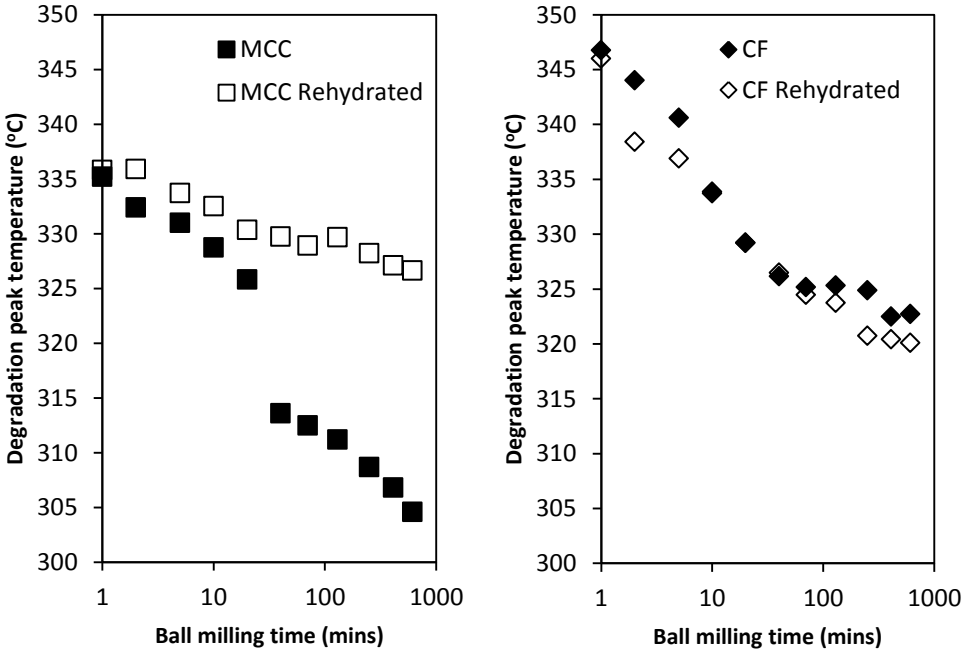

Figure 3.16 The peak degradation temperature (measured as the maximum height for each differential peak, as indicated by the arrows in Figure 3.15) of MCC (left) and CF (right), measured as the maximum peak DTA peak, as seen in Figure 3.15.

It is useful to again look at the moisture loss for the samples at 20 and 40 minutes where the cellulose becomes almost completely amorphous (Figure 3.17). There is little difference in the moisture loss for the CF samples whereas there is a large increase in the amount of moisture that is lost for the amorphous MCC (at 40

minutes). This is in agreement with the drop in degradation temperature seen in Figure 3.16. The physical desorption of water generally occurs between 25-150^{o}C whilst thermal dehydration occurs between 150-240^{o}C (Tang and Bacon, 1964, Bacon and Tang, 1964). Due to the highly polar nature of cellulose, the water is closely associated with the cellulose chains through hydrogen bonding (Scheirs *et al.*, 2001). For all the cellulose samples there is a small shoulder between 75-80^{o}C which is most apparent for CF that has not been milled. This may be due to the evaporation of the small amount of bulk water.

The peak moisture loss temperature shifts to a slightly higher temperature with ball milling (Figure 3.17). Using 2D ^{13}C-^{13}C NMR correlation spectroscopy and quantum chemistry computer simulations, Mori *et al.* (2012) have also found that amorphous cellulose has a more hydrophilic surface than crystalline cellulose. The amorphous cellulose may therefore bind water more tightly which will require more energy for the water to be released.

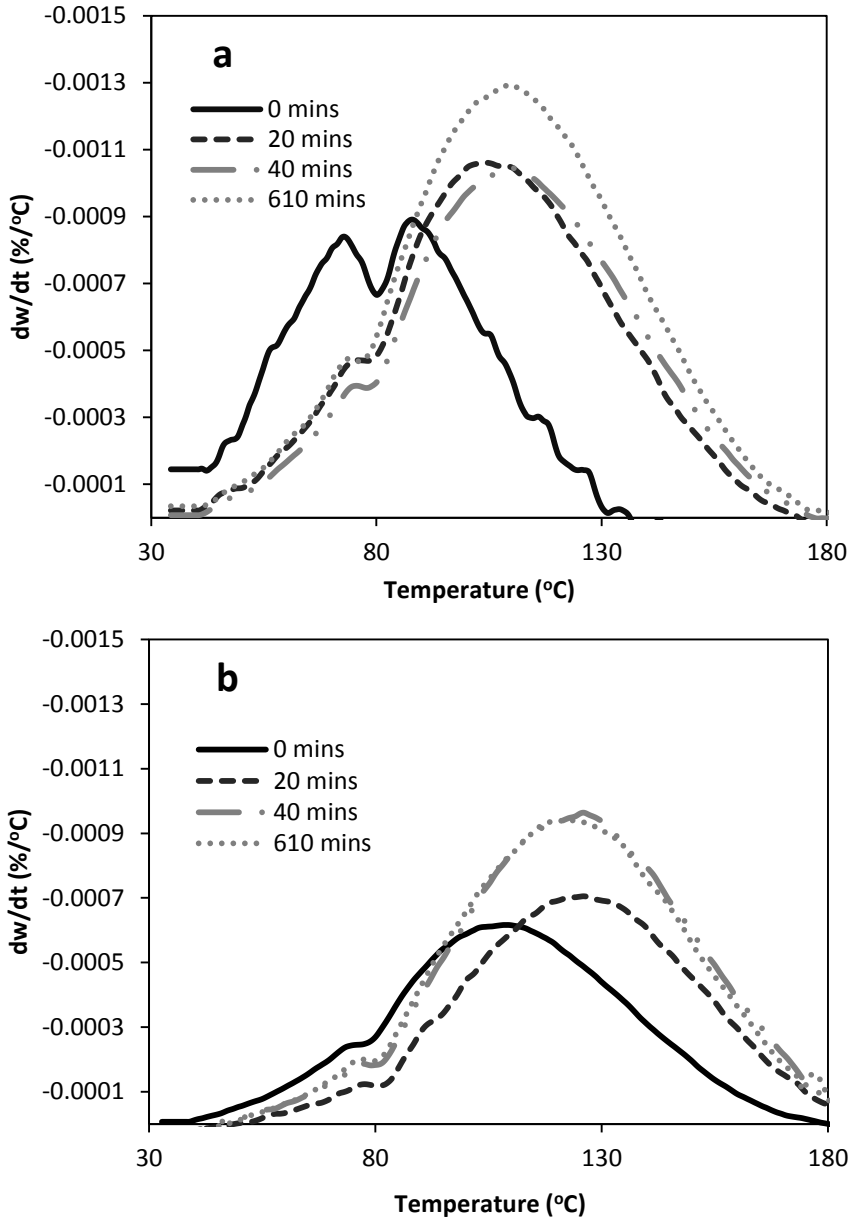

Figure 3.17 Differential thermal analysis showing the moisture loss of (a) CF and (b) MCC which have been ball milled for different lengths of time.

An interesting observation that should be pointed out is that all the amorphous samples (>40 minutes ball milling time) flowed out of the TGA pans at a temperature of above 250°C (Figure 3.18). This again indicates an increase in mobility of the amorphous samples compared to those that were partially crystalline. Wang *et al*. (2013) found that ball milled cellulose samples studied by TGA had gone through a liquid intermediate stage. SEM showed a cellular foam structure, with trapped air bubbles, was formed whilst for the non-ball milled samples the fibre integrity was

maintained up to 600°C. They attributed the formation of these liquid intermediates (mainly oligo-anhydrosugars) to be caused by dehydration and cross linking during the formation of furanic compounds. The yield of the furanic compounds was considerably higher for the ball milled samples compared to the control samples, possibly due to a combination of decreased DP and lower crystallinity, resulting in a lower activation energy. As discussed in the introduction a liquid intermediate stage is well reported (Lede, 2012).

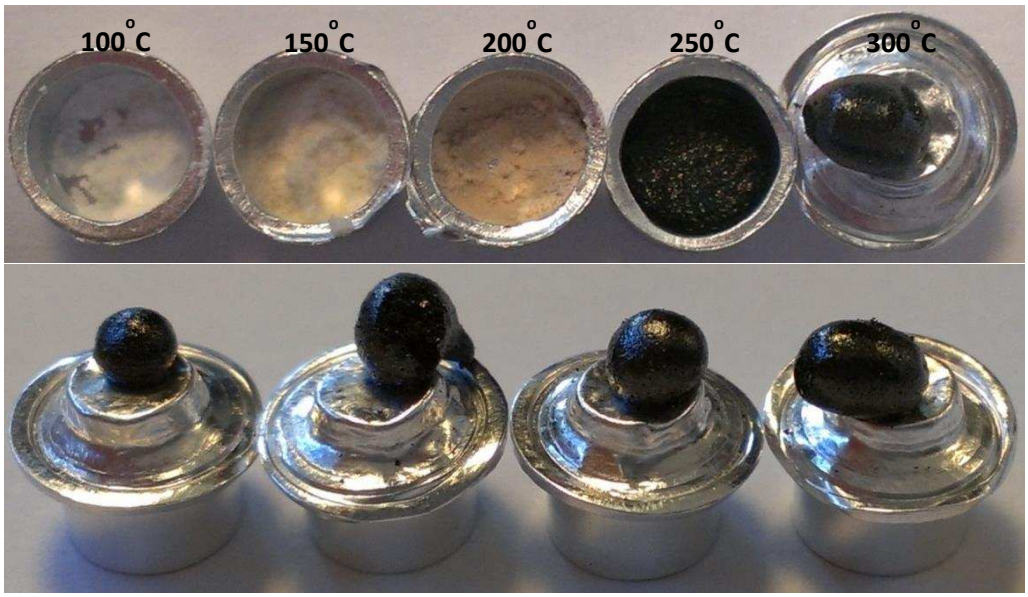

Figure 3.18 The top images show the degradation of MCC that was ball milled for 610 mins during heating in the TGA (the temperatures at which the samples were heated to are shown above each pot). The lower images show replicate samples that were heated to 450°C, where the degraded cellulose has exited the TGA pans during heating.

Using DSC, Figure 3.19 also shows that the degradation temperature of the ball milled amorphous sample is lower than that of the original MCC. The degradation temperature is lower than that shown in TGA as it is in air (oxidative) rather than nitrogen (inert). Below the degradation the crystalline MCC shows no transitions. The amorphous sample, however, shows two other peaks at about 50°C and 110°C. It is well reported that amorphous polymers show a thermal relaxation transition at about 50°C due to long range order that then requires time (in the order of days rather than hours) to return after heating (Appelqvist *et al.*, 1993, Gidley *et al.*,

1993). It will therefore not be seen in an immediate reheat. Paes *et al.* (2010) ascribed the peak to the 'melting' out of weak associations, most likely hydrogen bonds, as the endotherm was at a constant temperature regardless of moisture content. If the endothermic peak was due to physical aging it might be expected to shift to a higher temperature with increased moisture content. The exothermic peak at 110^{o}C is likely to be due to recrystallisation. Paes *et al.* (2010) found that on reheats this exothermic peak was not observed, but instead there was a higher level of meltable/freezable water due to the dehydrated recrystallised cellulose releasing water, as was also seen with DVS in Figure 3.12.

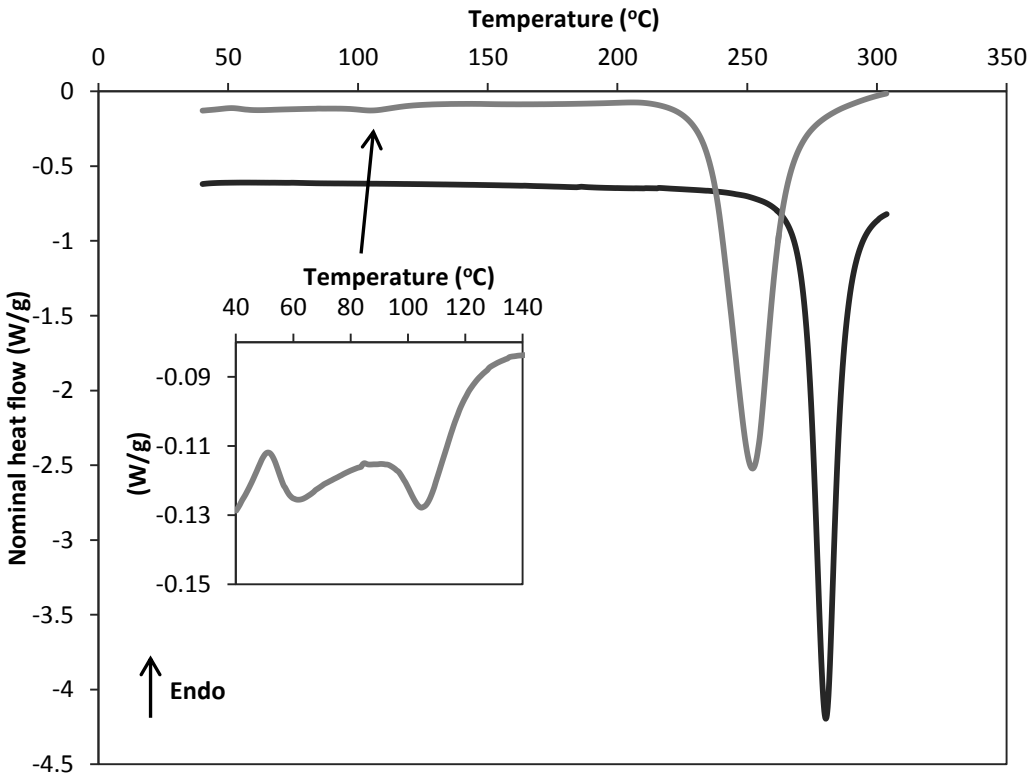

Figure 3.19 DSC spectra of MCC (black) and MCC which has been ball milled for 610 mins (grey). Insert graph shows the region of 40-140^{o}C expanded for the ball milled MCC.

Flash DSC is a newly available technique that enables the rapid heating and cooling of very small amounts of sample. It is primarily used for samples that melt and are therefore able to make a good contact with the chip sensor. The physical aging of maltose provides a good example of what the flash DSC is capable of (Figure 3.20).

The maltose was cured at 100°C and with longer aging the enthalpy of relaxation increases (Schmidt and Lammert, 1996, Lammert *et al.*, 1999, Noel *et al.*, 2005).

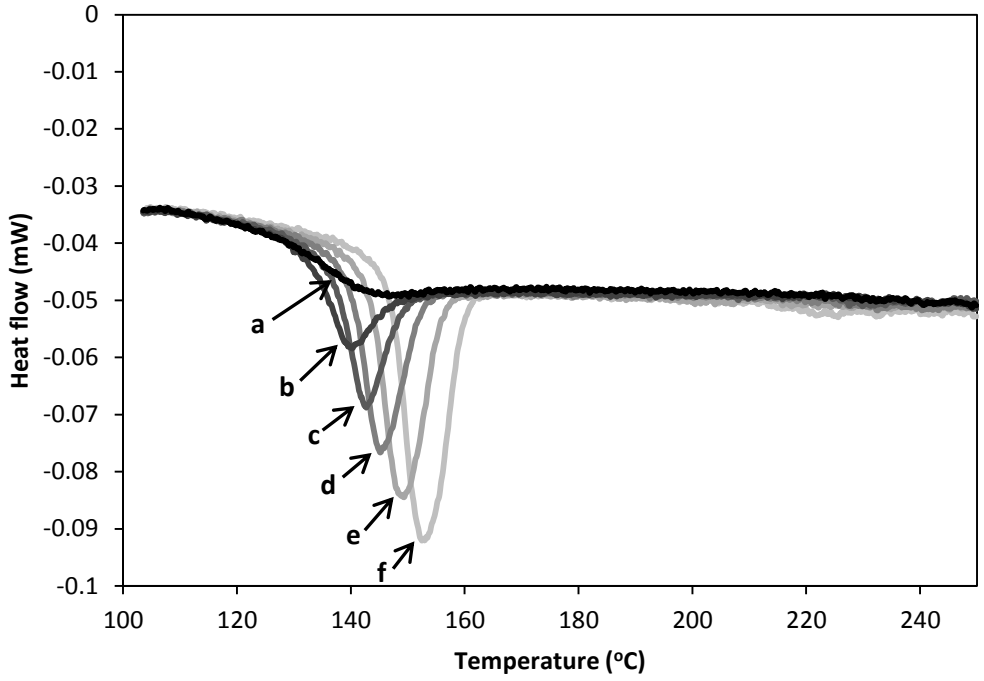

Figure 3.20 Flash DSC thermograms of maltose after curing at 100°C for (a) 1 second (b) 1 minute (c) 4 minutes (d) 16 minutes (e) 66.67 minutes and (f) 266.67 minutes.

Using flash DSC presents both an advantage and a drawback; the rapid heating and cooling rates (500 Ks^{-1}) should enable the measurement of any thermal transitions before degradation occurs. The obvious drawback being that crystalline cellulose does not melt so there is poor adherence to the sensor. Indeed, when MCC was run on the flash DSC it was very difficult to measure anything as the sample more often than not jumped off the sensor on the first heat. When the sample did stay in place there was very little direct contact with the sensor. Due to the jumping of the sample the initial heat produced very noisy data. Figure 3.21 shows the results of a run where some of the MCC did stay in place. No transition was seen for MCC.

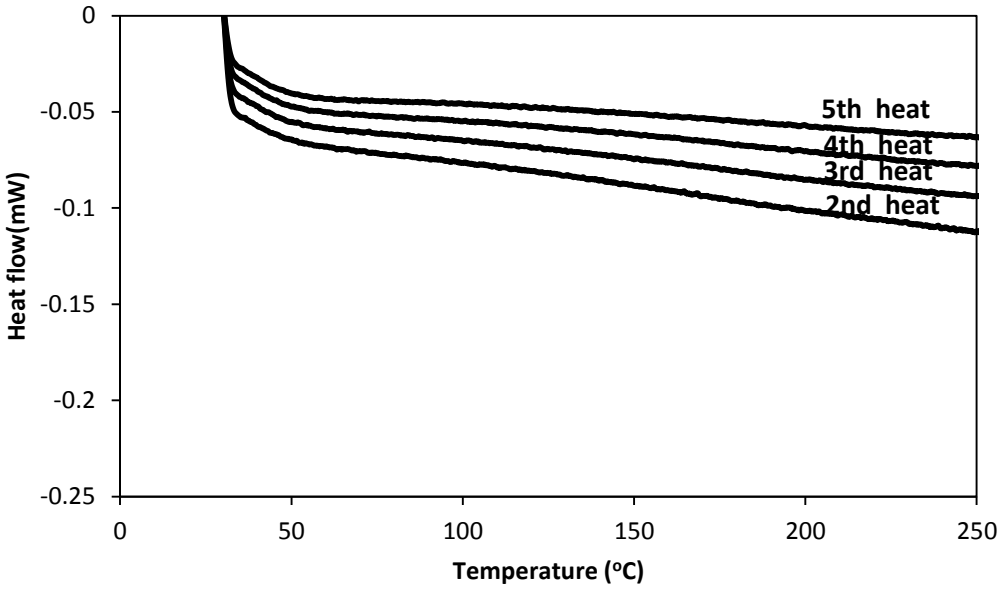

Figure 3.21 Flash DSC thermograms of MCC showing successive heats. The first heat is not shown due to excess noise.

The ball milled sample (610 minutes) on the other hand did appear to flow slightly and adhere to the sensor on the first run of five heating cycles. This enabled a better contact with the sensor and with a subsequent run of heating cycles a thermal transition is shown (Figure 3.22) with the mid-point of the glass transition at 176^{o}C. With each subsequent run the heat flow of the T_g reduces until by the 5th reheat the T_g is completely lost. This may well be due to the ball milled cellulose degrading with each successive heat and fuming off the chip and therefore decreasing the weight of the sample. This may also explain why the overall heat capacity decreases with further heating runs.

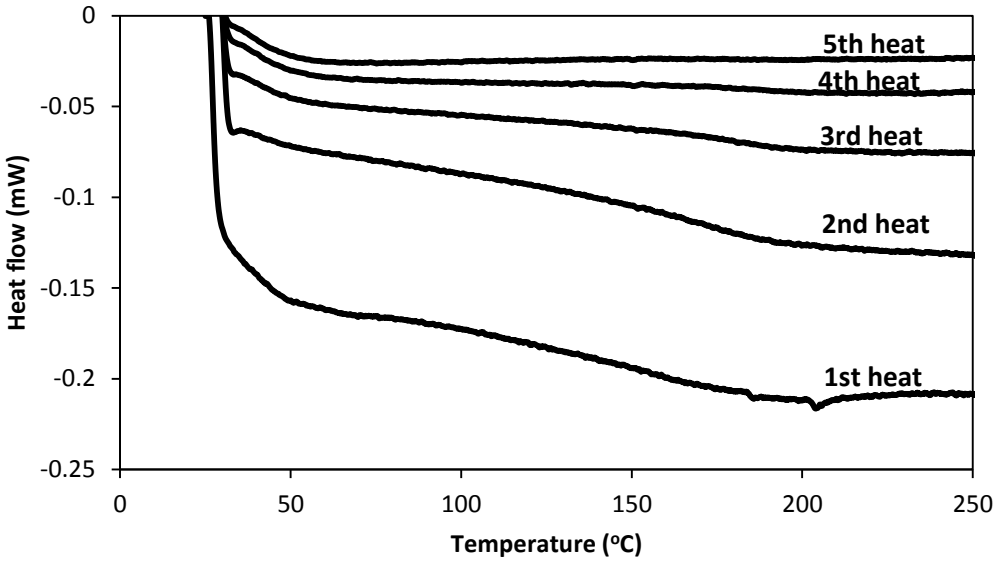

Figure 3.22 Flash DSC thermograms of MCC ball milled for 610 minutes showing successive heats.

Figure 3.23a shows that the maltose melts and forms a glass with a uniform shape. MCC does not melt (Figure 3.23b) whereas ball milled MCC does appear to flow as evidenced by the rounded and almost transparent sample in the middle of the sensor (Figure 3.23c). On both of the cellulose samples a ring is clearly visible around the heating element which is a result of the cellulose degrading. When the samples were viewed as the heating took place fumes were seen every time the samples were heated above 350°C.

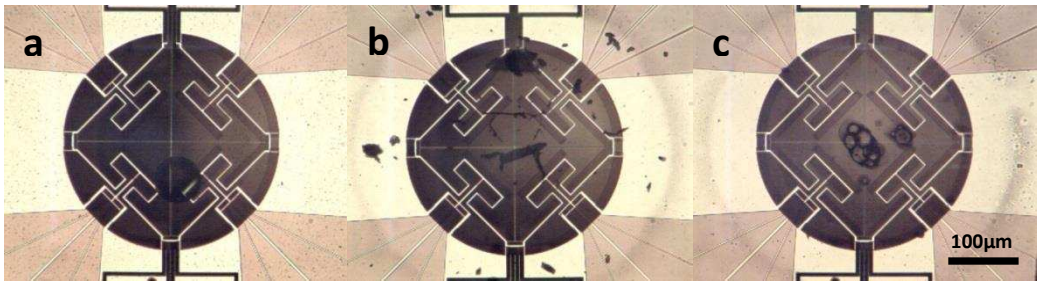

Figure 3.23 Flash DSC chips after use with (a) maltose (b) MCC and (c) MCC ball milled for 610 mins.

As the ball milled MCC appeared to flow slightly on the flash DSC chips, attempts were then made to thermoform cellulose on a larger scale so that the particulate structure could be disrupted creating a continuous material. Hot pressing has been used for thermoplastic starch in combination with methyl cellulose (Arvanitoyannis

and Biliaderis, 1999), PLA (Wang *et al.*, 2002), flax fibres (Romhány *et al.*, 2003) or eucalyptus pulp (Curvelo *et al.*, 2001). A temperature of 200^{o}C was chosen as this was higher than the T_g (Figure 3.22) but lower than the degradation temperature (Figure 3.19). Preliminary experiments on a small scale hot press were promising, producing a slightly transparent material. This was then scaled up using a 160 ton down-stroke press at a pressure of 90 bar (Figure 3.24). MCC, which is often used in the production of pharmaceutical tablets (Iloañusi and Schwartz, 1998, Sun, 2008), produced a compacted sheet, similar in texture to strong cardboard and there was a slight browning due to the heat (Figure 3.25a). Yamamura *et al.* (1997) have suggested that during the compaction of MCC, as well as cohesion between cellulose particles, there may be the formation of a regular long range intermolecular arrangement. The hot pressed ball milled MCC produced a much stronger sheet that cracked when removing from the mould. As can be seen from Figure 3.25b, part of the sheet turned a caramel brown colour. The differences in colour on the sheet are likely to be due to pressure differences during the hot press caused by uneven loading of the powder in the mould. The degradation temperature of ball milled MCC is above 200^{o}C (Figure 3.19) but the high pressure will reduce the degradation temperature (Zhang *et al.*, 2012). These areas were much harder to break by hand than the MCC sheet. Whilst visually, parts of the ball milled MCC sheet appears to have flowed and formed a continuous polymer melt due to its shiny surface, SEM images indicate the ball milled MCC has just been compacted (Figure 3.25b) and sintered as ball milled MCC particles were intact but fused together. This can be seen more clearly with the sheet that was composed of 70 wt% MCC that was ball milled for 610 minutes and 30 wt% CF (Figure 3.25c). The inability of ball milled MCC to lose its particulate structure is likely to be due to it recrystalising before it was able to flow.

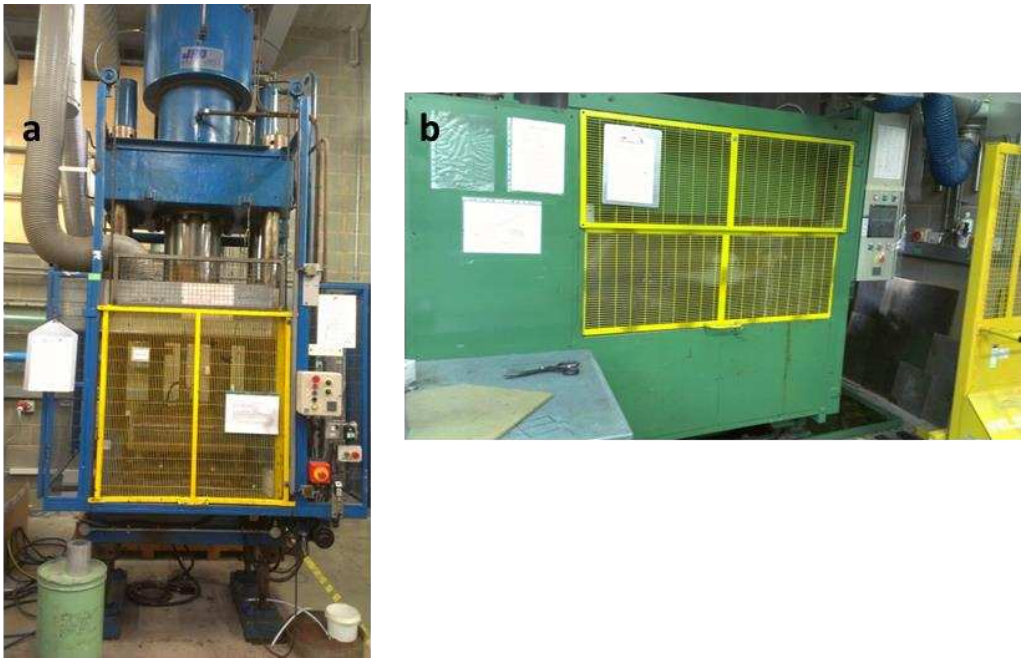

Figure 3.24 Pictures of (a) the down stroke hot press and (b) the up press to cool the sample whilst still under pressure.

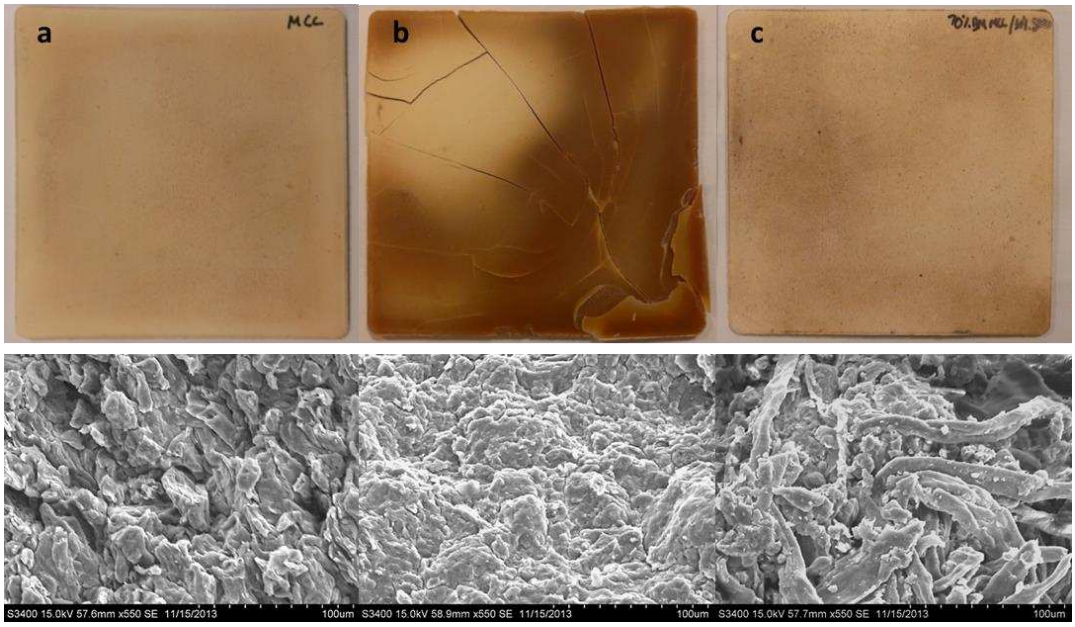

Figure 3.25 Cellulose pressed at 200°C (a) MCC (b) MCC ball milled for 610 minutes and (c) 70 wt% MCC ball milled for 610 mins + 30 wt% CF. Top are images of the pressed cellulose. Each tile is 8cm^2. Bottom images are the corresponding SEM images of the fractured surface.

3.4 Conclusion

Ball milling rapidly changes the structure of cellulose, both decreasing its crystallinity and viscosity average DP. Kinetic energy is transferred from the balls to the cellulose via collisions, rupturing the glycosidic bonds. When rehydrated, cellulose will recrystallise to its more thermodynamically stable type II polymorph unless there are

still some type I seed crystals present. At intermediate milling times a mixture of both polymorphs recrystallise. DP is the most important factor in the degradation temperature of CF whereas crystallinity is also important for dry ball milled MCC. DVS showed that if the RH is raised to 95% ball milled MCC will recrystallise which forces out water, lowering the weight of the sample. When cellulose becomes completely amorphous it will go through a liquid intermediate stage at a temperature above 250^{o}C. A liquid intermediate/melt stage is also seen with flash DSC. This enabled the measurement of a glass transition temperature. Attempts to thermoform amorphous cellulose were not successful which is likely to be due to recrystallisation before it flows.

Chapter 4. Reinforced polysaccharide biofoams

4.1 Introduction

Cellular solids or solid foams are comprised of cells which have solid edges or faces that fill space. They are found widely in nature, for instance cork, cancellous bone, wood, coral and sponge due to their high strength but light weight. Man-made foams have been manufactured since the early 20th century and have been used as packaging, cushioning and insulation materials. There are also many cellular solid foods, for example, bread and meringue.

Solid foams can be categorised into two types, based on cell structure, either open (also known as reticulated) or closed. Pores in open cell structured foams form an interconnected network and often result in a soft structure. Closed cell foams are often stronger and denser as the pores are not interconnected. Closed cell foams are particularly good as thermal insulators due to their poor conductivity of enclosed gas and good thermal shock resistance (Gibson and Ashby, 1988).

Aerogels are formed by removing liquid from a gel, for example by lyophilisation or super-critical CO_2 drying. This produces a structure that is lightweight, porous and has a large surface area as well as being mechanically strong. Thickened hydrocolloid solutions can also form sponges when dried but cannot strictly be referred to as aerogels. Due to the low solids content of most hydrocolloid solutions and gels the drying process is expensive and time consuming but there are many novel applications that can make the process economical, for example, for packaging, insulation and tissue scaffold/wound healing (Sharma *et al.*, 2013, Gupta *et al.*, 2010, Cardea *et al.*, 2013, Barbetta *et al.*, 2010, Croisier and Jerome, 2013, Rudaz *et al.*, 2014) as well as drug delivery (Vishal Gupta and Shivakumar, 2010, Garcia-Gonzalez *et al.*, 2011, Mehling *et al.*, 2009, Ulker and Erkey, 2014) and chemical sensing (Deligkaris *et al.*, 2010).

Traditionally, aerogels have been prepared from inorganic materials such as silica. There is now an increasing interest in producing aerogels from renewable, sustainable sources, particularly polysaccharides. Much of the current literature focuses on marine polysaccharides such as carrageenan and alginate (Hyland *et al.*, 2011, Sun and Tan, 2013). There is also a focus on micro/nanofibrillated cellulose aerogels as well as all cellulose composites (Duchemin *et al.*, 2010).

One of the most widespread ways of removing the liquid phase from a gel is by lyophilisation (freeze drying). The freezing rate is therefore important as it will dictate the size and direction of ice crystal formation. Faster freezing rates produce small ice crystals. Using micro-CT imaging Koehnke *et al.* (2012) showed they were able to produce a unidirectional aerogel by freezing in liquid nitrogen (-196^{o}C) using a temperature gradient with nanoreinforced xylan-cellulose composite foams. They found that samples with larger pores were stronger and stiffer than those with smaller pores and that samples with strong anisotropy of the pore structure in the loading direction were stronger than samples with non-directional freezing (random pore orientation). Wu *et al.* (2007) used a combination of collagen and chitosan and found that scaffolds fabricated at -20^{o}C and -80^{o}C had an open pore structure whereas the scaffolds fabricated at -196^{o}C had a parallel sheet structure. Stokols and Tuszynski (2004) created a linear pore structure with agarose aerogels by touching just the ends of glass vials containing agarose solution onto a block of dry ice surrounded by liquid nitrogen. The samples were allowed to freeze for 45 minutes and then freeze dried.

The production of nanofibrillated cellulose aerogels is particularly sensitive to the drying method. Jin *et al.* (2004) compared regular freeze drying, rapid freeze drying and solvent exchange. Regular freeze drying resulted in significant coalescence of the

microfibrils due to capillary effects whilst the solvent exchanged and dried aerogels gave a highly porous structure. Rapid freeze drying (freeze casting on a liquid nitrogen cooled metal plate) gave aerogel sheets with asymmetrical porosity.

Recently, Mikkonen *et al.* (2014) produced aerogels using guar gum and tamarind xyloglucan. They found that by using enzyme oxidisation of the polysaccharides the compressive modulus could be greatly increased. The modification also resulted in the aerogels no longer being water soluble which would help significantly for potential applications such as packaging.

One of the most important characteristics of a foam is its mechanical strength and stiffness (Young's modulus). Figure 4.1 shows a typical stress strain curve of a polysaccharide foam.

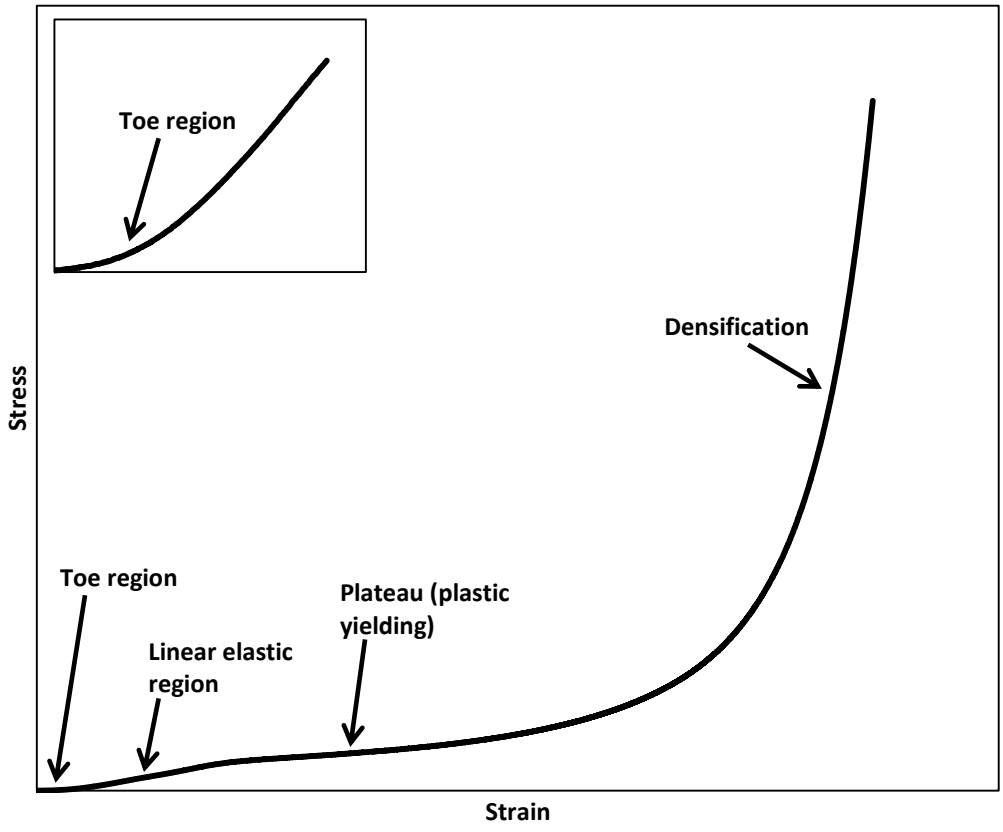

Figure 4.1 Stress-strain curve of a polysaccharide foam.

Due to the soft nature of foams, the initial portion of a stress-strain curve has a high deformation/low force characteristic known as the toe region caused by the alignment of the foam structure. The linear region, caused by the cell walls bending, follows the toe region and is used for the determination of Young's Modulus. The yield region is where permanent deformation starts. At high strain densification occurs as the cells collapse and compress. Foams are low density and generally have a relatively low Young's modulus compared to other materials (Figure 4.2).

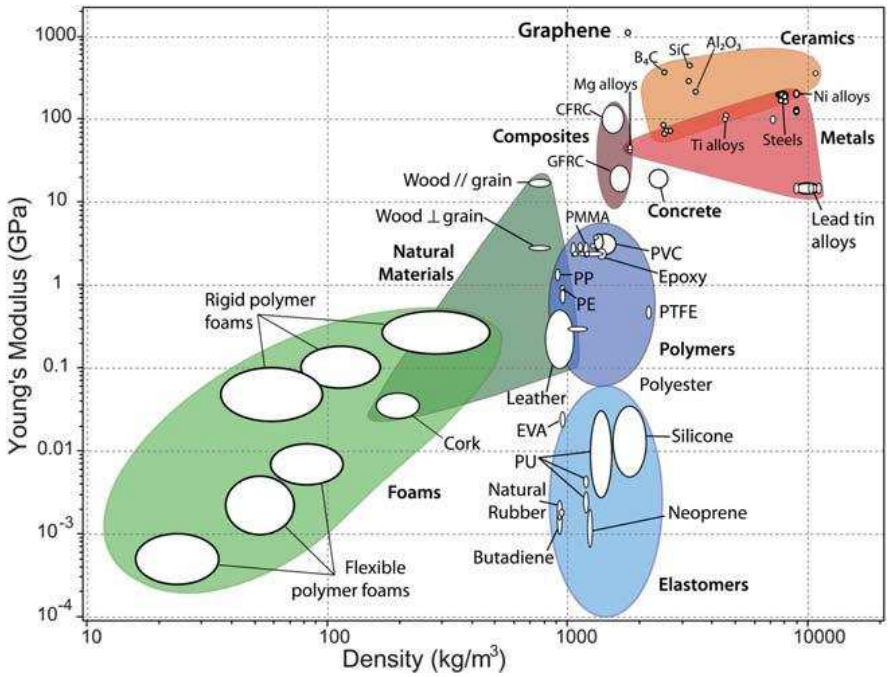

Figure 4.2 Chart of Young's modulus as a function of density (Verdejo *et al.*, 2011)

The mechanical strength of foams can be greatly improved by adding another component to reinforce the foam structure. One of the major factors in whether fibres will improve composite strength is their compatibility with the matrix polymer. Natural fibres therefore have much better adherence to polysaccharides such as starch due to their chemical similarities than to hydrophobic oil derived polymers such as polyester (Wollerdorfer and Bader, 1998).

Bergeret and Benezet (2011) used natural fibres such as cotton linters, hemp, sugarcane and coconut fibres to reinforce extruded starch biofoams which induced a density reduction of up to 33% as well as a decrease in water adsorption and increase in the mechanical properties. Similar studies using sugarcane fibres (Debiagi *et al.*, 2011), henequen and coconut (Aguilar-Palazuelos *et al.*, 2007), leafwood and paper pulp fibres (Averous and Boquillon, 2004), sisal, jute and cabuya (Torres *et al.*, 2007) and cellulose nanofibres (Hietala *et al.*, 2013) have all shown that the mechanical properties of the foams were greatly improved by fibre reinforcement. One of the major areas these new structures could be used is as an alternative loose fill packaging material.

Another polymer which has seen considerable interest in composite construction is polylactic acid (PLA) which is thermoplastic and derived from natural resources such as corn starch or sugarcane (Dicker *et al.*, 2014). Many studies have shown that PLA's mechanical properties can be improved by the addition of fibres (Sahari and Sapuan, 2011, Wambua *et al.*, 2003, Graupner *et al.*, 2009, Mukherjee and Kao, 2011). Neagu *et al.* (2009) produced PLA composite foams using supercritical CO_2. The addition of 5-10 wt% wood fibre significantly increased the stiffness and strength of the foam.

Water sorption can be incredibly important for the structural integretiy of cellulose solids. Some aerogels are designed to absorb as much water as possible, for instance wound dressings (Gupta *et al.*, 2010). Vishal Gupta and Shivakumar (2010) designed chitosan/poly(vinyl alcohol) superporous hydrogels which were able to swell and de-swell reversibly depending on the pH of media which enabled better drug delivery. Kuang *et al.* (2011) chemically modified starch to prepare fast swelling superabsorbant hydrogels which could be useful in a number of biomedical applications. However in many applications pronounced water absorption is not

desirable. Enzymatic oxidation of guar and xyloglucan has been used to slightly decrease the moisture uptake of aerogels (Mikkonen *et al.*, 2014).

Sundaram and Durance (2007) found that dried hydrocolloid hydrogels with the highest total pore area had the highest moisture content in sorption isotherms and that more interconnected pores resulted in higher moisture contents. They showed that hydrogels absorbed only small amounts of water at low relative humidity (RH) but large amounts at high RH, following a type III moisture sorption isotherm.

Locust bean gum (LBG) has a β-1,4-linked mannose backbone and approximately every fourth mannose unit is substituted with a 1,6-linked α-galactose residue. The distribution of galactose side chains is neither regular nor completely random (Dea *et al.*, 1986). LBG undergoes cryogelation when frozen due to association of the unsubstituted regions of the mannan backbone. LBG is used to reduce ice crystal recrystallisation rates in ice cream so as to provide a smoother texture (Patmore *et al.*, 2003, Regand and Goff, 2003, Doyle *et al.*, 2006). LBG is adsorbed onto cellulose fibres and has been used in papermaking (Swanson, 1961). Using ^{13}C NMR spectroscopy Newman and Hemmingson (1998) looked at interactions between LBG and cellulose. Fractions of LBG with a higher mannose to galactose (M:G) ratio were found to selectively bind to bleached kraft pulp and the fraction with a higher galactosyl substitution was washed from the sample. They suggested that most of the mannosyl residues were involved in generalised interactions with cellulose, not just the unsubstituted regions whereas the galactosyl residues were not involved. LBG has been found to interact synergistically with microcrystalline cellulose (MCC) (Dea *et al.*, 1986).

Fenugreek has a β-1,4-linked mannose backbone that is fully substituted with galactose residues and therefore does not undergo cryogelation. There have been

few studies on the interaction between cellulose and fenugreek but the sidechains of xyloglucan do not prevent it from binding to cellulose (Levy *et al.*, 1991). However galactomannans with less galactosyl residues tend to interact more with other polysaccharides (Dea *et al.*, 1986), for instance LBG forms a gel with xanthan whereas guar (M:G = 2:1) does not (Phillips and Williams, 2000). Fenugreek has no synergistic interaction with carboxymethylcellulose (Mathur, 2011).

This chapter seeks to identify any differences in foam structure caused by the cryo-gelation or non-gelation of the two galactomannans and to identify the reinforcement effect of different celluloses. Scoping experiments were also carried out to identify new methods of fibrillating cellulose through extrusion.

4.2 Materials and Methods

4.2.1 Materials

The celluloses used in this work are cellulose fibre (CF) and cellulose powder (CP) (Solka 900FCC and 300FCC respectively, International Fibre Corporation, USA) and Avicel MCC type PH-101 Ph Eur (Sigma Aldrich, UK). The polysaccharides used were fenugreek (Airgreen, Japan) and Locust bean gum (LBG 246) (Danisco, Denmark) which had weight average molecular weight of 4.05×10^6 and 2.72×10^6 g/mol respectively (please see Chapter 6, section 6.2.3, page 180 for the method of molecular weight measurement). Hydroxypropylcellulose (HPC) with a weight average molecular weight of 80,000 g/mol was purchased from Sigma Aldrich (UK).

4.2.2 Microfibrillation

2 wt% CP was swollen in water for 2 hours and then passed through a Niro Soavi Panda 2K high pressure homogeniser (GEA, Italy) at 1300 bar for a total of 15 passes. The microfibrillated cellulose (MFC) dispersion was then concentrated by centrifuging

at 2000g for 20 minutes and removing the excess water. The MFC dispersion was then diluted to its required concentration.

4.2.3 Light microscopy

Light microscope images were taken using a Leitz Diaplan microscope (Leica, Heidelberg, Germany) and a Pixelink PL-A600 (Ottawa, Canada) recording camera. MFC dispersions were dyed with Congo red. Hot stage pictures were taken using a TMHS 600 Linkam stage (Linkam Scientific Instruments, UK) and images were taken every 5 seconds with a heating rate of $10^{o}C\ min^{-1}$.

4.2.4 Gel and foam production

Polysaccharide gels and foams were made by first preparing concentrated polysaccharide solutions (≈2.5 wt%) by adding the polysaccharide powder slowly to water using a mixer and heating to $80^{o}C$ for 30 minutes until fully dissolved. The solutions were left overnight on a roller bed and then centrifuged at 4000 rpm for 40 minutes to remove as much of the insoluble particles as possible. The concentrations of the polysaccharide solutions were checked by oven drying and the solutions were then diluted to a concentration of 2 wt%. Cellulose suspensions were prepared to required concentrations (taking into account their moisture content) in distilled water and left to swell for 2 hours. The cellulose suspensions and polysaccharide solutions were then mixed together using a mixer. The mixtures were immediately frozen for 48 hours and then freeze dried for 7 days. The cellulose was added to the galagtomannan solutions at ratios of 1:1 to 1:6 galactomannan:cellulose. The foams with a ratio of 1:6, therefore, had six times as much cellulose filler as galactomannan matrix.

4.2.5 Texture analysis

Foams were removed from their pots after freeze drying and cut to a height of 15 mm with a sharp serrated knife (so as to remove the uneven top of the foams). The foams were then compressed using a TA.HD Plus Texture Analyser (Stable Micro Systems, UK) with a 100 kg load cell. All foams were compressed to a true strain of 0.4. The maximum force was the force at a true strain of 0.4. Figure 4.3 shows where the compression was stopped (dotted line) instead of completely crushing the foam (solid line). This enabled the additional measurement of height loss which was calculated by:

$$Height\ loss\ (\%) = \frac{Initial\ height - height\ after\ compression}{Inital\ height} \times 100 \qquad (4.1)$$

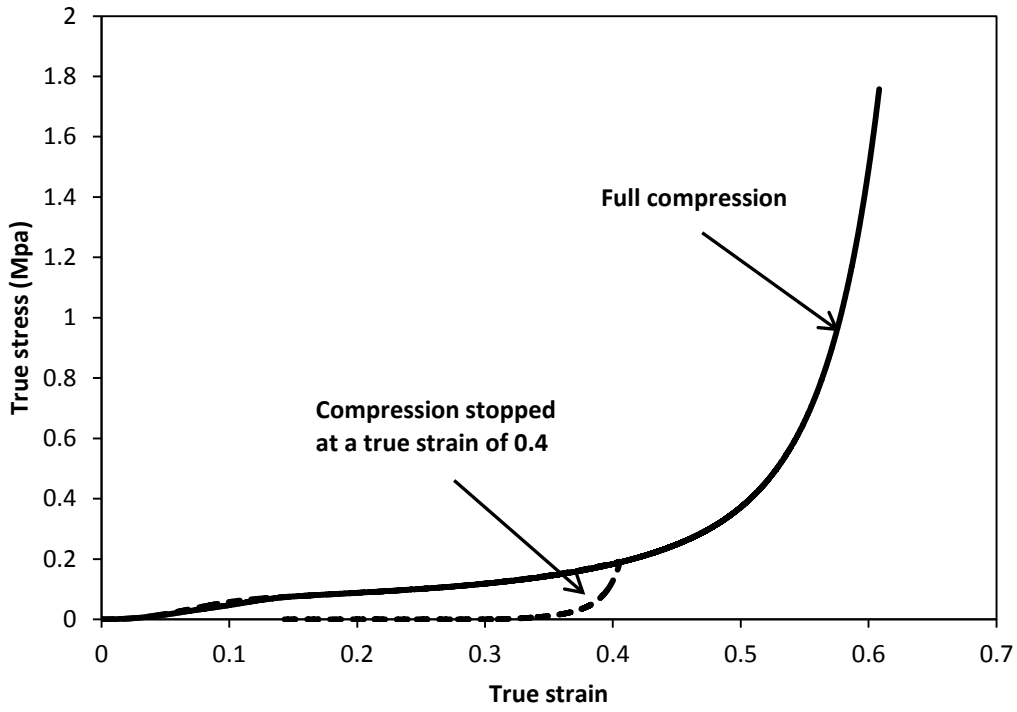

Figure 4.3 Stress-strain curve of a foam with a fenugreek to CF ratio of 1:4. The solid line shows full compression whereas the dotted line shows the true stress of a foam that was compressed to a true strain of 0.4 and then released.

Further calculations can be performed with the data provided by the texture analyser (i.e. distance and force) as follows:

Engineering stress is the applied load divided by the cross sectional area of a material, i.e. a force that deforms a body:

$$\sigma_E = \frac{F}{A_0} \tag{4.2}$$

Where F is the force and A_0 is the cross sectional area before deformation.

Engineering stain is the deformation of a material compared to its original size:

$$\epsilon_E = \frac{\Delta H}{H_0} \tag{4.3}$$

Where ΔH is the change in height and H_0 is the original height.

Both engineering stress and strain use fixed reference quantities such as the original cross sectional area or original height. These definitions are often accurate enough when the cross sectional area and height do not change substantially as force is applied. However, in some situations such as the compression of foams, these quantities can change substantially and thus must be accounted for. This is usually done by calculating the true stress and true stain.

The true stress is the applied load divided by the actual cross sectional area (which changes with time) of the material at that load:

$$\sigma_T = \frac{F}{A} = \frac{F}{A_0}.\frac{L}{L_0} = \sigma_E(1 + \epsilon_E) \tag{4.4}$$

Where A is the cross sectional area of the specimen at which the load is applied.

True strain equals the natural log of the quotient of current length over the original length. True strain is defined as the sum of all instantaneous engineering strains. True strain can be related back to engineering strain:

$$\epsilon_T = \ln\frac{L_f}{L_0} = \ln\frac{L_0 + \Delta L}{L_0} = \ln(1 + \epsilon_E) \quad (4.5)$$

Where L_f is final length.

Young's modulus is a measure of stiffness. It is the ratio of stress over strain in the linear viscoelastic region. Strain is unitless so Young's modulus has the same units as stress.

$$E = \frac{\sigma}{\epsilon} \quad (4.6)$$

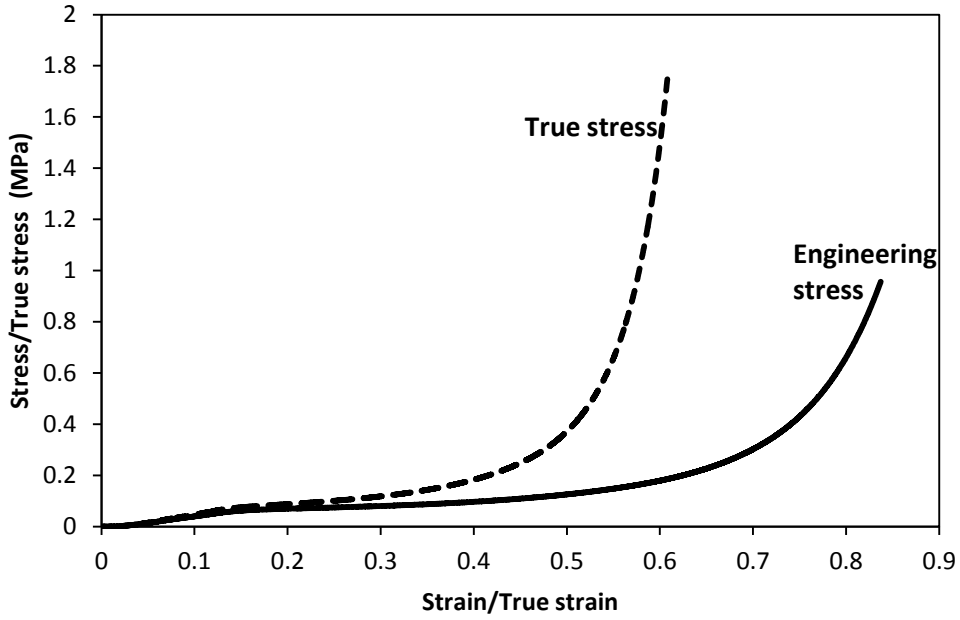

Figure 4.4 The engineering (solid line) and true (dashed line) stress strain curves of a foam with a fenugreek to CF ratio of 1:4.

As Figure 4.4 shows the values of engineering and true stress are very similar at low strain and only deviate at higher strain rates.

4.2.6 Bulk density

The bulk density of the foams was calculated by the following:

$$Bulk\ density = \frac{Weight\ of\ foam}{Volume\ of\ foam} \quad (4.7)$$

4.2.7 Moisture uptake

The polysaccharide foams were equilibrated over saturated salt solutions (Phosphorous Pentoxide RH≈2%, Potassium Carbonate RH=43% and Potassium Sulphate RH=97%) for 7 days. Moisture uptake was measured by the following:

$$Moisture\ uptake = \frac{Weight\ gain\ after\ 7\ days}{Initial\ weight}\ X\ 100 \quad (4.8)$$

4.2.8 Extrusion

For the initial fibrillation trials a Clextral BC-21 (Clextral Ltd, Firminy, France) was used which has a co-rotating twin-screw with a length of 400 mm, a barrel length to diameter ratio of 16:1 and screw speed of 200 rpm. The extruder was equipped with a pre-calibrated K-Tron Type T20 twin-screw volumetric feeder and a DKM-Clextral Type TD/2 water pump, which were used to control the solid feed and water inputs, respectively. The water flow rate was adjusted to give a moisture content of approximately 50 wt%.

The starch extrusion trials were performed on a co-rotating and intermeshing TSE 24 MC Extruder (Thermo Scientific, USA). The extruder barrel with a horizontally-split design is vertically segmented into 10 heating zones. The temperature profile along the extruder axis was maintained at 30, 30, 40, 40, 60, 60, 80, 100, 120, 140°C from the feed hopper to die. The twin-screws used had a diameter of 24 mm, length to diameter (L/D) ratio of 40:1 and were operated at screw speed of 200-400 rpm. The extrusion process was operated with a round die, a peristaltic pump for the supply of water (which was decreased from 100 L Hr^{-1} to 0.8 L Hr^{-1}) as plasticiser and two gravimetric feeders (Brabender Technology, Canada). One gravimetric feeder was used to feed the pre-mixed starch and cellulose powders (solid feed rate: 2 kg Hr^{-1}), and the other to feed maize grits which were used to clean the extruder. The extrudates produced were then equilibrated to different RH. In the course of the

extrusion process, pressure, torque, feeding rate, and the die temperature readings were monitored. The specific mechanical energy (SME) could then be calculated using the following equation:

$$SME = \left[2\,\pi\,\left(\frac{n}{60}\right)\,\tau\right]/MFR \tag{4.9}$$

Where n = screw speed, τ = torque and MFR = mass flow rate.

4.2.9 Radial Expansion Ratio (RER)

Radial expansion of extruded starch foams can be described by square of the ratio of the cross-sectional area of the foam to the die cross-section (Willett and Shogren, 2002):

$$RER = \left(\frac{R_f}{R_d}\right)^2 \tag{4.10}$$

Where R_f is the radius of the foam and R_d is the radius of the die. Extrudates were measured using a calliper and the RER was the average of 10 measurements.

4.2.10 C-Cell Mono image analyser

A C-Cell Mono imaging system (Calibre Control International Ltd, Warrington, UK) with a 75mm high resolution camera was used to capture images of the extrudate samples.

4.2.11 Capillary Rheometer

A Rosand RH7 twin bore Rosand Flowmaster RH7 capillary rheometer, (Bohlin Instruments, UK) was used. The sample was driven through a capillary die. The sample (70 wt% hydroxypropylcellulose 30 wt% MCC) was loaded into the barrel, allowed to equilibrate for 10 min and extruded at 140^{o}C. The extrusion was carried

out at ram speeds of 2, 5.63, 15.9, 44.7, 126, 355 and 1000 mm/s. The pressure was recorded as a function of the piston speed.

4.3 Results and Discussion

Figure 4.5 shows a freeze thaw cycle of each initial polysaccharide solution. As ice crystals form LBG is phase concentrated into the interstitial regions between the ice crystals and forms junction zones between the unsubstituted regions of the mannan backbone resulting in a gel-like network upon thawing. The gel structure can be seen in the thawed LBG micrograph in Figure 4.5 which shows the outline of where the ice crystals had been. Goff *et al.* (1999) found that the gel-like network formed after freezing becomes more distinct with temperature cycling. The authors found that there was no such structure formed with guar gum and therefore that LBG was more effective at inhibiting ice recrystallisation. Similarly to guar, in this work, fenugreek, which has a fully substituted backbone, was also unable to form a cryogel (Figure 4.5).

Therefore, to see if the cryogelation had any effect in increasing polymer-cellulose interaction, fenugreek was used as an alternative polymer. The particles seen in Figure 4.5 are part of the insoluble fraction that could not be removed even with significant centrifugation. The solutions therefore still contained a small fraction of impurities.

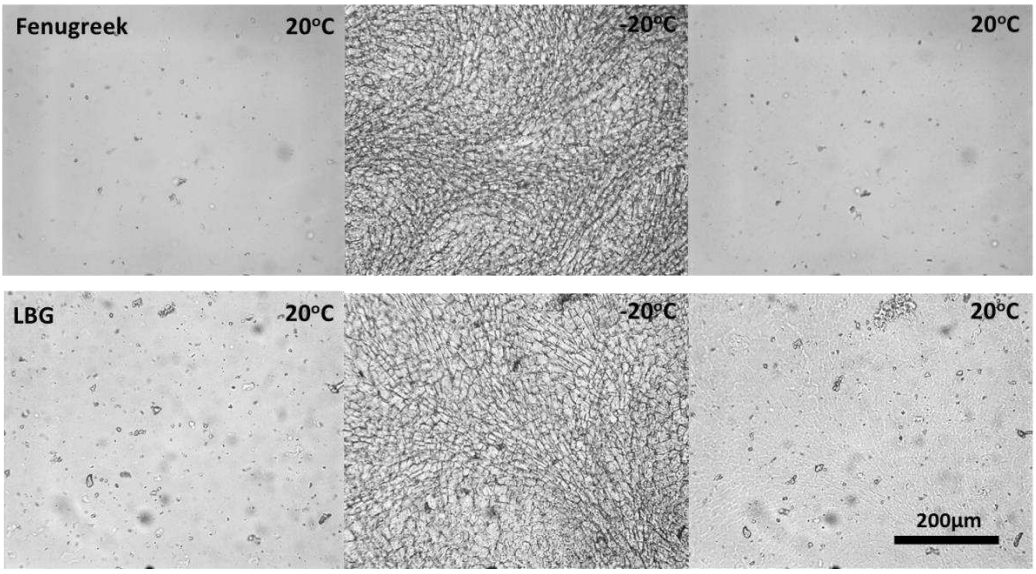

Figure 4.5 Light micrographs of a 1 wt% fenugreek aqueous solution (top) and a 1 wt% LBG aqueous solution (bottom) freeze thaw cycle from 20°C to -20°C and back to 20°C.

Both LBG and fenugreek create highly porous, interconnected and unordered open cell structured foams when freeze dried (Figure 4.6). The macroporous structure is due to the ice crystals acting as a template for the formation of pores (Lozinsky *et al.*, 2003). The pore size appears to be smaller for the LBG foam as would be expected due to its use in ice cream to slow down ice crystal growth (Patmore *et al.*, 2003). Fenugreek formed larger flat sheets, the edges of which show a fine fibril network. Foams with a similar morphology were created from alginate and chitosan gels (Hyland *et al.*, 2011). Sharma *et al.* (2013) produced carrageenan-gelatin cryogel foams with large and interconnected pores in the range of 60-100μm which would allow nutrient flow if used as a tissue scaffold. Using LBG-pectin-starch composites, Sundaram and Durance (2008) compared different drying methods; air, vacuum, freeze drying and microwave vacuum drying. They showed that compared to the other methods freeze dried gels showed a more collapsed pore structure which is common in food dehydration (Rassis *et al.*, 2002). Nussinovitch *et al.* (2004) used ImageJ, a public domain image processing program, to measure the fractal pore size distribution of freeze dried agar and fruit purees. The addition of fruit puree resulted

in small pores. Their method did have significant limitations as the pore numbers were calculated from 2-dimensional images of 3-dimensional structures. Stănescu *et al.* (2008) also used fractal analysis to provide a quantitative measure of the smoothness and therefore homogeneity as well as to give a better measure of the porosity of freeze dried collagen-chitosan matrices.

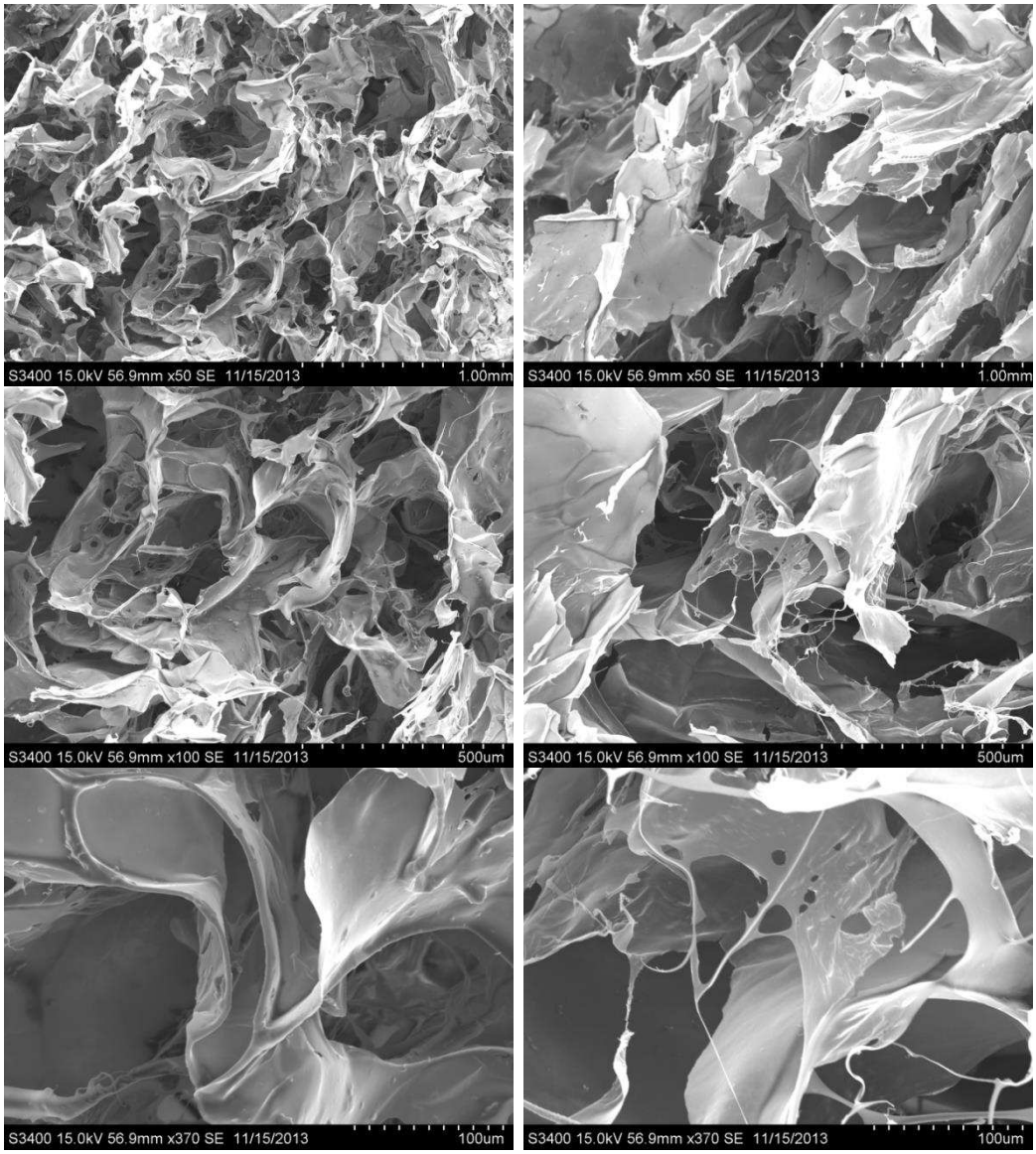

Figure 4.6 SEM micrographs of pure LBG (left) and fenugreek (right) foams at different magnifications. The scale bar is located in the bottom right corner of each micrograph.

Three celluloses were chosen as fibre reinforcements for the polysaccharide foams to identify the effect of fibre size and crystallinity. MCC is produced by acid hydrolysis of pulp resulting in a high crystallinity and small particle size and is widely used for

tableting, wet granulation and capsule filling. Cellulose fibres (CF) and cellulose powder (CP) are produced from the same source but CP is milled to a smaller particle size (Figure 4.7) which decreases its crystallinity and degree of polymerisation (Table 4.1). The average particle sizes are from the product specifications. The cellulose was added to the galagtomannan solutions at ratios of 1:1 to 1:6 galactomannan:cellulose. The foams with a ratio of 1:6, therefore, had six times as much cellulose filler as galactomannan matrix.

Table 4.1 Crystallinity from X-ray diffraction and viscosity average degree of polymerisation of the celluloses based on the average of three replicates. The average particle size is from the product specifications.

Cellulose	Crystallinity (%)	Degree of polymerisation	Average particle size (μm)
CF	41.5±0.15	1870	110
CP	27.4±0.1	1210	22
MCC	52.1±0.25	370	50

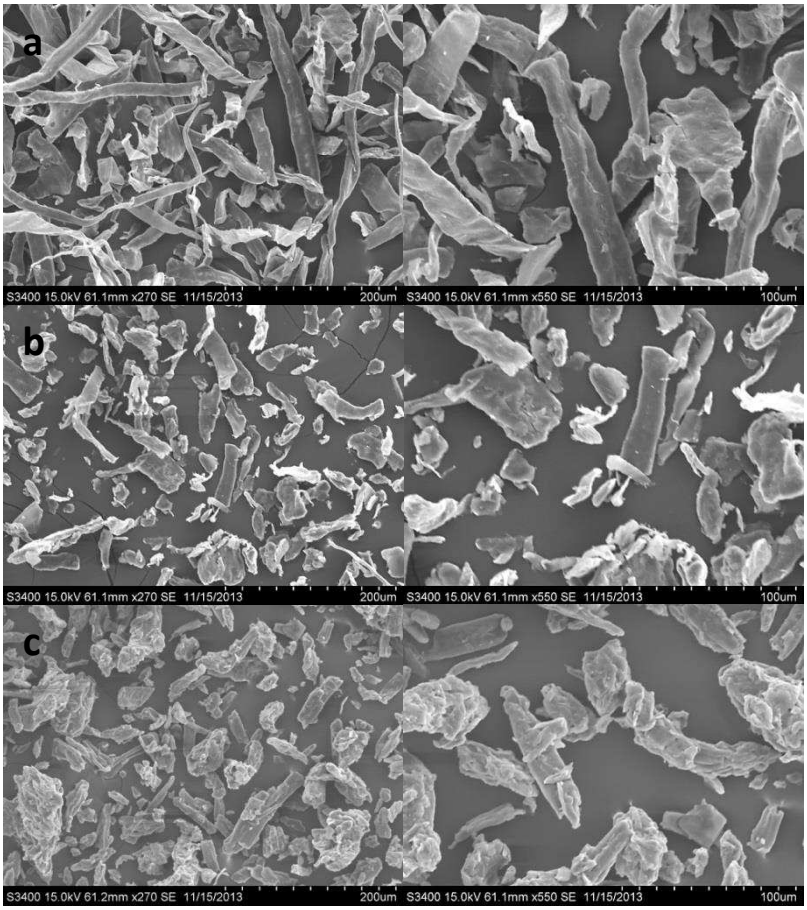

Figure 4.7 SEM micrographs of (a) CF (b) CP and (c) MCC at different magnifications.

The cell size of the foams containing CF at a ratio of 1:2 galactomannan:cellulose is smaller than the pure galactomannans foams (Figure 4.8). The addition of cellulose increases the solids content of the foams which will result in more sites for ice nucleation. During ice crystal growth the fibres appear to have been forced into the fenugreek cell wall sheets. The cellulose fibres are not aligned in either of the polysaccharide foams as there was no directional freezing.

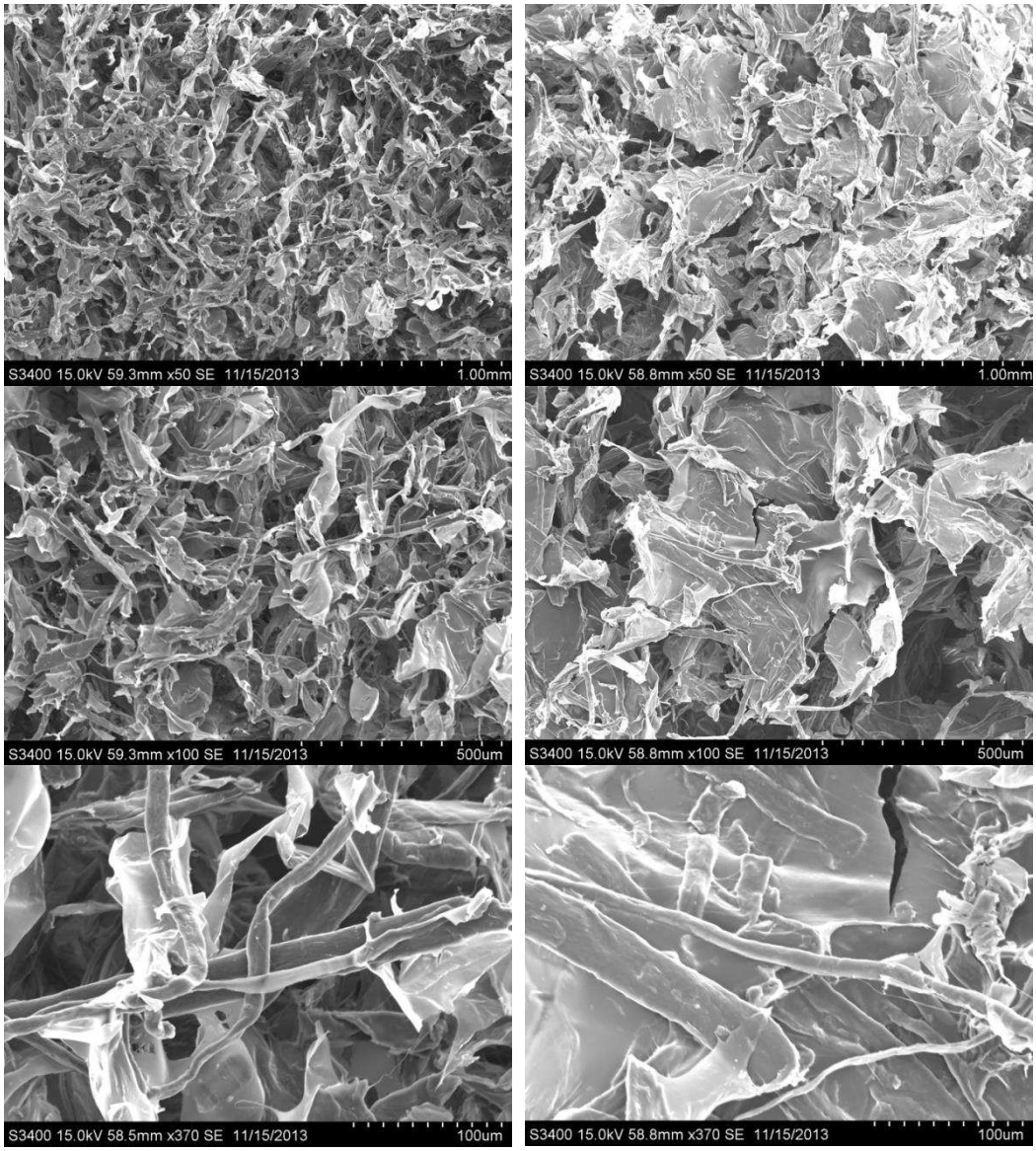

Figure 4.8 SEM micrographs of LBG (left) and fenugreek (right) foams with a 1:2 galactomannan:cellulose content.

A series of cellulose concentrations were added to the polysaccharide foams. Figure 4.9 shows typical stress strain curves for fenugreek foams with increasing content of MCC.

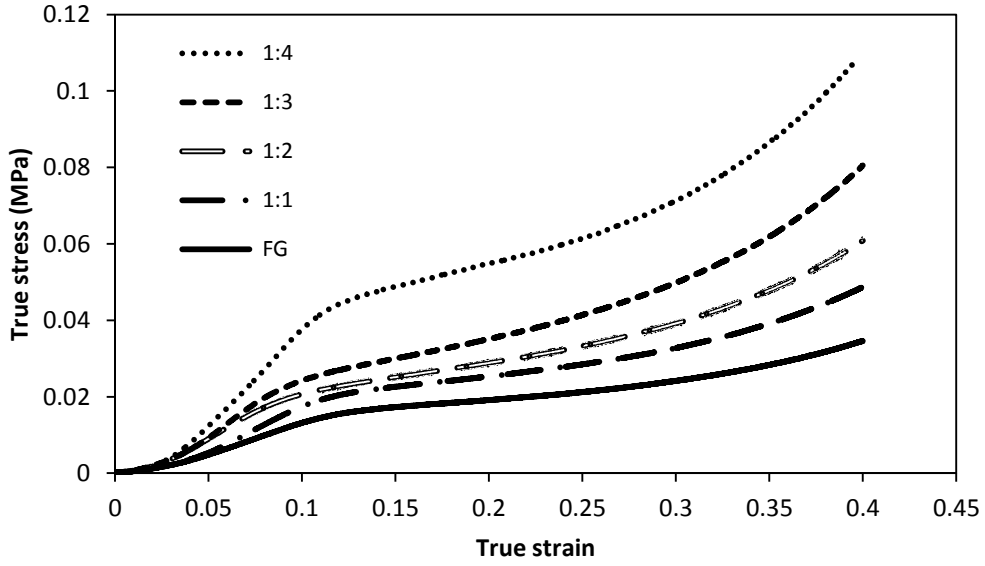

Figure 4.9 Typical stress strain curves for the fenugreek foams filled with MCC. The ratios represent the fenugreek:cellulose content, so 1:4 has four times as much cellulose filler as fenugreek matrix.

After compression both the fenugreek and LBG foams lose about 19% of their height (Figure 4.10). The plateau region of the foams is between a true strain of 0.15 and 0.25 (Figure 4.9) and at higher strain the foams begin to enter the zone of densification where the cell walls begin to buckle and touch during compression. When the compressive load is released, some of the cell walls are still adhered resulting in the foams being unable to spring back to their original height.

The height loss of both the LBG and fenugreek foams increases with increasing MCC concentration whilst both CP and CF have a much smaller impact on height loss (Figure 4.10). It might be expected that the foams containing MCC reach the level of densification before the other cellulose containing foams resulting in there being less spring back, however, when the 1:4 glactomannan to cellulose containing foams are compared, densification starts at the same strain value for each type of cellulose

(Figure 4.11). The difference is therefore likely to not be due to when densification occurs.

In the plant cell wall hemicelluloses bind to the surface of cellulose fibrils and act as tethers (Kiemle *et al.*, 2014). In Chapter 6 we will show that both LBG and fenugreek bind to the surface of CF and MCC in water, however, when the solvent is changed, whilst LBG still binds to the surface of CF it appears to be bound to MCC to a much lower level which may be due to its higher crystallinty (i.e. less regions available for hydrogen bonding). MCC has been shown to have weaker interactions with PLA compared to wood fibre (Mathew *et al.*, 2005). The authors proposed that the better interaction may have been due to greater roughness of the wood fibre. Other studies have shown that increasing the surface roughness of natural fibres increases the interaction with matrix polymers (Valadez-Gonzalez *et al.*, 1999, Herrera-Franco and Valadez-Gonzalez, 2005, Faruk *et al.*, 2012). A combination of lower surface roughness and higher crystallinity may therefore result in a lower interaction between MCC and the galactomannans than CP.

To produce the foams the galactomannans and celuloses were first mixed in water so there is likely to have been some interaction. It is unclear however, what effect the drying process would have on this interaction, although it might be assumed that the interaction between the galactomannan and cellulose will still be present as galactomannans are sometimes used in paper manufacture due to their fibre bonding ability (Prajapati *et al.*, 2013). If MCC is less tightly bound to the galactomannan matrix, during compression it will be able to move more freely. When the compression is then removed the MCC which has moved will inhibit the foams from springing back (Figure 4.10a). CP, which also has a low aspect ratio, similar to that of MCC (Figure 4.7), but a low crystallinity (Table 4.1) may have a higher level of

interaction with the galactomannan matrix than MCC and so only increases the height loss of the foams slightly (Figure 4.10b). CF has a much higher fibre size than either CP or MCC so is likely to have the highest flexibility and therefore does not stop the foam from regaining height after compression (Figure 4.10c).

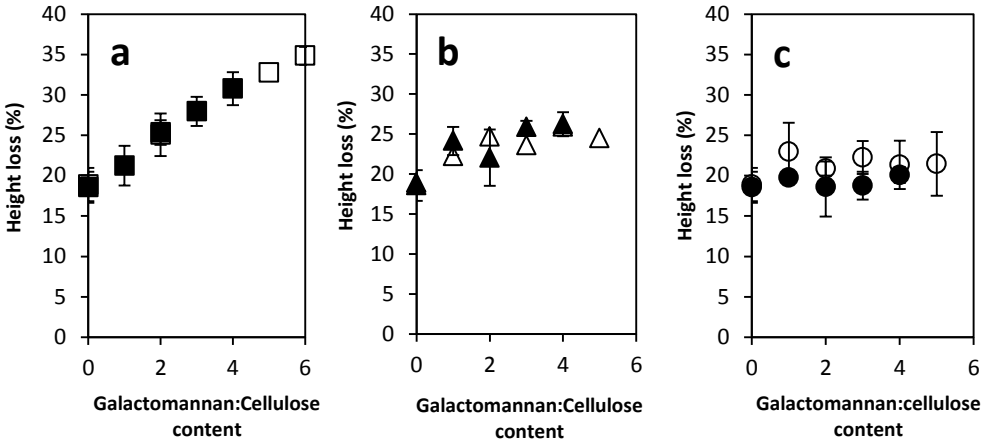

Figure 4.10 Height loss of fenugreek (solid) and LBG (hollow) foams after the compressive load is removed compared to the original height of the foams for (a) MCC (b) CP and (c) CF. The x axis represents the galactomannan:cellulose ratio.

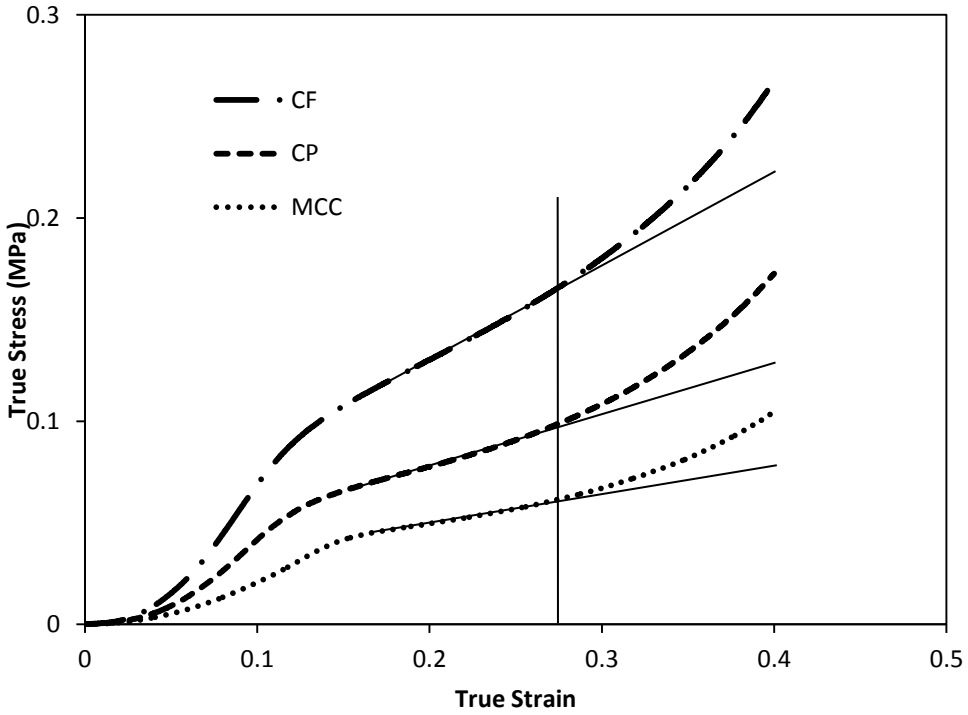

Figure 4.11 Stress strain graphs of fenugreek foams with a ratio of 1:4 fenugreek:cellulose measured with a texture analysiser. The solid lines indicate the plateau region. The vertical line indicates where densification begins.

Whilst both the pure LBG and fenugreek foams had the same height loss after compression (Figure 4.10) the maximum force required to compress the foams to a true strain value of 0.4 was greater for fenugreek compared to LBG (Figure 4.12) which may be due to its higher weight average molecular weight of 4.05 x 10^6 g/mol compared to 2.72 x 10^6 g/mol (please see the materials and methods section 4.2.1, page 99). Due to the differences in molecular weight it is difficult to see if there is any difference due to the cryogelation of LBG and it would therefore be useful in future work to use another polysaccharide of similar molecular weight to LBG to fully appreciate any differences in foam strength caused by cryogelation.

The addition of fibres to foams is known to increase their compressive modulus (Karthikeyan and Sankaran, 2004). Figure 4.12 shows that increasing cellulose content increases the maximum force required to compress the foams, however, there are differences between the celluloses. CF, which has the highest particle size and aspect ratio, provides the greatest reinforcement. It is well reported that the larger the fibre size the greater the reinforcement ability (Stark and Rowlands, 2003, Bouafif *et al.*, 2009, Migneault *et al.*, 2009). CP has a smaller particle size than CF and therefore provides lower reinforcement to the foams. MCC has a larger particle size than CP and so would be expected to provide greater reinforcement, however, this is not the case. MCC is actually composed of aggregates of cellulose crystals which can be seen in Figure 4.7. During the mixing process with the galactomannan solutions it is possible that these aggregates break up leaving the smaller individual crystals, however, disaggregation of MCC is only usually achieved by high pressure homogenisation (Kleinebudde *et al.*, 2000, Lee *et al.*, 2014) so it unlikely that the bench top mixer would induce sufficient shear to disaggregate the MCC, indeed, Mathew *et al.* (2005) found that even after extrusion, MCC remained as aggregates of crystalline fibrils.

As described above, the interaction between MCC and the galactomannan matrix may be weaker than that of CP. The better adhesion will result in the filler being able to provide greater reinforcement. The influence of filler/matrix interaction, which can depend on the size of the interface, strength of the interaction, filler anisotropy and filler orientation, on the strength of composites has been widely studied (Pukanszky, 1990, Dittenber and GangaRao, 2012, Dicker *et al.*, 2014).

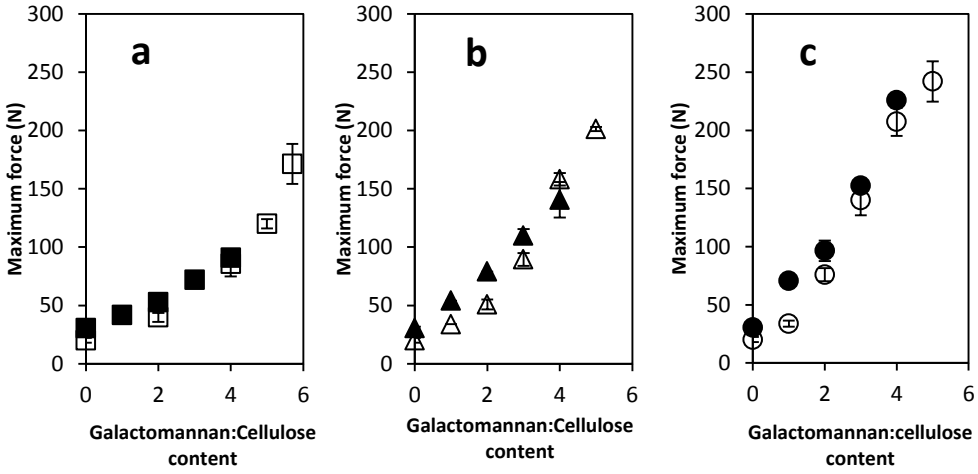

Figure 4.12 The maximum force required to compress fenugreek (solid) and LBG (hollow) foams to a true strain of 0.4 for (a) MCC (b) CP and (c) CF measured with a texture analyser. The x axis represents the galactomannan:cellulose ratio.

Young's modulus is a measure of stiffness. Fenugreek forms a stiffer foam than LBG even though it does not gel during freezing which again may be due to its higher molecular weight with a Young's modulus of 0.16 MPa compared to 0.09 MPa for LBG.

Mikkonen *et al.* (2014) prepared freeze dried polysaccharide foams from 1 wt% solutions, with guar (molecular weight 2600 kDa) and xyloglucan (molecular weight 1300 kDa) foams having compressive moduli of between 2 and 22 kPa.

The stiffness of the foams follows a similar trend to that of maximum force where increasing cellulose content increases the Young's modulus (Figure 4.13) which is consistent with previous reports of fibre composites (Bouafif *et al.*, 2009, Bledzki and

Gassan, 1999, Mukherjee and Kao, 2011, Bergeret and Benezet, 2011). There are larger differences between the galactomannans with LBG + cellulose foams being considerably less stiff than the fenugreek counterparts. This may be again due to the fenugreek's higher molecular weight.

Although CP had a greater reinforcing effect than MCC when compared using maximum force (Figure 4.12) they both impart the same level of stiffness to the foams with comparable value of Young's modulus (Figure 4.13). Young's modulus is measured during the initial linear region so particle size may be a more important factor.

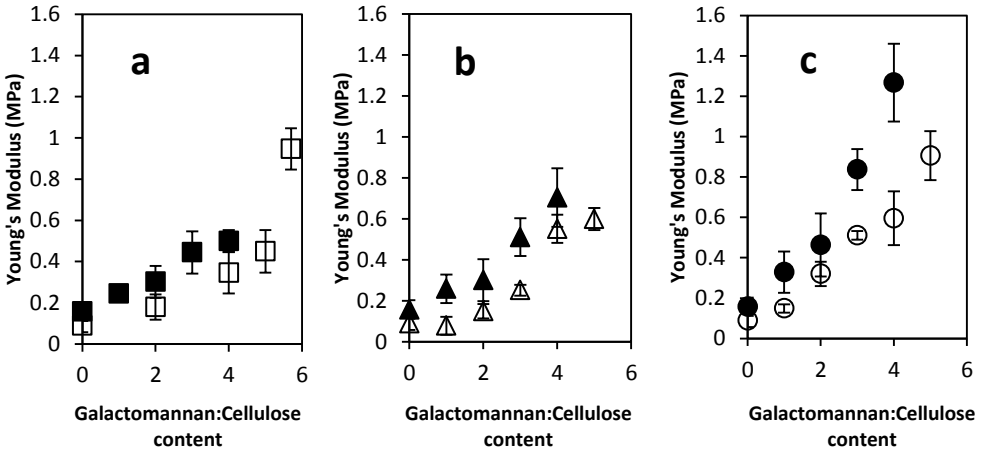

Figure 4.13 The Young's modulus of fenugreek (solid) and LBG (hollow) foams for (a) MCC (b) CP and (c) CF. The x axis represents the galactomannan:cellulose ratio.

The bulk modulus is proportional to the level of solids in the suspensions prior to freezing (Figure 4.14). By looking at the bulk density and Young's modulus of the foams, comparisons can be made with other polymer foams. Nussinovitch *et al.* (2004) produced freeze dried aerogels from 2 wt% agar solutions which had Young's modulus values of 0.2 MPa. The fenugreek foam in the present work compares favourably to this with a foam produced from a 1 wt% solution having a Young's modulus of 0.15 MPa (Figure 4.14). Sharma *et al.* (2013) produced freeze dried carrageean-gelatin cryogel matrices that regained their orginal lengh after 90%

compression. The Young's modulus of the cryogels with a density of 0.00207-0.00266 g/cm^3 was in the range of 4-11 kPa when measured dry. Surapolchai and Schiraldi (2010) produced cellulose aerogels by freeze drying sonicated MCC dispersions of between 5-10 wt%. They found that the modulus increased with increasing density, with 5 wt% solids giving a density of 0.056 g/cm^3 and a modulus of 17 kPa while foams with a solids content of 10 wt% had a density of 0.106 g/cm^3 and a modulus of 120 kPa. The authors found that by chemically modifying MCC by carboxymethylation the modulus of compression could be increased from a modulus of 120 kPa to 3442 kPa for foams with comparable densities.

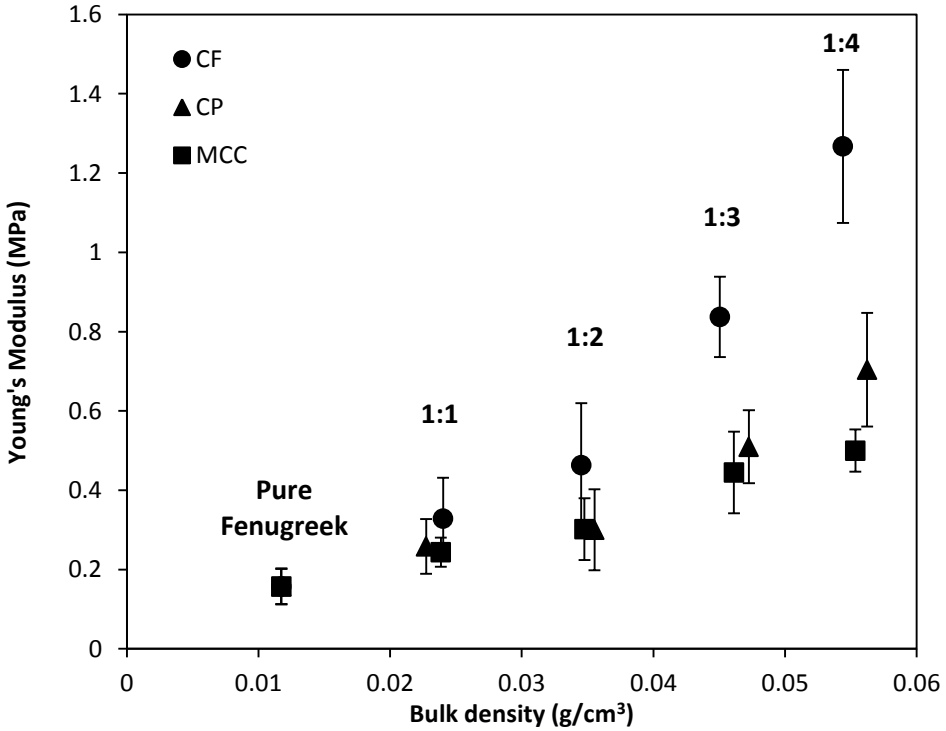

Figure 4.14 The Young's moduli of fenugreek foams against their bulk density for CF (circles), CP (triangles) and MCC (squares). The fenugreek:cellulose content are shown above.

Galactomannans and cellulose are highly hydrophilic so will absorb a high level of moisture. The foams were equilibrated for 7 days over saturated salt solutions to different relative humidities (RH). At a RH of 97% both the LBG and fenugreek foams shrink significantly whereas at 43% RH there is only slight shrinkage (Figure 4.15). The LBG foams shrink to a greater extent than the fenugreek foams. When CF is

incorporated at a ratio 1:4 (galactomannan:cellulose) the foams no longer shrink as the cellulose maintains the shape of the foam (Figure 4.16). Other fillers such as starch have been shown to reduce shrinkage of foams (Rassis *et al.*, 1998, Rassis *et al.*, 2002).

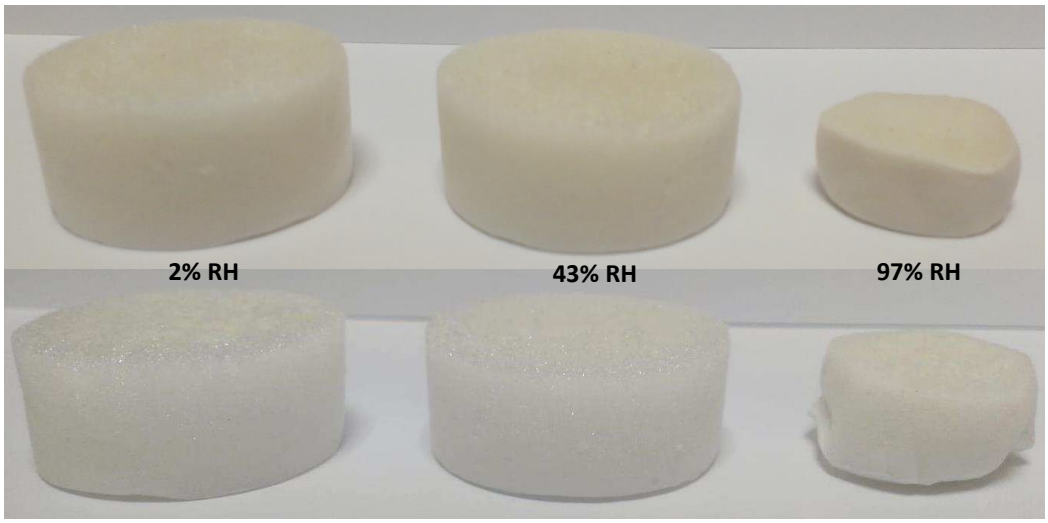

Figure 4.15 Galactomannan foams equilibrated at different RH, LBG (top) and fenugreek (bottom).

Figure 4.16 Foams at 97% RH LBG (top) and fenugreek (bottom) with pure galactomannan on the right and galactomannan + CF at a ratio of 1:4 on the left.

As the RH increases the foams absorb more water (Figure 4.17). Due to the higher solids content, the foams containing cellulose are able to absorb a greater amount of water than the pure galactomannan foams by weight (Figure 4.17a), however, as a percentage of the total increase, the pure galactomannan foams absorb more water

at an RH of 97% (Figure 4.17b). The pure fenugreek foams absorb a much larger amount of water compared to LBG at an RH of 97% which may indicate the more unstructured nature of fenugreek as it did not form a cryogel.

Due to the pure foam's high water uptake and shrinkage, when compressed, they are unable to spring back so lose much of their height (Figure 4.17c). The maximum force and Young's modulus of the foams are reduced with increasing water uptake (Figures 4.17d and 4.17e). Even though there is no shrinkage for the foams containing cellulose their mechanical properties are greatly impaired at high RH due to the hydration of the matrix. When the galactomannan foams were immersed in water they quickly dispersed, including those containing cellulose.

Sisal/polyester composites were reported to lose up to 13-31% of their strength when fully immersed in water compared to 95% RH (Dittenber and GangaRao, 2012). Other natural fibres such as flax and coir have also been shown to reduce in tensile strength with increased water absorption (Symington *et al.*, 2009).

A possible method in the future to reduce the level of moisture uptake and therefore increase the stability of cellulose based foams could be to waterproof the fibres and so decrease water absorbance. This can be achieved by wetting them with ethyl-cyanoacrylate monomer solutions containing inorganic nanoparticles and so encapsulating the fibres with a hydrophobic shell (Bayer *et al.*, 2011). This also leads to some antimicrobial activity. It would be of great interest to see if this method could also waterproof the galactomannan foams.

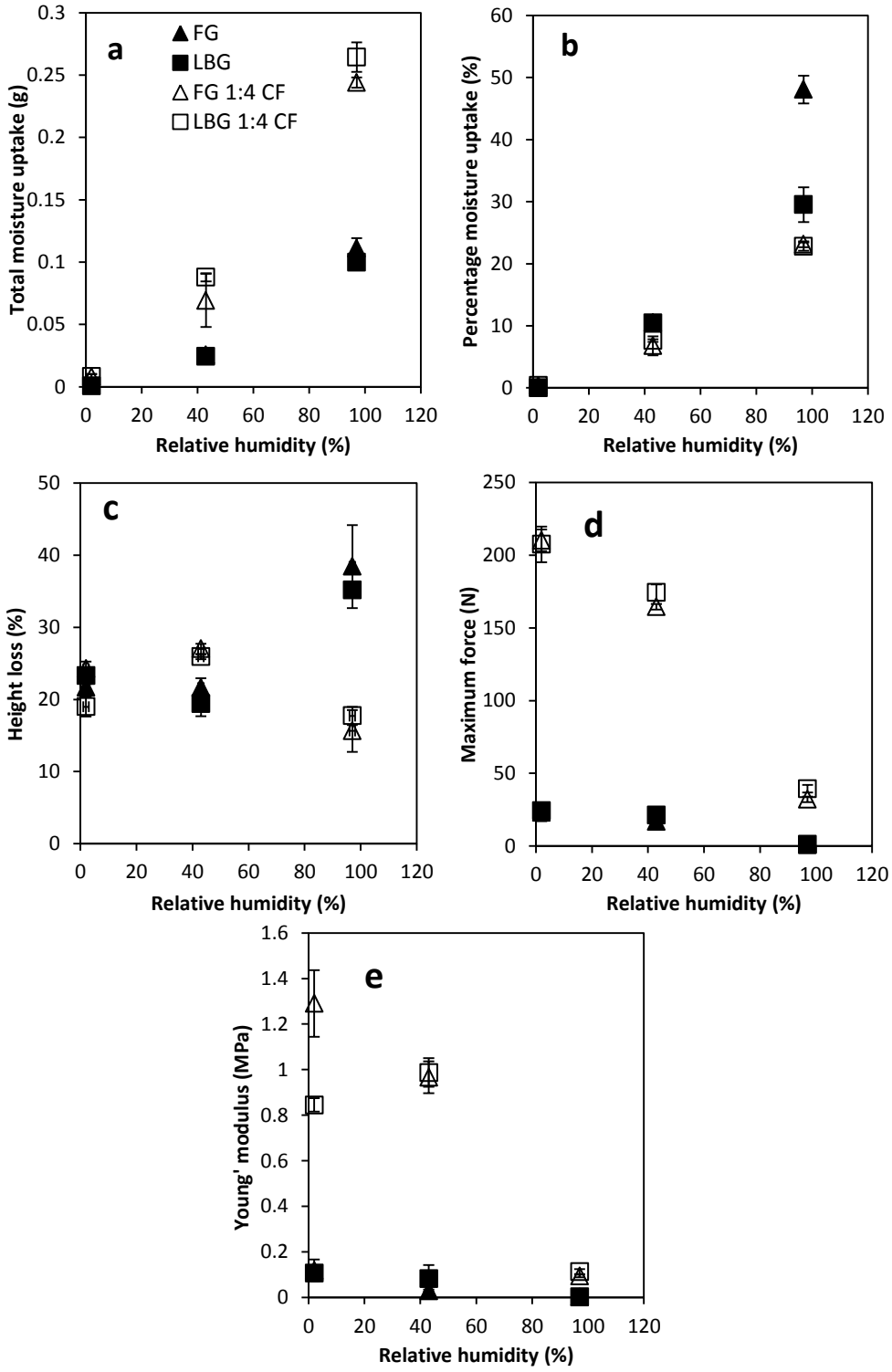

Figure 4.17 Polysaccharide foams equilibrated at different RH with (a) total moisture uptake (b) percentage moisture uptake (c) height loss (d) maximum force and (e) Young's modulus, showing pure galactomannan foams (solid symbols) and 1:4 galactomannan:cellulose (hollow symbols).

Microfibrillated cellulose (MFC) was produced by repeated passes of CP through a homogeniser, where the high shear and pressure peels away the microfibrils, greatly

increasing the surface area of the cellulose (Figure 4.18) (Spence *et al.*, 2011). Even at low concentrations (e.g. 1 wt%) MFC will from stable dispersions that have a high viscosity and do not sediment (Klemm *et al.*, 2011). MFC therefore has a much higher phase volume and space filling capacity than its original cellulose. A major drawback of using MFC is that it must be utilised in its wet state or the fibrils will aggregate upon drying (Peng *et al.*, 2012).

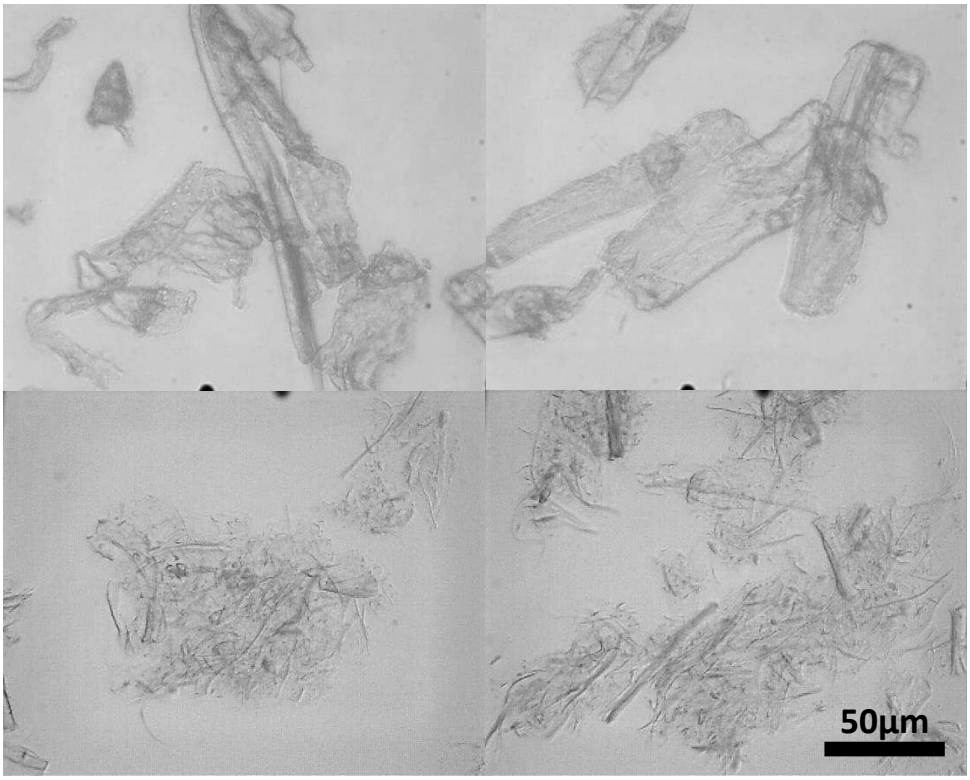

Figure 4.18 Light micrographs of CP before (top) and after (bottom) high pressure homogenisation.

MFC is able to reinforce LBG foams to a greater extent than CF at much lower concentrations due to the fibrillated network and higher surface area (Figure 4.19) (Nakagaito and Yano, 2005, Siro and Plackett, 2010). Zimmermann *et al.* (2010) found that fibrillated cellulose produced composites that had higher tensile strength and stiffness compared to the fibres from which they were produced. Homogenous fibrillation was more important for the mechanical properties than the degree of polymerisation (DP) of the cellulose. Svagan *et al.* (2010) produced freeze dried starch foams that contained up to 70 wt% MFC which had a combination of open and

closed cells and had negligible shrinkage. Unfortunately due to problems with equipment there was insufficient material to test with fenugreek foams.

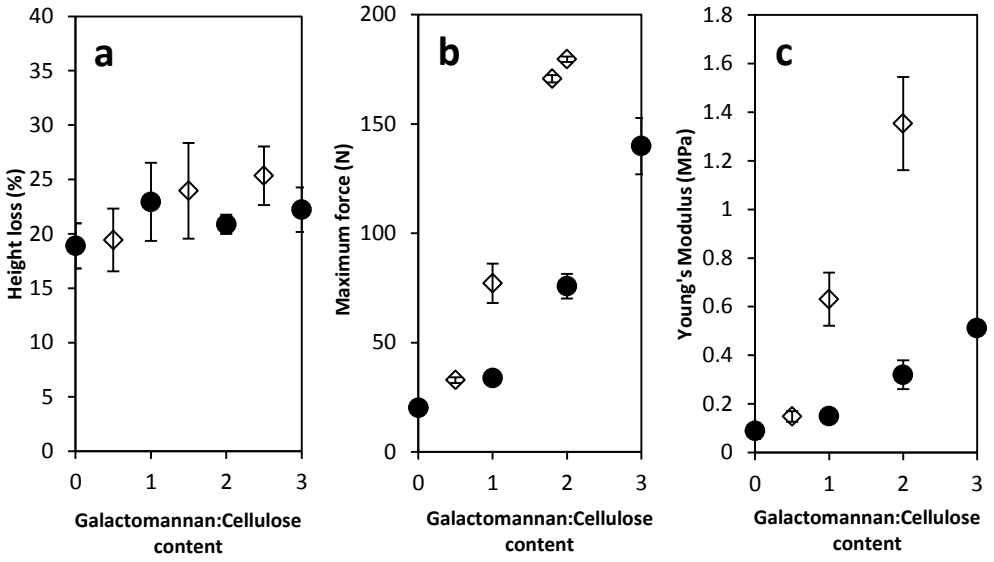

Figure 4.19 The (a) height loss (b) maximum force and (c) Young's modulus of LBG and MFC (hollow diamonds) and LBG and CP (solid circles) foams measured using a texture analyser. The x axis represents the galactomannan:cellulose ratio.

MFC is generally produced using high pressure homogenisation which is a highly energy intensive process. Pre-treatments such as TEMPO oxidation (Saito *et al.*, 2007), carboxymethylation (Eyholzer *et al.*, 2010b), enzyme treatment (Zhu *et al.*, 2011) and other mechanical pretreatments such as cryo-crushing and milling (Sandquist, 2013) have been used to reduce the energy needed to fibrillate cellulose. However, there has been little work to date on using extrusion as a method for cellulose fibrillation (Backfolk *et al.*, 2010).

To assess the viability of using extrusion to fibrillate cellulose, CF was passed through an extruder (Figure 4.20) with excess water at 90^{o}C. There were difficulties, for instance, the extruder did become blocked as the cellulose dried out at the end of the barrel due to water evaporating (Figure 4.21). Extrusion was partially succesful at fibrillating cellulose as can be seen in the micrographs of Figure 4.22 where the fibres have become "hairy" which was caused by the high shear forces in the extruder. The

fibrillation is not as extensive as that produced by high pressure homogenisation (Figure 4.18), but it is possible that with a longer barrel and repeated passes there would have been greater fibrillation, however, this initial experiment demonstrated that fibrillation is possible through extrusion. For future trials it would be useful to use a series of temperatures to identify if heating is necessary. When the extruded cellulose was dried most of the separated fibrills collapsed due to a process of hornification and the fibres clumped together (Figure 4.23).

Figure 4.20 The Clextral extruder used for the initial fibrillation experiments.

Figure 4.21 The extruder screws became blocked as the cellulose dried towards the end of the barrel.

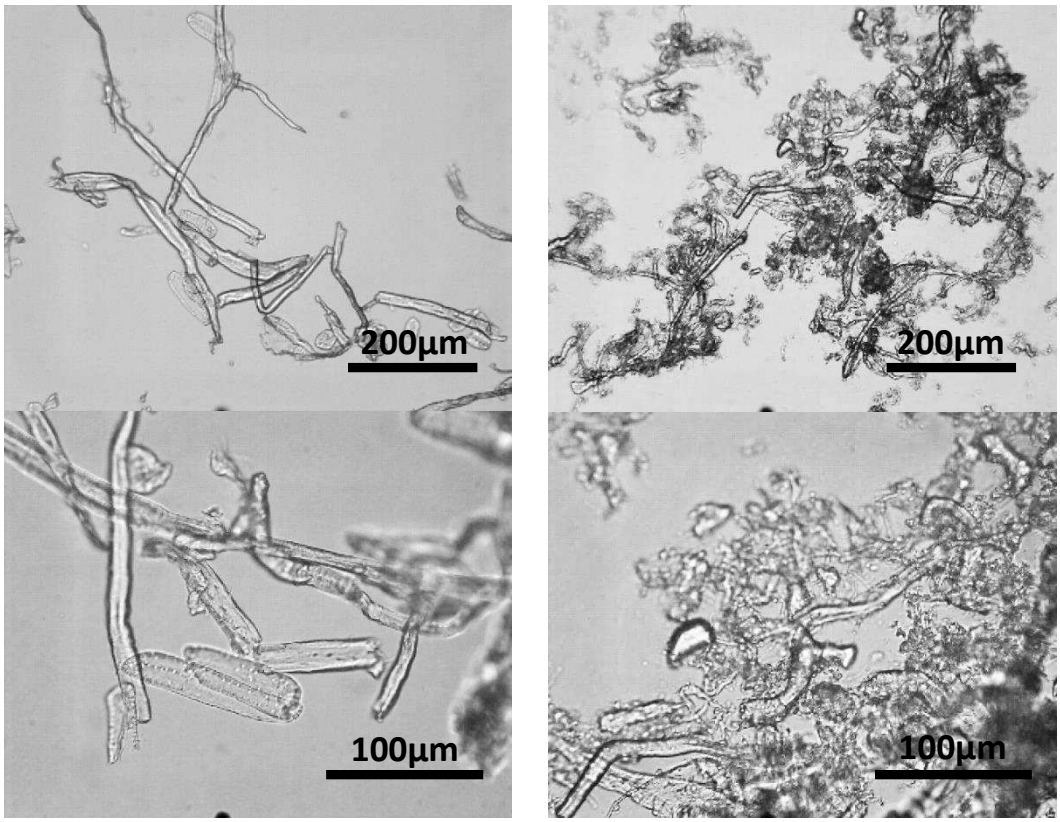

Figure 4.22 Light micrographs of CF before (left) and after (right) extrusion. The extruded CF had not been dried.

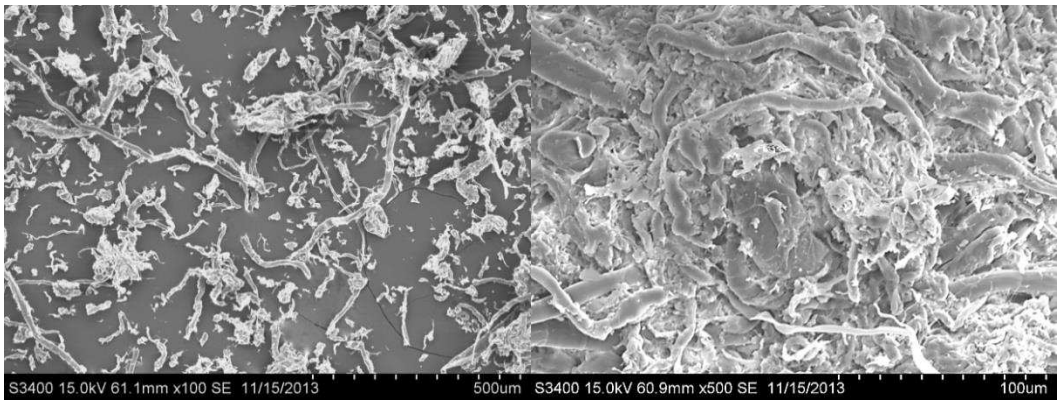

Figure 4.23 SEM micrographs of dried extruded CF.

Whilst freeze drying produces good foams it is both a costly and time intensive process (a week to produce a batch of foams). Extrusion is an alternative route to creating foam structures. Unfortunately, as extrusion is on a much larger scale, we were unable to secure sufficient quantities of the galactomannans. However, to

investigate extrusion as a method for cellulose reinforced foam production, starch was used as a matrix polymer.

Extrusion has been used in the food industry since the 1930s to produce pasta and later cooked extruded products such as expanded starch snacks. Modern starch extrusion literature often refers to thermoplastic starch (TPS) which is produced by extruding starch and a plasticiser at temperature of between 140-160^{o}C at high pressure and high shear. With plasticiser levels greater than 15-20 wt% TPS can be repeatedly softened and moulded (Carvalho, 2013). When the processing temperature is above 100^{o}C water will volatize resulting in an expanded material. This can be desirable if producing impact bearing materials such as foam packaging. Besides water, other low molecular weight plasticisers can be used, for instance urea, fructose, xylitol, sorbitol, maltitol, glycols and most commonly glycerol (vanSoest *et al.*, 1996, VanderBurgt *et al.*, 1996, Lourdin *et al.*, 1997, Gaudin *et al.*, 1999). By replacing water with another plasticiser the gelatinisation temperature is increased (Perry and Donald, 2000). Any crystalline order in the starch is destroyed during extrusion but, due to the mobility of the starch chains some recrystallisation will occur depending on the plasticiser content and temperature stored. This can result in TPS products becoming brittle over time.

The poor mechanical properties and water solubility of TPS materials can be greatly improved by using TPS as the matrix phase in composites. The addition of cellulose fibres should help reinforce TPS.

A key factor in extrusion is the water flow rate. Lowering the flow rate will greatly increase the specific mechanical energy (SME) (Figure 4.24) which is a measure of the energy per mass unit that is transferred to the material by mechanical imput during

extrusion (Domenech *et al.*, 2013). However, if the water flow rate was decreased too much the extruder became blocked (Figure 4.25).

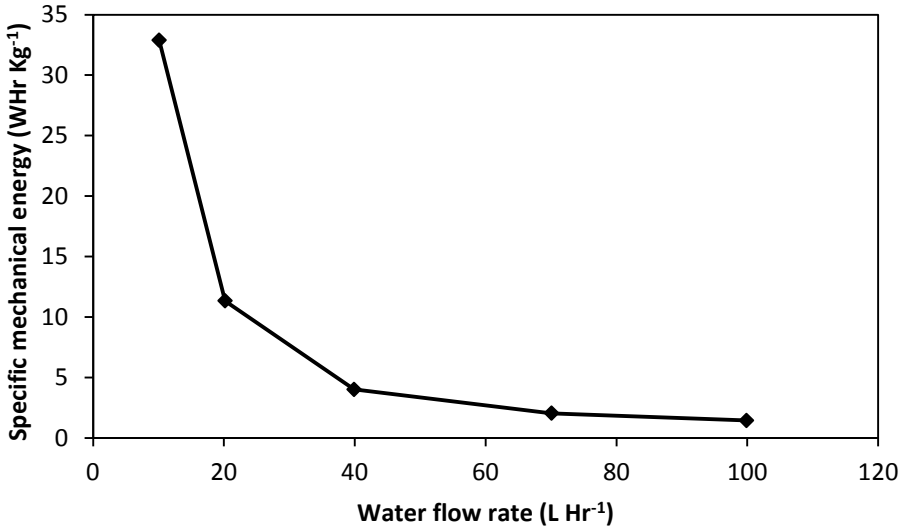

Figure 4.24 The specific mechanical energy at the die of the extruder of 70 wt% starch + 30 wt% CF at different water flow rates.

Although cellulose had been fibrillated when extruded on its own, when added to starch there was no fibrillation as the starch acted as a plasticiser/lubricant (Figure 4.26). The addition of cellulose did substantially change the structure of the starch extrudate (Figure 4.27) as the diamter of the extrudate was much decreased (Figure 4.28). Figure 4.29 shows that the cellulose fibres restricted the growth of the cells (bubbles caused by the expansion and evaporation of water at the extruder die). This effect has previously been observed by Bergeret and Benezet (2011) who described the decrease in cell size as due to the addition of fibres increasing the viscosity of the starch system. The addition of cellulose did not affect the water uptake for extrudate samples equilibrated to different RH (Figure 4.30).

Figure 4.25 The screws of the extruder became blocked at low water flow rates.

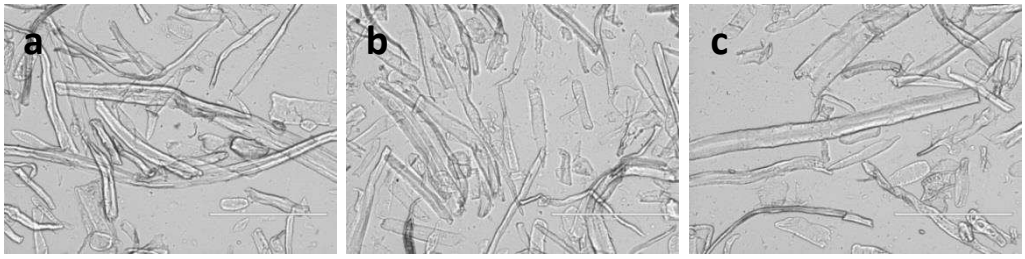

Figure 4.26 Light micrographs of 70 wt% Starch + 30 wt% CF after extrusion (a) 99.9 L Hr^{-1} water (b) 70.1 L Hr^{-1} water (c) 39.9 L Hr^{-1} water.

Figure 4.27 Extruded foams of 70 wt% starch + 30 wt% CF (top) and pure starch (bottom).

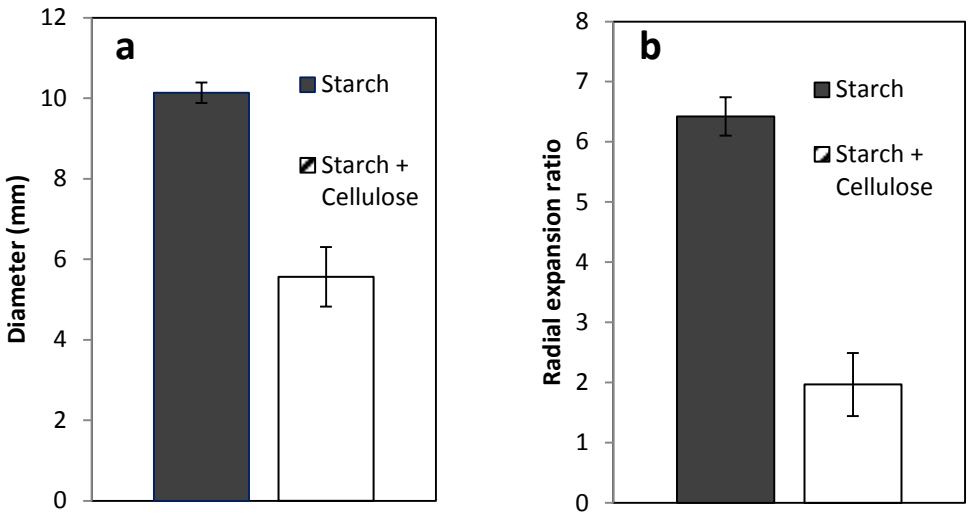

Figure 4.28 The (a) diameter and (b) radial expansion ratio of pure starch and 70 wt% starch + 30 wt% CF extrudates.

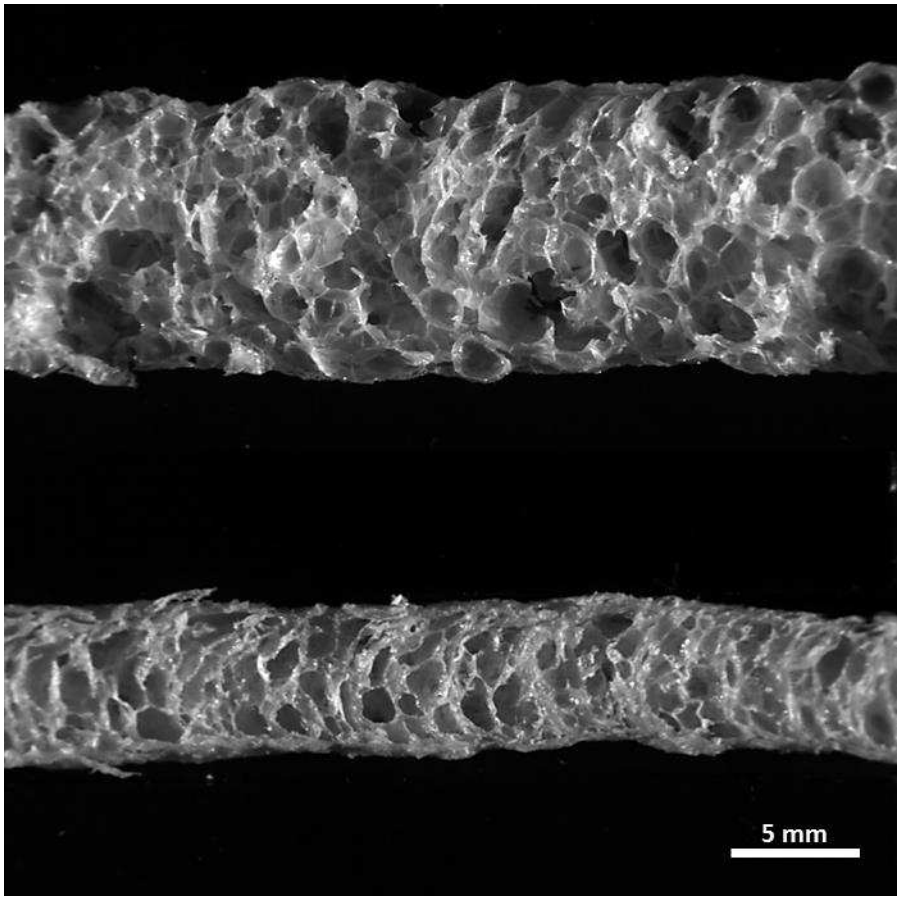

Figure 4.29 C Cell images of pure starch (top) and 70 wt% starch + 30 wt% CF (bottom) extrudates.

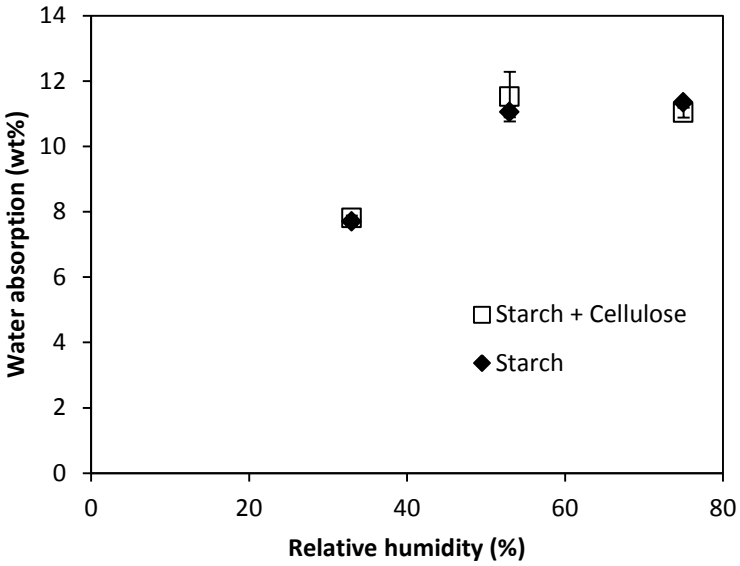

Figure 4.30 Water absorption at different RH of pure starch and 70 wt% starch + 30 wt% CF extrudates.

Further trials to produce foams were conducted on a capillary rheometer which consists of a heated tube with a piston which forces the contents of the tube through a capillary die at the base at varying shear speeds and is often used to model the shear within an extruder. Low molecular weight hydroxypropylcellulose (HPC), which is able to form a polymer melt at about 80^{o}C was used as the matrix material and cellulose at different concentrations was added. The low moisture content present in the cellulose was sufficient to act as a foaming agent when the sample was extruded at 140^{o}C. Continuous HPC + MCC foams were produced (Figure 4.31), even with 0.5 mm capillary die diameter (Figure 4.32). Zimmermann *et al.* (2004) have found that by incorporating just 5 wt% MFC into HPC composites there was a fivefold increase of the elongation to rupture.

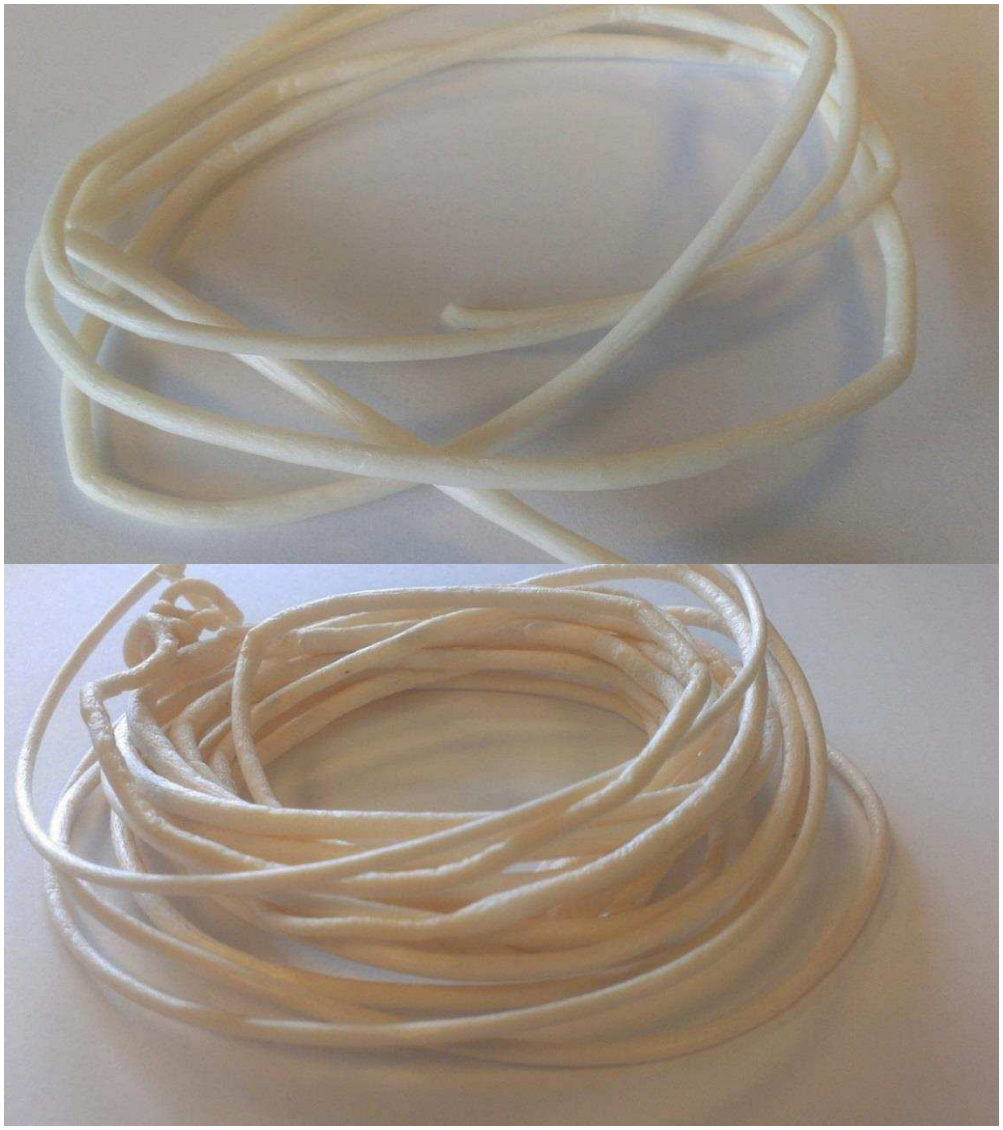

Figure 4.31 70 wt% HPC + 30 wt% MCC extrudate from the capillary rheometer.

Figure 4.32 70 wt% HPC + 30 wt% MCC extrudate from the capillary rheometer using a 0.5 mm diameter capillary die.

4.4 Conclusion

LBG gels during the freezing process (cryogelation). Whilst there were some observable differences in the morphology between the LBG and fenugreek foams, the cryogelation did not improve the foam strength with fenugreek producing slightly stronger and stiffer foams which is possibly due to its higher molecular weight. The pure polymer foams had a low density and low stength which could be improved considerably with the addition of cellulose acting as a filler. A high content of cellulose (at least 1:6 galactomannan:cellulose content) could be introduced to form stable structures. Increasing cellulose content increased the strength and stiffness of the polysaccharide foams with CF providing the greatest level of reinforcement which may have been due to its larger fibre size. CF provided a higher level of reinforcement than MCC which may be attributed to its lower crystallinity and surface roughness and so possibly higher matrix/fibre interactions. Both galactomannans foams absorbed a large amount of water at high RH which dramatically reduced their strength and stiffness. The addition of cellulose reduced shrinkage. MFC reinforced the foams to a much greater extent than the fibres, possibly due to its higher surface area and fibrilated structure. Extrusion was shown to fibrillate cellulose but more work is needed to find the best process parameters. Extrusion is also a useful process to produce cellulose reinforced starch foams.

Chapter 5. Cellulose in LiCl/urea/water

5.1 Introduction

Cellulose is insoluble in water and most common solvents, which is commonly attributed to its extensive intermolecular hydrogen bonding. To be able to use cellulose it is often dissolved and then regenerated to form regular fibres such as viscose and rayon. The solvents commonly used, such as carbon disulphide, are bad for the environment (Zhu *et al.*, 2006). Ionic liquids, which are commonly defined as salts that have a melting point below the boiling point of water, are 'greener' alternatives due to their ease of recycling, low vapour pressure, chemical stability and inflammablitiy (El Seoud *et al.*, 2007). The most commonly used ionic liquid is *N*-methylmorpholine *N*-oxide (NMMO), which has been used since 1987 in the production of Lyocell (under the trade name of Tencel by Courtaulds) (Borbély, 2008). Other ionic liquids that are gaining wider use in research include LiCl/*N*,*N*-dimethylacetamide (DMAc), LiCl/1,3-dimethyl-2-imidazolidinone (DMI) and DMSO/paraformaldehyde (PF) (Zhang *et al.*, 2005, Nishino *et al.*, 2004, Tamai *et al.*, 2004, Masson and Manley, 1991).

Molten salt hydrates are similar to ionic liquids but contain water which is tightly bound to the inner coordination sphere of the cation (Leipner *et al.*, 2000). Some inorganic molten salt hydrates are able to completely dissolve cellulose such as $LiClO_4 \cdot 3H_2O$, $LiSCN \cdot 2H_2O$, $ZnCl_2 \cdot 3H_2O$ and $(NCS)_2 \cdot 3H_2O$ (Zhang *et al.*, 2005, Fischer *et al.*, 2003, Xu and Chen, 1999, Fischer *et al.*, 1999) whilst other are only able to swell cellulose, such as $LiCl \cdot 2\text{-}5H_2O$, $LiNO_3 \cdot 2H_2O$ and $ZnCl_2 \cdot 4H_2O$ (Fischer *et al.*, 2003). Molten salt hydrates have also been shown to be non-derivatising (Lu and Shen, 2011) and are also inexpensive, nontoxic and easier to prepare than other non derivatising cellulose solvents (Sen *et al.*, 2013).

Swelling treatments are often employed in the textile industry as they can enhance the reactivity and accessibility of cellulose, change its pore structure to aid dye retention and help shape its structure (Jaturapiree *et al.*, 2008). In general, swelling is achieved using an alkali such as NaOH (Cuissinat and Navard, 2006). Recent work has shown that a mixture of LiCl, urea and water is able to swell cellulose to the same extent as NaOH (Tatarova *et al.*, 2010). Alkali sensitive reagents may therefore be used during the swelling treatment. The solution is noncorrosive, so reverse osmosis can be used for the recycling of LiCl and urea resulting in a lower toxicity of process effluents.

The interaction between lithium and cellulose was first investigated by Morgenstern *et al.* (1992) using ^{7}Li NMR. They showed there was increasing shielding of the ^{7}Li nuclei with increasing cellulose concentration indicating direct interactions between cellulose hydroxyl groups and lithium cations. Using ^{13}C NMR to analyse cellulose dissolved in $LiClO_4 \cdot 3H_2O$, $LiSCN \cdot 2H_2O$ or $ZnCl_2 \cdot 4H_2O$, Leipner *et al.* (2000) showed there was higher shielding of all the cellulose carbons except C_6 compared to cellulose dissolved in either $NaOH/H_2O$ or LiCl/DMAc which again indicated solvent cellulose interactions. This was further investigated by Brendler *et al.* (2001) using ^{7}Li NMR for a number of lithium salt hydrates. They found that the salt hydrates with less shielded lithium nuclei were only able to swell cellulose and not dissolve it. Recording ^{7}Li-^{1}H HOESY (Heteronuclear Overhauser Effect SpectroscopY) spectra, they also showed that cellobiose was part of the first coordination sphere of the lithium cation.

Some authors suggest that the amount of water present in the inner coordination sphere of the metal cation is the deciding factor in whether the molten salt hydrate will dissolve or only swell cellulose (Lu and Shen, 2011), for instance $ZnCl_2 \cdot 3H_2O$ will

dissolve bacterial cellulose whilst $ZnCl_2 \cdot 2H_2O$ and $ZnCl_2 \cdot 4H_2O$ will only swell cellulose. However, other authors have suggested that the cellulose hydroxyl groups hydrogen bond to the water molecules directly bonded to the metal cation (Sen *et al.*, 2013).

Tatarova *et al.* (2010) developed a LiCl/urea/water solution to treat fabrics. Urea was used as a co-solvent so that both urea and cellulose act as ligands for the lithium cation, and the urea stabilised solutions at ambient temperature. Urea has been found to significantly reduce the concentration needed of NaOH in caustic soda (Kunze and Fink, 2005). They found that the swelling of cellulose increased with decreasing water and urea content and described the mechanism of swelling as lithium-cellulose coordination complexes. The LiCl content of this solution is considerably lower than $LiCl \cdot 2H_2O$ but has similar properties and thus lowers the cost of usage (Tatarova *et al.*, 2012).

Whilst work has been done on the effect of LiCl/urea/water on type II celluloses (Tatarova *et al.*, 2010, Tatarova *et al.*, 2012), there has, as yet, been no work on the naturally occurring type I cellulose allomorph or ball milled cellulose. The following two chapters will address this and will also look at other natural plant polysaccharides in LiCl/urea/water.

5.2 Methods

5.2.1 Materials

The celluloses used in this work were cellulose fibre (CF) and cellulose powder (CP) (Solka 900FCC and 300FCC, International Fibre Corporation, USA), bacterial cellulose AxCel CG PX (CP Kelko, USA), eucalyptus pulp (Innovia, Cumbria, UK), cotton linters pulp (Shaanxi CHONYU Imp & Exp Co., Ltd, China), regenerated cellulose - Lyocell (Lenzig, Austria), and Avicel MCC type PH-101 Ph Eur (Sigma Aldrich, UK). Cotton

linters, eucalyptus and regenerated cellulose were ground for 1-2 minutes in a coffee grinder before use.

LiCl ≥99% and urea were purchased from Sigma Aldrich (UK).

5.2.2 LiCl/Urea/Water solution preparation

The swelling solution was prepared with 0.28:0.11:0.61 mol fractions of LiCl, urea and water respectively (Tatarova *et al.*, 2010). The water was added to the dry powders and stirred over heat until the solution turned clear. Any water lost as vapour when solutions were heated was replenished after the solutions were cooled. The final solution had a pH of 6.3.

5.2.3 Ball milling

The celluloses were milled using a Planetary Mill PULVERISETTE 5 at 200 rpm with 5 minutes milling followed by a 5 minute pause to allow heat to dissipate for a total milling time of 6 hours. Each pot (with zirconium balls) was filled with 10g of cellulose.

5.2.4 Rapid Visco Analyser (RVA)

The viscosity of celluloses in the swelling solution was measured using a Rapid Visco Analyzer (RVA) (Newport Scientific, Australia) with an initial shear rate of 200 rpm for 30s and then at 160 rpm for the remainder of the experiment. The initial temperature was 25^{o}C which was then increased after 5 minutes to 90^{o}C for 10 minutes (at a heating rate of 6.5^{o}C min^{-1}) and then cooled back down to 25^{o}C and held for a further 20 minutes for a total time of 45 minutes. Further experiments were run at a heating rate of 1^{o}C min^{-1} to match the DSC.

5.2.5 Light microscopy

Light microscope images were taken using a Leitz Diaplan microscope (Leica, Heidelberg, Germany) and a Pixelink PL-A600 (Ottawa, Canada) recording camera. Hot stage images were taken using a Linkam stage. Images were taken every 5 seconds and the temperature profile was the same as that used for the RVA.

5.2.6 Filtering

After the RVA treatment the cellulose samples were either washed immediately or washed after 24hrs in the swelling solution with either water or ethanol. The samples were then filtered with Whatman filter paper (Cat No 1001 090) and dried at 60^{o}C for 24 hours.

5.2.7 Wide angle X-ray diffraction

See Chapter 3, section 3.2.6, page 59.

5.2.8 Nitrogen analysis

Cellulose samples (50 mg) were weighed into the sample cells and the nitrogen content measured using a Nitrogen analyser (NA2000, Fisons Instruments, Milan, Italy). The method is based on the complete and instantaneous oxidation of the sample by combustion so the sample is converted into combustion products. The combustion gases pass through a reduction furnace and a chromatographic column to separate the gases. A thermal conductivity detector outputs a signal proportional to the concentration of nitrogen in the mixture.

5.2.9 ^{13}C Cross Polarization Magic Angle Spinning Nuclear Magnetic Resonance (CPMAS NMR)

See Chapter 3, section 3.2.7, page 60.

5.2.10 Rheology

Viscosity measurements were carried out using a Bohlin CVOR (Bohlin Instruments Ltd, Cirencester, UK), with a parallel plate (40 mm diameter, 1000 μm gap) geometry at 25^{o}C. Shear viscosity was monitored by increasing the shear rate from 0.00015 to 1000 s^{-1}. Zero shear values were obtained by using the Cross model within the Bohlin software.

Oscillatory rheology measurements were performed using a Bohlin CVO rheometer with a parallel plate geometry (40mm diameter and 1000 μm gap) at 25^{o}C. Amplitude sweeps were carried out to ensure measurements were within the linear viscoelastic region where the dynamic storage modulus (G') and loss modulus (G'') are independent of the stress amplitude. Frequency sweeps had an applied stress of 1 Pa.

5.2.11 Micro-differential scanning calorimetry (Micro-DSC)

Micro-DSC has an increased sensitivity when compared to conventional DSC due to the larger sample volume and lower scan rates. A Micro DSC III (Setaram, Caluire, France) was used which has cells made from Hastalloy which hold a volume of approximately 0.8 mL. 0.08g of starch or cellulose was weighed, followed by either water or the LiCl/urea/water solution, for a total sample weight of 0.8g. Samples were initially cooled to a starting temperature of 5^{o}C and run at rates of 1^{o}C min^{-1} up to 96^{o}C with four heating and cooling cycles. The reference cell was filled with either water or the LiCl/urea/water solution and matched for heat capacity with the sample. By ensuring they are matched, the calorimeter is balanced with the heat flow signal and is centred around the zero level, giving the most sensitive results.

5.3 Results

Six celluloses were initially used with the LiCl/urea/water swelling solution. A treatment temperature of 90°C was chosen as this had been shown to produce the highest level of swelling (Tatarova *et al.*, 2012). All celluloses showed an increase in viscosity upon cooling after the heat treatment (Figure 5.1). The possible cause of this increase in viscosity upon cooling will be discussed later in this chapter. Differences in viscosity are believed to be due to fibre size (aspect ratio), due to the higher hydrodynamic volume, (Milliken *et al.*, 1989, Djalili-Moghaddam and Toll, 2006) which can be seen in Figure 5.2.

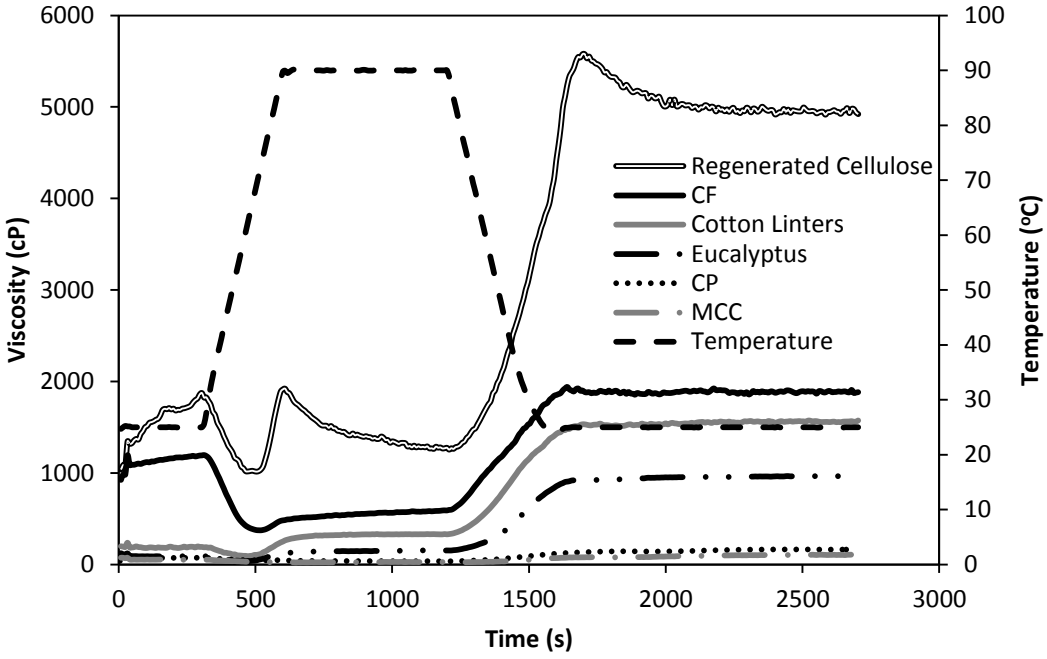

Figure 5.1 RVA viscosity profiles of celluloses in the LiCl/urea/water swelling solution at 5 wt% concentration.

Regenerated cellulose (Lyocell) clearly shows some swelling whereas it is much harder to see significant difference after treatment for the other celluloses (Figure 5.2). This may be because native cellulose does not swell to the same degree as regenerated cellulose, or more likely, it is more difficult to compare native fibres due to their natural differences in shape and size.

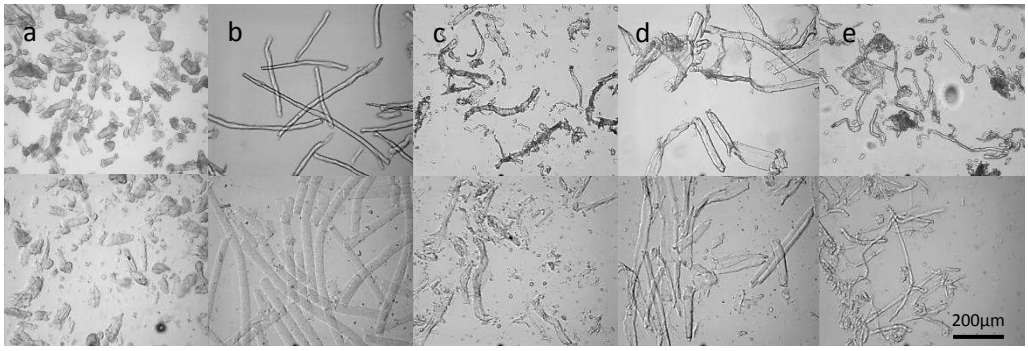

Figure 5.2 Light micrographs of celluloses before (top) and after (bottom) treatment in LiCl/urea/water (a) MCC (b) regenerated cellulose (c) cotton linters (d) CF (e) eucalyptus.

After treatment the celluloses were washed with either water or ethanol immediately or after 24 hours in the swelling solution at ambient temperature. The crystallinity of most of the celluloses decreased as a result of the treatment when washed immediately (Figure 5.3a). The ethanol washed samples had a greater reduction in crystallinity. Ethanol is not as effective as water as a solvent for either LiCl or urea. The solubility of LiCl in de-ionised water is high at 63.7g per 100 ml water compared to ethanol at only 42.4g per 100 ml water (Nayak *et al.*, 2008). This results in some of the salts still being trapped within the fibres and inhibiting recrystallisation. Nitrogen analysis confirms that less of the urea has been removed with the ethanol wash (Figure 5.4). When the fibres are left in the swelling solution at ambient temperature for 24 hours there is a greater reduction in crystallinity as the salts are able to penetrate further into the fibre and disrupt the crystal structure (Figure 5.3b).

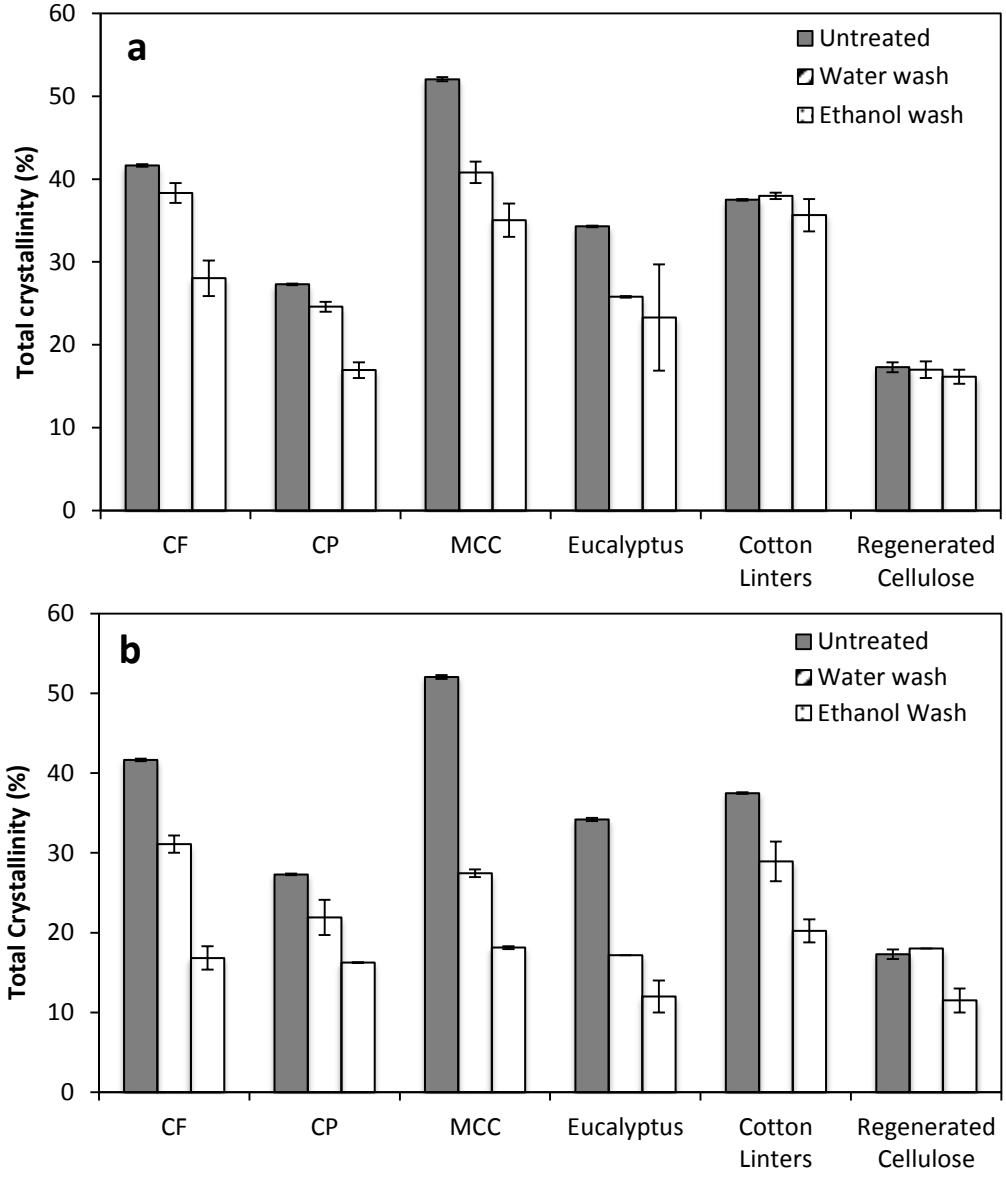

Figure 5.3 Cellulose crystallinity, measured by X-ray diffraction (XRD), after LiCl/urea/water treatment either (a) washed immediately or (b) washed 24 hours after treatment. The average of three samples is shown with error bars indicating the standard deviation.

Lyocell, Eucalyptus and cotton linters all had to be milled to prepare the samples so only microcrystalline cellulose (MCC), cellulose fibres (CF) and cellulose powder (CP) were used for later experiments so as to minimize any inhomogeneity effects.

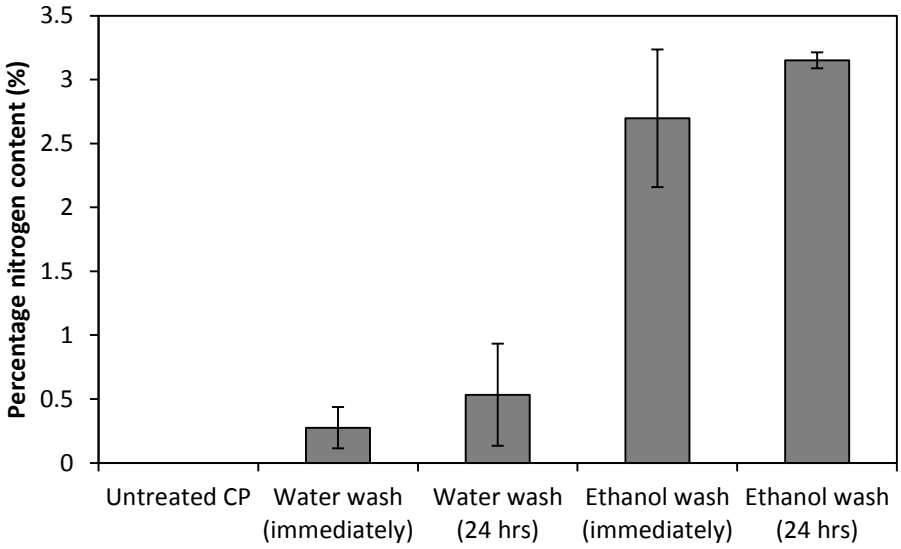

Figure 5.4 Nitrogen analysis of LiCl/urea/water treated CP which had either been washed in excess water or ethanol straight after treatment or 24 hours after treatment. The average of three samples is shown with error bars indicating the standard deviation.

Figure 5.3 shows the reduction in crystallinity when cellulose is treated for 10 minutes at 90°C (Figure 5.1). It might be expected that if cellulose is treated at 90°C for a longer time the crystallinity would decrease, however this was not the case (Figure 5.5). MCC was treated for different times at 90°C. The crystallinity of the MCC does not decrease between 10-90 minutes at 90°C. There is also no change in the final viscosity of the dispersions after treatment. Tatarova and Foster (2010) found that whilst the fibre diameter of cotton fibres slightly increased with heat when treated for 1 hour, there was little difference after 10 days. They also found that an increase in the temperature of the treatment resulted in an increase in viscosity upon cooling for Lyocell. They later showed there was in increase in the water retention value with an increase in temperature (Tatarova *et al.*, 2012).

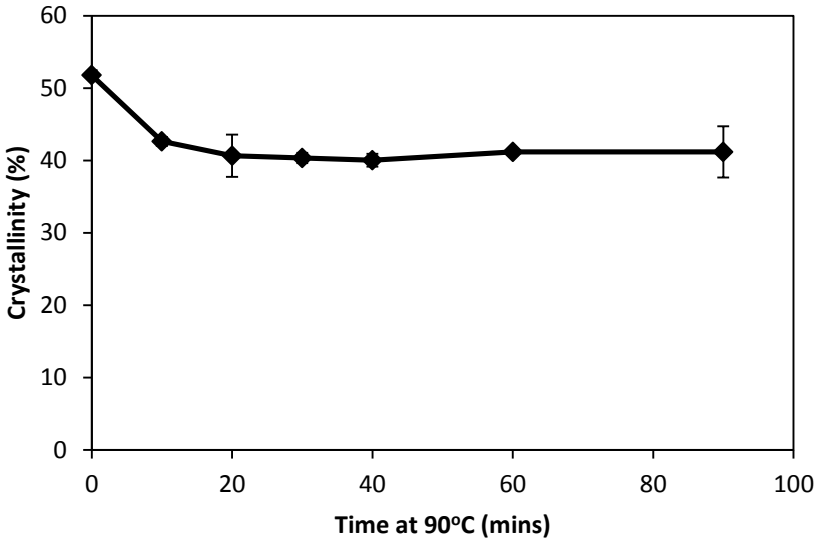

Figure 5.5 Crystallinity of MCC treated in LiCl/urea/water with different treatment times, measured using X-ray diffraction. The average of three samples is shown with error bars indicating the standard deviation.

Figure 5.6 shows ball milled (BM) MCC that has been treated in the RVA for 10 minutes or 90 minutes at 90°C and then regenerated in water. Both samples regenerate to the same crystallinity.

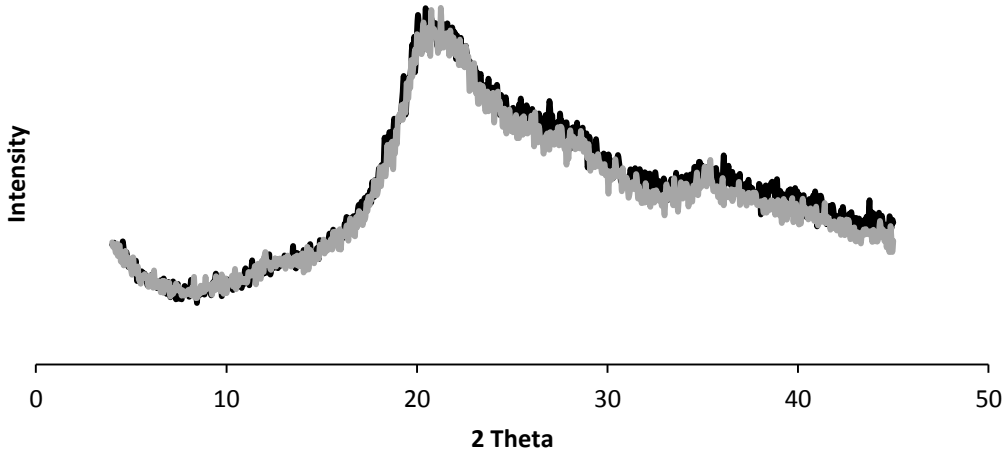

Figure 5.6 XRD spectra of ball milled MCC treated in LiCl/urea/water for either 10 minutes (black) or 90 minutes (grey) at 90°C.

When BM MCC is regenerated directly with water it recrystallises to a higher crystallinity (29%) than when treated and washed (24%) (Figure 5.7). The treated sample will still contains salt that will inhibit recrystallisation.

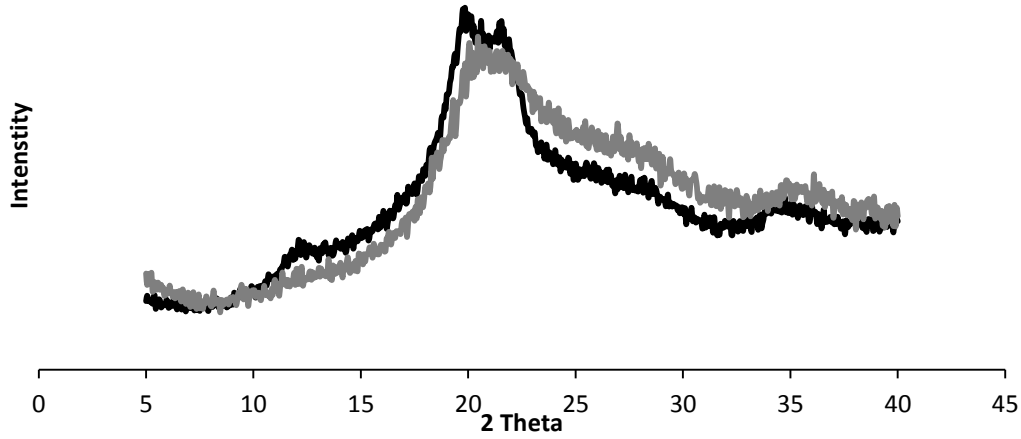

Figure 5.7 XRD spectra of ball milled MCC rehydrated in water (black) or treated in LiCl/urea/water and then water washed (grey).

While X-ray diffraction (XRD) shows that the crystallinities of the treated ball milled sample is lower than that of the water washed sample (Figure 5.7), NMR shows little difference between the samples (Figure 5.8).

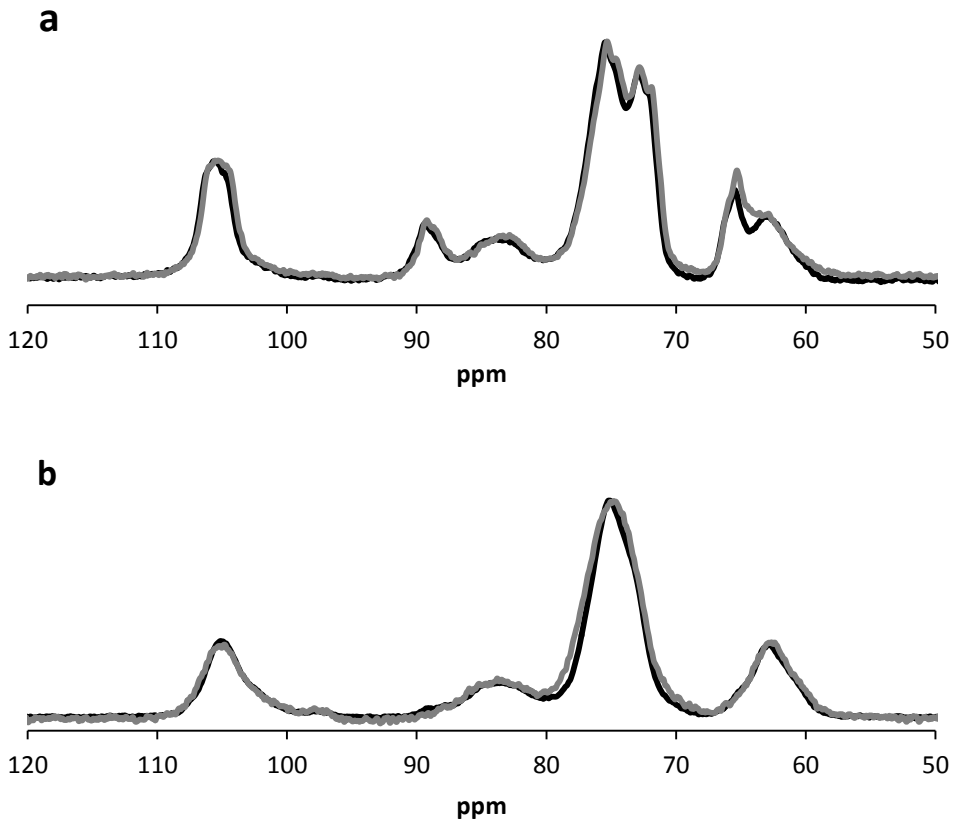

Figure 5.8 ^{13}C CPMAS NMR spectra of celluloses treated in LiCl/urea/water (grey) or untreated and rehydrated (water washed) (black) for (a) CF and (b) BM MCC.

Polarized microscopy is a useful tool to quickly identify crystallinity. Two polarizing filters are placed on the microscope at 90^{o} to each other. When the polarised light passes through a crystal it will be slightly rotated. This rotation will then enable the light to pass through the upper filter and so produce birefringence. Cross polar micrographs show that the cellulose fibres are still highly crystalline after treatment (Figure 5.9). Even the BM MCC shows some birefringence indicating that it must have recrystallised in the LiCl/urea/water solution.

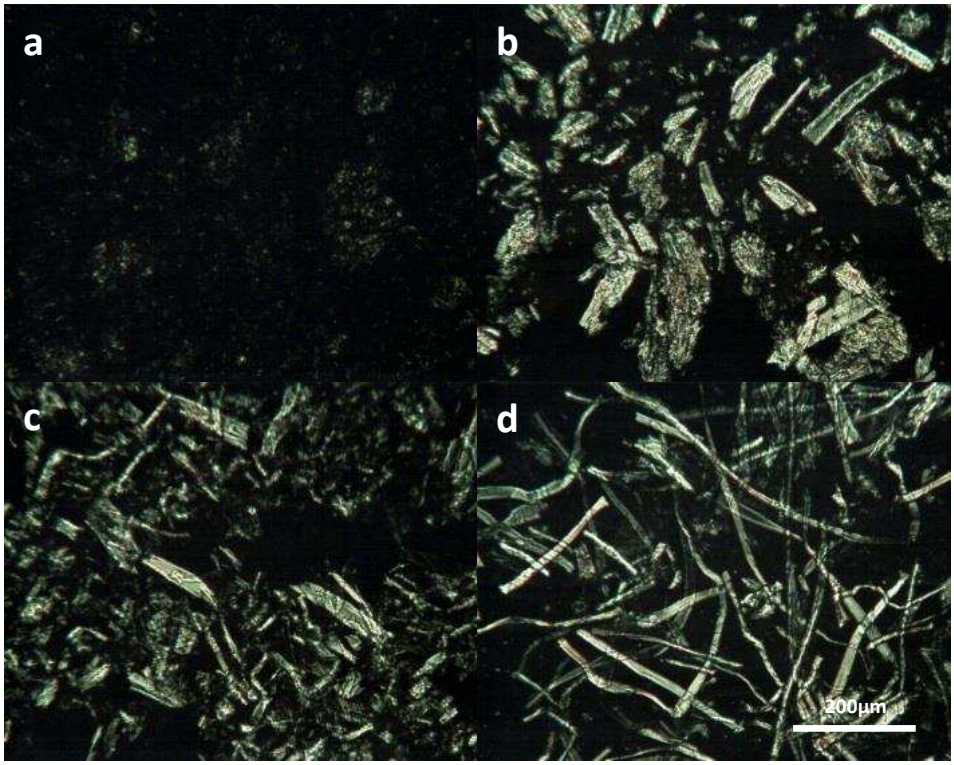

Figure 5.9 Cross polar micrographs of 5 wt% celluloses in the LiCl/urea/water solution after treatment (a) BM MCC (b) MCC (c) CP and (d) CF.

Using a hot stage on a light microscope allows the different heating stages to be investigated. Between 50-70^{o}C the particles begin to swell and aggregate (Figure 5.10a). This is shown in better detail in Figure 5.11 which is a more dilute dispersion (2.5 wt% compared to 5 wt% shown in Figure 5.10). Figure 5.10b shows that when the BM MCC is first dispersed into the swelling solution it immediately begins to recrystallise. When BM MCC is hydrated to a relative humidity (RH) of 95% it

recrystallises (Chapter 3), therefore, even though the swelling solution is a hydrogen bond disrupter (as it reduces cellulose crystallinity) there is sufficient water present that hydrogen bonds can actually be formed. As the heat increases the crystallinity is reduced.

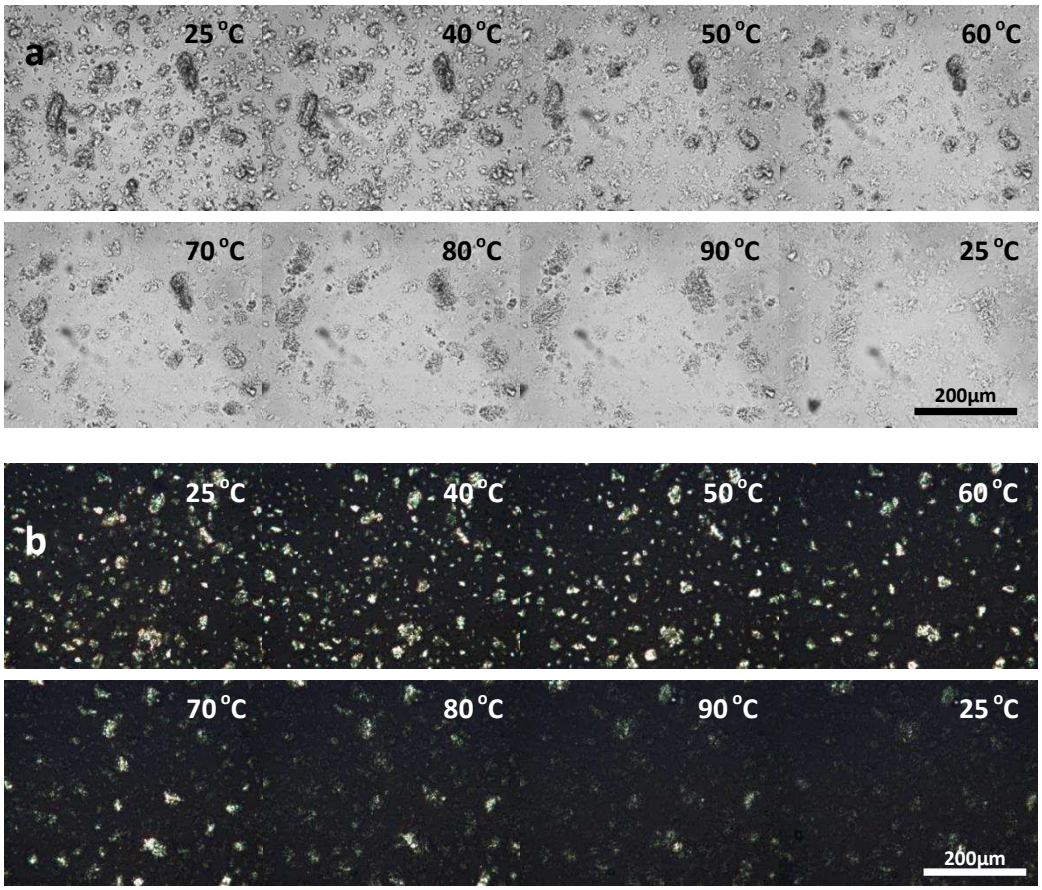

Figure 5.10 Hot-stage micrographs of 5 wt% BM MCC in the LiCl/urea/water solution showing (a) light micrographs and (b) cross polar micrographs.

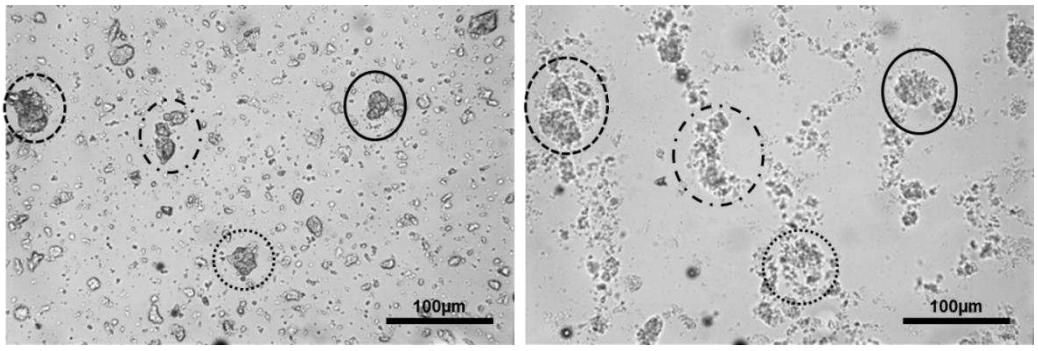

Figure 5.11 Hot-stage micrographs of 2.5 wt% BM MCC in the LiCl/urea/water solution at 25°C and 90°C. The circles indicate particles that have swollen.

There is little visual difference as CP is treated in the swelling solution (Figure 5.12). The decrease in crystallinity shown in Figure 5.3 is therefore likely to happen near the surface of the fibre.

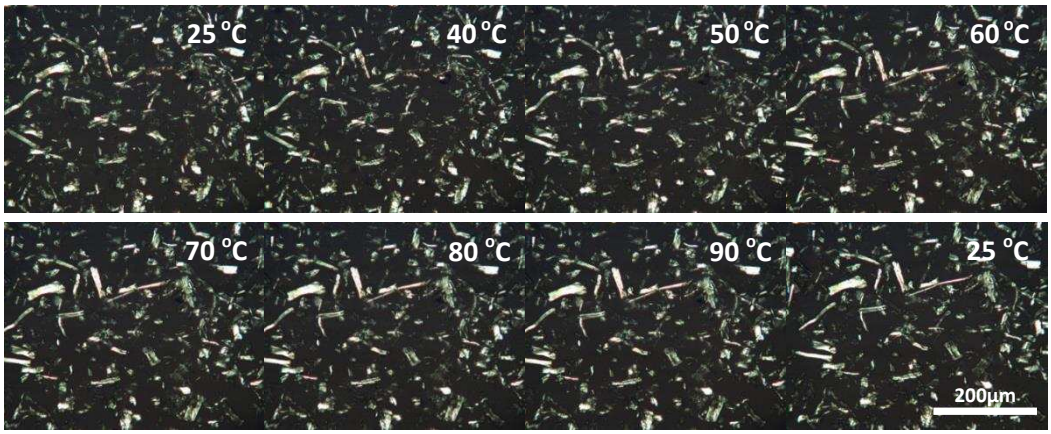

Figure 5.12 Cross polar hot-stage micrographs of 5 wt% CP in the LiCl/urea/water solution.

To get a better understanding of what is happening to cellulose in the swelling solution two different starches were used, potato starch (large granules) and rice starch (small granules), similar to the comparison made by Koganti *et al.* (2011 and 2014) on the effects of the cellulose dissolving solvent NMMO on starch dissolution.

Starch is composed of two polymers; amylose comprised of linear chains of α-1,4-linked anhydro-D-glucose units and amylopectin which has a high level of branching with α-1,6 linkages. Although both starch and cellulose are comprised of glucose monomers, the α-glycosidic linkage imparts a helical twist to the molecule as opposed to the flat ribbon structure of cellulose microfibrils. Starch granules have rings of crystallinity caused by amylopectin crystallites.

Native starch is insoluble in cold water but when heated will go through a process of gelatinisation. Above the gelatinisation temperature the granules will swell resulting in an increase in viscosity. Starch crystals will melt and amylose will leach out. The gelatinisation temperature is dependent on the starch-water ratio, pH, salt or sugar concentration and fat or protein content.

When starch is cooled it will go through a process of retrogradation as the linear portions of the amylose and amylopectin chains recrystallise. The temperature at which these complexes melt out are often considerably higher than the gelatinisation temperature.

In excess water, potato starch starts to swell at about 65°C (Figure 5.13a) and most of the crystal structure is lost by 70°C, as seen by the loss of birefringence (Figure 5.13b). Rice starch has a higher gelatinisation temperature so complete melting and hydration is only complete at 80°C (Figure 5.14).

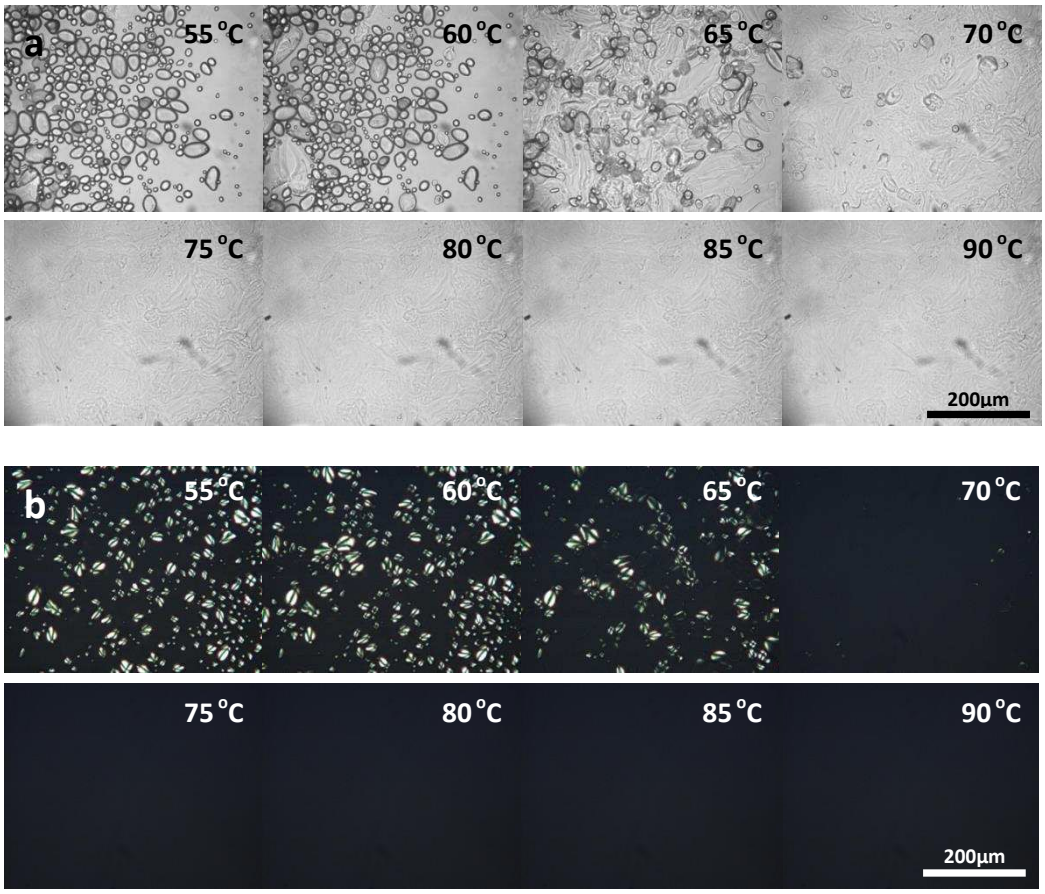

Figure 5.13 Hot-stage micrographs of 5 wt% potato starch in water showing (a) light micrographs and (b) cross polar micrographs.

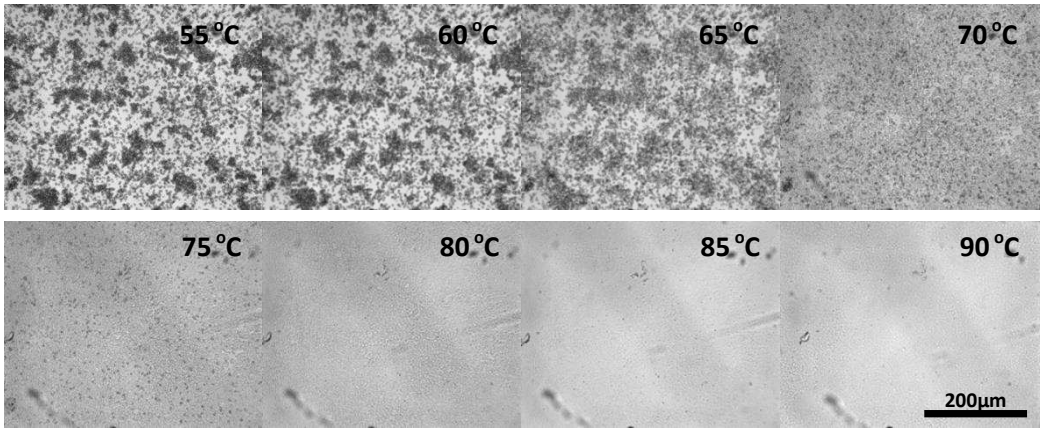

Figure 5.14 Hot-stage micrographs of 5 wt% rice starch in water.

In the LiCl/Urea/water solution the granules do not swell but instead are eroded from the outside as temperature increases (Figures 5.15 and 5.16). The starch is only fully dissolved at a temperature of 90°C. The starch granules still retain some of the crystallinity up to 80°C. Due to the smaller granule size of the rice starch, complete dissolution happens faster.

Koganti *et al.* (2011) used a series of NMMO/water solvents to dissolve starch. They found that NMMO concentrations between 50 and 60 wt% resulted in gelatinisation-like behaviour and only at NMMO concentrations above 70 wt% did the solvent erode the starch from the outside. This indicates that the water content of the LiCl/urea/water solution is low enough for there to be no gelatinisation.

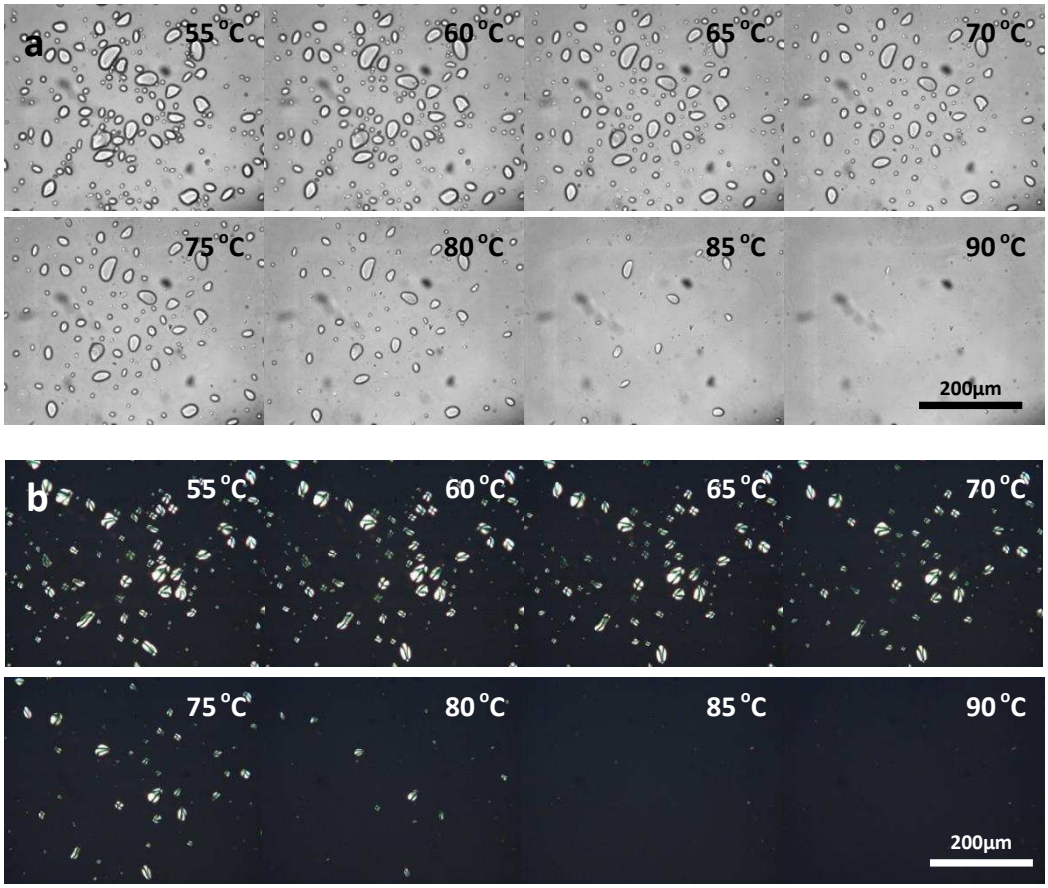

Figure 5.15 Hot-stage micrographs of 5 wt% potato starch in the LiCl/Urea/water solution showing (a) light micrographs and (b) cross polar micrographs.

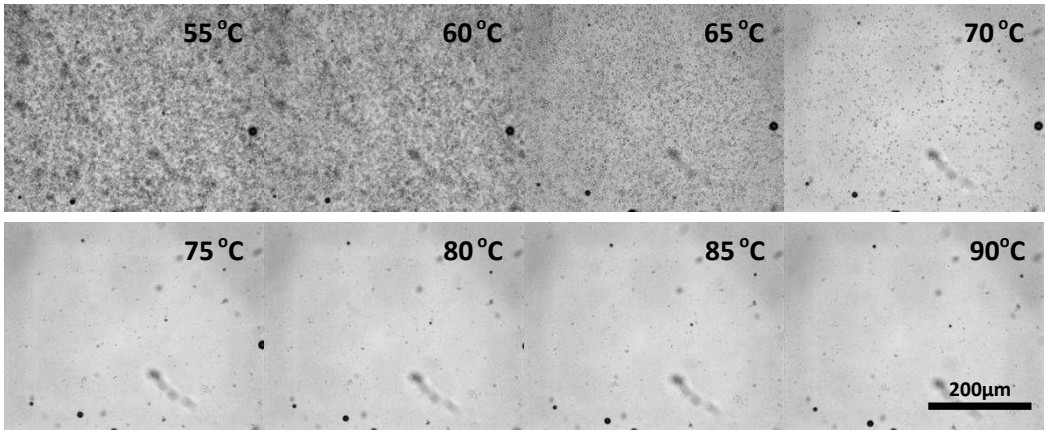

Figure 5.16 Hot-stage micrographs of 5 wt% rice starch in the LiCl/Urea/water solution.

Potato starch has a much greater viscosity in water compared to rice starch due to its larger granule size. However, after treatment in the LiCl/urea/water solution the two starches have the same viscosity (Figure 5.17). It is reported that potato starch has an amylose content of 20.1-31.0% and rice starch has an amylose content of 5-28.4% (Singh *et al.*, 2003). As the starches have a similar amount of amylose and

amylopectin, when fully dissolved in the LiCl/Urea/water solution their viscosity is matched. The original granule structure is now completely destroyed.

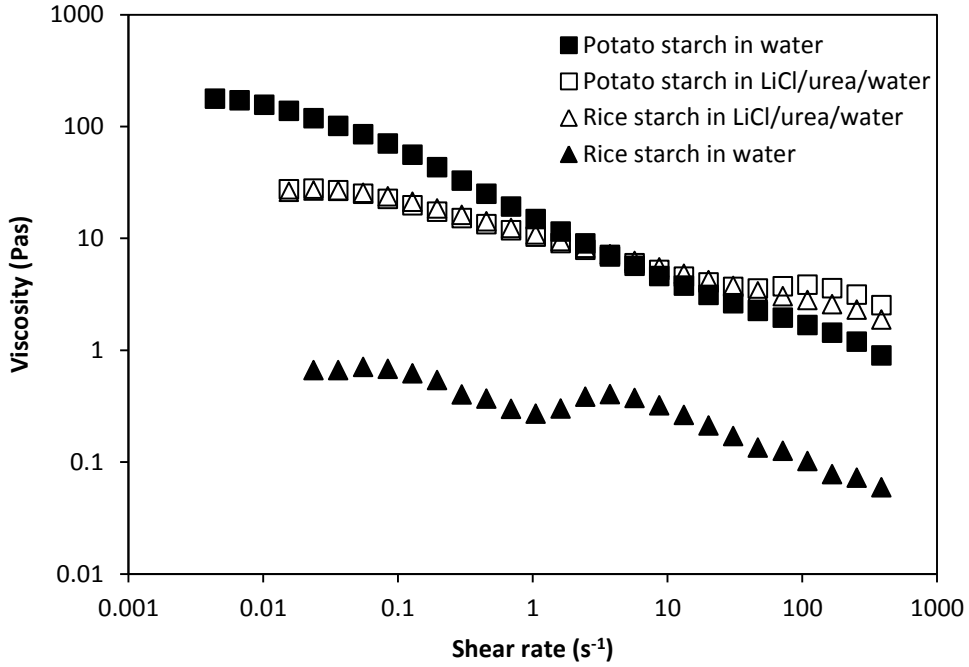

Figure 5.17 The viscosity 5 wt% starches in water (filled symbols) or LiCl/urea/water (hollow symbols) after treatment.

In the LiCl/urea/water solution the potato starch increases in viscosity during the initial heating to a lesser extent than rice starch due to its larger granule size (Figure 5.18). In water the potato starch increases to a greater viscosity than in the LiCl/urea/water due to the granules swelling, however, upon cooling the treated potato starch has a very large increase in viscosity which decreases with continued shear. This might suggest that there are some granule remnants which interact in a similar way to cellulose upon cooling. At the endpoint of the treatment these remnants are likely to have been fully solubilised as the viscosity starts to plateau. The viscosity increase upon cooling is not seen for the rice starch. The LiCl/urea/water solution is able to completely dissolve the rice starch within the treatment time due to its smaller granule size, therefore, leaving no granule remnants intact to interact upon cooling.

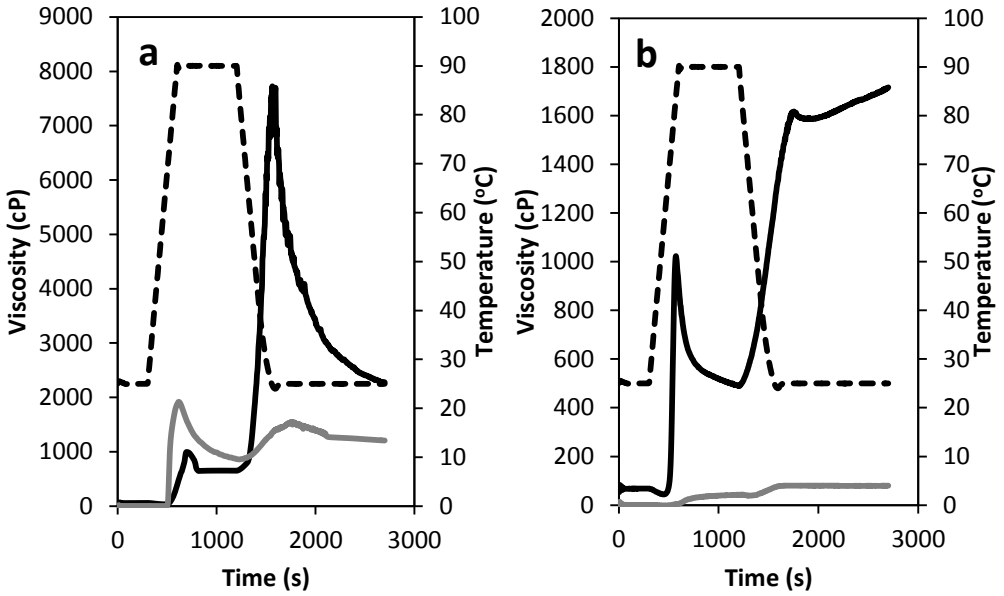

Figure 5.18 RVA viscosity profiles of 5 wt% starch in water (grey) or LiCl/Urea/water solution (black) for (a) potato and (b) rice.

In water, potato starch showed a frequency dependence and had a weak gel-like structure once gelatinised as the storage modulus (G') was higher than the loss modulus (G'') with no crossover (Figure 5.19) as is usual for native gelatinised starches (Chamberlain and Rao, 2000, Chaisawang and Suphantharika, 2006, Leite *et al.*, 2012). In the LiCl/urea/water solution potato starch shows viscous behaviour with G'' higher than G', also indicating starch goes through complete dissolution providing a polymeric solution with no granule remnants. Koganti *et al.* (2011) found that, for 5 wt% normal maize starch in NMMO concentrations of over 70 wt%, an increased viscosity response was observed whereas for concentrations of 50 wt% and below the system changed to produce a more elastic response, typical of swollen starch granules.

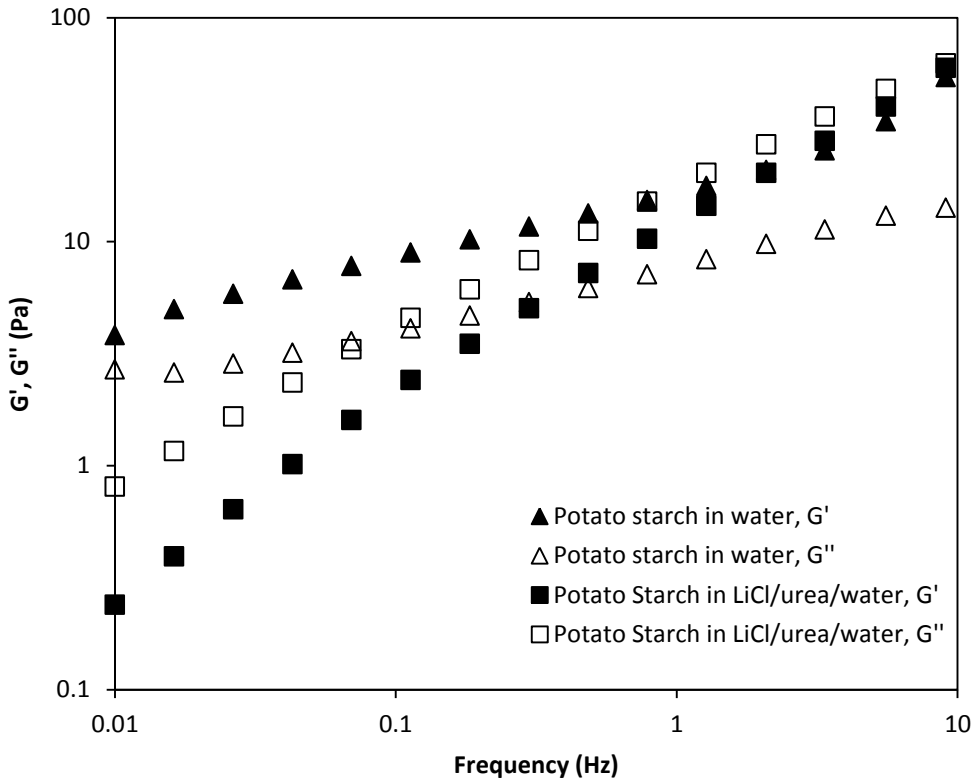

Figure 5.19 The dynamic moduli G' (filled symbols) and G'' (open symbols) of 5 wt% potato starch in water or LiCl/urea/water solution.

As a larger quantity of ball milled cellulose was required than in Chapter 3, a large ball mill was used. Both MCC and CF were milled for 6 hours which was found to produce a similar level of milling compared to 610 minutes in the smaller ball mill.

When the ball milled celluloses were treated they both had a very similar RVA profile (Figure 5.20). The degree of polymerisation (DP) of these samples was not measured, however, in Chapter 3 (section 3.3, page 66) it was shown that when MCC and CF were milled for 610 minutes they had a similar viscosity average DP (190 and 250 respectively) which may be why there is little difference between the ball milled samples. Upon cooling BM cellulose undergoes a large increase in viscosity which then drops with continued shear.

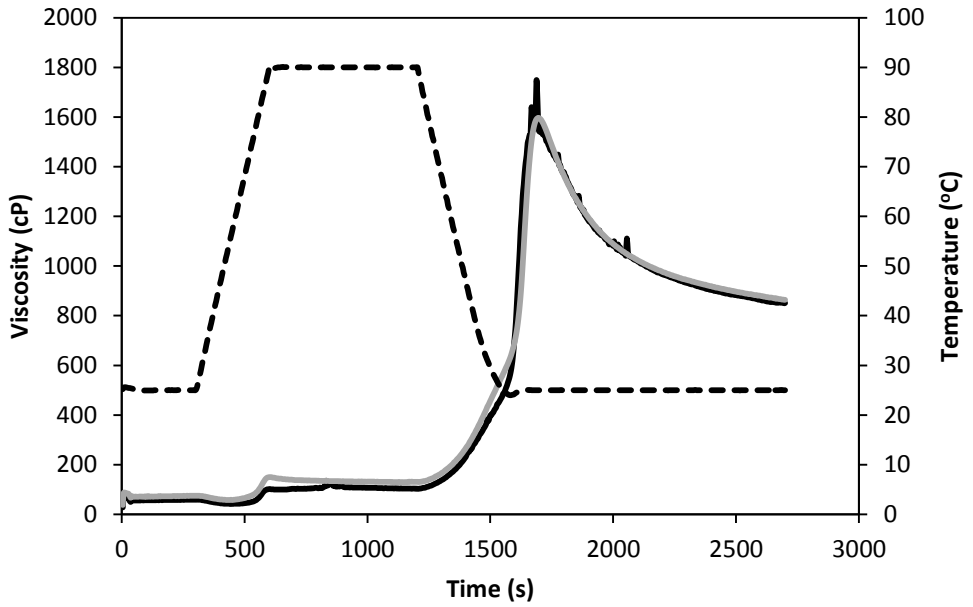

Figure 5.20 RVA profiles showing a comparison of 5 wt% ball milled MCC (black) and CF (grey) in the LiCl/urea/water solution.

After a second heat treatment the BM MCC repeats its large increase in viscosity upon cooling, and subsequent drop in viscosity with continued shear, whereas the starches return to their initial viscosities without an subsequent drop with subsequent shear as seen in the first run of the potto starch (Figure 5.21). Any interaction that causes the potato starch to increase in viscosity on the first run is completley lost by the second run and both starches have similar viscosities upon second cooling. The starch has a much higher viscosity than BM MCC as it is fully dissolved rather than just swollen due to its α-1,4 linkage compared to cellulose's β-1,4 glucose linkage.

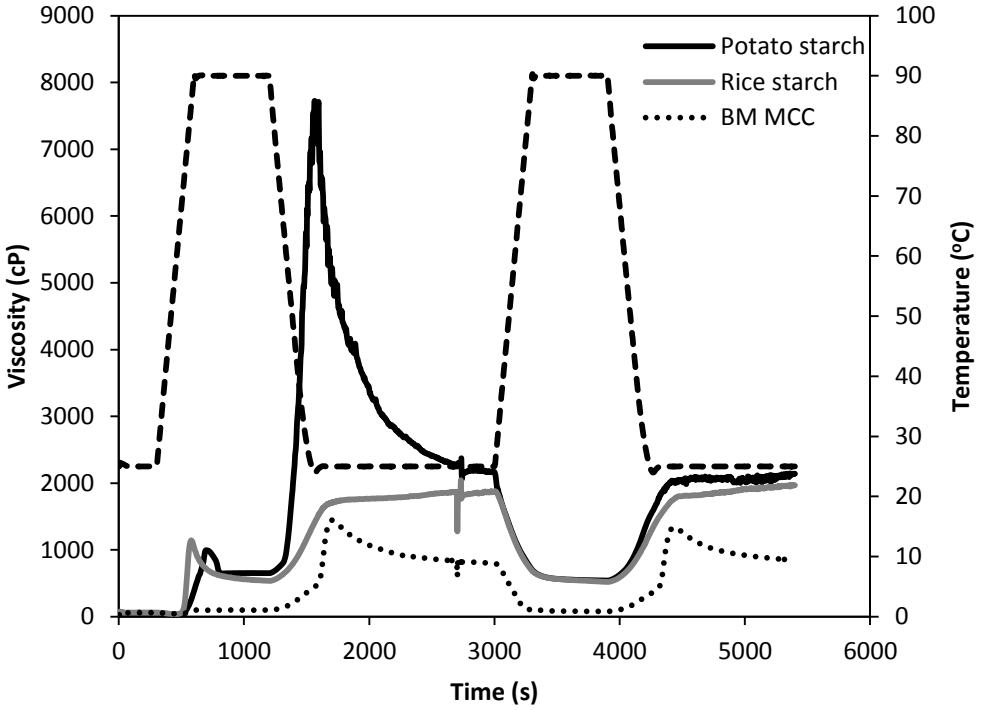

Figure 5.21 RVA profiles showing two heating runs of 5 wt% concentration of potato starch (black), rice starch (grey) and BM MCC (dotted) in the LiCl/urea/water solution.

The treated BM MCC dispersion was given a pre-shear for 60 seconds to completely break any structure that may have been formed. With increasing time before the viscosity was measured some structure was formed which resulted in a higher viscosity (Figure 5.22). At a shear rate of over 1 s^{-1} any structure is completely lost and all sampes have the same viscosity profile. The plateau (double knee) region from 0.015-0.15 s^{-1} is possibly caused by wall slip at low shear rates where the top plate is in contact with a thin layer of the liquid that has separated from the bulk (Meeker *et al.*, 2004, Buscall *et al.*, 1993). For future work it would be useful to try a serrated plate geometry which should negate any slip effects by providing voids to accommodate any separating liquid. If the double knee region is caused by slip, it indicates that for the samples with less structure there is less slip.

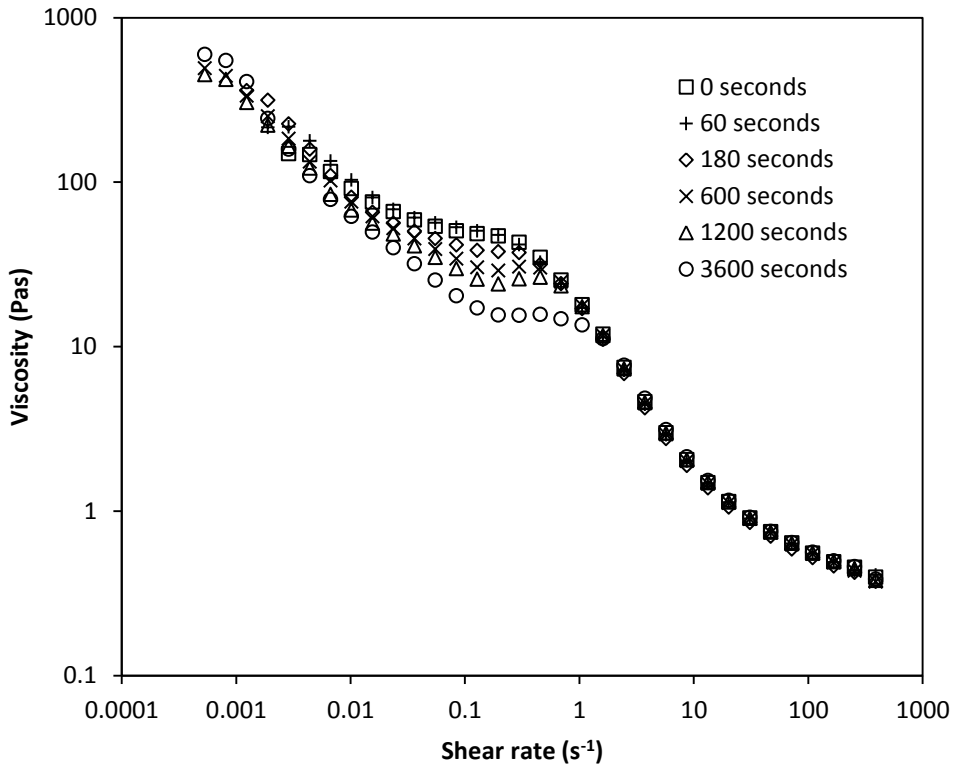

Figure 5.22 Viscosity of 5 wt% BM MCC in the LiCl/urea/water solution with different pause times (shown in the legend) after 60 second pre-shear.

The structure formed by BM MCC in LiCl/urea/water is characteristic of a weak gel with the elastic modulus (G') higher than the viscous modulus (G'') but with some frequency dependance (Figure 5.23) (Ikeda and Nishinari, 2001).

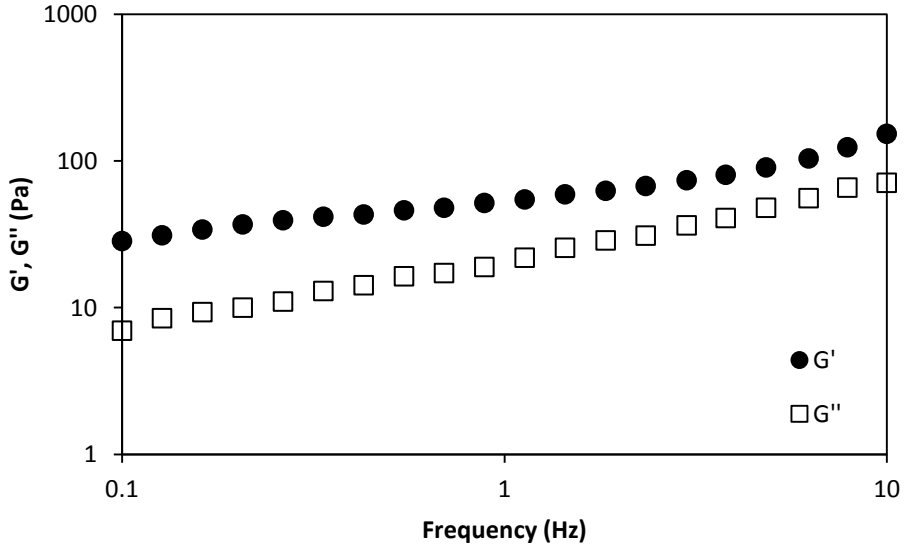

Figure 5.23 The dynamic moduli G' (filled symbols) and G'' (open symbols), measured at a shear stress of 1 Pa which was in the linear viscoelastic region (LVR), of 5 wt% BM MCC in LiCl/urea/water.

At a concentration of 5 wt% of MCC or CP the viscosity of the dispersions is too low to measure any structure formation. However, at a concentration of 10 wt% both cellulose dispersions increase in viscosity over time after an initial pre-shear (Figure 5.24).

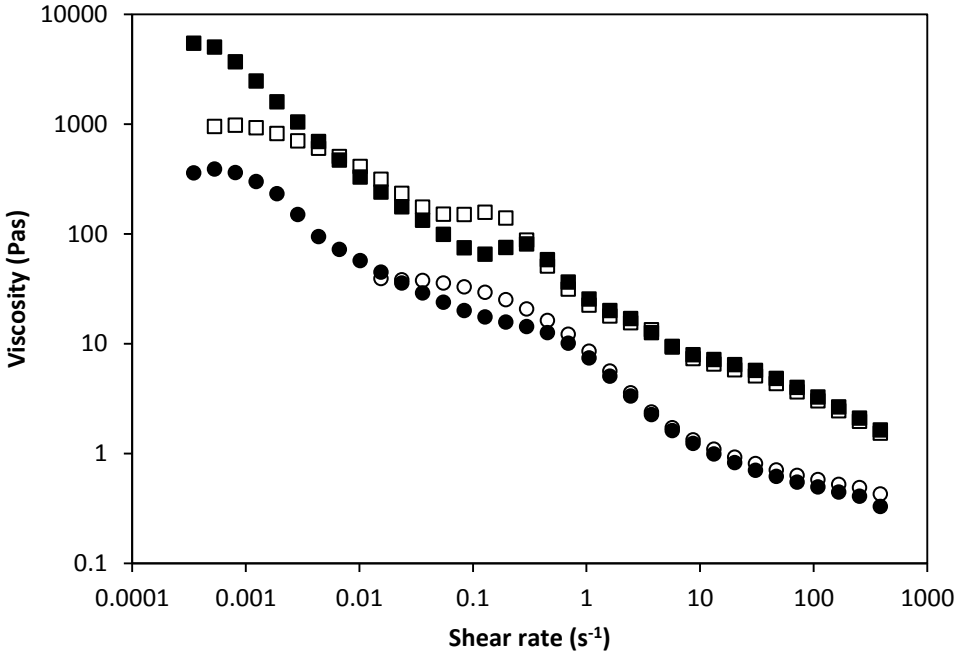

Figure 5.24 Viscosity of 10 wt% MCC (circles) and CP (square) pre-sheared for 60 seconds and then measured immediately (hollow symbols) or after one hour (filled symbols).

With increasing concentration, the viscosity of all the treated cellulose dispersions increase (Figure 5.25). The rheology of suspensions of rods in water, a Newtonian fluid, is dependant on the volume fraction and aspect ratio of the fibres (Milliken *et al.*, 1989). At lower concentration the fibres are able to freely move but upon increasing the concentration the fibres start to be disturbed by each other due to steric effects resulting in a shift in the slope as the dispersion moves from the dilute to semiconcentrated regime, known as the critical volume fraction $\emptyset_c$ (Pabst *et al.*, 2006). A similar effect is often seen for molecular solutions and described as the critical concentration (c^*) (Lue and Zhang, 2009). The $\emptyset_c$ will decrease with increasing apect ratio. CP and MCC show a $\emptyset_c$ at 8 and 9 wt%, respectively. There is little difference bewteen fibre size of CP and MCC when dry so the steeper slope of CP

may be explained by its lower crystallinity and therefore increased ability to swell compared to MCC, thereby having a larger volume fraction. CF has a much larger aspect ratio and so has a much higher viscosity than either CP or MCC at comparable concentrations. The BM MCC does not have a $\emptyset_c$ due to its particulate shape. At low concentrations it has a much higher viscosity than the other celluloses due to its larger surface area which allows for greater interaction and low crystallinity which enables it to swell to a much greater extent (Figure 5.11). CF also appears not to have a $\emptyset_c$ but due to its much higher size and aspect ratio this might be at a concentration lower than measured in this work.

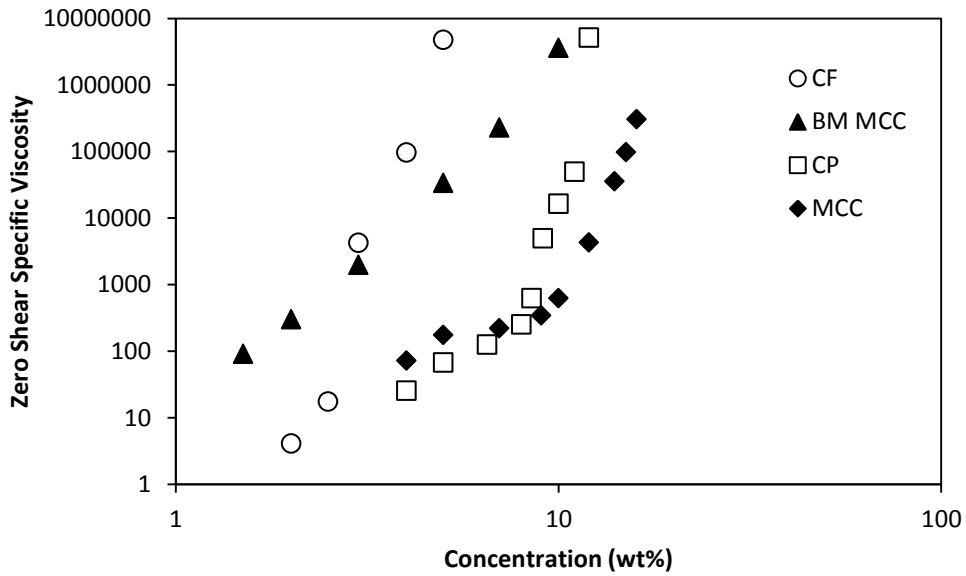

Figure 5.25 Zero shear viscosity of cellulose dispersions in the LiCl/urea/water solution.

Figure 5.26 shows the RVA profile of varying concentrations of BM MCC dispersions in the swelling solution. There appears to be a peak in viscosity upon cooling which is reminiscent of starch gelatinisation and may be a result of particle/aggregate disruption. Only BM MCC has a pronouced tailing off of its viscosity with continued shear upon cooling (Figure 5.26). As already shown in Figure 5.1, there is an increase in viscosity upon cooling for MCC (Figure 5.27), CP (Figure 5.28) and CF (Figure 5.29). MCC appears to have a slight incease in viscosity once at a steady temperature of

25°C (Figure 5.27), whereas, both CP and CF plateau when held at 25°C (Figures 5.28 and 5.29). When the celluloses are concentration matched at 5 wt% there is an initial increase in viscosity at a temperature of between 65-70°C. With an increase in concentration the temperature at which this initial increase begins is decreased so for 16 wt% MCC the temperature is just 43°C. Interestingly, all the celluloses show a similar temperature of increase when matched at the same concentration.

CF decreases in viscosity upon the initial heating (Figure 5.29) which was also seen for the other celluloses of high aspect ratio, lyocell and cotton linters (Figure 5.1). Due to their larger size the dispersions are already slightly viscous before the heat treatment.

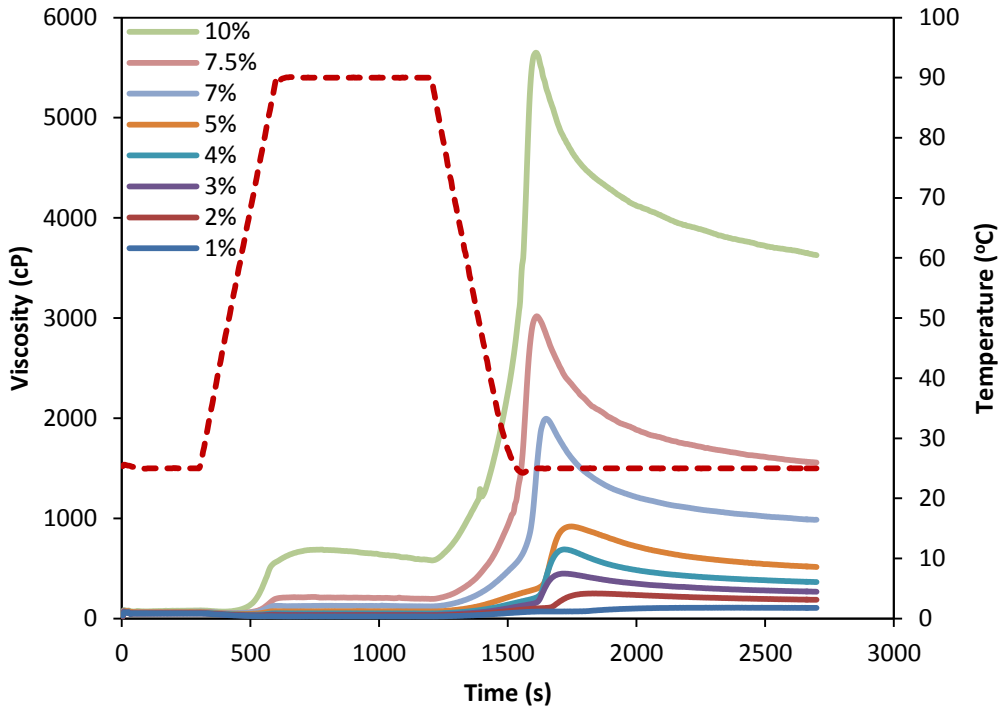

Figure 5.26 RVA viscosity profile for BM MCC in the LiCl/urea/water solution.

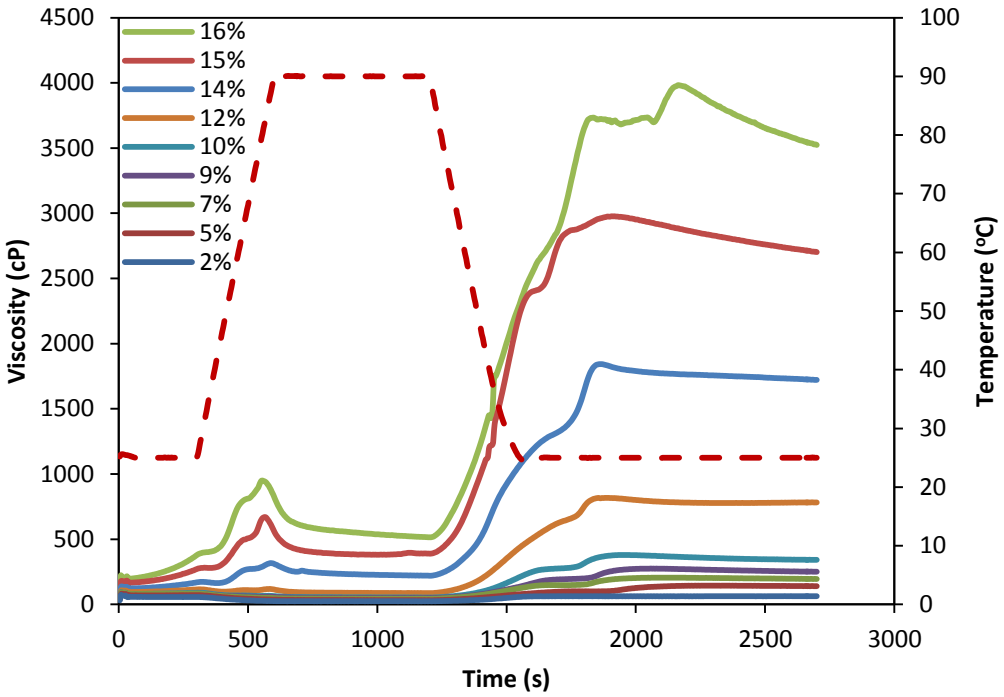

Figure 5.27 RVA viscosity profile for MCC in the LiCl/urea/water solution.

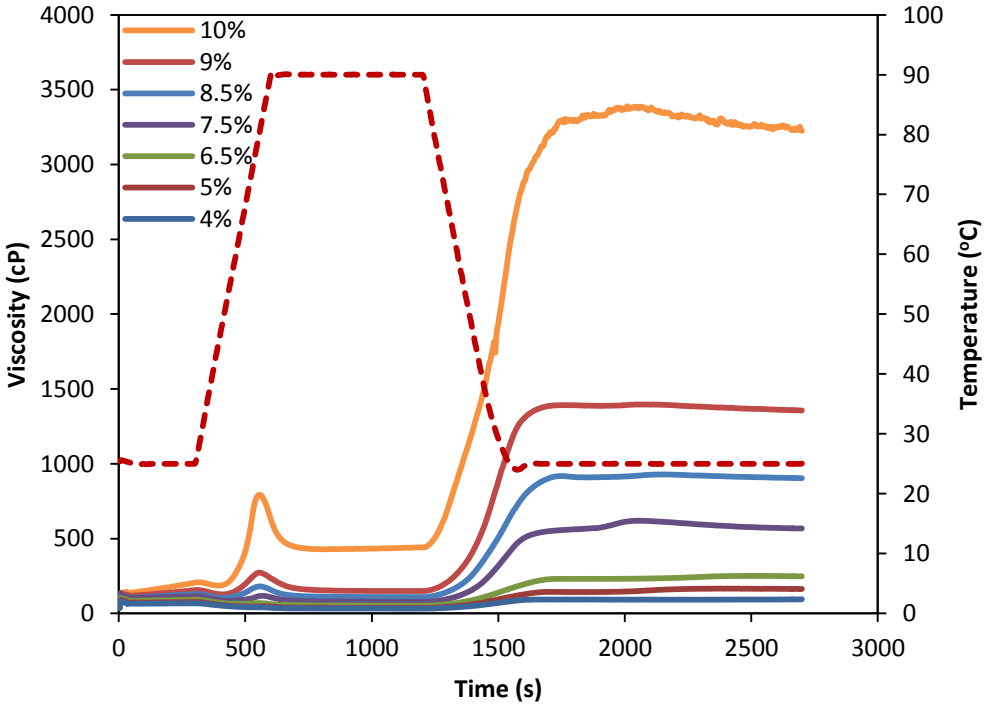

Figure 5.28 RVA viscosity profile for CP in the LiCl/urea/water solution.

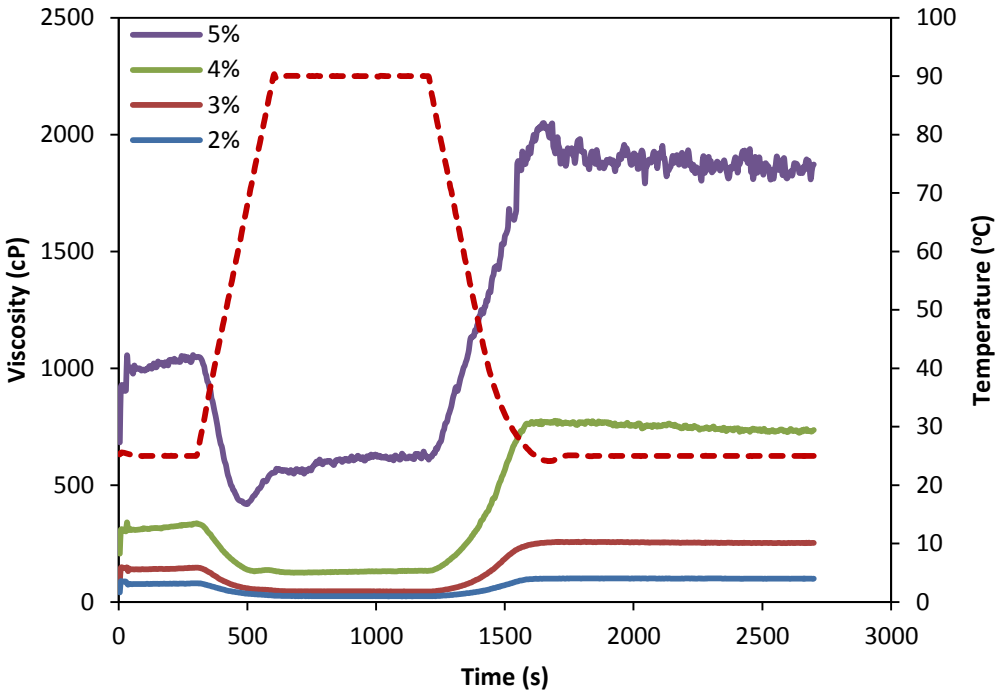

Figure 5.29 RVA viscosity profile for CF in the LiCl/urea/water solution.

In order to begin to understand the events taking place in the RVA, a differential scanning calorimetry (DSC) comparison was undertaken, and again compared to starch in this solvent system.

In excess water both potato and rice starch show gelatinisation endotherms (Figure 5.30) which are ascribed to the melting of the crystalline regions (Donovan, 1979), and reducing the volume fraction of water the endotherm is moved to higher temperatures. No phase transitions are seen on subsequent reheats as the melting temperature of retrograded starch is higher than 95°C (Liu *et al.*, 2007). In water, none of these celluloses are expected to show any phase transitions.

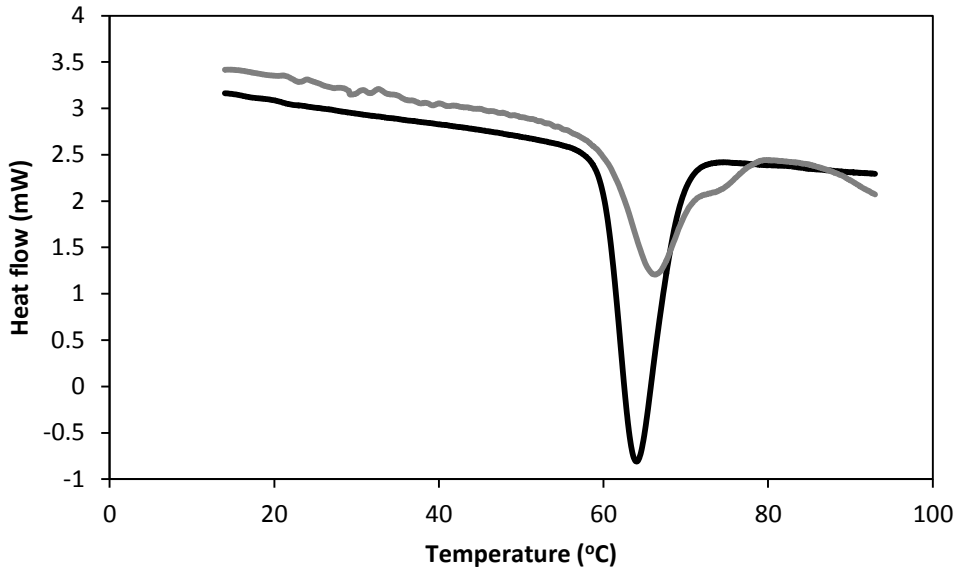

Figure 5.30 Micro DSC spectra of 10 wt% potato starch (black) and rice starch (grey) in water.

In the LiCl/urea/water solution the starches and celluloses all show very large exothermic peaks (Figure 5.31). Koganti *et al.* (2011) found that with increasing NMMO concentration the thermal transitions of starch transformed from endotherms to exotherms. The enthalpy of mixing is related to the breaking of polymer-polymer interactions and the formation of polymer-solvent interactions (Koganti, 2014). Whereas energy is required to melt starch crystalline regions in water, heat is released in the LiCl/urea/water system. The breaking of cellulose-cellulose or starch-starch hydrogen bonds is endotheric (Ramos *et al.*, 2011) but the the enthalpy of mixing i.e, the formation of hydrogen bonds with the LiCl/urea/water, is exothermic which appears to predominate here (Eq. 5.1).

$$\Delta H_{total} = \Delta H_{melting} + \Delta H_{mixing} \quad (5.1)$$

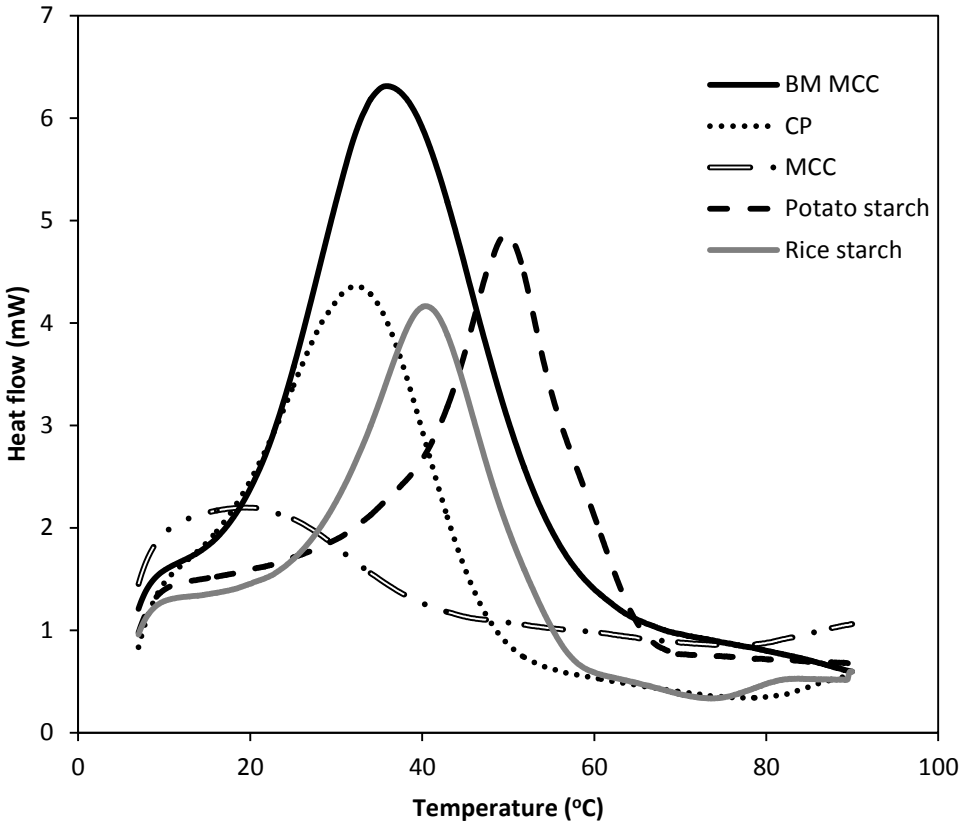

Figure 5.31 Micro DSC spectra of the first heat in the LiCl/urea/water solution.

BM MCC has the largest enthalpy whilst MCC is far smaller. The enthalpy is related to the availability of the polymer to form polymer-solvent interactions and is therefore negatively correlated to cellulose crystallinity. The unit cell of crystalline cellulose is anhydrous so will be unable to interact with the solvent until it is disrupted. MCC has a crystallinity almost double that of CP so it is harder for the swelling solution to penetrate MCC during the initial heat. Both starches have a similar total enthalpy.

Table 5.1 Enthalpy of celluloses and starches in LiCl/urea/water during their first heat, average of three replicates ± standard deviation, from Micro DSC measurements.

	Enthalpy (J/g)
BM MCC	-7.52 ± 0.39
CP	-5.85 ± 0.72
MCC	-1.71 ± 0.40
Potato starch	-4.69 ± 0.66
Rice starch	-4.12 ± 0.22

Upon cooling both BM MCC and MCC undergo exothermic transitions between 25-15^{o}C which indicates some structure formation (Figure 5.32). This is more pronounced for BM MCC presumably due to a combination of higher surface area and lower crystallinity. This structure is subsequently melted out between 40-60^{o}C. Both of these transitions are repeatable with further runs. It is difficult to detect any transitions for CP on either heating or cooling runs. Similarly, both BM MCC and MCC have a tailing off of viscosity at 25^{o}C after the initial heating in the RVA, indicating the breakdown of structure caused by shear, whereas CP has a constant viscosity demonstrating there is no structure breakdown. CP has a substantially higher viscosity average DP (1210) compared to MCC (370) and BM MCC (190) which may result in a lower mobility.

The transitions observed for MCC and BM MCC are reminiscent of the thermal transitions seen for methylcellulose where a large endothermic peak is seen on heating (Takahashi *et al.*, 2001). At low temperature, methylcellulose is soluble in water. It is generally agreed that the hydrophobic methyl groups (CH_3) inhibit hydrogen bonding of the polymer chains (Li, 2002). Water molecules are hydrogen bonded along the polymer molecule and cage-like structures of water molecules are ordered around the methyl groups. The water molecules are therefore not free and random but possess a degree of order (Li *et al.*, 2002). Heating a solution of methylcellulose leads to the destruction of the cage-like structures of water and exposes the methyl groups which are then able to form hydrophobic associations. There is a corresponding morphological change from random coils to hydrophobic aggregates (Wang *et al.*, 2006). The energy needed for the destruction of the cage structures is larger than the energy required for the formation of hydrophobic associations (which occur within the same temperature range) resulting in the total energy being endothermic (an entropy increasing process). The cooling process is

exothermic as the hydrophobic associations will be broken and the cage structures will be reformed so the entropy change will be negative. The temperature of degelation is 30^{o}C lower than the gelation temperature (60^{o}C). The thermal hysteresis indicates that the kinetics of the hydrophobic dissociation is not an exact reversal of the association during heating (Xu and Li, 2005).

The enthalpy of the transitions of cellulose in LiCl/urea/water is much smaller than those of methylcellulose indicating that they are only a surface effect. This is in agreement with the fact that MCC is still highly crystalline in LiCl/urea/water. BM MCC has higher enthalpy values compared to MCC due to its larger surface area.

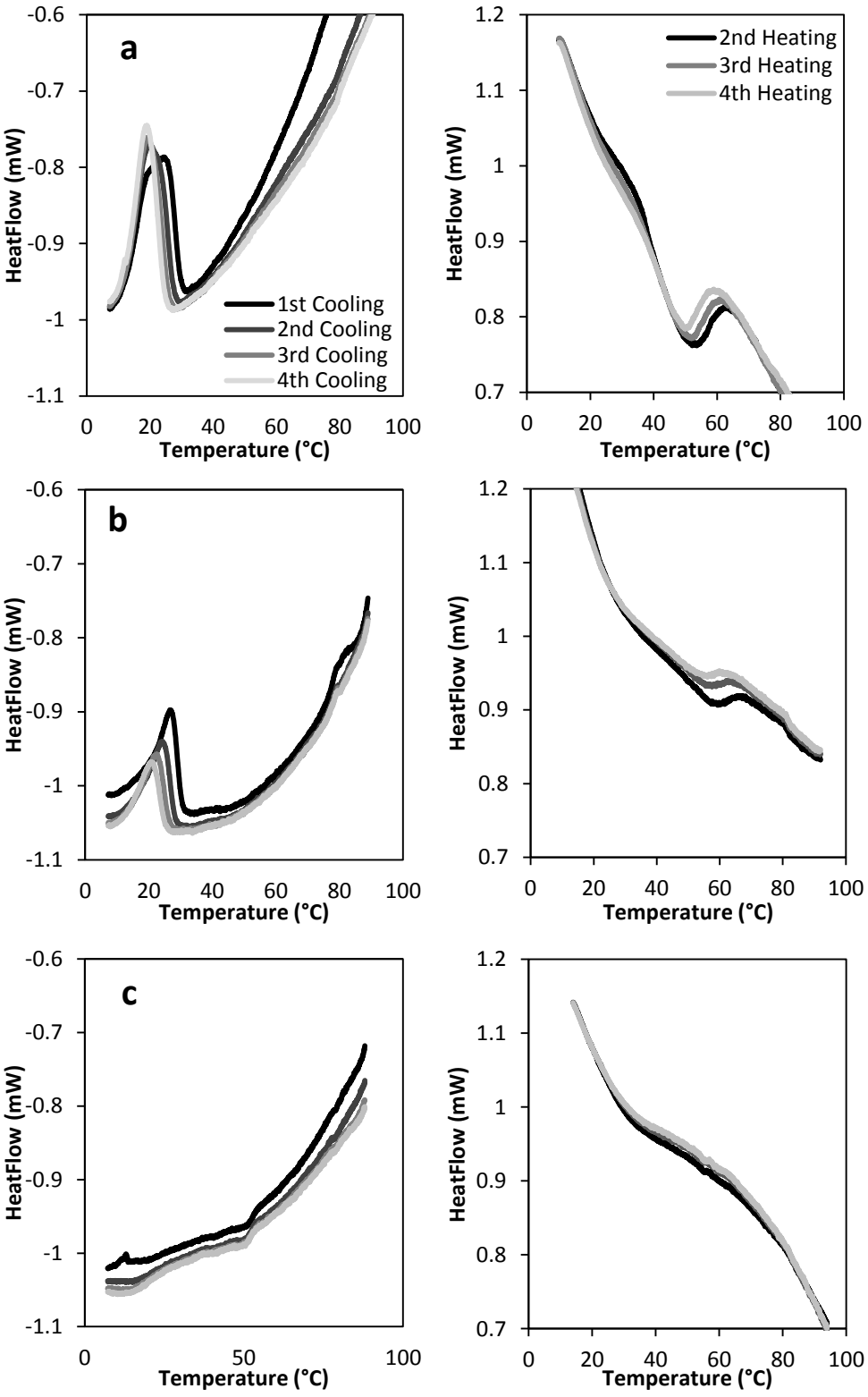

Figure 5.32 Micro DSC spectra of 10 wt% cellulose in the LiCl/urea/water solution cooling (left) and heating (right) for (a) BM MCC (b) MCC and (c) CP.

In order to investigate the scan rate dependance and to probe further the origin of the RVA viscosity increases, the heating rate of the RVA was matched to that of the

Micro DSC. During the initial heat BM MCC has a steep increase in viscosity at about 33^{o}C which is the temperature of peak heat flow (Figure 5.33). This is the point at which the cellulose particles start to swell and aggregate. At the peak viscosity at 70^{o}C the heat flow plateaus indicating molecular dispersion. This peak is not seen in Figure 5.26 for BM cellulose, however, it is seen for both MCC and CP (Figures 5.27 and 5.28). A slower heating rate is required to see the peak for BM MCC. Upon cooling the viscosity increases slowly until 34^{o}C where there is a sharp increase in viscosity which correlates with the start point of the exotherm. On the second heating run the correlation between heat flow and viscosity is not quite so clear as the viscosity drops with increasing temperature but begins to plateau when the exotherm is completed. During the second cooling run the viscosity increases again matches the exotherm start point which is shifted 1^{o}C lower than in the first run. The onset of this peak continues to shift to lower temperatures with subsequent runs (Figure 5.33). After the initial endotherm which shows that the heat of mixing is dominating, the subsequent endotherms and exotherms match what might be expected for conforational change.

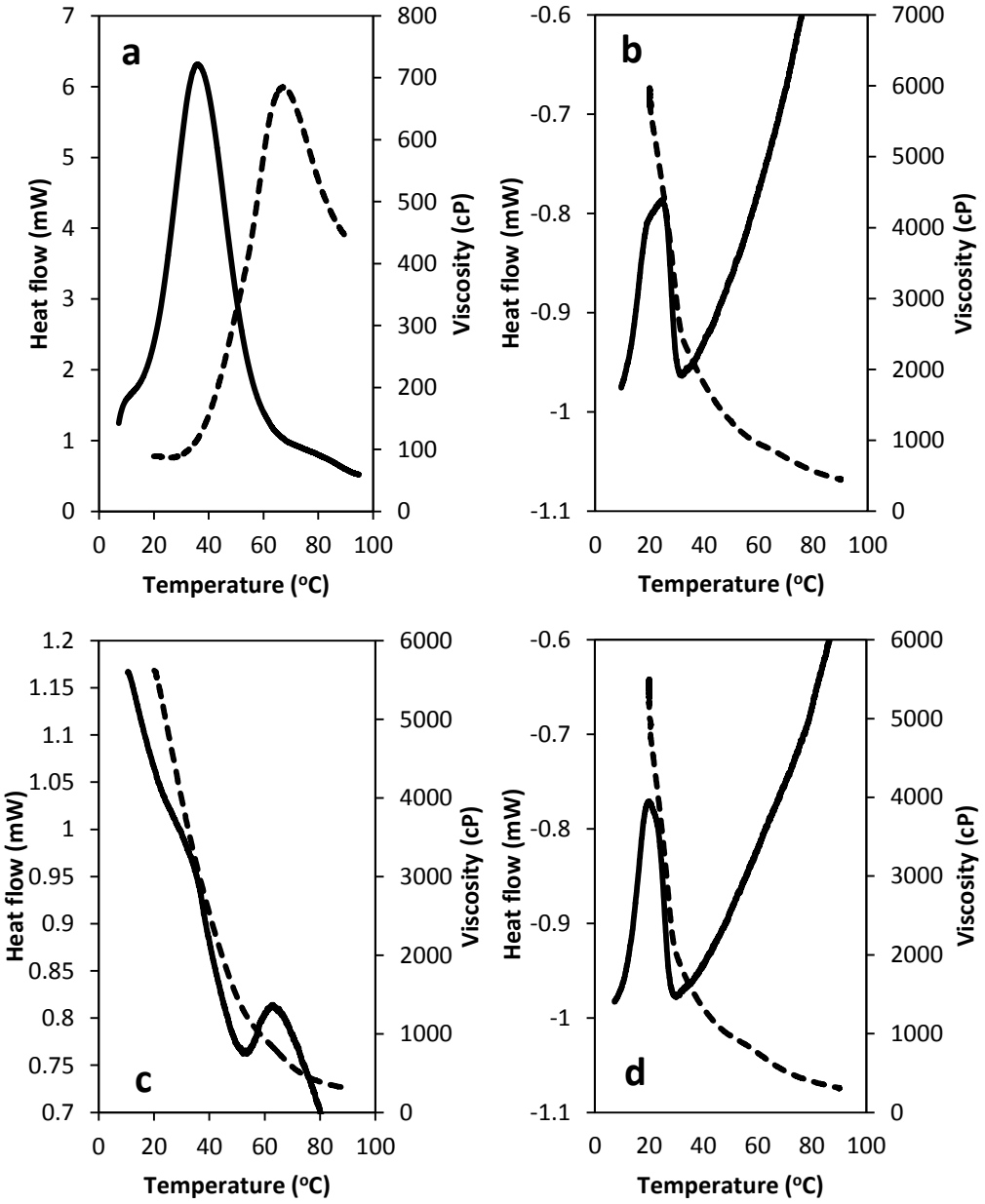

Figure 5.33 Heat flow from Micro DSC (solid line) and viscosity (dotted line) against temperature for 10 wt% BM MCC in the LiCl/urea/water solution showing the (a) first heat (b) first cool (c) second heat and (d) second cool. The RVA heating rate was matched to that of the Micro DSC at 1°C min^{-1}.

Upon cooling potato starch in LiCl/urea/water undergoes a slight exothermic transition with a peak at about 90°C (Figure 5.34). It is much harder to detect any transition for rice starch upon cooling although on the second cooling run there is a small exothermic peak. Both starches have clear endothermic peaks between 60-80°C which decrease in size with each subsequent run.

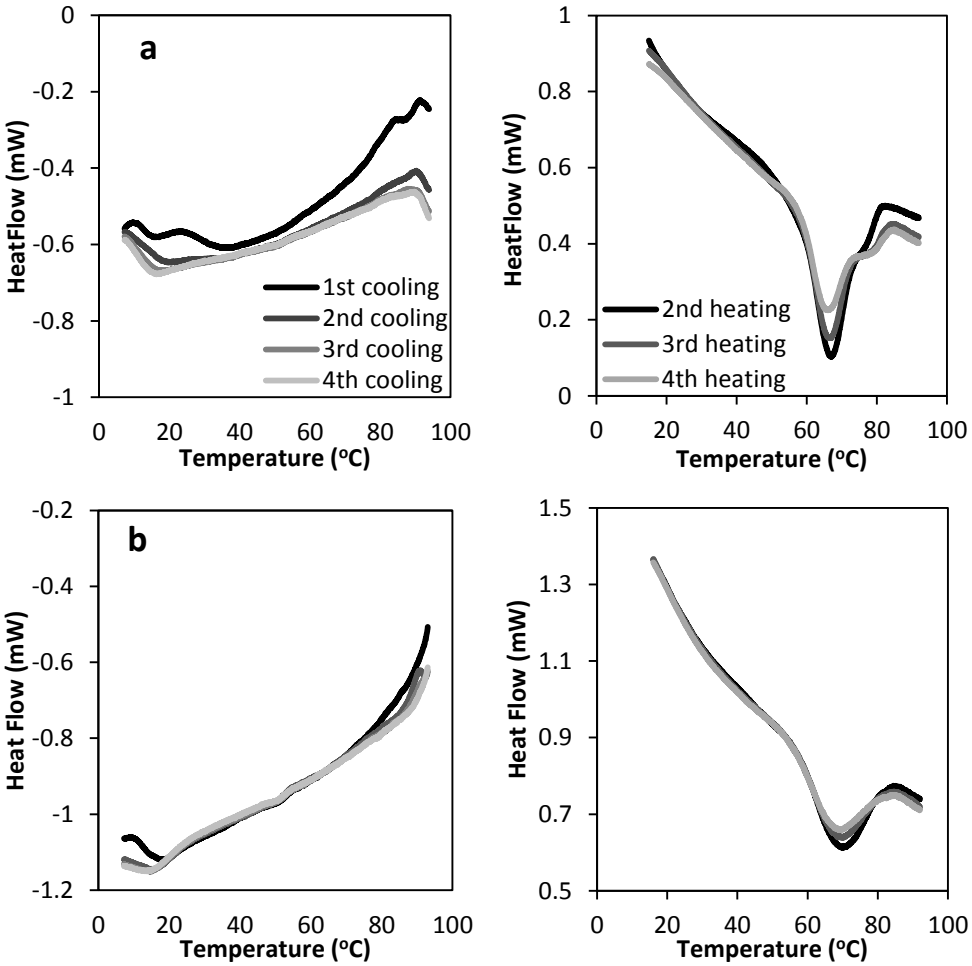

Figure 5.34 Micro DSC spectra of 10 wt% starch in LiCl/urea/water solution cooling (left) and heating (right) for (a) potato and (b) rice.

5.4 Discussion

Recently Lindman *et al.* (2010) discussed the causes of cellulose insolubility in water. The cellulose community generally explain it by the large number of hydrogen bonds present. However Lindman *et al.* point out that other molecules with a high number of hydrogen bonds are highly soluble such as glucose and dextran. If only intermolecular hydrogen bonding is the cause of cellulose insolubility then glucose or dextran should self-associate and phase separate, however this is obviously not the case. This discrepancy therefore shows that hydrogen bonding is not the sole reason for cellulose insolubility. An answer to this may be the amphiphilicity of cellulose

(Biermann *et al.*, 2001). Cyclodextrin (a ring of glucose molecules) is highly soluble in water yet is able to incorporate very non polar molecules into the interior of the ring, showing that glucose molecules can have very different polarity within a chain. The flat ribbons of cellulose chains may therefore have sides of different polarity (Yamane *et al.*, 2006). The hydrophilic nature of cellulose is caused by the hydroxyl groups located in the equatorial direction whereas the axial direction of the glucopyranose rings is hydrophobic because of the hydrogen atoms of the C-H bonds, which means that cellulose molecules have structural anisotropy. Lindeman et al. go on to explain that this may explain the excellent solubility of cellulose in amphiphilic solvents such as ionic liquids and that co-solutes such as PEG and urea, which weaken hydrophobic interactions also help in the aqueous solubility of cellulose. Cellulose dissolved in 10 wt% $NaOH/H_2O$ gels at a temperature above 25^{o}C (Medronho *et al.*, 2012). However, when betain derivative, an amphiphilic co-solute, is added the temperature of gelation is increased by 10^{o}C which the authors attribute to the amphiphilic co-solute reducing the number of hydrophobic interactions that are responsible for aggregation.

It has been noted that, as with the clouding phenomenon seen with some non-ionic polymers with increased temperature (Lindman and Karlström, 2009), cellulose dissolution may sometimes be favoured at lower temperatures. As temperature increases, the polar conformations around the C-C bonds which favour interactions with a polar solvent, shift to less polar conformations and so increase the overall hydrophobicity of the cellulose chains (Lindman *et al.*, 2010).

Amorphous cellulose is able to partially recrystallise immediately in the LiCl/urea/water solution at ambient temperature as the BM MCC is birefringent (Figure 5.10). Bergenstråhle *et al.* (2010) used molecular dynamic simulations of

short cello-oligomers in aqueous solution to estimate the contributions of hydrophobic stacking and hydrogen bonding to the insolubility of crystalline cellulose. They found that hydrophobic association and hydrogen bonding favour crystal packing over solubilisation which is partially a consequence of the planar topology of the rigid flat cellulose ribbons. The authors go on to say that even though their model is based on the native crystalline structure of cellulose they would expect the amorphous regions to behave in a similar way as the hydrophobic surfaces if the chains are paired together in such a way that they exclude water and that many intermolecular hydrogen bonds exist.

Recently, mesoscale modeling of cellulose-water interactions has shown that at ambient temperature the surface of cellulose fibres have at least a monomolecular layer of water associated with it (Khazraji and Robert, 2013). The authors found that cellulose-water interactions are exothermic reactions as there is an increase in entropy which is denoted by a negative heat flow.

It might be argued that the intial heating of cellulose in LiCl/urea/water solution "activates" the particles by swelling them. This is the large exotherm seen in Figure 5.31 of the first heating of the dispersions in the Micro DSC. Hyrdogen bonding on the surface of the cellulose particles/fibres is broken and the swelling solution penetrates further as the temperature increases. This causes the increase in viscosity found by Tatarova and Foster (2010) where 1.4 wt% lyocell had an increase in final viscosity from 70cP to 300cP when heated to 60^{o}C or 95^{o}C respectively. The initial heat destroys some of the crystalline regions (Figure 5.3). At high temperature (90^{o}C) there appears to be a maximum level the swelling solution is able to disrupt the crystalline regions as the crystallinity does not reduce with longer heat treatments (Figure 5.5). Due to the swelling, the cellulose chains are able to more freely change

their conformation between a predominantly hydrophobic or hydrophilic structure in a similar way to methylcellulose. As the temperature increases the cellulose becomes more hydrophobic (Medronho *et al.*, 2012, Lindman *et al.*, 2010) which halts the extremely polar solution from decrystallising the ordered regions. The ability of amorphous cellulose chains, located on the surface of the fibres, to change conformation is likely to be limited by their DP (Figure 5.32). Cellulose has been found to be decreasingly soluble in NaOH with increasing DP (Le Moigne and Navard, 2010). This conformational change is likely to be a twisting of the cellulose chains to reduce the contact of their hydrophobic sides with water at higher temperature.

At a temperature of 60-75^{o}C the viscosity then falls (Figures 5.26, 5.27, 5.28 and 5.33) as the gel-like structure is melted out. Upon cooling, between 35-20^{o}C, the gel-like structure is reformed, as shown by both RVA and Micro DSC results (Figure 5.33). As has been shown by the cross polar micrographs of BM MCC, cellulose is able to form hydrogen bonds at lower temperatures. This structure formation may then be as a result of the conformational change from predominantly hydrophobic to hydrophilic. The primarily hydrophilic cellulose structures water and forms a cellulose-cellulose network which becomes stronger over time (Figure 5.22).

The endothermic peak seen on subsequent reheats between 35-65^{o}C may then be due to a shift from a predominantly hydrophilic structure to a hydrophobic structure. This disrupts the surrounding water and effectively melts out any structure that was formed at a lower temperature.

The LiCl/urea/water solution is unable to completely dissolve cellulose but does solubilise starch. Koganti *et al.* (2011) found that NMMO at concentrations of 70 wt% and above were able to dissolve starch but only at concentrations above 86 wt% was the NMMO able to solubilise cellulose. If the water content of the LiCl/urea/water

solution was decreased then it could be expected to completely dissolve cellulose, however, this is not possible when using a starting temperature at ambient as the salt will come out of solution at such high concentrations.

An alternative explanation to the sudden aggregation of the BM MCC particles seen in Figure 5.11 at approximately 65^{o}C may be a change in phase behaviour due to the solubilty of the outer cellulose chains. Below the lower critical solution temperature, the cellulose may be partially miscible with the LiCl/urea/water solution, but above the lower critical solution temperature the Gibbs free energy become positive. The unfavourable entropy of mixing then causes the cellulose particles to aggregate.

5.5 Conclusion

A LiCl/urea/water solution is able to swell cellulose and decrease its crystallinity. The decrease in crystallinity is increased over time at ambient temperature but not with longer treatments at 90^{o}C. Over time at ambient temperature the treated cellulose dispersions form a gel-like network. BM MCC is able to recrystallise in the LiCl/urea/water solution when first rehydrated showing that there is enough water present to allow some degree of hydrogen bonding. MCC and CP have a similar particle size but CP is able to reach a much higher viscosity at higher concentrations as it has a lower crystallinity and thus is able to swell to a higher degree. The mechanism of gelation may be due to a change in cellulose conformation from predominantly hydrophobic at high temperature to hydrophilic at lower temperatures but may be dependent on the mobility and therefore DP of the cellulose.

Starch granules are eroded from the outside and do not swell in the LiCl/urea/water solution. The two starches have an equal final viscosity after treatment as they have

a similar amylose:amylopectin content showing that they are completely molecular solutions with no granular remnants.

Chapter 6. Natural polysaccharides in LiCl/urea/water

6.1 Introduction

The swelling and dissolution of cellulose in molten salt hydrates and ionic liquids will enable the design of novel composites in combination with other polymers, and in particular cell wall polysaccharides. Before these composites can be designed, however, it is important to understand what effects these solvents have on the properties of the cell wall polysaccharides.

Hofmeister (1888) was the first to recognise that electrolytes have differing effects on proteins by either increasing their solubility (salting in) or increasing precipitation (salting out). Heydweiller (1910) later discovered that salts dissolved in water increased the surface tension of the solution-air interface where anions were the major influencer. The variation in surface tension followed the Hofmeister series where anions are arranged in order of increasing electrostatic surface potential difference:

$$CO_3^{2-} > SO_4^{2-} > IO_3^- > F^- > BrO_3^- > Cl^- > NO_3^- > Br^- > ClO_3^- > I^- > ClO_4^-$$

The order of some of the cations in the Hofmeister series are:

$$NH_4^+ > K^+ > Na^+ > Li^+ > Mg^{2+} > Ca^{2+}$$

The ions to the left of the series decrease the solubility of nonpoar molecules (salting out) and are referred to as chaotropes as they exhibit weaker interactions with water than water itself and so do not interfere to a great degree with hydrogen bonding whereas the ions with a high charge density, to the right of the series, are refered to as kosmotropes as they exhibit stronger interactions with water molecules than water itself and so are able to break water-water hydrogen bonds. The Hofmeister series has generally been derived from experimental results, but recently dos Santos *et al.* (2010), for the first time, have derived a theoretical model of the lyotropic (Hofmeister) series.

Kosmotropes are usually small, strongly hydrated ions and are able to structure water, while chaotropes are generally large and poorly hydrated so break the structure of water. A simple method of assessing the nature of an electrolyte is to measure its effect on the viscosity of water. As salt concentrations increase, kosmotropes will increase the viscosity of water whilst chaotropes will decrease it (Wiggins, 2002).

Chloride ions are weakly chaotropic but the behaviour of a halide salt will normally be determined by the stronger metal ion. Therefore, the overall power of a LiCl solution will be kosmotropic. Urea is a chaotrope but acts as a kosmotrope at high concentrations and is able to denature proteins at concentrations of 4-5M (Russo, 2008). Urea is commonly refered to as a hydrogen bond breaker (McGrane *et al.*, 2004). It has been found to increase the intrinsic viscosity of chitosan by breaking intramolecular hydrogen bonds allowing the molecules to exist in a more extended form (Tsaih and Chen, 1997). The concentration of urea required to disrupt the intramolecular hydrogen bonds increased with increasing molecular weight (Chen and Tsaih, 2000).

Urea, as a chaotrope, acts as a co-solvent by promoting a better solvating interaction between the solute and water (Breslow and Guo, 1990). It breaks the structure of water in the bulk and disrupts the hydrophobic parts of non-ionic surfactants (Deguchi and Meguro, 1975). The unfolding process of ribonuclease by urea and LiCl have been compared (Ahmad, 1983). Urea is able to cause complete denaturation where the unfolded molecule acts as a linear random coil whereas the addition of LiCl leads to incomplete unfolding. When low concentrations of LiCl (i.e. below the concentration it is able to denature ribonulcease alone) were added to urea solutions, the salt actually stabilised the protein against urea denaturation (Ahmad,

1984). This may be due to the ability of the carbonyl oxygen of the urea molecules to form strong complexes with the lithium ions.

Dextran, a high molecular weight α-1-6-linked glucose polymer, has been studied in a number of solvents to identify solvent effects on polymer conformation (Antoniou *et al.*, 2010). Dextran's intrinsic viscosity and coil volume (V_{coil}) was found to double from water to ethanolamine and the hydrodynamic coil radius (R_{coil}) increased from 15.7 to 19.3 nm. The authors suggest that hydrogen bonding is the most important factor that determined solubility. The coil radius of dextran in the other solvents (which were either hydrogen acceptors or donors) increased in a linear order water→ethylene glycol→formamide→DMSO where the Hansen solubility parameter (δ_H) decreased with each solvent, which is a measure of the cohesive energy due to hydrogen bonding (Hansen, 2012).

Due to the hydrogen bond breaking nature of ionic liquids they are excellent solvents for polysaccharides. Using 1-butyl-3-methylimidazolium chloride (BmimCl) as a solvent, Horinaka *et al.* (2012) found that three different galactomannans, guar, tara and locust bean gum (LBG) with mannose to galactose (M:G) ratios of 2:1, 3:1, and 4:1 respectively all had a random coil conformation in concentrated solution and that the galactose side groups caused no conformational changes. 1-allyl-3-methylimidazolium chloride (AmimCl) and BmimCl was used to dissolve 5 wt% konjac (Li *et al.*, 2011). Konjac was found to swell at ambient temperature and dissolve above 60^{o}C forming clear viscous solutions. With increasing temperature the dissolution time decreased, however, the molecular weight also decreased indicating at least some level of degradation.

Ionic liquids have been used to prepare polysaccharide gel structures. Xanthan gum is an anionic polyelectrolyte and only able to form a weak gel network alone and is

usually added to other polysaccharides such as LBG to form synergistic, firm, thermoreversible gels (Copetti *et al.*, 1997), however, at concentrations of 9.1-50 wt% in BmimCl xanthan is able to form a firm gel when left standing at room temperature (Izawa and Kadokawa, 2010). A 9.1 wt% xanthan gum/BmimCl gel could then be converted into a hydrogel by soaking in water. The xanthan became ionically cross-linked (Izawa *et al.*, 2009).

The authors subsequently produced ion gels with fenugreek, guar and LBG (Kadokawa *et al.*, 2013). They found that LBG constructed a looser gel network due to its lower galactose content. Fenugreek produced the strongest gels which the authors attributed to crystalline structures that were formed for fenugreek and guar but not LBG. However, they did not show the molecular weights of the galactomannans which are likely to have a large impact on mechanical properties.

Four different polysaccharides, fenugreek, LBG, konjac and xyloglucan have been chosen to identify any solvent effects of the LiCl/urea/water solution. The binding of the polysaccharides to cellulose in the different solvent environments has also been investigated.

6.2 Materials and Methods

6.2.1 Materials

The polysaccharides used were; Konjac glucomannan from the tubers of *Amorphophallus Konjac, K. Koch*: Propol RS (Shimizu Chemical Corporation, Japan), Xyloglucan from tamarind seed (Dainippon Pharmaceutical Company, Japan), Fenugreek Gum Powder T (Air Green Co., Ltd, Japan) and Locust bean gum (Danisco, Norway).

The celluloses used were cellulose fibre (CF) (Solka 900FCC, International Fibre Corporation, USA) and Avicel MCC type PH-101 Ph Eur (Sigma Aldrich, UK). Ball milled MCC was produced as described in chapter 5.

LiCl ≥99%, urea, fluorescein isothiocyanate (FTIC) and rhodamine B were purchased from Sigma Aldrich (UK). Dimethyl sulfoxide (99.8%), toluene (99.8%), pyridine (99.5%) were purchased from Acros Organics (UK) and dibutyltin dilaurate (95%) was purchased from Alfa Aesar (UK).

6.2.2 Sugar Analysis

Sugar analysis was kindly performed by Nofima (Norway).

6.2.3 Molecular weight measurement

Molecular weight measurements were kindly performed by Nofima (Norway). Dried sample was mixed with water ca. 1 mg/ml. Each sample was treated twice as follows: cooked for 5 min in a boiling water bath followed by vigorous shaking in Precellys shaker for two cycles of 30 seconds (default program, without beads). All samples were then made to 0.1 M sodium nitrate, 0.02 wt% sodium azide and then filtered through a 0.8 µm filter. Finally 100 µl was injected into the SEC-MALS system. This system comprised a Shimadzu autosampler and pump, Dawn helios light scattering detector (8 angles), Optilab T-rEX refractive index detector, and a viscostar II viscometer (all detectors from Wyatt, USA). The columns were maintained at 25 °C and comprising two serially connected Tosoh Bioscience TSK gel Bioscience G5000 and G6000 PWXL SEC columns operated at a flow rate of 0.5 ml min^{-1}. Pullulan (NP2) with a certified molecular weight of 4.23 x 105 from PSS, Germany was injected as a positive control (certified reference standard). The refractive index increment (dn/dc) was not individually determined for each sample and was taken to be 0.147 for all samples. Nor was the second viral coefficient (A2) determined. It was taken as

being zero. Forward extrapolation (to smaller masses) of molar mass data was done via fitting of an exponential function. All data were processed with Astra 6 Software from Wyatt.

6.2.4 LiCl/Urea/Water solution preparation

See chapter 5, section 5.2.2, page 136.

6.2.5 Hemicellulose purification

Initially, hemicellulose powders were added to the LiCl/urea/water solution but there was great difficulty in dissolving the hemicelluloses. This may have been due to the small amounts of insoluble impurities present in the samples. The following purification step was then employed:

Hemicellulose stock solutions were prepared by stirring the powders in deionised water and heating to 80^{o}C for 30 minutes. The solutions were then left on a roller bed overnight at room temperature. The hemicellulose solutions were then centrifuged at 2000g for 20 minutes at 20^{o}C. When powders were needed for the swelling treatment, the supernatant was freeze dried and the freeze dried material dispersed in the LiCl/urea/water solution.

6.2.6 Rapid Visco Analyser (RVA)

See chapter 5, section 5.24, page 136.

6.2.7 Rheology

Rheological measurements of the polymer solutions were carried out using a Bohlin CVO rheometer (Bohlin Instruments Ltd, Cirencester, UK) with cone and plate (4^{o} cone angle/40mm diameter and 150 µm gap) and double gap (for low viscosity measurements) geometries at 25^{o}C. Zero shear values were obtained by using the Cross model within the Bohlin software.

Oscillatory rheology measurements were performed using a Bohlin CVO rheometer with a cone and plate geometry (4^{o} cone angle/40mm diameter and 150 µm gap) at 25^{o}C. Amplitude sweeps were carried out to ensure measurements were within the linear viscoelastic region where the dynamic storage modulus (G') and loss modulus (G'') are independent of the stress amplitude. Frequency sweeps had an applied stress of 1 Pa.

Intrinsic viscosities were estimated using the single point method described in Chapter 4 using rotational rheometry data.

6.2.8 Capillary Rheometer

Water was mixed with unpurified polysaccharide powders in a food mixer. The hydrated mixture was then placed in the pre-heated (80^{o}C) capillary of a Rosand Flowmaster Capillary Rheometer RH-7 (Malvern Instruments Ltd, UK). Samples were immediately run to avoid too much moisture loss at a series of 10 shear rates from 2-1000 Pas.

6.2.9 Surface tension measurements

The surface tension of 0.04 wt% concentrations of the polysaccharide in either water or LiCl/urea/water was measured using a Profile Analysis Tensiometer 1 (Sinterface, Germany) at a temperature of 25^{o}C. After thorough cleaning with the respective solvent a pendant drop was formed on a needle and the profile of the drop was measured over time using the tensiometer software.

6.2.10 Dialysis

Polysaccharide solutions were dialysed after treatment to remove the salts using BioDesignDialysis Tubing (D106) 8000 MWCO (BioDesign Inc, New York, USA). The dialysed samples were then freeze dried to remove water.

6.2.11 ^{13}C Cross Polarization Magic Angle Spinning Nuclear Magnetic Resonance (CPMAS NMR)

See chapter 3, section 3.2.7, page 59.

6.2.12 Fourier Transformed Infrared Spectra (FTIR)

The FTIR spectra of the polysaccharides were recorded using a Brucker IFS48 spectrometer with a DTGS detector equipped with an ATR single reflectance cell with a diamond crystal (45 incidence angle) golden gate cell (Graseby-Space Ltd, Orpington, UK). For each measurement the spectra was obtained from the average of 128 scans at a resolution of 4 cm^{-1} against an empty background. Spectra were base line corrected.

6.2.13 Fluorescent tagging

Fluorescent tagging was kindly carried out by Latifah Jasmini (Chemical Engineering, University of Nottingham). LBG and fenugreek were labelled with Rhodamine B and konjac and xyloglucan were labelled with fluorescein isothiocyanate (FTIC). To a two-necked-100 ml-round bottom flask equipped with a magnetic stir bar, the polysaccharide (0.5g) and fluorescent marker (50 mg) were added. The flask was purged with argon before adding dry dimethylsulfoxide (50 ml) and subsequently attached to the condenser. Pyridine (0.1 ml) and dibutyltin dilaurate (50 mg) were then added to the flask. The reaction was heated at 95^{o}C for 24 h. The modified polysaccharide was filtered and washed with ethanol before drying *in vacuo*.

6.2.14 Confocal laser scanning microscopy (CLSM)

Polysaccharides were matched to a specific viscosity of 100 in either water or LiCl/urea/water. 0.01g of each polysaccharide was replaced with the fluorescently labelled sample. Samples were then run in the RVA with the same profile used above in 6.2.6. After treatment an aliquot of the sample was deposited onto a glass slide

and covered with a cover slip. A Leica TCS SP5 confocal laser scanning microscope (CLSM) equipped with an inverted microscope was used in single photon mode with an Ar laser with a Leica objective lens (10 X 0.4 IMM/dry/HC PL APO). Different excitation wavelengths were used depending on which florescent sample was used (Table 6.1).

Table 6.1 Excitation and emission wavelengths of the fluorescent samples.

	Excitation (nm)	Emission (nm)
Rhodamine B	540	625
FITC	495	519

6.3 Results and Discussion

Sugar analysis gives a clear indication as to the structure of the polysaccharides (Table 6.2). LBG has a mannose to galactose (M:G) ratio of 2.9:1 which is lower than the 4:1 ratio usually found in the literature (Naoi *et al.*, 2002). The M:G ratio of fenugreek is in better agreement with the literature at 1.1:1 (Mathur and Mathur, 2005, Mathur, 2011, Brummer *et al.*, 2003). Both LBG and fenugreek contain a number of other sugars which may be from a small fraction of other hemicelluloses. The percentage sum of the yield compared to the starting material is in agreement with the amount of insoluble material that is removed during the purification step (≈20 wt%) described in the methods section (Section 6.2.5, page 181).

Table 6.2 Sugar analysis with yields described as wt% of dried starting material showing the yields of arabinose (Ara), rhamnose (Rha), fucose (Fuc), xylose (Xyl), glucuronic acid (GlcA), galacturonic acid (GalA), mannose (Man), galactose (Gal) and glucose (Glc).

	Ara	Rha	Fuc	Xyl	GlcA	GalA	Man	Gal	Glc	Sum
LBG	1.8	0.4	0.0	0.9	0.4	1.2	55.1	19.3	1.7	80.8
Fenugreek	0.3	0.2	0.0	0.8	0.0	0.6	43.5	39.1	0.4	84.9
Konjac	0.0	0.0	0.0	0.4	0.1	0.3	44.1	3.5	26.1	74.5
Xyloglucan	1.4	0.2	0.0	28.8	0.2	0.6	4.0	14.4	13.2	62.8

The mannose to glucose ratio of konjac is 1.7:1 which is close to 1.6:1 often described in the literature for the β-(1-4)-linked backbone (Williams *et al.*, 2000). Konjac also has a low level of branching (≈8%) at the β-(1-6)-glucosyl units (Nishinari *et al.*, 2007). There is also small fraction of galactose branching (≈5%) (Buckeridge *et al.*, 2000).

Xyloglucan has a cellulosic-like β-1,4-linked glucan backbone highly substituted with α-D-linked xylospyranosyl residues attached at O-6 which can be further substituted with other sugar residues. The proportion of glucose from the sugar analysis is much lower than would be expected as it should be at least a little higher than xylose. This is likely to be a result of incomplete acid hydrolysis as the cellulose backbone is much harder to break down than the other sugar side units. This would then explain the low sum value of 62.3% of the dried starting material. This sample of xyloglucan has no fucose side units as it is a storage polysaccharide from tamarind seeds rather than from the primary cell wall (Buckeridge, 2010). The fucosyl residues have been suggested to increase the adsorption affinity to cellulose (Hayashi *et al.*, 1994) due to a flatter conformation of the polymer which increases its capacity to bind to cellulose (Levy *et al.*, 1991). Therefore, in aqueous solution this xyloglucan will have a flexible random coil configuration (Ren *et al.*, 2004). There is also quite a high degree of galactosylation which may further decrease interactivity with cellulose (de Lima and Buckeridge, 2001) although the fine structure distribution is important. Uneven distribution of galactose may favour a higher binding capacity if the galactosyl residues are at one side of the polysaccharide molecule which would expose the glucose backbone (de Lima and Buckeridge, 2001) whereas a uniform distribution of galactose side units would lead to a more twisted backbone and therefore lower the binding capacity (Levy *et al.*, 1997). Tamarind seed xyloglucan is composed of a regular patter of Xly-substitution where the majority of the molecule is composed of

repetitive units of Glc_4:Xyl_3 (York *et al.*, 1990). The sugar analysis results which show a xylose:galactose ratio of 2:1 may indicate that this xyloglucan has a repetitive subunit of XLLG + XLXG or XLLG + XXLG where X corresponds to α-D-Xyl-(1-6)-Glc, L corresponds to a xylose residue substituted at O-2 with β-Gal and G denotes an unbranched glucose residue (Buckeridge *et al.*, 1992, Nishinari *et al.*, 2007). There is also a smaller fraction of arabinose side units. The mannose is likely to be from other hemicelluloses that have not been removed.

Fenugreek has the highest weight average molecular weight of the polysaccharides used (Table 6.3) and is much larger than LBG although it has a lower intrinsic viscosity in water. These results are in line with some authors such as Wu *et al.* (2009) who found that LBG had a molecular weight of 2.08 x 10^6 g/mol and intrinsic viscosity of 14.2 dl/g and that fenugreek had a molecular weight of 3.23 x 10^6 g/mol and an intrinsic viscosity of 15.10 dl/g. Pollard *et al.* (2008) found that different commercial LBG samples had molecular weights in the range of 0.86 - 1.0 x 10^6 g/mol and intrinsic viscosities in the range of 12.4 -13.9 dl/g while Andrade *et al.* (1999) found that purifying LBG increased its molecular weight from 2.03 to 2.29 x 10^6 g/mol and intrinsic viscosity from 13.5-14.0 to 15.2-15.7 dl/g. Brummer *et al.* (2003) found that LBG had a molecular weight of 1.2 x 10^6 g/mol and an intrinsic viscosity of 14.38 dl/g while fenugreek had a larger molecular weight of 1.4 x 10^6 g/mol but a smaller intrinsic viscosity of 9.61 dl/g. The authors also found that LBG had a larger radius of gyration (R_g) than fenugreek, at 82.88 nm compared to 75.08 nm respectively. They account for this disparity between molecular weight and intrinsic viscosity by noting previous research which has found that the addition of galactosyl residues on the mannan backbone induces a reduction in chain dimensions (Petkowicz *et al.*, 1998). Using molecular modelling, Wang and Somasundaran (2007) found that guar forms a more compacted helical structure than LBG (which has a stiffer chain) due to the

increase in galactose side chains which increases intra-molecular hydrogen bonding. Fenugreek is even more highly substituted than guar and so is likely to form an even tighter structure. For galactomannans with intermediate M:G ratios such as guar and tara the galactosyl distribution pattern is also of importance for overall conformation (Wu *et al.*, 2012).

Table 6.3 Molecular weights measured by SEC MALS and intrinsic viscosities measured by rotational rheometry, of each of the polysaccharides. The average of three replicates for each intrinsic viscosity is shown ± the standard deviation.

	Weight average molecular weight (10^6 g/mol)	[η] in Water (dl/g)	[η] in LiCl/urea/water (dl/g)
LBG	2.72	17.5 ± 0.2	10.8 ± 0.1
Fenugreek	4.045	15.2 ± 0.1	55.6 ± 2.8
Konjac	2.06	15.7 ± 0.4	17.3 ± 0.4
Xyloglucan	1.48	2.7 ± 0.1	5.1 ± 0.1

Goycoolea *et al.* (1995) previously found that LBG had an intrinsic viscosity of 12.1 dl/g in 1M NaCl but this decreased to just 5.2 dl/g in 1M NaOH. Upon neutralisation the viscosity substantially increased which showed the effects were not wholly due to depolymerisation. They suggested that LBG does not form completely molecular solutions but is in fact associated due to the unsubstituted regions of the mannan backbone. These associations or 'hyperentaglements' are broken by alkali resulting in a reduction in viscosity. They showed that guar also undergoes a slight decrease in intrinsic viscosity in alkaline conditions from 12.5 to 11.9 dl/g. The decrease is much smaller than LBG as there are fewer unsubstituted regions on the mannan backbone due to a higher galactose content.

Doyle *et al.* (2009), using the same method as Goycoolea *et al.* (1995) but with fenugreek, found that the addition of 1M NaOH decreased the intrinsic viscosity from 16.0 to 12.0 dl/g. With increasing NaOH concentration the intrinsic viscosity

decreased until levelling off at concentration of 3M. This was explained by the alkali causing the ionisation of the hydroxyl groups (from –OH to $–O^-$) which caused electrostatic repulsion and inhibited hyperentanglement. As fenugreek is fully substituted and so does not have any part of the backbone free for mannan-mannan interaction, Doyle *et al.* (2009) proposed a new theory of hyperentanglement where there are transient associations in the crystallographic *a* plane where galactose side chains lay above or below one another exposing the mannan backbone for weak intermolecular associations as well as the more permanent mannan-mannan associations in the *b* crystallographic plane for less substituted galactomannan.

Richardson *et al.* (1998) found that the addition of sucrose up to a concentration of 10 wt% decreased the intrinsic viscosity of LBG which the authors suggested was due to an decrease in polymer/polymer associations again suggesting that the intrinsic viscosity in water is artificially high due to aggregates. There was an increase in the intrinsic viscosity for both LBG and guar at a sucrose concentration of 20 wt% which may have been due to an increase in the solvent quality but it was then subsequently decreased at a concentration of 40 wt% which may have been due to competition for water which enhanced polymer contraction. They also found that guar was more compact than LBG due to its higher galactose content.

In this study, the decrease in LBG's intrinsic viscosity is less than might be expected (17.5 to 10.8 dl/g) when compared to the work of Goycoolea *et al.* (1995). This might indicate that whilst intermolecular associations are disrupted there is also a decrease in intramolecular hydrogen bonding which expands the overall conformation of the individual LBG molecules.

Konjac has a molecular weight of about 2×10^6 g/mol which is in the range that has previously been reported (Dave *et al.*, 1998, Parry, 2010). Konjac is often described

as having a semi flexible coil conformation in aqueous solution (Kok *et al.*, 2009, Li and Xie, 2006) although recent work has suggested that it has an ordered single helix in neutral, dilute solution although at high temperatures (>60^{o}C), high NaOH (>0.45M) or high urea (>4.0M) the order is lost resulting in a random coil conformation (Wang *et al.*, 2011).

Storage xyloglucans are known to have high molecular weights of up to 2 x 10^6 g/mol (Mishra and Malhotra, 2009). Xyloglucan decreases in its level of interaction with increased molecular weight (Lima *et al.*, 2004). Lima *et al.* (2004) have suggested a mechanism where storage xyloglucans are first synthesised as low molecular weight polymers and then assembled into bigger complexes at the end of polysaccharide deposition.

The zero shear viscosity of the polysaccharides was compared in pure water and in the LiCl/urea/water solution. Specific viscosity takes into account the differences in the solvent viscosities. By plotting concentration against zero shear specific viscosity on a log-log scale different solution regimes can be differentiated (McCleary *et al.*, 1985). All the polysaccharides used show a linear relationship between concentration and viscosity at low concentrations which then changes at a critical concentration (c^*) to a power law relationship as the concentration increases due to the formation of an entangled polymer network.

The viscosity at low concentrations (below 0.1 wt%) of LBG is lower in the LiCl/urea/water solution than water (Figure 6.1) which is in agreement with the decrease in intrinsic viscosity (Table 6.3). At higher concentrations, LBG's viscosity is similar in both solvents. Fenugreek on the other hand has a much higher viscosity in LiCl/urea/water. Similarly xyloglucan also has a considerably higher viscosity in

LiCl/urea/water whereas there is only a minimal increase for konjac (Figures 6.2 and Table 6.3).

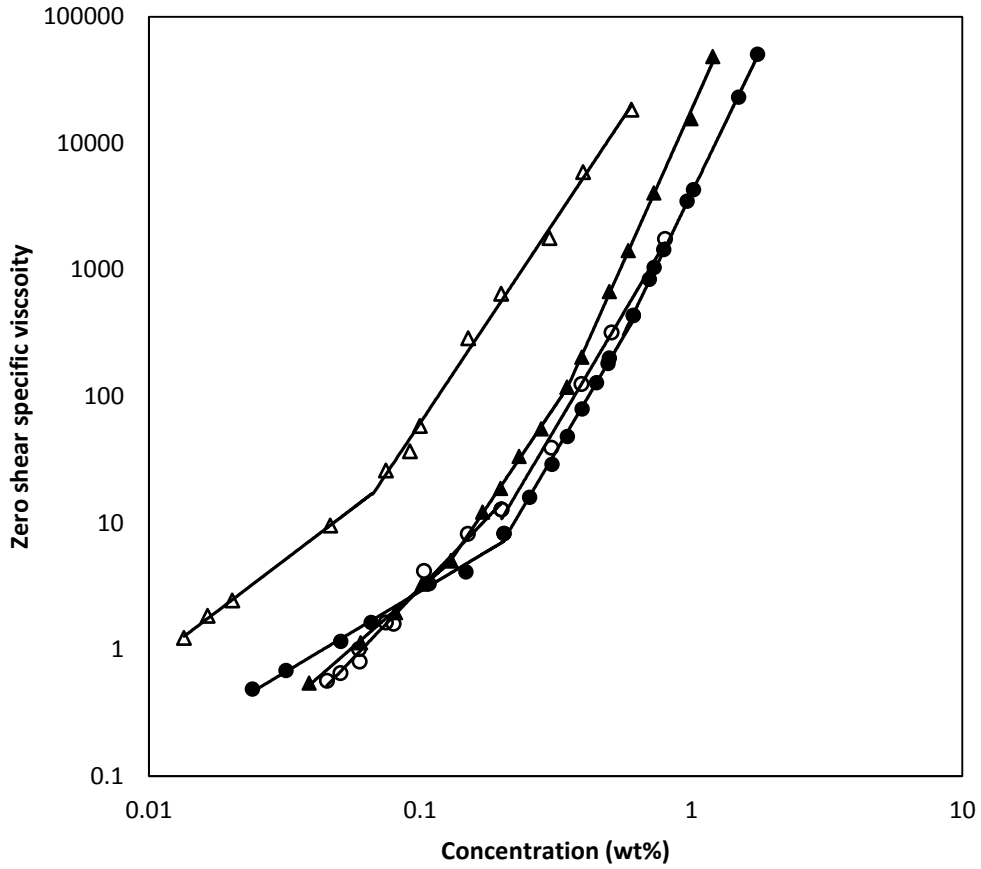

Figure 6.1 The zero shear specific viscosity of fenugreek (triangles) and LBG (circles) in water (filled symbols) or the LiCl/urea/water solution (open symbols) at 25°C.

Aqueous LiCl solutions have previously been found to not affect the intrinsic viscosity of guar up to a salt concentration of 4.1 mol/L (Ma and Pawlik, 2007). However, a saturated solution of LiCl increased the intrinsic viscosity of guar from 11.7 to 21.7 dl/g. Urea had no effect on the intrinsic viscosity up to a concentration of 1 mol/L but at 4 mol/L concentration the intrinsic viscosity increased to 14.5 dl/g although, interestingly, the intrinsic viscosity decreased slightly for a saturated urea solution. Saturated solutions of cesium chloride (CsCl) decreased guar's intrinsic viscosity. Ma and Pawlik (2007) account for these differences by the solvent quality of the different salt solutions. Saturated CsCl (a chaotrope and thus a water-structure breaker) is a

better solvent than water so fully solubilises guar by dissociating any aggregates between the unsubstituted mannan chains. They suggest that saturated LiCl and NaCl (kosmotropes) solutions actually increase the level of aggregation by the Li^+ and Na^+ binding water molecules into their hydration sheaths leaving little water to hydrate/solubilise the polymer chains thereby making polymer-polymer interactions more favourable than polymer-solvent interactions. This competitive hydration model does not correlate, however, with their results for urea. They suggest that the hydrogen bond breaking properties of urea do not occur at the low guar concentrations level they studied. The authors exclude conformation change as a possible cause in altering the intrinsic viscosity due to the non-ionic nature of guar and so insist there can be no screening of anionic functional groups.

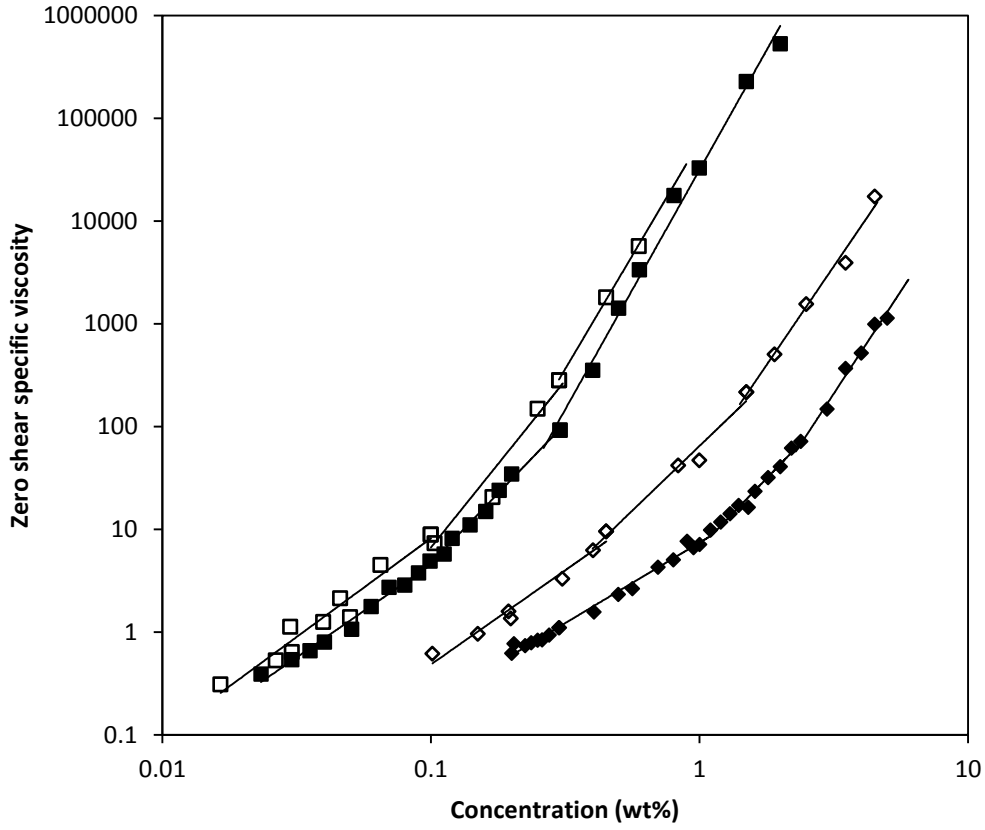

Figure 6.2 The zero shear specific viscosity of konjac (squares) and xyloglucan (diamonds) in water (filled symbols) or the LiCl/urea/water solution (open symbols) at 25°C.

Recently, researchers have begun to dispute idea that water structure breaking and making is central to the Hofmeister series (Zhang and Cremer, 2006) and that rather, direct ion-macromolecule interactions are the major driving force. Using femto-second mid-infrared pump-probe spectrocopy, Omta *et al.* (2003) found that the water strucutre outside the hydration shell of the ion was not influenced by the ion.

A model of hydrogen bond breaking causing conformational change gives a more complete picture as to what may be happening in both the present chapter and the work of Ma and Pawlik (2007). The intrinsic viscosity of LBG does decrease in LiCl/urea/water due to the break-up of aggregates but conformational change increases the viscosity of fenugreek and xyloglucan. If competition for water was the major factor then konjac should also increase in viscosity to a similar level, but it does not as it does not undergo significant conformational change.

In water all polysaccharides show viscoelastic liquid-like behaviour where the storage modulus (G') is below the loss modulus (G'') at low frequencies (Figure 6.3). At higher frequencies the systems have a solid-like behaviour with G' higher than G'' and there is less frequency dependence due to polymer entanglement (Clark and Ross-Murphy, 2009). This feature is found for many random-coil polysaccharides in the concentrated regime (Wientjes *et al.*, 2001).

None of the polysaccharides used gel independently. The crossover frequency of fenugreek can be shifted to higher values when the protein content is reduced (Youssef *et al.*, 2009).

Native xyloglucan does not gel (Wang *et al.*, 1997, Nishinari and Takahashi, 2003), however, tamarind xyloglucan has been found to gel by the removal of 35% of the galactose side chains (Shirakawa *et al.*, 1998). Gels were formed upon heating but

returned to the sol state on cooling indicating that hydrophobic interactions were important, in a similar way to methylcellulose (Brun-Graeppi *et al.*, 2010). Xyloglucan is also able to gel with the addition of alcohol (Yuguchi *et al.*, 2004).

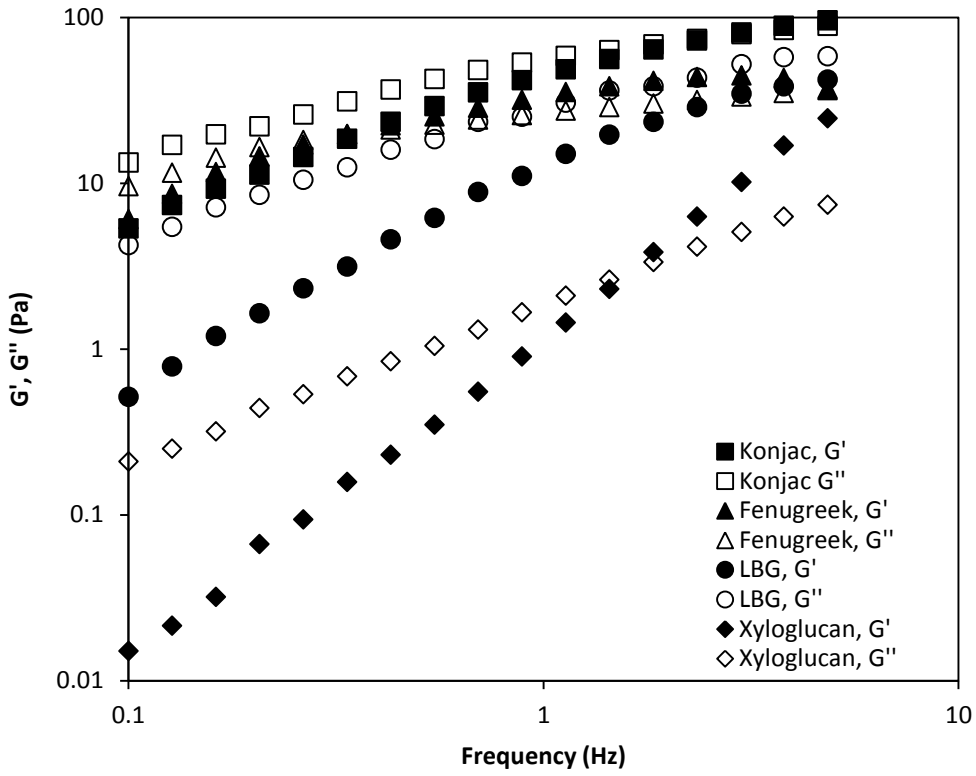

Figure 6.3 The dynamic moduli G' (filled symbols) and G'' (open symbols) of 1 wt% polysaccharide solutions in water at 25°C.

In the LiCl/urea/water solvent both fenugreek and konjac show a viscoelastic solid behaviour indicating a higher level of entanglement whereas LBG still has a liquid-like behaviour (Figure 6.4). This may be due to LBG's smaller size in LiCl/urea/water caused by disaggregation leading to smaller molecules and therefore less entanglement. Xyloglucan also shows liquid-like behaviour which may be due to its lower molecular weight.

Recently, Horinaka *et al.* (2012) used 1-butyl-3-methylimidazolium chloride (BmimCl) to solubilise guar, tara and LBG. They found that concentrated solutions (5-20 wt%)

showed angular frequency dependence curves of the storage and loss modulus which is characteristic of entangled polymer chains in solution.

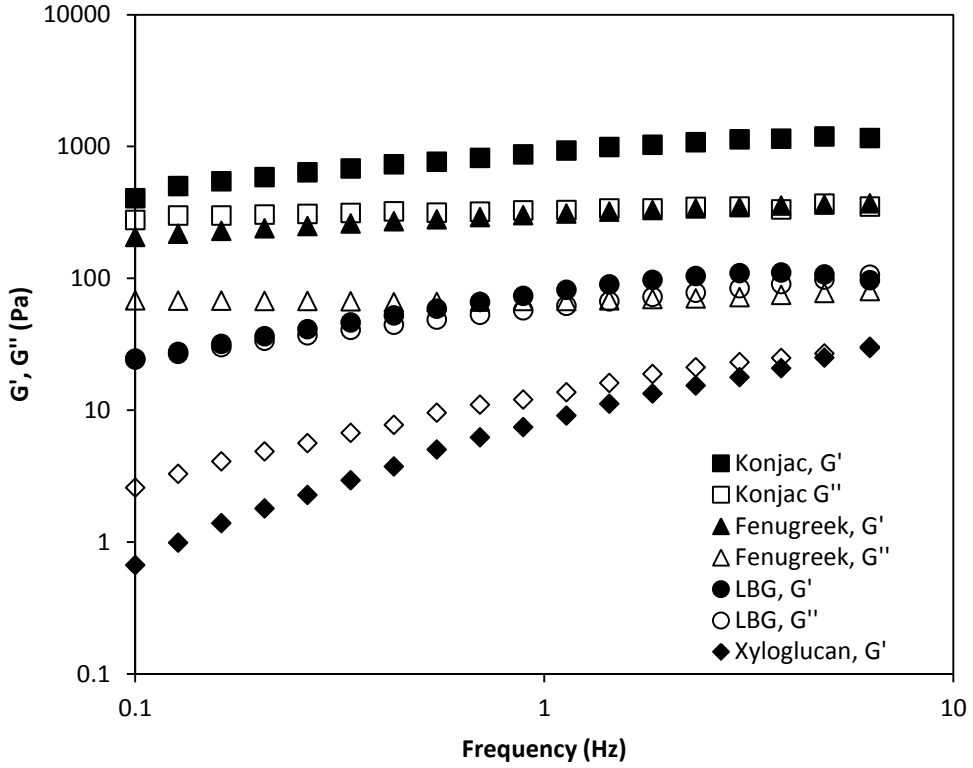

Figure 6.4 The dynamic moduli G' (filled symbols) and G'' (open symbols) of 1 wt% polysaccharide solutions in LiCl/urea/water at 25°C.

There is a growing interest in the extrusion of polysaccharides which modifies their properties, for instance, xanthan forms a particulate structure which has much quicker hydration rates than unmodified powder (Sereno *et al.*, 2007). A capillary rheometer is able to measure the shear viscosity and shear stress of highly concentrated polysaccharide mixtures which helps cast light on what is happening within an extruder. Most polysaccharides form long ribbon-like strings in concentration ranges between 20-60 wt%. Figure 6.5 shows an example of ribbons of LBG at different concentrations. Other polysaccharides that also produce these ribbons include konjac, pectin, carrageenan and xanthan. Fenugreek, however, did not produce ribbons in concentrations above 30 wt% and even at a concentration of 20 wt% the ribbons were only able to achieve a length of about 4cm before breaking

(Figure 6.5). A possible explanation of this unusual behaviour is that fenugreek is amphiphilic (Garti *et al.*, 1997, Yildiz and Oner, 2014). Fenugreek has been found to have adsorption isotherms (onto the oil/water interface) more characteristic of amphiphilic biopolymers than those of other gums (18mg/m^2 compared to 2.8mg/m^2 for LBG and 4mg/m^2 for guar) (Garti, 2005). To investigate this further, surface tension measurements were performed.

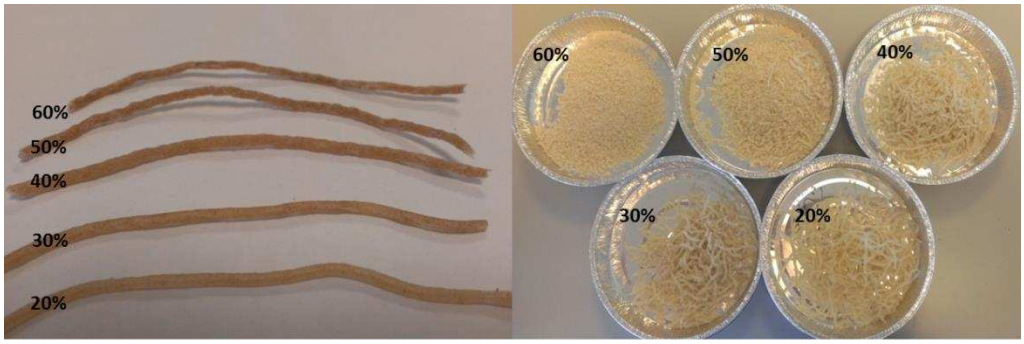

Figure 6.5 LBG (left) and fenugreek (right) extruded from a capillary rheometer. Numbers next to each sample represents the concentration of polysaccharide.

Surface tension is the ability of a liquid to resist an external force on its surface due to a greater attraction of the solvent molecules to each other than to the air. A useful way of measuring surface tension is the pendant drop method where a drop of liquid is suspended from the end of a tube. A camera measures any change in the shape of the droplet over time. Surfactants have the ability to lower surface tension by adsorbing at the interface between liquid and air.

Fenugreek is known to be surface active although there is some disagreement as to how much the small protein fraction aids with this (Mathur, 2011, Mathur and Mathur, 2005, Brummer *et al.*, 2003). There are also reports of LBG surface activity but to a much lower extent, for instance Wu *et al.* (2009) found that 0.5 wt% concentration of fenugreek reduced the interfacial tension of water to 58 mN/m whilst LBG was only able to reduce interfacial tension to 64 mN/m. Some studies have shown that after removing protein from LBG and fenugreek the surface activity

was not affected (Garti and Reichman, 1994, Garti *et al.*, 1997) while other studies have reported that purified LBG shows no surface activity (Gaonkar, 1991). More recent studies have shown that the removal of protein from fenugreek does reduce surface activity but does not completley remove it (Youssef *et al.*, 2009). Wu *et al.* (2009) have concluded that whilst protein contaminants will provide some surface activity they are not the major factor responsible for surface activity and that the M:G ratio and fine structure was the major cause.

0.04 wt% fenugreek lowers the surface tension of water whereas 0.04 wt% LBG has no effect (Figure 6.6). The LiCl/urea/water solution has a higher surface tension than that of water which is shown by the increase of almost 20 mN/m (Figure 6.7). Both LiCl and urea increase the surface tension of water (Aveyard, 1982). At high concentrations of 10M at 20^{o}C urea increases the surface of water to 75 mN/m (Šišková *et al.*, 1985). Surface tension values as high as 180 mN/m have been found for concentrated solution of LiCl (Liu *et al.*, 2011). The surface tension is related to how much the salts structure water (Weissenborn and Pugh, 1996). LiCl is therefore the major influencer on the overall surface tension.

In LiCl/urea/water fenugreek again reduces the surface tension (Figure 6.7). Over a much longer time period LBG does also reduce the surface tension slightly. It is possible that if the LBG in water had been left for a longer time it would also have reduced the surface tension of water to some degree as the surface tension was only measured for 1500 seconds in water but took 2000 seconds to start to decrease in LiCl//urea/water (Figure 6.7). The purification of the polysaccharides was only done using centrifugation to remove the bulk of the insoluble fraction so there is likely to still be some protein present in the samples, although protein content was not measured. These surface tension measurements do show that fenugreek is a better

surfactant indicating it might have more of an amphiphilic characteristic than LBG. It would be useful for future work to assess the surface activity of xyloglucan as the main chain has been found to be partially hydrophobic while the galactose moieties are hydrophilic (Umemura and Yuguchi, 2009).

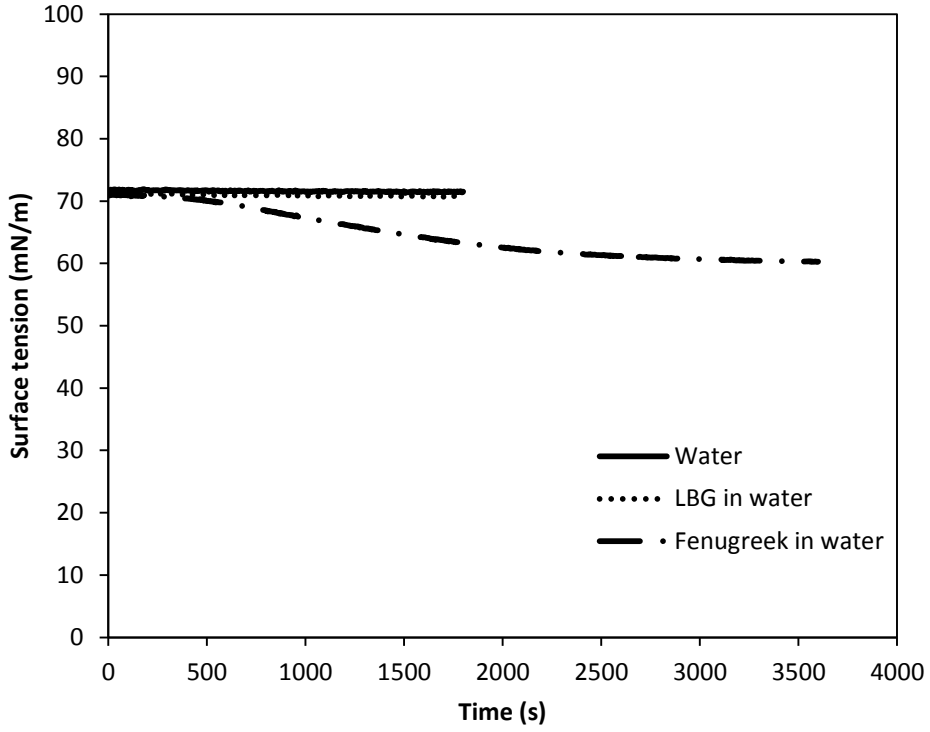

Figure 6.6 Tensiometer data showing the surface tension of 0.04 wt% galactomannans in water.

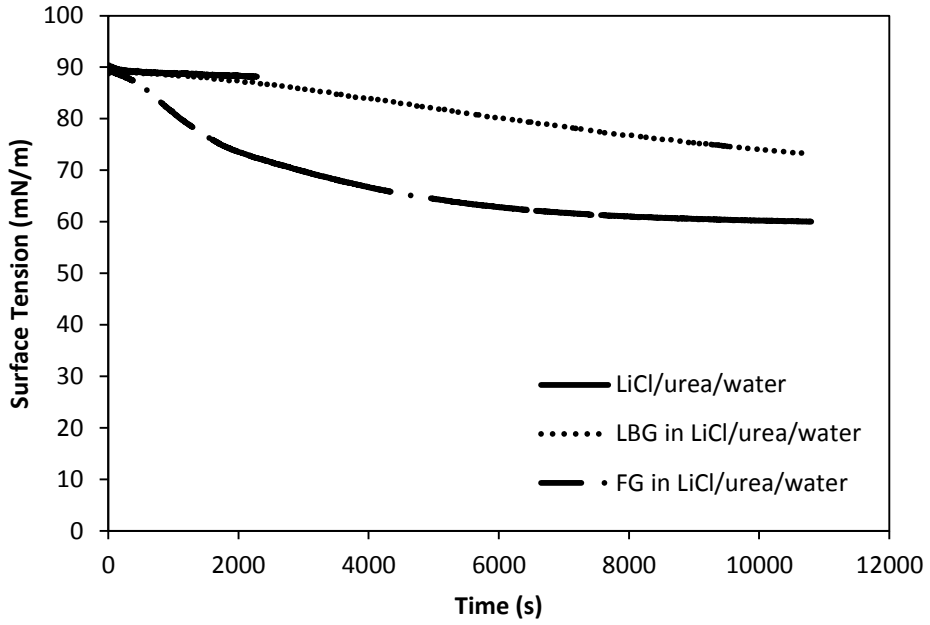

Figure 6.7 Tensiometer data showing the surface tension of 0.04 wt% galactomannans in LiCl/urea/water.

β-1,4 glucans, β-mannans and β-xylans cause a much greater reduction in the freedom of movement of water molecules than α-galactans, α-mannans, α-xylans and α-glucans, which results in their surface minimisation and concomitant reduction in water solubility (Chaplin, 2003). Hydrophobic molecules prefer a less dense aqueous environment than hydrophilic molecules which prefer a denser aqueous environment. Low density water is therefore a good solvent for hydrophobic molecules as they need to order the water around them which tends to happen at low temperatures (Chaplin, 2000, Chaplin, 2001). Xylose units are more hydrophobic than galactose or glucose as they have one less OH group (Picout *et al.*, 2003). With the removal of some galactose side chains (>35%) using fungal β-galactosidase, concentrated xyloglucan solutions are able to gel at high temperature due to the aggregation of hydrophobic domains to minimise the hydrophobic surface area in contact with the bulk water (Brun-Graeppi *et al.*, 2010). The mannan backbone of

fenugreek is sheilded by the galactose side chains resulting in the backbone being hydrophobic (Mathur, 2011, Dionísio and Grenha, 2012).

Urea is able to disrupt hydrophobic interactions by disordering water structure (de Xammar Oro, 2001) although the influence of urea on hydrophobic interactions is controversial (Cho *et al.*, 2006). Urea at a concentration of 7M was able to disrupt the hydrophobic domains of chitosan (Philippova *et al.*, 2001). Urea may therefore be causing conformational change by both breaking hydrogen bonds and disrupting the hydrophobic domains of both fenugreek and xyloglucan which leads to the large increase in viscosity.

Ivory nut mannan is an example of nearly pure mannan (Putaux, 2005). It is insoluble in water which is usually attributed to the strong mannan-mannan intermolecular associations. With increasing galactose content these interactions are weakened by the steric hindrance of the side units which increases aqueous solubility. LBG is able to form gels following a freeze-thaw treatment whereas the more highly substituted guar is not. Similarly to cellulose, mannan I is the native crystalline state which can be converted to mannan II after alkali treatment (Chanzy *et al.*, 1979) although mannan II is also found in nature (*Codium fragile*) (Marchessault *et al.*, 1990). In contrast with cellulose, native crystal forms of mannan have an anti-parallel chain packing of two-fold helices (Chanzy *et al.*, 1987). All galactomannans, regardless of their level of substitution have a broadly similar three-dimensional crystal structure with an anti-parallel sheet stabilised by mannan-mannan hydrogen bonding (Song *et al.*, 1989). Any spaces where a galactose molecule would otherwise be will be filled by a water molecule and thus a loss in crystallinity upon drying is found due to a collapse in the structure. Due to fenugreek's higher galactose substitution it shows markedly less loss of crystallinity upon drying than LBG, tara or guar (Song *et al.*, 1989).

^{13}C CPMAS NMR is primarily used to identify order at the molecular level rather than crystalline structure (Gidley *et al.*, 1991). Gidley *et al.* (1991) compared guar, LBG and konjac using ^{13}C CPMAS NMR. They found that all the dry samples (8-10 wt% H_2O) had broad spectral features with only limited resolution of signals (i.e. amorphous) and that hydration (30 wt%) led to narrower resonances and increased resolution. This hydration-induced conformational adjustment has also been seen for other polysaccharides such as agarose and kappa- and iota-carrageenan (Saitô *et al.*, 1990). Ivory nut mannan, however, does have sharp resonances for the dry powder. These sharp signals indicate the crystalline structure of the mannan which has also been found with XRD (Atkins *et al.*, 1988). Hydration broadened these features in CPMAS NMR and XRD which indicated a decrease in both crystalline and molecular order (Gidley *et al.*, 1991).

Samples of the treated and untreated polysaccharides were dialysed to remove the solvent and freeze dried. The ^{13}C CPMAS NMR spectrum of the treated fenugreek sample has slightly more resolved peaks than those of the untreated sample (Figure 6.8a) which indicates there was a small increase in molecular order. Whilst fenugreek is generally referred to having a M:G ratio of 1:1 (Mathur and Mathur, 2005), in this study it was found to be just higher at 1.11:1 (Table 6.2), which suggests 48% galactose substitution, so there may be enough free mannose to allow for very occasional hydrophobic ordering when the fenugreek contracts as the solvent is removed causing minor aggregates.

The NMR spectra show a large difference between the treated and untreated LBG samples (Figure 6.8b). Although both samples were in pure aqueous solution before drying as all the salts should have been removed by dialysis the treated LBG sample appears to have much greater molecular order than the untreated sample as shown

by the sharper peaks. The spectrum seen in Figure 6.8b for the treated LBG is very similar to that of mannan II from *Codium fragile* (Marchessault *et al.*, 1990). This could be interpreted as the galactose residues have been removed during treatment leaving behind almost pure mannan chains that are able to crystallise but this is not born out from the FTIR spectra in Figure 6.9b where there is almost no change meaning there has been very little, if any, chemical modification. As seen by the decrease in intrinsic viscosity the LBG aggregates are broken by the LiCl/urea/water solvent. When the solvent is replaced by water these smaller LBG molecules will once again aggregate due to the unsubstituted regions on the LBG mannan backbone which are hydrophobic (Picout *et al.*, 2003). However due to their smaller starting size they will be able to produce greater molecular order. β-glucans have been found to gel faster and produce gels with greater G' values as the molecular weight decreases (Brummer *et al.*, 2014).

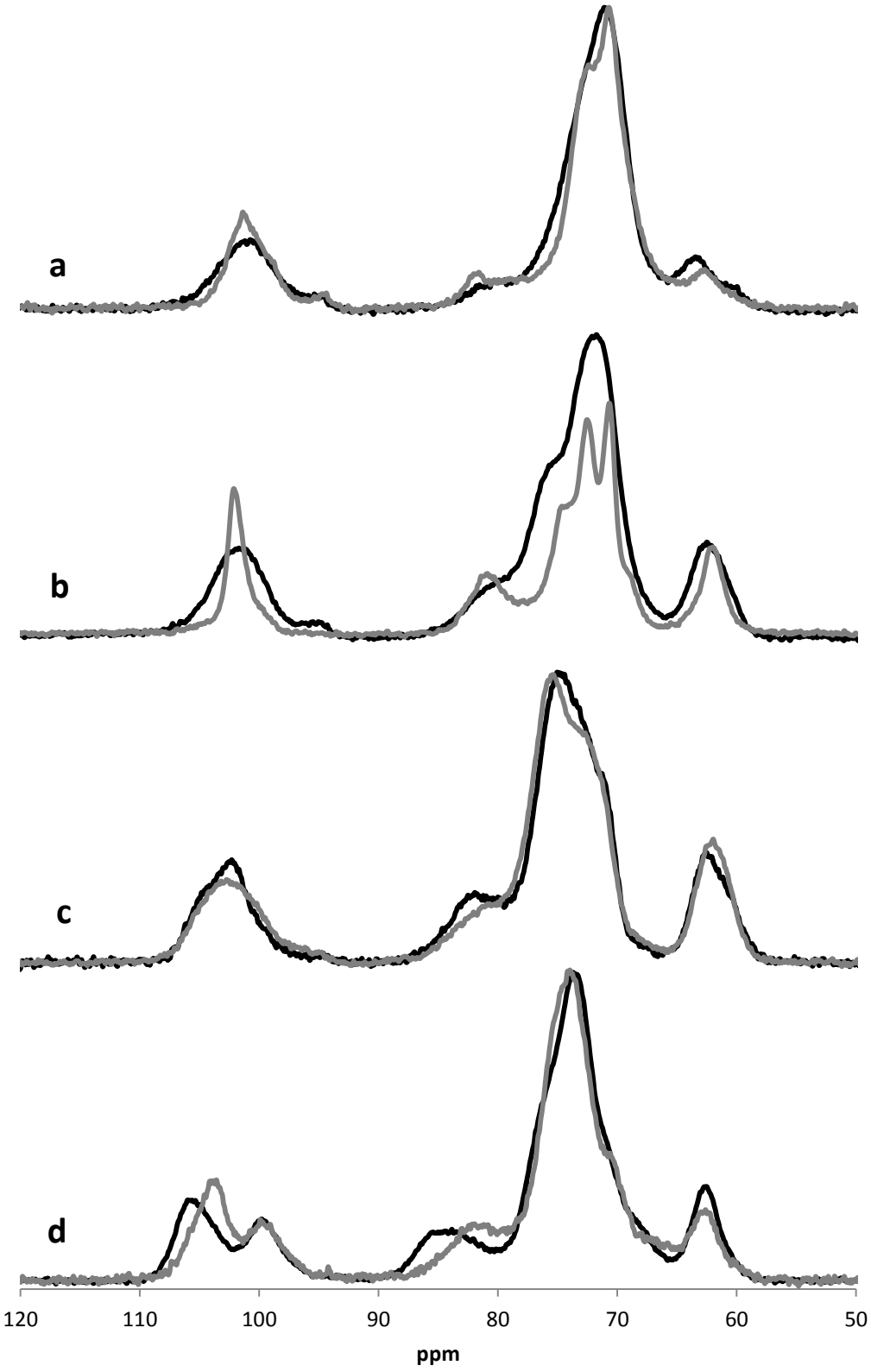

Figure 6.8 ^{13}C CPMAS NMR spectra of polysaccharide samples that were either treated in LiCl/urea/water and dried (grey) or untreated (black), for (a) fenugreek (b) LBG (c) konjac and (d) xyloglucan.

Guar has a crystalline structure in a relative humidity (RH) range of 40-80% where the mannose backbone and galactose side chains form antiparallel planar sheets (Cheng *et al.*, 2002). Cheng *et al.* (2002) found that under low osmotic pressure urea did break the hydrogen bonding structure of the native guar crystalline structure but at high osmotic pressure urea seemed to be able to hydrogen bond to the guar to form a new crystalline structure. It may also be possible therefore that the crystal structure of LBG, seen by NMR, was actually produced before dialysis and drying.

The peak at 99-100 ppm can be assigned to the xylose C1 of xyloglucan (Whitney *et al.*, 1995, Bootten *et al.*, 2008) and does not shift for the treated samples (Figure 6.8d). The chemical shift at 82.5 ppm is assigned to the C4 glucan chain (Ha *et al.*, 1997). The peak at 105.8 ppm for the untreated xyloglucan corresponds to the C1 (1,4-Glc) region of the glucose backbone (Dick-Pérez *et al.*, 2011) shifts to 103.8 ppm after treatment. A parallel can be drawn from starch as the C1 region of starch is known to shift from about 102 ppm to 105 ppm as it becomes more amorphous (Gidley and Bociek, 1988, Gidley, 1992). If the xyloglucan has become more crystalline then its conformation is expected to change somewhat.

Early XRD studies of crystalline tamarind seed xyloglucan found that it had a flat, ribbon-like two-fold helical conformation for the main chain (Taylor and Atkins, 1985). The main chain of the oligomer XXXG has been found to have a twisted conformation in aqueous solution (Picard *et al.*, 2000). Using a model with 12 glucose residues as the main chain and 6 galactose and three xylose residues as side chains Umemura and Yuguchi (2005) found that in aqueous solution, xyloglucan had either a flat restricted or twisted backbone both had a tendency to contract which was caused by side chains binding to the main glucan chain through intra molecular hydrogen bonding.

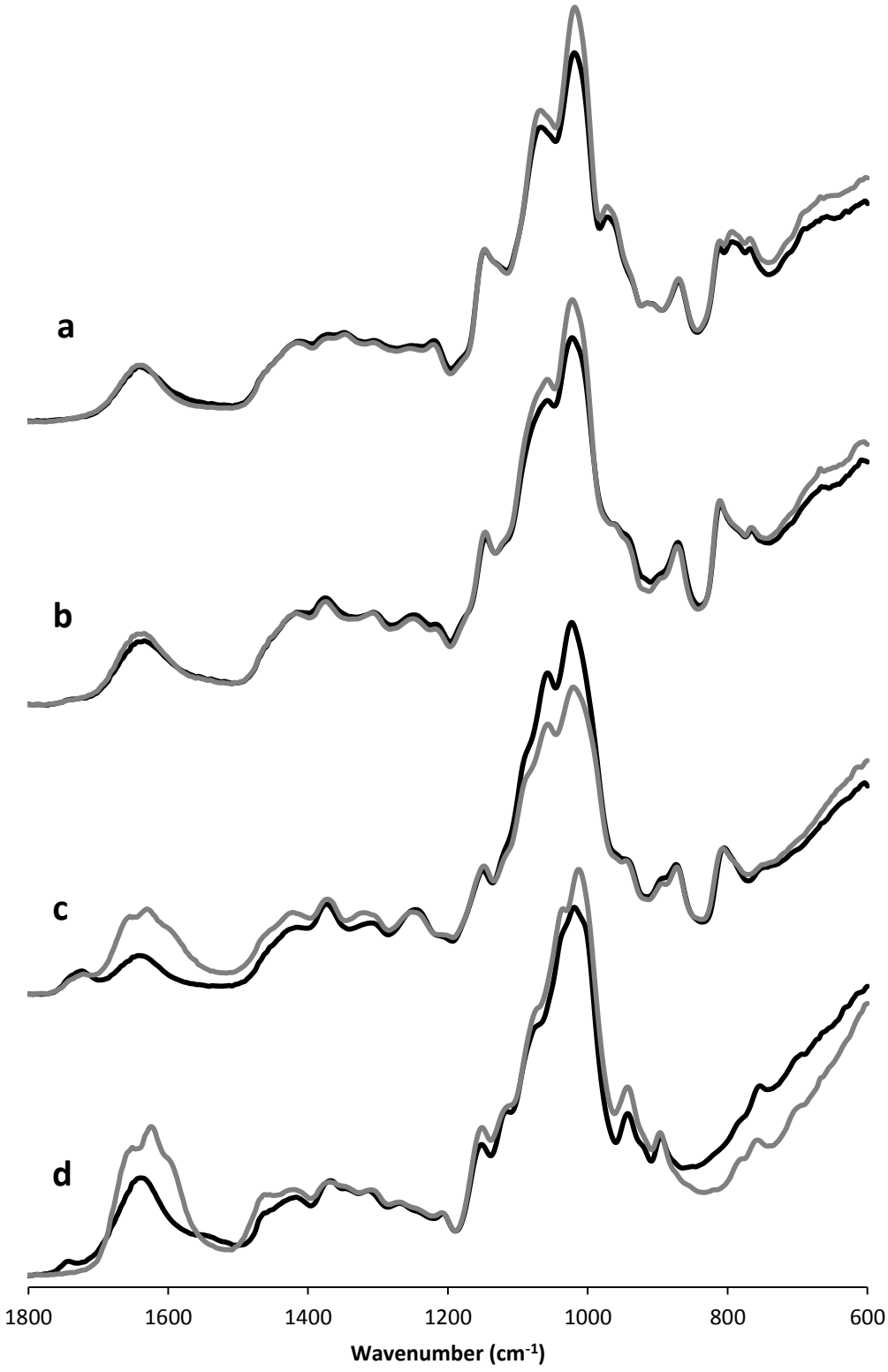

Figure 6.9 FTIR spectra of polysaccharide samples that were either treated in LiCl/urea/water and dried (grey) or untreated (black), polysaccharides for (a) fenugreek (b) LBG (c) konjac and (d) xyloglucan.

The addition of the LiCl/urea/water will break the intramolecular hydrogen bonding which will allow the cellulosic backbone to have a flatter, more extended conformation. As the salt is removed by dialysis the xyloglucan chains may aggregate in a more uniform way due to the extended conformation which is shown by the increase in molecular order from the NMR results.

During dialysis konjac underwent gelation (Figure 6.10). Gelation of konjac can be achieved by alkali treatment, causing deacetylation (Penroj *et al.*, 2005). This does not appear to be the cause of gelation for this system as the pH of the LiCl/urea/water solution was 6.3 and gelation occurred during the removal of the salts. Figure 6.11 shows acetyl carbon peaks for both the untreated and treated konjac samples at 22 ppm (Bootten *et al.*, 2004). While the data is noisy the peaks appear to be the same size for both samples which indicates that the acetyl groups have not been removed during treatment. Gelation has been reported for non-deacetylated konjacs at concentrations of 7 wt% or higher (Zhang *et al.*, 2001). During dialysis the concentration is likely have decreased from its initial 1 wt% so it is extremely unlikely to have exceeded 7 wt% at any point. It has been reported that konjac solutions above 1 wt% can form gels at ambient temperature but this is over the time scale of months (Williams *et al.*, 2000).

Figure 6.10 Image of konjac gelation after LiCl/urea/water treatment and subsequent dialysis.

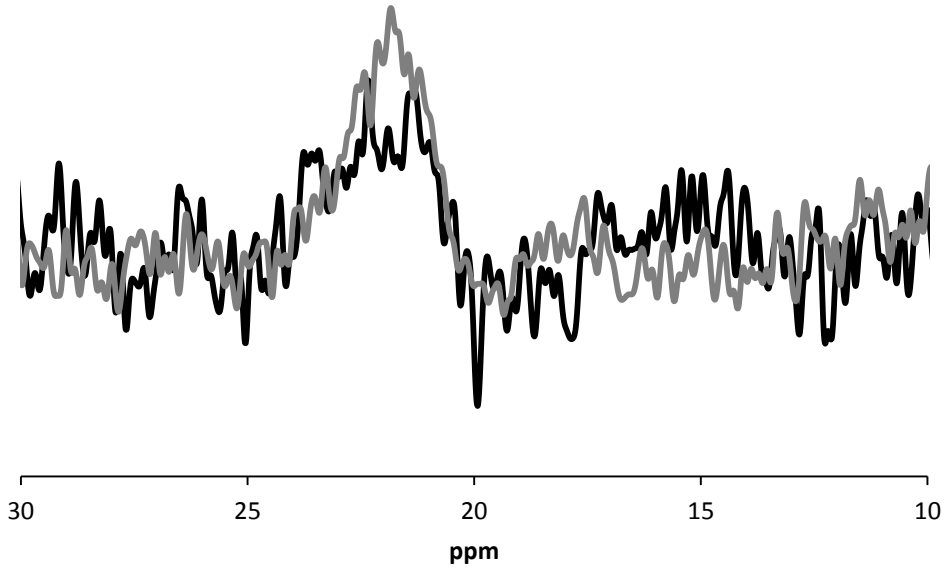

Figure 6.11 ^{13}C CPMAS NMR spectra of the acetyl region for LiCl/urea/water treated (grey) and untreated (black) konjac.

Whilst the LiCl/urea/water solvent does not deacetylate konjac it does appear to negate the effect of the acetyl groups which may be due to ionic screening which thus enables it to gel over time (Winzor *et al.*, 2004). Although konjac does produce order (gel) during dialysis the order is lost upon drying as there is little difference in the NMR spectra of the treated and untreated samples (Figure 6.8d).

FTIR is a useful method to identify any chemical or physical changes. Both fenugreek and LBG appear to undergo no chemical changes during treatment as the treated and untreated spectra are very similar (Figures 6.11a and 6.11b). There is an increase in absorption at 1024 cm^{-1} which is due to C-O stretching in the C-O-C linkage which may indicate an increase in order (Savitha Prashanth *et al.*, 2006) as well as an increase at 1077 cm^{-1} which are complex vibrations that relate to the linkage between the galactose residue and the mannan main chain (Risica *et al.*, 2005). Stretching peaks of the $–CH_3$ groups at 1736 cm^{-1} are assigned to the aceto groups in konjac (Figure 6.9c) (Maeda *et al.*, 1980). There is little difference between the treated and untreated sample again indicating the acetyl groups have not been removed. There is a slight increase in the absorption band at 1636 cm^{-1} which has previously identified as intra-molecular hydrogen bonds (Li *et al.*, 2011). The characteristic absorption bands of mannose are between 810 and 880 cm^{-1} and do not change (Xiao *et al.*, 2001). The peaks at 1080 and 1022 cm^{-1} are assigned to the stretching of C-O-C where there is a small decrease in intensity.

FTIR results suggest that none of the polysaccharides undergo any chemical modification during treatment indicating that the differences seen between the solvents are as a result of conformational changes. Fenugreek has the largest molecular weight of the polysaccharides tested yet has a comparatively low viscosity. Due to its high level of galactose substitution it has a very compacted structure as the galactose side chains form intramolecular hydrogen bonds (Petkowicz *et al.*, 1998, Wang and Somasundaran, 2007). When dissolved in the LiCl/urea/solvent these intramolecular hydrogen bonds are broken which allows the molecule to expand to a much larger conformation. The intermolecular associations between LBG molecules are broken resulting in a decrease in intrinsic viscosity. Whilst the number of intramolecular hydrogen bonds will be less for LBG due to the low number of

galactose side chains, their breakage will also result in a slight expansion which explains why there is no overall decrease in viscosity at semi-dilute and concentrated solution regimes. Konjac is a linear molecule with only a very low level of branching which may explain why there is only a slight increase in the viscosity in LiCl/urea/water. Xyloglucan is highly branched and thus has a compacted conformation. It behaves in a similar way to fenugreek in the LiCl/urea/water solvent where intramolecular hydrogen bonds are broken and hydrophobic regions are disrupted resulting in a large increase in viscosity.

Whitney *et al.* (1998) used bacterial cellulose to investigate interactions between cellulose and mannans. Konjac was found to form highly heterogeneous structures with bacterial cellulose with the glucomannan cross-linking the cellulose ribbons in a similar way to that seen by xyloglucan (Carpita and Gibeaut, 1993). Whitney *et al.* (1998) also found that galactomannan interaction followed the order of galactose substitution, so that LBG with the lowest substitution had greater interaction that the fully substituted fenugreek indicating that the galactosyl substitution was a significant barrier to incorporation with cellulose fibrils. The unsubstituted mannan backbone is able to adopt the extended cellulose conformation so LBG was also able to form cross-links between the cellulose fibrils.

Investigations on the adsorption onto the surface of talc revealed that the most important driving force for both LBG and guar was hydrogen bonding as urea, a hydrogen bond breaker, markedly reduced adsorption and that both polymers were found to adsorb flat on the solid to increase the number of OH groups that were in contact with the surface (Wang and Somasundaran, 2007). There was no effect of M:G ratio on adsorption. Wang and Somasundaran (2007) also found by computer modelling that in an aqueous environment both polymers had a helical structure but

guar had a more complicated structure than LBG because of the increase in galactose units along the mannose chain.

Figure 6.12 shows confocal micrographs of microcrystalline cellulose (MCC) and fenugreek in water. Figure 6.12c shows that the fluorescently labelled fenugreek binds to the surface of MCC. The following confocal micrographs (Figures 6.14-6.19) will show the labelled polysaccharide so as to provide a clearer picture. There will also be galactomannan in solution that is not bound to the cellulose; however, the bound galactomannan will be much more concentrated meaning that it is more visible in the micrographs.

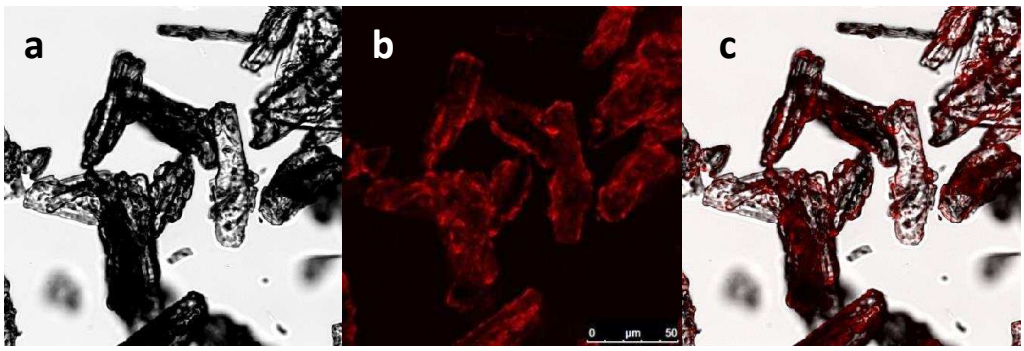

Figure 6.12 Confocal micrographs of MCC and fenugreek in water where (a) is the optical light microscopy showing the cellulose (b) is the fluorescent image showing the fluorescently labelled polysaccharide and (c) is a combination of the two.

LBG has previously been found to bind to cellulose (Mishima *et al.*, 1998). In water both LBG and fenugreek (Figures 6.14a and 6.14b) appear to bind to the surface of the cellulose fibres (CF). With no quantitative values it is not possible to state if there is any difference between the two galactomannans. From the work of Whitney *et al.* (1998) it would be expected that fenugreek would bind to a much lesser degree than LBG but visually there appears to be little difference between the galactomannans. In the LiCl/urea/water solution LBG is still bound to the cellulose (Figure 6.13c) whereas there seems to be no interaction between the fenugreek and cellulose (Figure 6.13d).

It should be noted, however, that the fluorescently labelled fenugreek was far less soluble in LiCl/urea/water which can be seen by the bright specs.

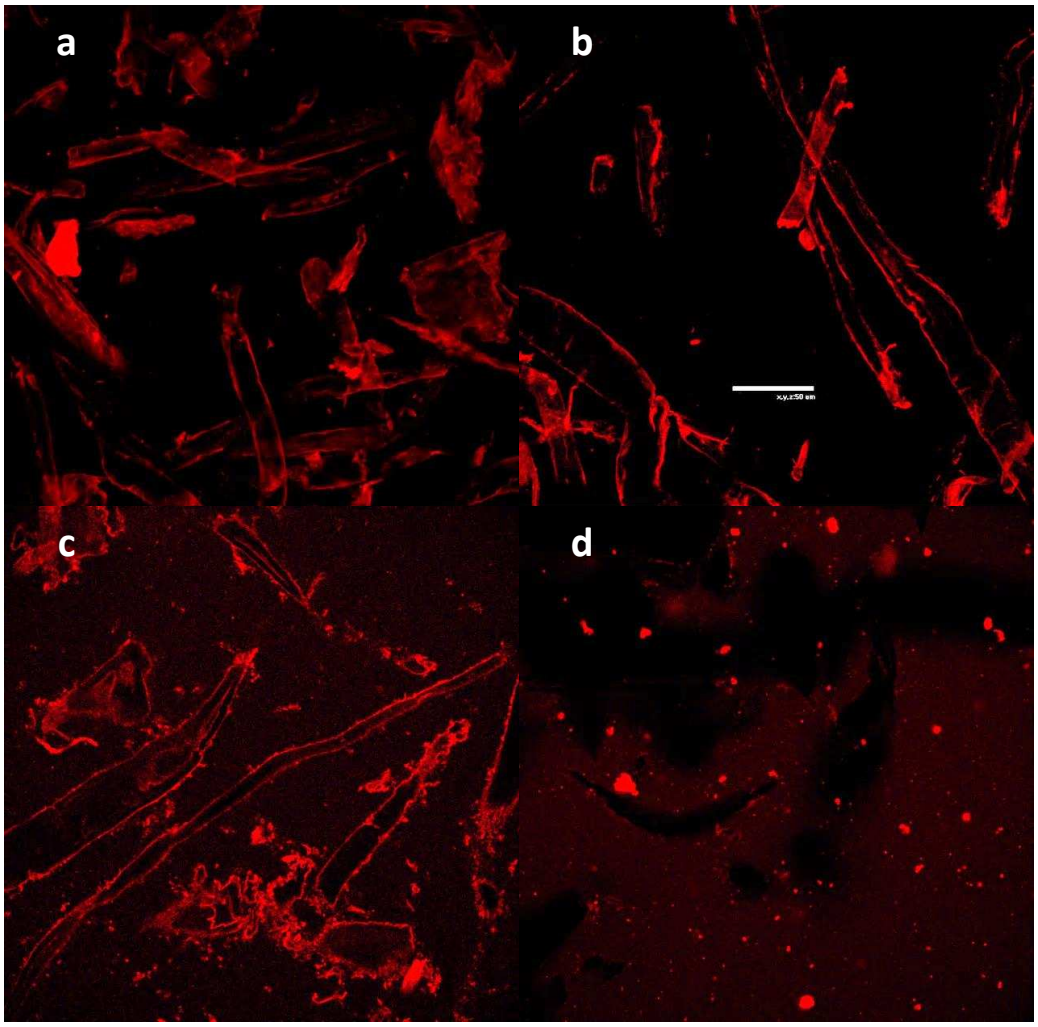

Figure 6.13 Confocal micrographs showing galactomannans and CF in different solvents (a) LBG in water (b) fenugreek in water (c) LBG in LiCl/urea/water solution and (d) fenugreek in LiCl/urea/water solution. Scale bar is 50 µm.

A comparative experiment was undertaken, now using MCC instead of CF and in water both LBG and fenugreek appear to bind to MCC (Figure 6.14). In LiCl/urea/water LBG appears to bind to a lesser extent to MCC than it did to CF (c.f. Figures 6.14c and 6.15c). This may be as a result of MCC's higher crystallinity. Fenugreek does not bind to MCC at all in LiCl/urea/water (Figure 6.14d).

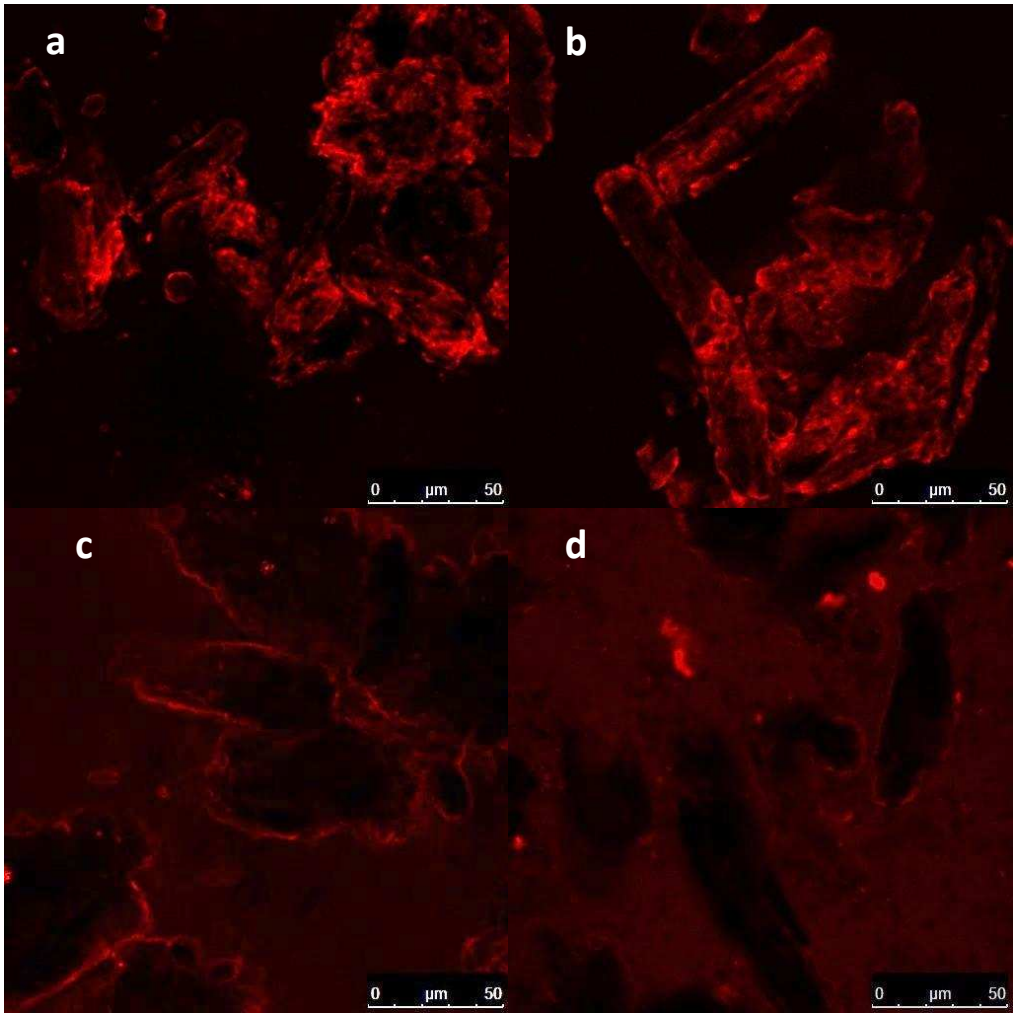

Figure 6.14 Confocal micrographs showing galactomannans and MCC in different solvents (a) LBG in water (b) fenugreek in water (c) LBG in LiCl/urea/water solution and (d) fenugreek in LiCl/urea/water solution.

Now investigating the interaction between LBG and fenugreek with physically processed ball milled (BM) MCC LBG and fenugreek both appear to bind in LiCl/urea/water (Figure 6.15). The arrows point to a part of each image where there is no cellulose. For the LBG sample this area is dark as the majority of the LBG has bound to the cellulose whereas in the fenugreek sample there is still a significant amount of polymer that is not bound.

The confocal micrographs of galactomannan and cellulose suggest that by decreasing the crystallinity of cellulose the binding of galactomannans increase. de Lima and Buckeridge (2001) found the opposite trend where MCC was able to bind three times

as much xyloglucan as cellulose fibres which the authors accounted for by the increase in surface area.

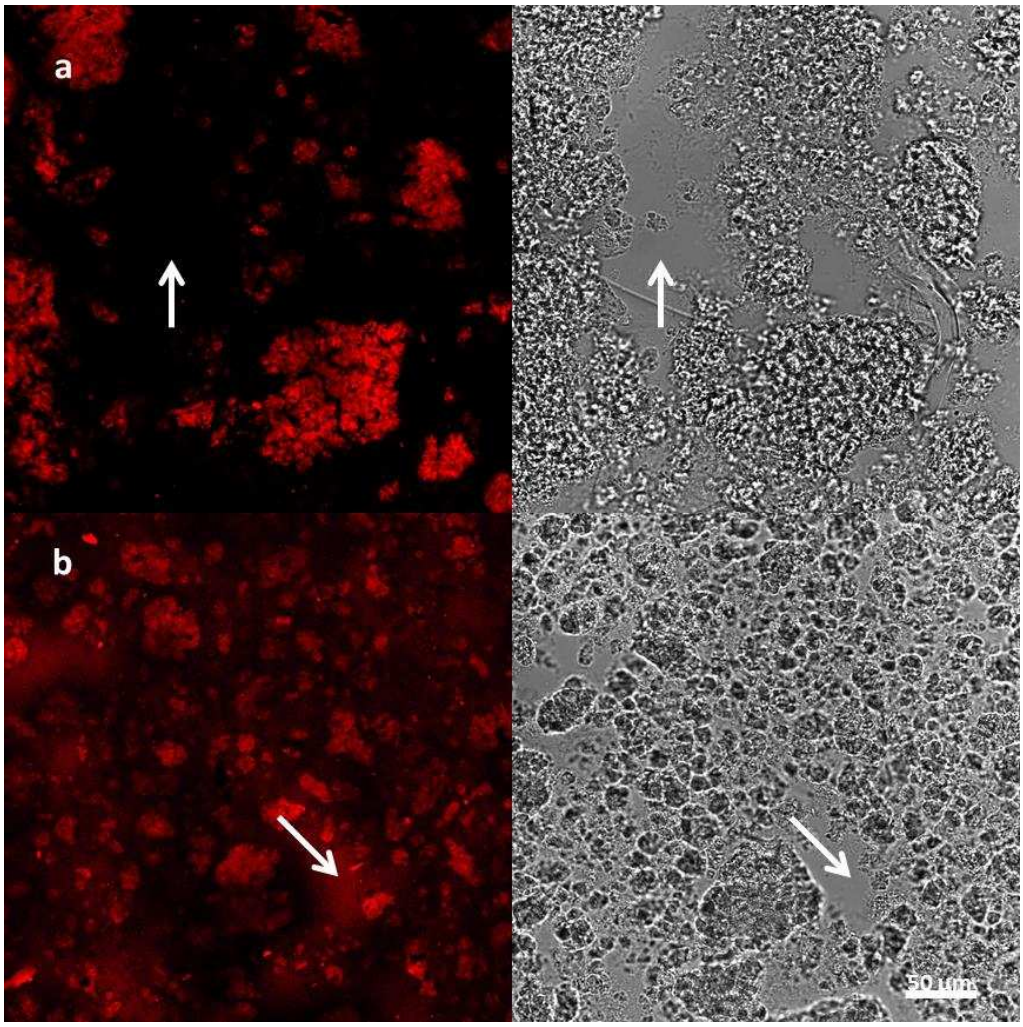

Figure 6.15 Confocal micrographs of BM MCC in LiCl/urea/water with (a) LBG and (b) fenugreek. The light micrographs of the same image are shown on the right. The arrows point to a part of each image where there is no cellulose.

In this study, in water, xyloglucan does not bind to either MCC (Figure 6.16) or CF (Figure 6.17). This is likely due to the absence of fucose side chains which have been shown to aid interaction due to the flatter conformation on the main chain (Levy *et al.*, 1991, Hayashi *et al.*, 1994). Xyloglucan has a tightly bound conformation in water but in LiCl/urea/water the side chains unfold as intramolecular hydrogen bonds are broken. This exposes the glucose backbone and enables the xyloglucan to bind to cellulose (Figures 6.17 and 6.18, bottom row of micrographs). de Lima and

Buckeridge (2001) found there was a slightly higher interaction between cellulose and xyloglucan at a pH of 6.0 (between the range of pH 2-8) whilst temperature had no effect between the range of 5-60^{o}C. The pH of the LiCl/urea/water solvent is 6.3 so the change in pH may also increase the level of binding of xyloglucan but this is unlikely to be the sole reason, as the increase found by de Lima and Buckeridge (2001) was small.

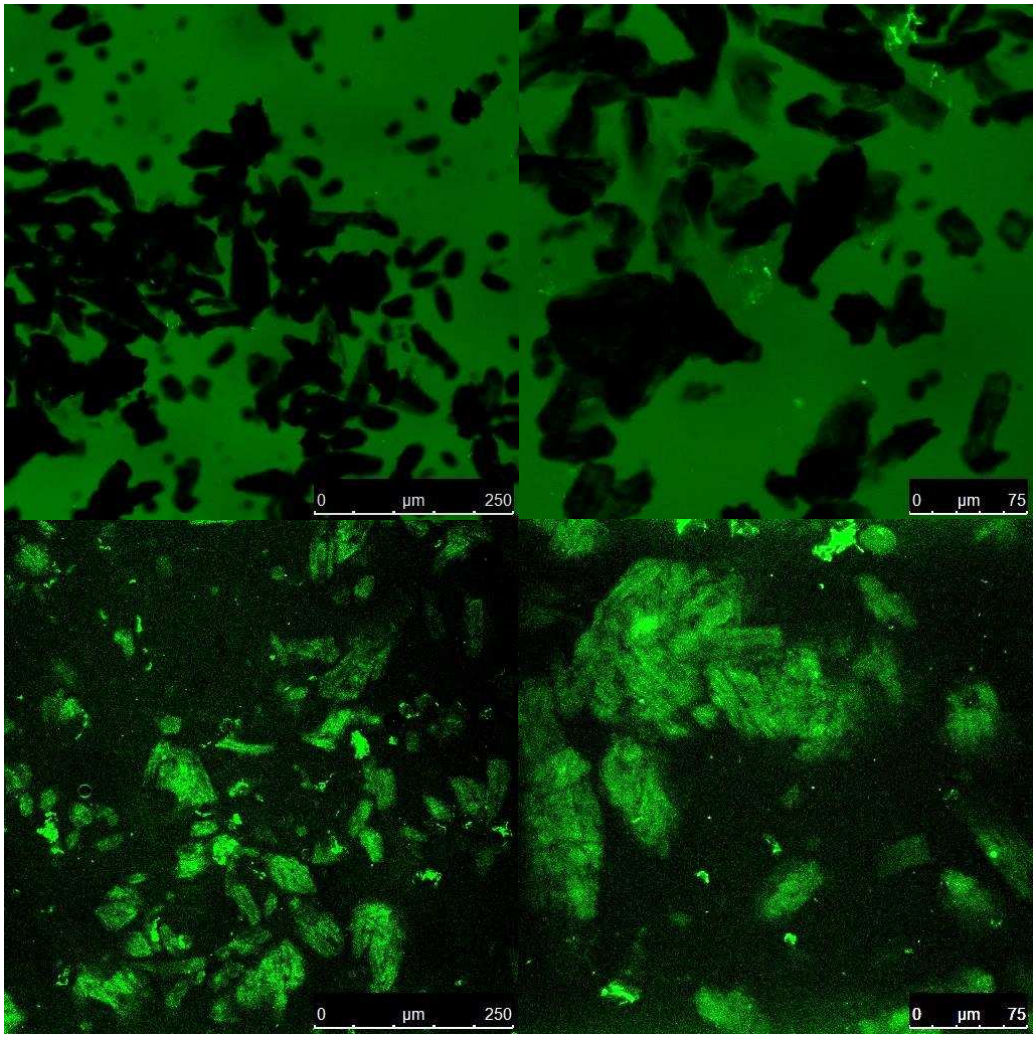

Figure 6.16 Confocal micrographs showing xyloglucan with MCC in water (top) or in LiCl/urea/water (bottom).

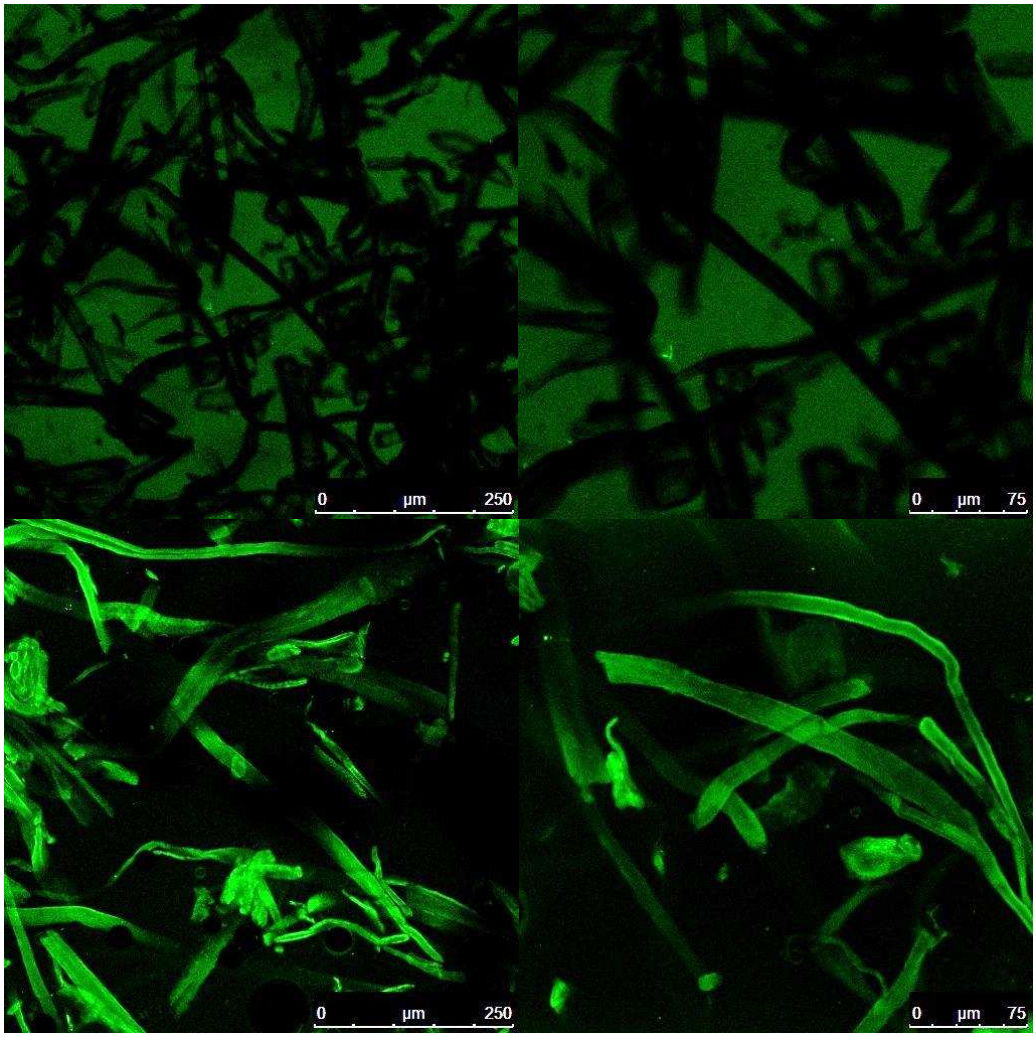

Figure 6.17 Confocal micrographs showing xyloglucan with CF in water (top) and LiCl/urea/water (bottom).

Due to problems drying the fluorescently labelled konjac there was a large amount that remained undissolved (the very bright specs on each image) (Figure 6.18). It is therefore difficult to be completely confident with the images. However, the confocal micrographs appear to suggest that konjac does not bind to cellulose in either water of LiCl/urea/water. As there are minimal solvent effects for konjac (Figure 6.2), it might be expected that it would behave in a similar manner in both solvents. The acetate groups that provide konjac with its water solubility may also inhibit interaction with cellulose. It would be interesting to see if konjac would bind to cellulose during dialysis in a similar way to its gel formation shown in Figure 6.10 when the acetate groups are screened.

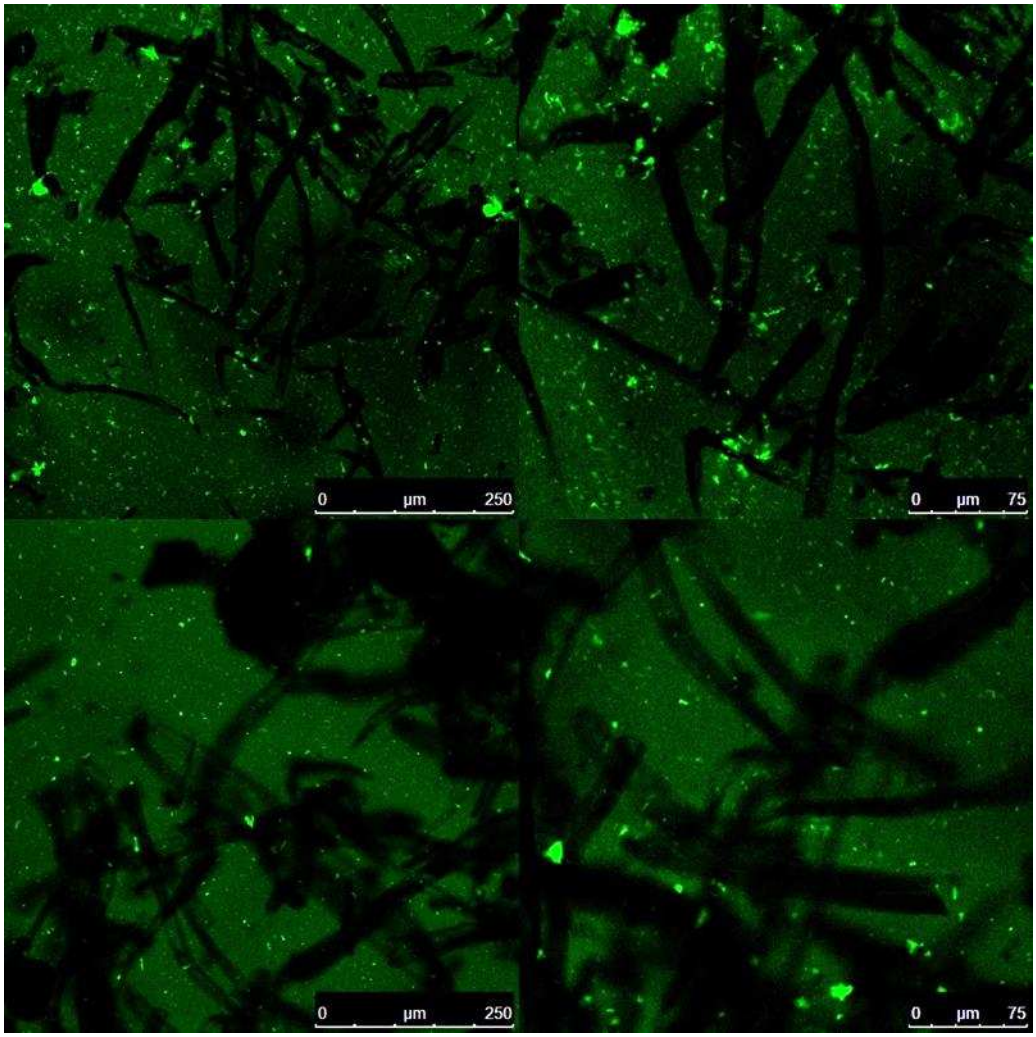

Figure 6.18 Confocal micrographs of CF with konjac in water (top) and LiCl/urea/water (bottom).

The confocal micrographs only provide a qualitative understanding of the polymer-cellulose binding so it would be useful to quantify this in future work. This could be achieved using the method of Mishima *et al.* (1998) where they packed columns with cellulose and solutions of each polysaccharide were then applied to the column and the amount of carbohydrate eluted was measured calorimetrically.

6.4 Conclusion

LiCl/urea/water appears to be able to break both intra and intermolecular hydrogen bonds and disrupts hydrophobic domains. This may result in the conformational change from tightly bound and compact in water to a more extended conformation

in LiCl/urea/water for fenugreek and xyloglucan which are both highly branched. LBG aggregates are also broken lowering its intrinsic viscosity. At high concentrations the expansion of the smaller molecules results in no overall change in viscosity. Konjac, which is only minimally branched, does not undergo any significant conformational change from water to LiCl/urea/water.

Both the fluorescently labelled LBG and fenugreek bind to cellulose in water. The conformational change of fenugreek in LiCl/urea/water seems to inhibit binding to cellulose whereas xyloglucan does bind to cellulose in LiCl/urea/water but does not in water. The results of konjac binding are inconclusive but suggest that it does not bind to cellulose in either water or LiCl/urea/water. It is, however, unclear as to what affect the fluorescent labelling may have on the properties of these polysaccharides so further work needs to be done using alternative fluorescent markers to confirm the results.

LiCl/urea/water is a useful solvent for hemicelluloses as it disrupts many of the intramolecular associations. Branched polysaccharides therefore may have a larger hydrodynamic volume resulting in a higher viscosity when compared to water whilst disaggregation will result in a reduction in viscosity.

Chapter 7. Conclusions and future work

7.1 Conclusions and future work

Cellulose is the most abundant natural polymer on earth but due to its insolubility in water and most common solvents has seen little use in the construction of advanced materials in its native state (Klemm *et al.*, 2005); however, this is rapidly changing with the increasing interest in nano-cellulose and renewable matrix polymers (Eichhorn *et al.*, 2010, Habibi *et al.*, 2010, Moon *et al.*, 2011, Klemm *et al.*, 2011). This work has focussed on gaining a better understanding of the affects of different mechanical and chemical pre-treatments on cellulose and other plant polysaccharides.

Ball milling is a useful method of mechanical disrupting the crystalline structure of cellulose (Paes *et al.*, 2010, Avolio *et al.*, 2012, Abbaszadeh *et al.*, 2014). The main findings from the first section of this work are that:

- Ball milling results in the loss of crystalline structure and reduction in the viscosity average degree of polymerisation (DP) and degradation temperature
- In excess water, the presence of seed crystals results in partial recrystallisation back to type I cellulose, while completely amorphous cellulose will recrystallise to a type II crystal structure
- The degradation temperature is related to DP and to a lesser extent crystallinity
- Unlike traditional calorimetric methods, Flash differential scanning calorimetry (DSC) is able to measure a glass transition (T_g) for amorphous cellulose
- Hot pressing is unable to disrupt the particulate structure of amorphous cellulose which is likely to be due to recrystallisation before it is able to flow

To further investigate ways of utilising cellulose to create structures, freeze dried foams, reinforced with cellulose were compared. Two galactomannans were chosen; locust bean gum (LBG) which is able to undergo cryogelation (Patmore *et al.*, 2003, Goff *et al.*, 1999) and fenugreek which does not form a cryogel due to its fully substituted backbone. Results show that:

- Molecular weight is more important than cryogelation in the strength and stiffness of galactomannan foams
- A large amount of cellulose (up to six times as much cellulose as galactomannan matrix) was able to be incorporated into the galactomannan foams which added greater reinforcement by increasing the strength and stiffness of the foams
- The level of galactomannan/cellulose interaction is related to cellulose crystallinity and surface roughness
- Increased interaction results in stronger foams
- Microfibrillated cellulose (MFC) provided the greatest reinforcement due to its larger surface area and fibrillated structure
- Extrusion is able to fibrillate cellulose

Further work is needed to assess the most suitable parameters, such as; screw speed and configuration, barrel length, water flow rate and temperature, but extrusion of cellulose composites will be a more cost effective and quicker fabrication method than freeze drying. It would be of great interest in the future to see if galactomannan foams could be produced using extrusion and co-processed with cellulose as it is

being fibrillated which should increase the level of interaction and therefore have superior mechanical properties. In future work it would also be useful to assess the reinforcement properties of cellulose nanowhiskers in galactomannan foams.

A further method of utilising cellulose is through the use of a swelling treatment. Work by Tatarova *et al.* (2010) has shown that a LiCl/urea/water solution is able to swell regenerated cellulose to the same extent as traditional alkali treatments but it has the advantage of being recyclable. In this work we have looked at a range of native celluloses in LiCl/urea/water which have shown that:

- There is a reduction in crystallinity
- Cellulose is 'activated' during the initial heat with LiCl/urea/water
- The ability of amorphous cellulose polymer chains, located on the surface of the fibres, to change conformation is likely to be limited by their DP
- At ambient temperature the cellulose dispersions formed a weak gel-like network
- This structure is melted out at 60^{o}C due to a change in cellulose conformation from predominantly hydrophilic to hydrophobic surfaces
- Starch granules are eroded from the outside rather than swollen, as seen with ionic liquids, which allows for complete dissolution

It would be useful to explore further the changes in cellulose conformation using molecular modelling.

Straw, which contains lignin and hemicelluloses as well as cellulose, was shown to swell in LiCl/urea/water which may open up new ways of structuring plant cell wall material. To produce these structures it is important to understand what effect the solvent has on different hemicelluloses.

In this work, four hemicelluloses were chosen; LBG, fenugreek, konjac and xyloglucan. Fenugreek and xyloglucan, which are highly branched have a tightly bound conformation in water due to the high number of intramolecular associations, however, in LiCl/urea/water many of the inter and intramolecular associations may have been broken resulting in their relative viscosity increasing compared to their viscosity in water. Konjac which is predominantly linear with little branching did not change in conformation and so there was little change in viscosity. LBG has large unsubstituted regions of its backbone which results in the mannan regions aggregating, often referred to as hyperentanglement (Doyle *et al.*, 2009). In LiCl/urea/water these aggregates are broken causing a decrease in viscosity (Goycoolea *et al.*, 1995). When the LBG was subsequently dried the aggregates were able to reform resulting in an increase in molecular order. This work shows that:

- LiCl/urea/water breaks many of the inter and intramolecular associations of the hemicelluloses used in this work
- In LiCl/urea/water intramolecular associations may be broken resulting in conformational change and an increase in viscosity for branched polymers
- LiCl/urea/water may also causes disaggregation due to the breakage of intermolecular associations which leads to a decrease in viscosity for aggregated polymers

It would be useful in future work to measure the radius of gyration of the polysaccharides in the different solvent environments to confirm that there is a conformational change.

Confocal microscopy was used to identify any interaction between the hemicelluloses (which were fluorescently labelled) and cellulose. Both LBG and fenugreek appeared to bind to the surface of cellulose fibrils in water. It is, however,

unclear as to what affect the fluorescent labelling may have on the properties of these polysaccharides. By changing the conformation of fenugreek using LiCl/urea/water it is no longer able to bind to cellulose fibres. Xyloglucan on the other hand is unable to bind to cellulose in water, but by changing its conformation it will bind to the surface of cellulose fibrils. Due to problems with the drying process of fluorescently labelled konjac the results are less clear, although it appears that in both water and LiCl/urea/water konjac does not interact with cellulose, however, as konjac has been shown to gel during the removal of the solvent, it would be useful to investigate whether it will interact with cellulose as it gels.

It would also be useful to investigate other branched polymers such as 'hairy' pectin to further show that the conformational changes shown above are due to the breakage of intramolecular associations. This work opens up the possibility of increasing the interaction between certain polymers and cellulose. It would also be interesting to see if these interactions were carried over into the dry state which would provide a new route to designing novel materials.

This work has attempted to show that by using chemical or mechanical treatments there is huge potential in utilising native cellulose to create composite structures that are renewable and biodegradable but also could have properties that are as good if not better than traditional oil based materials.

References

ABBASZADEH, A., MACNAUGHTAN, W. & FOSTER, T. J. 2014. The effect of ball milling and rehydration on powdered mixtures of hydrocolloids. *Carbohydrate Polymers,* 102, 978-985.

ABDELMOULEH, M., BOUFI, S., BELGACEM, M. N. & DUFRESNE, A. 2007. Short natural-fibre reinforced polyethylene and natural rubber composites: Effect of silane coupling agents and fibres loading. *Composites Science and Technology,* 67, 1627-1639.

AGODA-TANDJAWA, G., DURAND, S., BEROT, S., BLASSEL, C., GAILLARD, C., GARNIER, C. & DOUBLIER, J. L. 2010. Rheological characterization of microfibrillated cellulose suspensions after freezing. *Carbohydrate Polymers,* 80, 677-686.

AGODA-TANDJAWA, G., DURAND, S., GAILLARD, C., GARNIER, C. & DOUBLIER, J. L. 2012. Rheological behaviour and microstructure of microfibrillated cellulose suspensions/low-methoxyl pectin mixed systems. Effect of calcium ions. *Carbohydrate Polymers,* 87, 1045-1057.

AGUILAR-PALAZUELOS, E., ZAZUETA-MORALES, J. D. J., JIMÉNEZ-ARÉVALO, O. A. & MARTÍNEZ-BUSTOS, F. 2007. Mechanical and structural properties of expanded extrudates produced from blends of native starches and natural fibers of henequen and coconut. *Starch-Stärke,* 59, 533-542.

AHMAD, F. 1983. Free energy changes in ribonuclease A denaturation. Effect of urea, guanidine hydrochloride, and lithium salts. *Journal of Biological Chemistry,* 258, 11143-11146.

AHMAD, F. 1984. Free energy changes in denaturation of ribonuclease A by mixed denaturants. Effects of combinations of guanidine hydrochloride and one of the denaturants lithium bromide, lithium chloride, and sodium bromide. *Journal of Biological Chemistry,* 259, 4183-4186.

AHMED, S. & JONES, F. 1990. A review of particulate reinforcement theories for polymer composites. *Journal of Materials Science,* 25, 4933-4942.

ALBERSHEIM, P., DARVILL, A. G., ONEILL, M. A., SCHOLS, H. A. & VORAGEN, A. G. J. 1996. An hypothesis: The same six polysaccharides are components of the primary cell walls of all higher plants. *Pectins and Pectinases,* 14, 47-55.

ANDERSON, J. W., BAIRD, P., DAVIS, R. H., JR., FERRERI, S., KNUDTSON, M., KORAYM, A., WATERS, V. & WILLIAMS, C. L. 2009. Health benefits of dietary fiber. *Nutrition Reviews,* 67, 188-205.

ANDRADE, C., AZERO, E., LUCIANO, L. & GONÇALVES, M. 1999. Solution properties of the galactomannans extracted from the seeds of Caesalpinia pulcherrima and Cassia javanica: comparison with locust bean gum. *International Journal of Biological Macromolecules,* 26, 181-185.

ANDRESEN, M., JOHANSSON, L.-S., TANEM, B. S. & STENIUS, P. 2006. Properties and characterization of hydrophobized microfibrillated cellulose. *Cellulose,* 13, 665-677.

ANG, J. F. 1991. Water retention capacity and viscosity effect of powdered cellulose. *Journal of Food Science,* 56, 1682-1684.

ANG, J. F. & MILLER, W. B. 1991. Multiple functions of powdered cellulose as food ingredient *Cereal Foods World,* 36, 558-&.

ANTONIOU, E., BUITRAGO, C., TSIANOU, M. & ALEXANDRIDIS, P. 2010. Solvent effects on polysaccharide conformation. *Carbohydrate Polymers,* 79, 380-390.

APPELQVIST, I. A. M., COOKE, D., GIDLEY, M. J. & LANE, S. J. 1993. Thermal-properties of polysaccharides at low moisture .1. An endothermic melting

process and water-carbohydrate interactions. *Carbohydrate Polymers,* 20, 291-299.

ARAKI, J., WADA, M., KUGA, S. & OKANO, T. 1998. Flow properties of microcrystalline cellulose suspension prepared by acid treatment of native cellulose. *Colloids and Surfaces a-Physicochemical and Engineering Aspects,* 142, 75-82.

ARVANITOYANNIS, I. & BILIADERIS, C. G. 1999. Physical properties of polyol-plasticized edible blends made of methyl cellulose and soluble starch. *Carbohydrate Polymers,* 38, 47-58.

ATKINS, E., FARNELL, S., BURDEN, C., MACKIE, W. & SHELDRICK, B. 1988. Crystalline structure and packing of mannan I. *Biopolymers,* 27, 1097-1105.

AULIN, C., GALLSTEDT, M., LARSSON, T., SALMEN, L. & LINDSTROM, T. 2011. Novel nanocellulose-based barriers. *Abstracts of Papers of the American Chemical Society,* 241.

AVELLA, M., AVOLIO, R., BONADIES, I., CARFAGNA, C., ERRICO, M. E. & GENTILE, G. 2010. Effect of compatibilization on thermal degradation kinetics of HDPE-based composites containing cellulose reinforcements. *Journal of Thermal Analysis and Calorimetry,* 102, 975-982.

AVEROUS, L. & BOQUILLON, N. 2004. Biocomposites based on plasticized starch: thermal and mechanical behaviours. *Carbohydrate Polymers,* 56, 111-122.

AVEYARD, R. 1982. A surface tension approach to the salting-out of nonpolar nonelectrolytes. *Canadian journal of chemistry,* 60, 1317-1326.

AVOLIO, R., BONADIESA, I., CAPITANI, D., ERRICO, M. E., GENTILE, G. & AVELLA, M. 2012. A multitechnique approach to assess the effect of ball milling on cellulose. *Carbohydrate Polymers,* 87, 265-273.

AZEREDO, H. M. C., MATTOSO, L. H. C., WOOD, D., WILLIAMS, T. G., AVENA-BUSTILLOS, R. J. & MCHUGH, T. H. 2009. Nanocomposite Edible Films from Mango Puree Reinforced with Cellulose Nanofibers. *Journal of Food Science,* 74, N31-N35.

BACK, E. L., HTUN, M. T., JACKSON, M. & JOHANSON, F. 1967. Effect of auto-cross linking reactions on thermal softening of cellulose. *Textile Research Journal,* 37, 432-&.

BACKFOLK, K., HARLIN, A., HEISKANEN, I. & LAITINEN, R. 2010. Process for the production of microfibrillated cellulose in an extruder and microfibrillated cellulose produced according to the process. Google Patents.

BACON, R. & TANG, M. 1964. Carbonization of cellulose fibers—II. Physical property study. *Carbon,* 2, 221-225.

BAHETI, V. & MILITKY, J. 2013. Reinforcement of Wet Milled Jute Nano/Micro Particles in Polyvinyl Alcohol Films. *Fibers and Polymers,* 14, 133-137.

BAI, W., HOLBERY, J. & LI, K. C. 2009. A technique for production of nanocrystalline cellulose with a narrow size distribution. *Cellulose,* 16, 455-465.

BARBETTA, A., CARRINO, A., COSTANTINI, M. & DENTINI, M. 2010. Polysaccharide based scaffolds obtained by freezing the external phase of gas-in-liquid foams. *Soft Matter,* 6, 5213-5224.

BARONEPEL, O., GHARYAL, P. K. & SCHINDLER, M. 1988. Pectins as mediators of wall porosity in soybean cells. *Planta,* 175, 389-395.

BATES, S., ZOGRAFI, G., ENGERS, D., MORRIS, K., CROWLEY, K. & NEWMAN, A. 2006. Analysis of amorphous and nanocrystalline solids from their X-ray diffraction patterns. *Pharmaceutical Research,* 23, 2333-2349.

BATZER, H. & KREIBICH, U. T. 1981. Influence of water on thermal transitions in natural polymers and synthetic polyamides. *Polymer Bulletin,* 5, 585-590.

BAYER, I. S., FRAGOULI, D., ATTANASIO, A., SORCE, B., BERTONI, G., BRESCIA, R., DI CORATO, R., PELLEGRINO, T., KALYVA, M. & SABELLA, S. 2011. Water-repellent cellulose fiber networks with multifunctional properties. *Acs Applied Materials & Interfaces,* 3, 4024-4031.

BECK-CANDANEDO, S., ROMAN, M. & GRAY, D. G. 2005. Effect of reaction conditions on the properties and behavior of wood cellulose nanocrystal suspensions. *Biomacromolecules,* 6, 1048-1054.

BENOIT, M., RODRIGUES, A., VIGIER, K. D. O., FOURRE, E., BARRAULT, J., TATIBOUET, J.-M. & JEROME, F. 2012. Combination of ball-milling and non-thermal atmospheric plasma as physical treatments for the saccharification of microcrystalline cellulose. *Green Chemistry,* 14, 2212-2215.

BENZION, O. & NUSSINOVITCH, A. 1997. Physical properties of hydrocolloid wet glues. *Food Hydrocolloids,* 11, 429-442.

BERGENSTRÅHLE, M., WOHLERT, J., HIMMEL, M. E. & BRADY, J. W. 2010. Simulation studies of the insolubility of cellulose. *Carbohydrate Research,* 345, 2060-2066.

BERGERET, A. & BENEZET, J. C. 2011. Natural Fibre-Reinforced Biofoams. *International Journal of Polymer Science*.

BERTRAN, M. S. & DALE, B. E. 1986. Determination of cellulose accessibility by differential scanning calorimetry. *Journal of Applied Polymer Science,* 32, 4241-4253.

BHUIYAN, M. T. R., HIRAI, N. & SOBUE, N. 2000. Changes of crystallinity in wood cellulose by heat treatment under dried and moist conditions. *Journal of Wood Science,* 46, 431-436.

BIERMANN, O., HÄDICKE, E., KOLTZENBURG, S. & MÜLLER-PLATHE, F. 2001. Hydrophilicity and lipophilicity of cellulose crystal surfaces. *Angewandte Chemie International Edition,* 40, 3822-3825.

BLANSHARD, J. M. V. 1987. Starch granule stucture and function: a physiochemical approach. *In:* GALLIARD, T. (ed.) *Starch: Properties and Potential.* New York: John Wiley & Sons.

BLEDZKI, A. & GASSAN, J. 1999. Composites reinforced with cellulose based fibres. *Progress in Polymer Science,* 24, 221-274.

BODROS, E., PILLIN, I., MONTRELAY, N. & BALEY, C. 2007. Could biopolymers reinforced by randomly scattered flax fibre be used in structural applications? *Composites Science and Technology,* 67, 462-470.

BOOTTEN, T. J., HARRIS, P. J., MELTON, L. D. & NEWMAN, R. H. 2004. Solid-state ^{13}C NMR spectroscopy shows that the xyloglucans in the primary cell walls of mung bean (Vigna radiata L.) occur in different domains: a new model for xyloglucan–cellulose interactions in the cell wall. *Journal of Experimental Botany,* 55, 571-583.

BOOTTEN, T. J., HARRIS, P. J., MELTON, L. D. & NEWMAN, R. H. 2008. WAXS and ^{13}C NMR study of Gluconoacetobacter xylinus cellulose in composites with tamarind xyloglucan. *Carbohydrate Research,* 343, 221-229.

BORBÉLY, É. 2008. Lyocell, The New Generation of Regenerated Cellulose. *Acta Polytechnica Hungarica,* 5, 11-18.

BOUAFIF, H., KOUBAA, A., PERRÉ, P. & CLOUTIER, A. 2009. Effects of fiber characteristics on the physical and mechanical properties of wood plastic composites. *Composites Part A: Applied Science and Manufacturing,* 40, 1975-1981.

BOUTIN, O., FERRER, M. & LEDE, J. 2002. Flash pyrolysis of cellulose pellets submitted to a concentrated radiation: experiments and modelling. ***Chemical Engineering Science,*** **57, 15-25.**

BOUTIN, O., LEDE, J., OLALDE, G. & FERRIERE, A. 1999. Solar flash pyrolysis of biomass direct measurement of the optical properties of biomass components. ***Journal De Physique Iv,*** **9, 367-372.**

BRENDLER, E., FISCHER, S. & LEIPNER, H. 2001. ^{7}Li NMR as probe for solvent–cellulose interactions in cellulose dissolution. ***Cellulose,*** **8, 283-288.**

BRESLOW, R. & GUO, T. 1990. Surface tension measurements show that chaotropic salting-in denaturants are not just water-structure breakers. ***Proceedings of the National Academy of Sciences,*** **87, 167-169.**

BROWN, R. M. & SAXENA, I. M. 2000. Cellulose biosynthesis: A model for understanding the assembly of biopolymers. ***Plant Physiology and Biochemistry,*** **38, 57-67.**

BRUCE, D. M., HOBSON, R. N., FARRENT, J. W. & HEPWORTH, D. G. 2005. High-performance composites from low-cost plant primary cell walls. ***Composites Part a-Applied Science and Manufacturing,*** **36, 1486-1493.**

BRUMMER, Y., CUI, W. & WANG, Q. 2003. Extraction, purification and physicochemical characterization of fenugreek gum. ***Food Hydrocolloids,*** **17, 229-236.**

BRUMMER, Y., DEFELICE, C., WU, Y., KWONG, M., WOOD, P. J. & TOSH, S. M. 2014. Textural and Rheological Properties of Oat Beta-Glucan Gels with Varying Molecular Weight Composition. ***Journal of Agricultural and Food Chemistry,*** **62, 3160-3167.**

BRUN-GRAEPPI, A. K., RICHARD, C., BESSODES, M., SCHERMAN, D., NARITA, T., DUCOURET, G. & MERTEN, O.-W. 2010. Study on the sol–gel transition of xyloglucan hydrogels. ***Carbohydrate Polymers,*** **80, 555-562.**

BUCKERIDGE, M. S. 2010. Seed cell wall storage polysaccharides: models to understand cell wall biosynthesis and degradation. ***Plant Physiology,*** **154, 1017-1023.**

BUCKERIDGE, M. S., PESSOA DOS SANTOS, H. & TINÉ, M. A. S. 2000. Mobilisation of storage cell wall polysaccharides in seeds. ***Plant Physiology and Biochemistry,*** **38, 141-156.**

BUCKERIDGE, M. S., ROCHA, D. C., REID, J. & DIETRICH, S. 1992. Xyloglucan structure and post-germinative metabolism in seeds of Copaifera langsdorfii from savanna and forest populations. ***Physiologia Plantarum,*** **86, 145-151.**

BUSCALL, R., MCGOWAN, J. I. & MORTON-JONES, A. J. 1993. The rheology of concentrated dispersions of weakly attracting colloidal particles with and without wall slip. ***Journal of Rheology (1978-present),*** **37, 621-641.**

CAFFALL, K. H. & MOHNEN, D. 2009. The structure, function, and biosynthesis of plant cell wall pectic polysaccharides. ***Carbohydrate Research,*** **344, 1879-1900.**

CALAHORRA, M., CORTAZAR, M., EGUIAZABAL, J. & GUZMÁN, G. 1989. Thermogravimetric analysis of cellulose: effect of the molecular weight on thermal decomposition. ***Journal of Applied Polymer Science,*** **37, 3305-3314.**

CARDEA, S., BALDINO, L., DE MARCO, I., PISANTI, P. & REVERCHON, E. 2013. Supercritical Gel Drying of Polymeric Hydrogels for Tissue Engineering Applications. ***Chemical Engineering Transactions,*** **32, 1123-1128.**

CARPITA, N. C. & GIBEAUT, D. M. 1993. Structural models of primary cell walls in flowering plants: consistency of molecular structure with the physical properties of the walls during growth. *The Plant Journal,* 3, 1-30.

CARVALHO, A. J. F. 2013. Starch: Marjor sources, properties and applications as thermoplastic materials. *In:* EBNESAJJAD, S. (ed.) *Handbook of Biopolymers and Biodegradable Plastics.* Elsevier.

CHAISAWANG, M. & SUPHANTHARIKA, M. 2006. Pasting and rheological properties of native and anionic tapioca starches as modified by guar gum and xanthan gum. *Food Hydrocolloids,* 20, 641-649.

CHAMBERLAIN, E. & RAO, M. 2000. Effect of concentration on rheological properties of acid-hydrolyzed amylopectin solutions. *Food Hydrocolloids,* 14, 163-171.

CHANLIAUD, E. & GIDLEY, M. J. 1999. In vitro synthesis and properties of pectin/Acetobacter xylinus cellulose composites. *Plant Journal,* 20, 25-35.

CHANZY, H., DUBE, M., MARCHESSAULT, R. & REVOL, J. 1979. Single crystals and oriented crystallization of ivory nut mannan. *Biopolymers,* 18, 887-898.

CHANZY, H., PEREZ, S., MILLER, D. P., PARADOSSI, G. & WINTER, W. T. 1987. An electron diffraction study of the mannan I crystal and molecular structure. *Macromolecules,* 20, 2407-2413.

CHAPLIN, M. 2000. A proposal for the structuring of water. *Biophysical chemistry,* 83, 211-221.

CHAPLIN, M. F. 2001. Water: its importance to life. *Biochemistry and Molecular Biology Education,* 29, 54-59.

CHAPLIN, M. F. 2003. Fibre and water binding. *Proceedings of the Nutrition Society,* 62, 223-227.

CHEETHAM, N. W. H. & TAO, L. P. 1998. Variation in crystalline type with amylose content in maize starch granules: an X-ray powder diffraction study. *Carbohydrate Polymers,* 36, 277-284.

CHEN, R. H. & TSAIH, M. L. 2000. Urea-induced conformational changes of chitosan molecules and the shift of break point of Mark–Houwink equation by increasing urea concentration. *Journal of Applied Polymer Science,* 75, 452-457.

CHENG, Q. Z., WANG, S. Q., LEE, S. H. & RIALS, T. G. 2006. Composite Materials from microfibrils isolated from regenerated cellulose fibers. *Abstracts of Papers of the American Chemical Society,* 231, 84-CELL.

CHENG, Y., PRUD'HOMME, R. K., CHIK, J. & RAU, D. C. 2002. Measurement of forces between galactomannan polymer chains: effect of hydrogen bonding. *Macromolecules,* 35, 10155-10161.

CHO, J., HEUZEY, M.-C., BÉGIN, A. & CARREAU, P. J. 2006. Effect of urea on solution behavior and heat-induced gelationof chitosan-β-glycerophosphate. *Carbohydrate Polymers,* 63, 507-518.

CHRISTIERNIN, M., HENRIKSSON, G., LINDSTROM, M. E., BRUMER, H., TEERI, T. T., LINDSTROM, T. & LAINE, J. 2003. The effects of xyloglucan on the properties of paper made from bleached kraft pulp. *Nordic Pulp & Paper Research Journal,* 18, 182-187.

CIOLACU, D. & POPA, V. I. 2006. On the thermal degradation of cellulose allomorphs. *Cellulose Chemistry and Technology,* 40, 445-449.

CLARK, A. & ROSS-MURPHY, S. B. 2009. *Biopolymer network assembly: measurement and theory*, Elsevier: London, UK.

COLLINSON, S. R. & THIELEMANS, W. 2010. The catalytic oxidation of biomass to new materials focusing on starch, cellulose and lignin. *Coordination Chemistry Reviews,* 254, 1854-1870.

COPETTI, G., GRASSI, M., LAPASIN, R. & PRICL, S. 1997. Synergistic gelation of xanthan gum with locust bean gum: a rheological investigation. *Glycoconjugate journal,* 14, 951-961.

COSGROVE, D. J. 2000. Expansive growth of plant cell walls. *Plant Physiology and Biochemistry,* 38, 109-124.

CROISIER, F. & JEROME, C. 2013. Chitosan-based biomaterials for tissue engineering. *European Polymer Journal,* 49, 780-792.

CSISZAR, E. & FEKETE, E. 2011. Microstructure and Surface Properties of Fibrous and Ground Cellulosic Substrates. *Langmuir,* 27, 8444-8450.

CSISZAR, E., FEKETE, E., TOTH, A., BANDI, E., KOCZKA, B. & SAJO, I. 2013. Effect of particle size on the surface properties and morphology of ground flax. *Carbohydrate Polymers,* 94, 927-933.

CUISSINAT, C. & NAVARD, P. Swelling and dissolution of cellulose part II: Free floating cotton and wood fibres in NaOH–water–additives systems. Macromolecular Symposia, 2006. Wiley Online Library, 19-30.

CURVELO, A., DE CARVALHO, A. & AGNELLI, J. 2001. Thermoplastic starch–cellulosic fibers composites: preliminary results. *Carbohydrate Polymers,* 45, 183-188.

DAAS, P. J. H., MEYER-HANSEN, K., SCHOLS, H. A., DE RUITER, G. A. & VORAGEN, A. G. J. 1999. Investigation of the non-esterified galacturonic acid distribution in pectin with endopolygalacturonase. *Carbohydrate Research,* 318, 135-145.

DAMMSTROM, S., SALMEN, L. & GATENHOLM, P. 2005. The effect of moisture on the dynamical mechanical properties of bacterial cellulose/glucuronoxylan nanocomposites. *Polymer,* 46, 10364-10371.

DAUENHAUER, P. J., COLBY, J. L., BALONEK, C. M., SUSZYNSKI, W. J. & SCHMIDT, L. D. 2009. Reactive boiling of cellulose for integrated catalysis through an intermediate liquid. *Green Chemistry,* 11, 1555-1561.

DAVE, V., SHETH, M., MCCARTHY, S. P., RATTO, J. A. & KAPLAN, D. L. 1998. Liquid crystalline, rheological and thermal properties of konjac glucomannan. *Polymer,* 39, 1139-1148.

DAY, L., XU, M., OISETH, S. K., LUNDIN, L. & HEMAR, Y. 2010. Dynamic rheological properties of plant cell-wall particle dispersions. *Colloids and Surfaces B-Biointerfaces,* 81, 461-467.

DE LIMA, D. U. & BUCKERIDGE, M. S. 2001. Interaction between cellulose and storage xyloglucans: the influence of the degree of galactosylation. *Carbohydrate Polymers,* 46, 157-163.

DE RODRIGUEZ, N. L. G., THIELEMANS, W. & DUFRESNE, A. 2006. Sisal cellulose whiskers reinforced polyvinyl acetate nanocomposites. *Cellulose,* 13, 261-270.

DE XAMMAR ORO, J. R. 2001. Role of co-solute in biomolecular stability: glucose, urea and the water structure. *Journal of biological physics,* 27, 73-79.

DEA, I. C. M., CLARK, A. H. & MCCLEARY, B. V. 1986. Effect of the molecular fine structure of galactomannans on their interaction properties - the role of unsubstituted sides. *Food Hydrocolloids,* 1, 129-140.

DEBIAGI, F., MALI, S., GROSSMANN, M. V. E. & YAMASHITA, F. 2011. Biodegradable foams based on starch, polyvinyl alcohol, chitosan and sugarcane fibers obtained by extrusion. *Brazilian Archives of Biology and Technology,* 54, 1043-1052.

DEGUCHI, K. & MEGURO, K. 1975. The effects of inorganic salts and urea on the micellar structure of nonionic surfactant. *Journal of Colloid and Interface Science,* 50, 223-227.

DELIGKARIS, K., TADELE, T. S., OLTHUIS, W. & VAN DEN BERG, A. 2010. Hydrogel-based devices for biomedical applications. *Sensors and Actuators B-Chemical,* 147, 765-774.

DELMER, D. P. & AMOR, Y. 1995. Cellulose biosynthesis. *Plant Cell,* 7, 987-1000.

DICK-PÉREZ, M., ZHANG, Y., HAYES, J., SALAZAR, A., ZABOTINA, O. A. & HONG, M. 2011. Structure and interactions of plant cell-wall polysaccharides by two- and three-dimensional magic-angle-spinning solid-state NMR. *Biochemistry,* 50, 989-1000.

DICKER, M. P., DUCKWORTH, P. F., BAKER, A. B., FRANCOIS, G., HAZZARD, M. K. & WEAVER, P. M. 2014. Green composites: A review of material attributes and complementary applications. *Composites Part A: Applied Science and Manufacturing,* 56, 280-289.

DIONÍSIO, M. & GRENHA, A. 2012. Locust bean gum: exploring its potential for biopharmaceutical applications. *Journal of pharmacy & bioallied sciences,* 4, 175.

DITTENBER, D. B. & GANGARAO, H. V. 2012. Critical review of recent publications on use of natural composites in infrastructure. *Composites Part A: Applied Science and Manufacturing,* 43, 1419-1429.

DJALILI-MOGHADDAM, M. & TOLL, S. 2006. Fibre suspension rheology: effect of concentration, aspect ratio and fibre size. *Rheologica acta,* 45, 315-320.

DOMENECH, T., PEUVREL-DISDIER, E. & VERGNES, B. 2013. The importance of specific mechanical energy during twin screw extrusion of organoclay based polypropylene nanocomposites. *Composites Science and Technology,* 75, 7-14.

DOMVOGLOU, D., WORTMANN, F., TAYLOR, J. & IBBETT, R. 2010. Controlled accessibility Lewis acid catalysed thermal reactions of regenerated cellulosic fibres. *Cellulose,* 17, 757-770.

DONOVAN, J. W. 1979. Phase transitions of the starch–water system. *Biopolymers,* 18, 263-275.

DOS SANTOS, A. P., DIEHL, A. & LEVIN, Y. 2010. Surface tensions, surface potentials, and the Hofmeister series of electrolyte solutions. *Langmuir,* 26, 10778-10783.

DOYLE, J. P., GIANNOULI, P., MARTIN, E. J., BROOKS, M. & MORRIS, E. R. 2006. Effect of sugars, galactose content and chainlength on freeze-thaw gelation of galactomannans. *Carbohydrate Polymers,* 64, 391-401.

DOYLE, J. P., LYONS, G. & MORRIS, E. R. 2009. New proposals on "hyperentanglement" of galactomannans: Solution viscosity of fenugreek gum under neutral and alkaline conditions. *Food Hydrocolloids,* 23, 1501-1510.

DUCHEMIN, B. J. C., STAIGER, M. P., TUCKER, N. & NEWMAN, R. H. 2010. Aerocellulose Based on All-Cellulose Composites. *Journal of Applied Polymer Science,* 115, 216-221.

DUFRESNE, A. 2012. *Nanocellulose: from nature to high performance tailored materials*, Walter de Gruyter.

EBRINGEROVA, A. 2006. Structural diversity and application potential of hemicelluloses. *Macromolecular Symposia,* 232, 1-12.

EICHHORN, S., BAILLIE, C., ZAFEIROPOULOS, N., MWAIKAMBO, L., ANSELL, M., DUFRESNE, A., ENTWISTLE, K., HERRERA-FRANCO, P., ESCAMILLA, G. &

GROOM, L. 2001. Review: current international research into cellulosic fibres and composites. *Journal of Materials Science,* 36, 2107-2131.

EICHHORN, S. J., DUFRESNE, A., ARANGUREN, M., MARCOVICH, N. E., CAPADONA, J. R., ROWAN, S. J., WEDER, C., THIELEMANS, W., ROMAN, M., RENNECKAR, S., GINDL, W., VEIGEL, S., KECKES, J., YANO, H., ABE, K., NOGI, M., NAKAGAITO, A. N., MANGALAM, A., SIMONSEN, J., BENIGHT, A. S., BISMARCK, A., BERGLUND, L. A. & PEIJS, T. 2010. Review: current international research into cellulose nanofibres and nanocomposites. *Journal of Materials Science,* 45, 1-33.

EKLOF, J. M. & BRUMER, H. 2010. The XTH Gene Family: An Update on Enzyme Structure, Function, and Phylogeny in Xyloglucan Remodeling. *Plant Physiology,* 153, 456-466.

EL SEOUD, O. A., KOSCHELLA, A., FIDALE, L. C., DORN, S. & HEINZE, T. 2007. Applications of ionic liquids in carbohydrate chemistry: A window of opportunities. *Biomacromolecules,* 8, 2629-2647.

ELAZZOUZI-HAFRAOUI, S., NISHIYAMA, Y., PUTAUX, J. L., HEUX, L., DUBREUIL, F. & ROCHAS, C. 2008. The shape and size distribution of crystalline nanoparticles prepared by acid hydrolysis of native cellulose. *Biomacromolecules,* 9, 57-65.

ELLIS, W. D. & O'DELL, J. L. 1999. Wood-polymer composites made with acrylic monomers, isocyanate, and maleic anhydride. *Journal of Applied Polymer Science,* 73, 2493-2505.

EVANS, R. & WALLIS, A. F. A. 1989. Cellulose molecular weights determined by viscometry. *Journal of Applied Polymer Science,* 37, 2331-2340.

EYHOLZER, C., BORDEANU, N., LOPEZ-SUEVOS, F., RENTSCH, D., ZIMMERMANN, T. & OKSMAN, K. 2010a. Preparation and characterization of water-redispersible nanofibrillated cellulose in powder form. *Cellulose,* 17, 19-30.

EYHOLZER, C., LOPEZ-SUEVOS, F., TINGAUT, P., ZIMMERMANN, T. & OKSMAN, K. 2010b. Reinforcing effect of carboxymethylated nanofibrillated cellulose powder on hydroxypropyl cellulose. *Cellulose,* 17, 793-802.

EYHOLZER, C., ZIMMERMANN, T. & OKSMAN, K. 2010c. Water-redispersible, nanofibrillated cellulose powder for polymer reinforcement. *Abstracts of Papers of the American Chemical Society,* 239.

FARUK, O., BLEDZKI, A. K., FINK, H.-P. & SAIN, M. 2012. Biocomposites reinforced with natural fibers: 2000–2010. *Progress in Polymer Science,* 37, 1552-1596.

FAVIER, V., CHANZY, H. & CAVAILLE, J. Y. 1995. Polymer nanocomposites reinforced by cellulose whiskers. *Macromolecules,* 28, 6365-6367.

FENGEL, D. & WEGENER, G. 1984. *Wood: Chemistry, ultrastructure, reactions,* Berlin, Germany, De Gruyter.

FIEDLER, B., GOJNY, F. H., WICHMANN, M. H., NOLTE, M. & SCHULTE, K. 2006. Fundamental aspects of nano-reinforced composites. *Composites Science and Technology,* 66, 3115-3125.

FINK, H. P., WEIGEL, P., PURZ, H. J. & GANSTER, J. 2001. Structure formation of regenerated cellulose materials from NMMO-solutions. *Progress in Polymer Science,* 26, 1473-1524.

FISCHER, S., LEIPNER, H., THÜMMLER, K., BRENDLER, E. & PETERS, J. 2003. Inorganic molten salts as solvents for cellulose. *Cellulose,* 10, 227-236.

FISCHER, S., VOIGT, W. & FISCHER, K. 1999. The behaviour of cellulose in hydrated melts of the composition LiXčn H2O (X= I−, NO3−, CH3COO−, ClO4−). *Cellulose,* 6, 213-219.

FOSTER, T. J. 2011. Natural structuring with cell wall materials. *Food Hydrocolloids,* 25, 1828-1832.

FRANKS, N. E. 1980. *Regenerated cellulose fibre product containing sodium alignate or lignosulphonate crosslinked with formaldehyde*.

FRATZL, P. & WEINKAMER, R. 2007. Nature's hierarchical materials. *Progress in Materials Science,* 52, 1263-1334.

FU, S.-Y., FENG, X.-Q., LAUKE, B. & MAI, Y.-W. 2008. Effects of particle size, particle/matrix interface adhesion and particle loading on mechanical properties of particulate–polymer composites. *Composites Part B: Engineering,* 39, 933-961.

GALLANT, D. J., BOUCHET, B. & BALDWIN, P. M. 1997. Microscopy of starch: Evidence of a new level of granule organization. *Carbohydrate Polymers,* 32, 177-191.

GAONKAR, A. G. 1991. Surface and interfacial activities and emulsion characteristics of some food hydrocolloids. *Food Hydrocolloids,* 5, 329-337.

GARCIA-GONZALEZ, C. A., ALNAIEF, M. & SMIRNOVA, I. 2011. Polysaccharide-based aerogels-Promising biodegradable carriers for drug delivery systems. *Carbohydrate Polymers,* 86, 1425-1438.

GARTI, N. 2005. Food Emulsifiers: Structure-Reactivity Relationships, Designs and Applications. *In:* MARANGONI, A. G. & NARINE, S. S. (eds.) *Physical Properties of Lipids.* New York, USA: Marcel Dekker Inc.

GARTI, N., MADAR, Z., ASERIN, A. & STERNHEIM, B. 1997. Fenugreek galactomannans as food emulsifiers. *Food Science and Technology-Lebensmittel-Wissenschaft & Technologie,* 30, 305-311.

GARTI, N. & REICHMAN, D. 1994. Surface properties and emulsification activity of galactomannans. *Food Hydrocolloids,* 8, 155-173.

GAUDIN, S., LOURDIN, D., LE BOTLAN, D., ILARI, J. L. & COLONNA, P. 1999. Plasticisation and mobility in starch-sorbitol films. *Journal of Cereal Science,* 29, 273-284.

GHOZALI, M. & HARYONO, A. 2013. Effect of Size of Cellulose Particle as Filler in the PVC Biocomposites on Their Thermal and Mechanical Properties. *Nanotechnology Applications in Energy and Environment,* 737, 67-73.

GIBSON, L. J. & ASHBY, M. F. 1988. *Cellular Solids Structure and Properties,* Oxford, Pergamon Press.

GIDLEY, M., MCARTHUR, A. & UNDERWOOD, D. 1991. ^{13}C NMR characterization of molecular structures in powders, hydrates and gels of galactomannans and glucomannans. *Food Hydrocolloids,* 5, 129-140.

GIDLEY, M. J. 1992. High-resolution solid-state NMR of food materials. *Trends in Food Science & Technology,* 3, 231-236.

GIDLEY, M. J. & BOCIEK, S. M. 1988. Carbon-13 CP/MAS NMR studies of amylose inclusion complexes, cyclodextrins, and the amorphous phase of starch granules: relationships between glycosidic linkage conformation and solid-state carbon-13 chemical shifts. *Journal of the American Chemical Society,* 110, 3820-3829.

GIDLEY, M. J., COOKE, D. & WARDSMITH, S. 1993. Low moisture polysaccharide systems: Thermal and spectroscopic aspects. *Glassy State in Foods*, 303-316.

GINDL, W. & KECKES, J. 2005. All-cellulose nanocomposite. *Polymer,* 46, 10221-10225.

GLAHN, P. E. 1982. Hydrocolloid stailization of protein suspensions at low pH. *Progress in Food and Nutrition Science,* 6, 171-177.

GOFF, H., FERDINANDO, D. & SCHORSCH, C. 1999. Fluorescence microscopy to study galactomannan structure in frozen sucrose and milk protein solutions. *Food Hydrocolloids,* 13, 353-362.

GOYCOOLEA, F. M., MORRIS, E. R. & GIDLEY, M. J. 1995. Viscosity of galactomannans at alkaline and neutral pH - evidence of hyperentanglement in solution *Carbohydrate Polymers,* 27, 69-71.

GRAUPNER, N., HERRMANN, A. S. & MUESSIG, J. 2009. Natural and man-made cellulose fibre-reinforced poly(lactic acid) (PLA) composites: An overview about mechanical characteristics and application areas. *Composites Part a-Applied Science and Manufacturing,* 40, 810-821.

GRUBER, E. & GRUBER, R. 1981. Viscosimetrical determination of the degree of polymerization of cellulose. *Papier,* 35, 133-141.

GUPTA, B., AGARWAL, R. & ALAM, M. S. 2010. Textile-based smart wound dressings. *Indian Journal of Fibre & Textile Research,* 35, 174-187.

HA, M.-A., APPERLEY, D. C. & JARVIS, M. C. 1997. Molecular rigidity in dry and hydrated onion cell walls. *Plant Physiology,* 115, 593-598.

HABIBI, Y., LUCIA, L. A. & ROJAS, O. J. 2010. Cellulose Nanocrystals: Chemistry, Self-Assembly, and Applications. *Chemical Reviews,* 110, 3479-3500.

HAJJI, F. 2014. *Phase transition of semi-crystalline biopolymers in low-water environments.* Doctor of Philosophy, University of Nottingham.

HAJJI, F., MITCHELL, J. R. & FOSTER, T. J. Relationship between the conformational structure and processability of hydrocolloids. *In:* P. A. WILLILAMS, G. O. P., ed. Gums and stabilisers for the food industry 16, 28.7.2011 2011 Wageningen, The Netherlands. RSC Publishing, 67-76.

HANSEN, C. M. 2012. *Hansen solubility parameters: a user's handbook*, CRC press.

HAYASHI, T., OGAWA, K. & MITSUISHI, Y. 1994. Characterisation of the adsorption of xyloglucan to cellulose *Plant and Cell Physiology,* 35, 1199-1205.

HEPWORTH, D. G. & BRUCE, D. M. 2000a. The mechanical properties of a composite manufactured from non-fibrous vegetable tissue and PVA. *Composites Part a-Applied Science and Manufacturing,* 31, 283-285.

HEPWORTH, D. G. & BRUCE, D. M. 2000b. A method of calculating the mechanical properties of nanoscopic plant cell wall components from tissue properties. *Journal of Materials Science,* 35, 5861-5865.

HERRERA-FRANCO, P. & VALADEZ-GONZALEZ, A. 2005. A study of the mechanical properties of short natural-fiber reinforced composites. *Composites Part B: Engineering,* 36, 597-608.

HERRICK, F. W., CASEBIER, R. L., HAMILTON, J. K. & SANDBERG, K. R. Microfibrillated cellulose: morphology and accessibility. *In:* SARKO, A., ed. The Ninth Cellulose Conference. Applied Polymer Symposia, 1983 New York City. Wiley, 797-813.

HERTH, W. & MEYER, Y. 1977. Ultrastructural and chemical analysis of wall fibrils synthesised by tobacco mesophyll protoplasts *Biologie Cellulaire,* 30, 33-40.

HETTRICH, K., FISCHER, S., SCHRODER, N., ENGELHARDT, J., DRECHSLER, U. & LOTH, F. 2006. Derivatization and characterization of xylan from oat spelts. *Macromolecular Symposia,* 232, 37-48.

HEYDWEILLER, A. 1910. Concerning the physical characteristics of solutions in correlation. II. Surface tension and electronic conductivity of watery salt solutions. *Ann. Phys,* 33, 145-185.

HIETALA, M., MATHEW, A. P. & OKSMAN, K. 2013. Bionanocomposites of thermoplastic starch and cellulose nanofibers manufactured using twin-screw extrusion. *European Polymer Journal,* 49, 950-956.

HOFMEISTER, F. 1888. On the understanding of the effects of salts. *Arch. Exp. Pathol. Pharmakol.(Leipzig),* 24, 247-260.

HORINAKA, J.-I., YASUDA, R. & TAKIGAWA, T. 2012. Rheological properties of concentrated solutions of galactomannans in an ionic liquid. *Carbohydrate Polymers,* 89, 1018-1021.

HOWSMON, J. A. & MARCHESSAULT, R. H. 1959. The ball-milling of cellulose fibers and recrystallization effects. *Journal of Applied Polymer Science,* 1, 313-322.

HU, H., ZHANG, Y., LIU, X., HUANG, Z., CHEN, Y., YANG, M., QIN, X. & FENG, Z. 2014. Structural changes and enhanced accessibility of natural cellulose pretreated by mechanical activation. *Polymer Bulletin,* 71, 453-464.

HUANG, F.-Y. 2012. Thermal Properties and Thermal Degradation of Cellulose Tri-Stearate (CTs). *Polymers,* 4, 1012-1024.

HUANG, Z., WANG, N., ZHANG, Y., HU, H. & LUO, Y. 2012. Effect of mechanical activation pretreatment on the properties of sugarcane bagasse/poly(vinyl chloride) composites. *Composites Part a-Applied Science and Manufacturing,* 43, 114-120.

HYLAND, L. L., TARABAN, M. B., HAMMOUDA, B. & YU, Y. B. 2011. Mutually Reinforced Multicomponent Polysaccharide Networks. *Biopolymers,* 95, 840-851.

IBBETT, R. N., DOMVOGLOU, D. & FASCHING, M. 2007. Characterisation of the supramolecular structure of chemically and physically modified regenerated cellulosic fibres by means of high-resolution Carbon-13 solid-state NMR. *Polymer,* 48, 1287-1296.

IKEDA, S. & NISHINARI, K. 2001. "Weak gel"-type rheological properties of aqueous dispersions of nonaggregated κ-carrageenan helices. *Journal of Agricultural and Food Chemistry,* 49, 4436-4441.

ILOAÑUSI, N. O. & SCHWARTZ, J. B. 1998. The effect of wax on compaction of microcrystalline cellulose beads made by extrusion and spheronization. *Drug development and industrial pharmacy,* 24, 37-44.

IMBERTY, A., CHANZY, H., PEREZ, S., BULEON, A. & TRAN, V. 1988. The double-helical nature of the crystalline part of a-starch *Journal of Molecular Biology,* 201, 365-378.

IMBERTY, A. & PEREZ, S. 1988. A revisit to the 3-dimensional structure of B-type starch *Biopolymers,* 27, 1205-1221.

IMMERGUT, E. H. & EIRICH, F. R. 1953. Intrinsic viscosities and molecular weights of cellulose and cellulose derivatives. *Industrial and Engineering Chemistry,* 45, 2500-2511.

INOUE, H., YANO, S., ENDO, T., SAKAKI, T. & SAWAYAMA, S. 2008. Combining hot-compressed water and ball milling pretreatments to improve the efficiency of the enzymatic hydrolysis of eucalyptus. *Biotechnology for Biofuels,* 1.

ISO 2009. Pulps — Determination of limiting viscosity number in cupriethylenediamine (CED) solution. Geneva: International Standard Organisation.

IWAMOTO, S., KAI, W., ISOGAI, A. & IWATA, T. 2009. Elastic Modulus of Single Cellulose Microfibrils from Tunicate Measured by Atomic Force Microscopy. *Biomacromolecules,* 10, 2571-2576.

IYER, P. B., SREENIVASAN, S., CHIDAMBARESWARAN, P. K. & PATIL, N. B. 1984. Crystallisation of amorphous cellulose *Textile Research Journal,* 54, 732-735.

IZAWA, H. & KADOKAWA, J.-I. 2010. Preparation and characterizations of functional ionic liquid-gel and hydrogel materials of xanthan gum. *Journal of Materials Chemistry,* 20, 5235-5241.

IZAWA, H., KANEKO, Y. & KADOKAWA, J.-I. 2009. Unique gel of xanthan gum with ionic liquid and its conversion into high performance hydrogel. *J. Mater. Chem.,* 19, 6969-6972.

JATURAPIREE, A., EHRHARDT, A., GRONER, S., OEZTUERK, H. B., SIROKA, B. & BECHTOLD, T. 2008. Treatment in swelling solutions modifying cellulose fiber reactivity - Part 1: Accessibility and sorption. *Macromolecular Symposia,* 262, 39-49.

JIN, H., NISHIYAMA, Y., WADA, M. & KUGA, S. 2004. Nanofibrillar cellulose aerogels. *Colloids and Surfaces a-Physicochemical and Engineering Aspects,* 240, 63-67.

KABBERT, R., GOWOREK, S. & KUNZEK, H. 1997. Preparation of single-cell material from enzymatically disintegrated apple tissue - changes in structure and functional properties. *Zeitschrift Fur Lebensmittel-Untersuchung Und-Forschung a-Food Research and Technology,* 205, 380-387.

KADOKAWA, J.-I., KATO, T., SETOYAMA, M. & YAMAMOTO, K. 2013. Preparation of Galactomannan-Based Materials Compatibilized with Ionic Liquids. *Journal of Polymers and the Environment,* 21, 512-519.

KARTHIKEYAN, C. & SANKARAN, S. 2004. Elastic behaviour of plain and fibre-reinforced syntactic foams under compression. *Materials Letters,* 58, 995-999.

KASAPIS, S. 1999. The elastic moduli of the microcrystalline cellulose-gelatin blends. *Food Hydrocolloids,* 13, 543-546.

KEENER, T. J., STUART, R. K. & BROWN, T. K. 2004. Maleated coupling agents for natural fibre composites. *Composites Part a-Applied Science and Manufacturing,* 35, 357-362.

KHAN, F., PILPEL, N. & INGHAM, S. 1988. The effect of moisture on the density, compaction and tensile strength of microcrystalline cellulose. *Powder technology,* 54, 161-164.

KHAZRAJI, A. C. & ROBERT, S. 2013. Self-assembly and intermolecular forces when cellulose and water interact using molecular modeling. *Journal of Nanomaterials,* 2013, 48.

KIEMLE, S. N., ZHANG, X., ESKER, A. R., TORIZ, G., GATENHOLM, P. & COSGROVE, D. J. 2014. Role of (1, 3)(1, 4)-β-Glucan in Cell Walls: Interaction with Cellulose. *Biomacromolecules,* 15, 1727-1736.

KIM, U. J., KUGA, S., WADA, M. & OKANO, T. 1999. Anomaly in periodate oxidation of crystalline cellulose. *Abstracts of Papers of the American Chemical Society,* 217, 041-CELL.

KLEINEBUDDE, P., JUMAA, M. & EL SALEH, F. 2000. Influence of degree of polymerization on behavior of cellulose during homogenization and extrusion/spheronization. *AAPS PharmSci,* 2, 18-27.

KLEMM, D., HEUBLEIN, B., FINK, H. P. & BOHN, A. 2005. Cellulose: Fascinating biopolymer and sustainable raw material. *Angewandte Chemie-International Edition,* 44, 3358-3393.

KLEMM, D., KRAMER, F., MORITZ, S., LINDSTROM, T., ANKERFORS, M., GRAY, D. & DORRIS, A. 2011. Nanocelluloses: A New Family of Nature-Based Materials. *Angewandte Chemie-International Edition,* 50, 5438-5466.

KOBAYASHI, M., MATOH, T. & AZUMA, J. 1996. Two chains of rhamnogalacturonan II are cross-linked by borate-diol ester bonds in higher plant cell walls. *Plant Physiology,* 110, 1017-1020.

KOCHERBITOV, V., ULVENLUND, S., KOBER, M., JARRING, K. & ARNEBRANT, T. 2008. Hydration of microcrystalline cellulose and milled cellulose studied by sorption calorimetry. *Journal of Physical Chemistry B,* 112, 3728-3734.

KOEHNKE, T., LIN, A., ELDER, T., THELIANDER, H. & RAGAUSKAS, A. J. 2012. Nanoreinforced xylan-cellulose composite foams by freeze-casting. *Green Chemistry,* 14, 1864-1869.

KOGANTI, N. 2014. *Solvent effects on the dissolution and regeneration of cellulose and starch.* Doctor of Philosophy, University of Notingham.

KOGANTI, N., MITCHELL, J. R., IBBETT, R. N. & FOSTER, T. J. 2011. Solvent Effects on Starch Dissolution and Gelatinization. *Biomacromolecules,* 12, 2888-2893.

KOH, L. W. & KASAPIS, S. 2011. Orientation of short microcrystalline cellulose fibers in a gelatin matrix. *Food Hydrocolloids,* 25, 1402-1405.

KOK, M. S., ABDELHAMEED, A. S., ANG, S., MORRIS, G. A. & HARDING, S. E. 2009. A novel global hydrodynamic analysis of the molecular flexibility of the dietary fibre polysaccharide konjac glucomannan. *Food Hydrocolloids,* 23, 1910-1917.

KOTCHARIAN, A., KUNZEK, H. & DONGOWSKI, G. 2004. The influence of variety on the enzymatic degradation of carrots and on functional and physiological properties of the cell wall materials. *Food Chemistry,* 87, 231-245.

KREZE, T., JELER, S. & STRNAD, S. 2002. Correlation between structure characteristics and adsorption properties of regenerated cellulose fibers. *Materials Research Innovations,* 5, 277-283.

KROONBATENBURG, L. M. J., KROON, J. & NORTHOLT, M. G. 1986. Chain modulus and intramolecular hydrogen-bonding in native and regenerated cellulose fibres. *Polymer Communications,* 27, 290-292.

KUANG, J., YUK, K. Y. & HUH, K. M. 2011. Polysaccharide-based superporous hydrogels with fast swelling and superabsorbent properties. *Carbohydrate Polymers,* 83, 284-290.

KUNZE, J. & FINK, H. P. Structural changes and activation of cellulose by caustic soda solution with urea. Macromolecular Symposia, 2005. Wiley Online Library, 175-188.

KUNZEK, H., KABBERT, R. & GLOYNA, D. 1999. Aspects of material science in food processing: changes in plant cell walls of fruits and vegetables. *Zeitschrift Fur Lebensmittel-Untersuchung Und-Forschung a-Food Research and Technology,* 208, 233-250.

KUNZEK, H., MULLER, S., VETTER, S. & GODECK, R. 2002. The significance of physico chemical properties of plant cell wall materials for the development of innovative food products. *European Food Research and Technology,* 214, 361-376.

LAMMERT, A. M., LAMMERT, R. M. & SCHMIDT, S. J. 1999. Physical aging of maltose glasses as measured by standard and modulated differential scanning calorimetry. *Journal of Thermal Analysis and Calorimetry,* 55, 949-975.

LANGAN, P., NISHIYAMA, Y. & CHANZY, H. 1999. A revised structure and hydrogen-bonding system in cellulose II from a neutron fiber diffraction analysis. *Journal of the American Chemical Society,* 121, 9940-9946.

LAYCOCK, B. G. & HALLEY, P. J. 2014. Starch applications: state of market and new trends.

LE MOIGNE, N. & NAVARD, P. 2010. Dissolution mechanisms of wood cellulose fibres in NaOH–water. *Cellulose,* 17, 31-45.

LEDE, J. 2012. Cellulose pyrolysis kinetics: An historical review on the existence and role of intermediate active cellulose. *Journal of Analytical and Applied Pyrolysis,* 94, 17-32.

LEDE, J., BLANCHARD, F. & BOUTIN, O. 2002. Radiant flash pyrolysis of cellulose pellets: products and mechanisms involved in transient and steady state conditions. *Fuel,* 81, 1269-1279.

LEDE, J. & BOUTIN, O. 1999. Flash pyrolysis of biomass submitted to a concentrated radiation. Application to the study of the primary steps of cellulose decomposition. *Abstracts of Papers of the American Chemical Society,* 217, U807-U807.

LEE, J.-A., YOON, M.-J., LEE, E.-S., LIM, D.-Y. & KIM, K.-Y. 2014. Preparation and characterization of cellulose nanofibers (CNFs) from microcrystalline cellulose (MCC) and CNF/polyamide 6 composites. *Macromolecular Research,* 22, 738-745.

LEE, S.-H., TERAMOTO, Y. & ENDO, T. 2010. Enhancement of enzymatic accessibility by fibrillation of woody biomass using batch-type kneader with twin-screw elements. *Bioresource Technology,* 101, 769-774.

LEIPNER, H., FISCHER, S., BRENDLER, E. & VOIGT, W. 2000. Structural changes of cellulose dissolved in molten salt hydrates. *Macromolecular Chemistry and Physics,* 201, 2041-2049.

LEITE, T. D., NICOLETI, J. F., PENNA, A. L. B. & FRANCO, C. M. L. 2012. Effect of addition of different hydrocolloids on pasting, thermal, and rheological properties of cassava starch. *Food Science and Technology (Campinas),* 32, 579-587.

LEROUGE, P., ONEILL, M. A., DARVILL, A. G. & ALBERSHEIM, P. 1993. Structural characterisation of endo-gylcanae-generated oligoglycosyl side-chains of rhamnogalactuonan-I. *Carbohydrate Research,* 243, 359-371.

LEVY, S., MACLACHLAN, G. & STAEHELIN, L. A. 1997. Xyloglucan sidechains modulate binding to cellulose during in vitro binding assays as predicted by conformational dynamics simulations. *The Plant Journal,* 11, 373-386.

LEVY, S., YORK, W. S., STUIKEPRILL, R., MEYER, B. & STAEHELIN, L. A. 1991. Simulations of the static and dynamic molecular conformations of xyloglucan - The role of the fucosylated side chain in specific side chain folding *Plant Journal,* 1, 195-215.

LI, B. & XIE, B. 2006. Single molecular chain geometry of konjac glucomannan as a high quality dietary fiber in East Asia. *Food Research International,* 39, 127-132.

LI, D., ZHANG, L. & WAN, C. 2011. Dissolution of Konjac glucomannan with room temperature ionic liquids. *Journal of Wuhan University of Technology-Mater. Sci. Ed.,* 26, 703-709.

LI, L. 2002. Thermal gelation of methylcellulose in water: scaling and thermoreversibility. *Macromolecules,* 35, 5990-5998.

LI, L., SHAN, H., YUE, C., LAM, Y., TAM, K. & HU, X. 2002. Thermally induced association and dissociation of methylcellulose in aqueous solutions. *Langmuir,* 18, 7291-7298.

LIMA, D. U., LOH, W. & BUCKERIDGE, M. S. 2004. Xyloglucan-cellulose interaction depends on the sidechains and molecular weight of xyloglucan. *Plant Physiology and Biochemistry,* 42, 389-394.

LIMA, D. U., OLIVEIRA, R. C. & BUCKERIDGE, M. O. 2003. Seed storage hemicelluloses as wet-end additives in papermaking. *Carbohydrate Polymers,* 52, 367-373.

LIN, Z., HUANG, H., ZHANG, H., ZHANG, L., YAN, L. & CHEN, J. 2010. Ball Milling Pretreatment of Corn Stover for Enhancing the Efficiency of Enzymatic Hydrolysis. *Applied Biochemistry and Biotechnology,* 162, 1872-1880.

LINDMAN, B. & KARLSTRÖM, G. 2009. Nonionic polymers and surfactants: temperature anomalies revisited. *Comptes Rendus Chimie,* 12, 121-128.

LINDMAN, B., KARLSTRÖM, G. & STIGSSON, L. 2010. On the mechanism of dissolution of cellulose. *Journal of molecular liquids,* 156, 76-81.

LIU, H., YU, L., CHEN, L. & LI, L. 2007. Retrogradation of corn starch after thermal treatment at different temperatures. *Carbohydrate Polymers,* 69, 756-762.

LIU, X., YI, X. & JIANG, Y. 2011. Mass transfer performance comparison of two commonly used liquid desiccants: LiBr and LiCl aqueous solutions. *Energy Conversion and management,* 52, 180-190.

LOJEWSKI, T., ZIEBA, K. & LOJEWSKA, J. 2010. Size exclusion chromatography and viscometry in paper degradation studies. New Mark-Houwink coefficients for cellulose in cupri-ethylenediamine. *Journal of Chromatography A,* 1217, 6462-6468.

LOPEZ-RUBIO, A., FLANAGAN, B. M., GILBERT, E. P. & GIDLEY, M. J. 2008. A novel approach for calculating starch crystallinity and its correlation with double helix content: A combined XRD and NMR study. *Biopolymers,* 89, 761-768.

LOURDIN, D., BIZOT, H. & COLONNA, P. 1997. ''Antiplasticization'' in starch-glycerol films? *Journal of Applied Polymer Science,* 63, 1047-1053.

LOZINSKY, V. I., GALAEV, I. Y., PLIEVA, F. M., SAVINA, I. N., JUNGVID, H. & MATTIASSON, B. 2003. Polymeric cryogels as promising materials of biotechnological interest. *TRENDS in Biotechnology,* 21, 445-451.

LU, X. & SHEN, X. 2011. Solubility of bacteria cellulose in zinc chloride aqueous solutions. *Carbohydrate Polymers,* 86, 239-244.

LUCCA, P. A. & TEPPER, B. J. 1994. Fat replacers and the functionality of fat in foods. *Trends in Food Science & Technology,* 5, 12-19.

LUE, A. & ZHANG, L. 2009. Rheological behaviors in the regimes from dilute to concentrated in cellulose solutions dissolved at low temperature. *Macromolecular Bioscience,* 9, 488-496.

LUO, W., WANG, J., LIU, X., LI, H., PAN, H., GU, Q. & YU, X. 2013. A facile and efficient pretreatment of corncob for bioproduction of butanol. *Bioresource Technology,* 140, 86-89.

LYND, L. R., WEIMER, P. J., VAN ZYL, W. H. & PRETORIUS, I. S. 2002. Microbial cellulose utilization: Fundamentals and biotechnology. *Microbiology and Molecular Biology Reviews,* 66, 506-+.

MA, X. D. & PAWLIK, M. 2007. Intrinsic viscosities and Huggins constants of guar gum in alkali metal chloride solutions. *Carbohydrate Polymers,* 70, 15-24.

MAEDA, M., SHIMAHARA, H. & SUGIYAMA, N. 1980. Detailed examination of the branched structure of Konjac glucomannan [pasta made from starch of devil's tongue, Amorphophalus konjac]. *Agricultural and Biological Chemistry*.

MANI, P. & SATYANARAYANA, K. G. 1990. Effects of the surface treatments of lignocellulosic fibres on their debonding stress *Journal of Adhesion Science and Technology,* 4, 17-24.

MARCHESSAULT, R., TAYLOR, M. & WINTER, W. 1990. ^{13}C CP/MAS NMR spectra of poly-β-D (1→ 4) mannose: mannan. *Canadian journal of chemistry,* 68, 1192-1195.

MARLETT, J. A., MCBURNEY, M. I. & SLAVIN, J. L. 2002. Position of the American Dietetic Association: Health implications of dietary fiber. *Journal of the American Dietetic Association,* 102, 993-1000.

MARXFIGINI, M. 1978. Significance of intrinsic viscosity ratio of unsubstituted and nitrated cellulose in different solvents. *Angewandte Makromolekulare Chemie,* 72, 161-171.

MASSON, J. F. & MANLEY, R. S. J. 1991. Miscible blends of cellulose and poly (vinylpyrrolidone). *Macromolecules,* 24, 6670-6679.

MATHEW, A. P., OKSMAN, K. & SAIN, M. 2005. Mechanical properties of biodegradable composites from poly lactic acid (PLA) and microcrystalline cellulose (MCC). *Journal of Applied Polymer Science,* 97, 2014-2025.

MATHUR, N. 2011. *Industrial galactomannan polysaccharides*, CRC Press.

MATHUR, V. & MATHUR, N. 2005. Fenugreek and other lesser known legume galactomannan-polysaccharides: scope for developments. *Journal of Scientific and Industrial research,* 64, 475.

MATSUDA, Y., KOWSAKA, K., OKAJIMA, K. & KAMIDE, K. 1992. Structural change of cellulose contained in immature cotton boll during its growth *Polymer International,* 27, 347-351.

MAVRAKIS, C. & KIOSSEOGLOU, V. 2008. The structural characteristics and mechanical properties of biopolymer/mastic gum microsized particles composites. *Food Hydrocolloids,* 22, 854-861.

MCCLEARY, B. V., CLARK, A. H., DEA, I. C. M. & REES, D. A. 1985. The fine structures of carob and guar galactomannans. *Carbohydrate Research,* 139, 237-260.

MCGRANE, S. J., MAINWARING, D. E., CORNELL, H. J. & RIX, C. J. 2004. The role of hydrogen bonding in amylose gelation. *Starch-Stärke,* 56, 122-131.

MCNEIL, M., DARVILL, A. G., FRY, S. C. & ALBERSHEIM, P. 1984. Structure and function of the primatary cell walls of plants. *Annual Review of Biochemistry,* 53, 625-663.

MEDRONHO, B., ROMANO, A., MIGUEL, M. G., STIGSSON, L. & LINDMAN, B. 2012. Rationalizing cellulose (in) solubility: reviewing basic physicochemical aspects and role of hydrophobic interactions. *Cellulose,* 19, 581-587.

MEEKER, S. P., BONNECAZE, R. T. & CLOITRE, M. 2004. Slip and flow in pastes of soft particles: Direct observation and rheology. *Journal of Rheology (1978-present),* 48, 1295-1320.

MEHLING, T., SMIRNOVA, I., GUENTHER, U. & NEUBERT, R. H. H. 2009. Polysaccharide-based aerogels as drug carriers. *Journal of Non-Crystalline Solids,* 355, 2472-2479.

MIGNEAULT, S., KOUBAA, A., ERCHIQUI, F., CHAALA, A., ENGLUND, K. & WOLCOTT, M. P. 2009. Effects of processing method and fiber size on the structure and properties of wood–plastic composites. *Composites Part A: Applied Science and Manufacturing,* 40, 80-85.

MIHRANYAN, A., LLAGOSTERA, A. P., KARMHAG, R., STRØMME, M. & EK, R. 2004. Moisture sorption by cellulose powders of varying crystallinity. *International Journal of Pharmaceutics,* 269, 433-442.

MIHRANYAN, A. & STRØMME, M. 2004. Capillary condensation of moisture in fractal pores of native cellulose powders. *Chemical physics letters,* 393, 389-392.

MIKKONEN, K. S., MATHEW, A. P., PIRKKALAINEN, K., SERIMAA, R., XU, C., WILLFOR, S., OKSMAN, K. & TENKANEN, M. 2010. Glucomannan composite films with cellulose nanowhiskers. ***Cellulose,*** **17, 69-81.**

MIKKONEN, K. S., PARIKKA, K., SUURONEN, J.-P., GHAFAR, A., SERIMAA, R. & TENKANEN, M. 2014. Enzymatic oxidation as a potential new route to produce polysaccharide aerogels. ***Rsc Advances,*** **4, 11884-11892.**

MILLIKEN, W. J., GOTTLIEB, M., GRAHAM, A. L., MONDY, L. A. & POWELL, R. L. 1989. The viscosity-volume fraction relation for suspensions of rod-like particles by falling-ball rheometry. ***Journal of Fluid Mechanics,*** **202, 217-232.**

MISHIMA, T., HISAMATSU, M., YORK, W. S., TERANISHI, K. & YAMADA, T. 1998. Adhesion of beta-D-glucans to cellulose. ***Carbohydrate Research,*** **308, 389-395.**

MISHRA, A. & MALHOTRA, A. V. 2009. Tamarind xyloglucan: a polysaccharide with versatile application potential. ***Journal of Materials Chemistry,*** **19, 8528-8536.**

MOHANTY, A. K., MISRA, M. & DRZAL, L. T. 2002. Sustainable bio-composites from renewable resources: Opportunities and challenges in the green materials world. ***Journal of Polymers and the Environment,*** **10, 19-26.**

MOON, R. J., MARTINI, A., NAIRN, J., SIMONSEN, J. & YOUNGBLOOD, J. 2011. Cellulose nanomaterials review: structure, properties and nanocomposites. ***Chemical Society Reviews,*** **40, 3941-3994.**

MORAN, J. I., ALVAREZ, V. A., CYRAS, V. P. & VAZQUEZ, A. 2008. Extraction of cellulose and preparation of nanocellulose from sisal fibers. ***Cellulose,*** **15, 149-159.**

MORGENSTERN, B., KAMMER, H., BERGER, W. & SKRABAL, P. 1992. ^{7}Li-NMR study on cellulose/LiCl/NN-dimethylacetamide solutions. ***Acta polymerica,*** **43, 356-357.**

MORI, T., CHIKAYAMA, E., TSUBOI, Y., ISHIDA, N., SHISA, N., NORITAKE, Y., MORIYA, S. & KIKUCHI, J. 2012. Exploring the conformational space of amorphous cellulose using NMR chemical shifts. ***Carbohydrate Polymers,*** **90, 1197-1203.**

MORRISON, W. R., TESTER, R. F., SNAPE, C. E., LAW, R. & GIDLEY, M. J. 1993. Swelling and gelatinisation of cereal starches 4 - Some effects of lipid-complexed amylose and free amylose in waxy and normal barley starches. ***Cereal Chemistry,*** **70, 385-391.**

MUKHERJEE, T. & KAO, N. 2011. PLA based biopolymer reinforced with natural fibre: a review. ***Journal of Polymers and the Environment,*** **19, 714-725.**

NADA, A. M. A. & HASSAN, M. L. 2000. Thermal behavior of cellulose and some cellulose derivatives. ***Polymer Degradation and Stability,*** **67, 111-115.**

NAKAGAITO, A. & YANO, H. 2005. Novel high-strength biocomposites based on microfibrillated cellulose having nano-order-unit web-like network structure. ***Applied Physics A,*** **80, 155-159.**

NAOI, S., HATAKEYAMA, T. & HATAKEYAMA, H. 2002. Phase transition of locust bean gum-, tara gum-and guar gum-water systems. ***Journal of Thermal Analysis and Calorimetry,*** **70, 841-852.**

NAYAK, J. N., CHEN, Y. & KIM, J. 2008. Removal of impurities from cellulose films after their regeneration from cellulose dissolved in DMAc/LiCl solvent system. ***Industrial & Engineering Chemistry Research,*** **47, 1702-1706.**

NEAGU, R., CUÉNOUD, M., BERTHOLD, F., BOURBAN, P., GAMSTEDT, E. & LINDSTRÖMM, M. J. 2009. Processing and mechanical properties of novel wood fibre composites foams. ***Proceedings of ICCM17, Edinburgh, UK.***

NEWMAN, R. H. & HEMMINGSON, J. A. 1998. Interactions between locust bean gum and cellulose characterized by C-13 nmr spectroscopy. *Carbohydrate Polymers,* 36, 167-172.

NISHINARI, K. & TAKAHASHI, R. 2003. Interaction in polysaccharide solutions and gels. *Current Opinion in Colloid & Interface Science,* 8, 396-400.

NISHINARI, K., TAKEMASA, M., ZHANG, H. & TAKAHASHI, R. 2007. Storage plant polysaccharides: xyloglucans, galactomannans, glucomannans. *Comprehensive glycoscience: from chemistry to systems biology, 1st edn. Elsevier, Oxford*.

NISHINO, T., MATSUDA, I. & HIRAO, K. 2004. All-cellulose composite. *Macromolecules,* 37, 7683-7687.

NISHIYAMA, Y., LANGAN, P. & CHANZY, H. 2002. Crystal structure and hydrogen-bonding system in cellulose 1 beta from synchrotron X-ray and neutron fiber diffraction. *Journal of the American Chemical Society,* 124, 9074-9082.

NOEL, T. R., PARKER, R., BROWNSEY, G. J., FARHAT, I. A., MACNAUGHTAN, W. & RING, S. G. 2005. Physical aging of starch, maltodextrin, and maltose. *Journal of Agricultural and Food Chemistry,* 53, 8580-8585.

NORDIN, S. B., NYREN, J. O. & BACK, E. L. 1973. Molten cellulose produced in a laser beam *Svensk Papperstidning-Nordisk Cellulosa,* 76, 609-610.

NORDIN, S. B., NYREN, J. O. & BACK, E. L. 1974. Indication of molten cellulose produced in a laser beam. *Textile Research Journal,* 44, 152-154.

NUSSINOVITCH, A., JAFFE, N. & GILLILOV, M. 2004. Fractal pore-size distribution on freeze-dried agar-texturized fruit surfaces. *Food Hydrocolloids,* 18, 825-835.

NUWAMANYA, E., BAGUMA, Y., WEMBABAZI, E. & RUBAIHAYO, P. 2011. A comparative study of the physicochemical properties of starches from root, tuber and cereal crops. *African Journal of Biotechnology,* 10, 12018-12030.

O'NEILL, M. A., WARRENFELTZ, D., KATES, K., PELLERIN, P., DOCO, T., DARVILL, A. G. & ALBERSHEIM, P. 1996. Rhamnogalacturonan-II, a pectic polysaccharide in the walls of growing plant cell, forms a dimer that is covalently cross-linked by a borate ester - In vitro conditions for the formation and hydrolysis of the dimer. *Journal of Biological Chemistry,* 271, 22923-22930.

OKSMAN, K., SKRIFVARS, M. & SELIN, J. F. 2003. Natural fibres as reinforcement in polylactic acid (PLA) composites. *Composites Science and Technology,* 63, 1317-1324.

OMTA, A. W., KROPMAN, M. F., WOUTERSEN, S. & BAKKER, H. J. 2003. Negligible effect of ions on the hydrogen-bond structure in liquid water. *Science,* 301, 347-349.

OZTURK, H. B., ABU-ROUS, M., MACNAUGHTAN, B., SCHUSTER, K. C., MITCHELL, J. R. & BECHTOLD, T. 2010. Changes in the Inter- and Intra- Fibrillar Structure of Lyocell (TENCEL (R)) Fibers after KOH Treatment. *In:* HEINZE, T., JANURA, M. & KOSCHELLA, A. (eds.) *Utilization of Lignocellulosic Materials.* Weinheim: Wiley-V C H Verlag Gmbh.

PAAKKO, M., ANKERFORS, M., KOSONEN, H., NYKANEN, A., AHOLA, S., OSTERBERG, M., RUOKOLAINEN, J., LAINE, J., LARSSON, P. T., IKKALA, O. & LINDSTROM, T. 2007. Enzymatic hydrolysis combined with mechanical shearing and high-pressure homogenization for nanoscale cellulose fibrils and strong gels. *Biomacromolecules,* 8, 1934-1941.

PABST, W., GREGOROVÁ, E. & BERTHOLD, C. 2006. Particle shape and suspension rheology of short-fiber systems. *Journal of the European Ceramic Society,* 26, 149-160.

PAES, S. S., SUN, S. M., MACNAUGHTAN, W., IBBETT, R., GANSTER, J., FOSTER, T. J. & MITCHELL, J. R. 2010. The glass transition and crystallization of ball milled cellulose. *Cellulose,* 17, 693-709.

PARK, S., BAKER, J. O., HIMMEL, M. E., PARILLA, P. A. & JOHNSON, D. K. 2010. Cellulose crystallinity index: measurement techniques and their impact on interpreting cellulase performance. *Biotechnology for Biofuels,* 3.

PARK, Y., HUNTER, D. J., SPIEGELMAN, D., BERGKVIST, L., BERRINO, F., VAN DEN BRANDT, P. A., BURING, J. E., COLDITZ, G. A., FREUDENHEIM, J. L., FUCHS, C. S., GIOVANNUCCI, E., GOLDBOHM, R. A., GRAHAM, S., HARNACK, L., HARTMAN, A. M., JACOBS, D. R., KATO, I., KROGH, V., LEITZMANN, M. F., MCCULLOUGH, M. L., MILLER, A. B., PIETINEN, P., ROHAN, T. E., SCHATZKIN, A., WILLETT, W. C., WOLK, A., ZELENIUCH-JACQUOTTE, A., ZHANG, S. M. M. & SMITH-WARNER, S. A. 2005. Dietary fiber intake and risk of colorectal cancer - A pooled analysis of prospective cohort studies. *Jama-Journal of the American Medical Association,* 294, 2849-2857.

PARRY, J.-M. 2010. Konjac Glucomannan. *In:* IMESON, A. (ed.) *Food Stabilisers, Thickeners and Gelling Agents.* Chichester, UK: Wiley-Blackwell.

PATMORE, J. V., GOFF, H. D. & FERNANDES, S. 2003. Cryo-gelation of galactomannans in ice cream model systems. *Food Hydrocolloids,* 17, 161-169.

PAULY, M. & SCHELLER, H. V. 2000. O-Acetylation of plant cell wall polysaccharides: identification and partial characterization of a rhamnogalacturonan O-acetyl-transferase from potato suspension-cultured cells. *Planta,* 210, 659-667.

PEDERSOLI, J. L. J. 2000. Effect of cellulose crystallinity on the progress of thermal oxidative degradation of paper. *Journal of Applied Polymer Science,* 78, 61-66.

PENG, H., LI, H., LUO, H. & XU, J. 2013. A novel combined pretreatment of ball milling and microwave irradiation for enhancing enzymatic hydrolysis of microcrystalline cellulose. *Bioresource Technology,* 130, 81-87.

PENG, X.-W., REN, J.-L., ZHONG, L.-X. & SUN, R.-C. 2011. Nanocomposite Films Based on Xylan-Rich Hemicelluloses and Cellulose Nanofibers with Enhanced Mechanical Properties. *Biomacromolecules,* 12, 3321-3329.

PENG, Y., GARDNER, D. J. & HAN, Y. 2012. Drying cellulose nanofibrils: in search of a suitable method. *Cellulose,* 19, 91-102.

PENROJ, P., MITCHELL, J., HILL, S. & GANJANAGUNCHORN, W. 2005. Effect of konjac glucomannan deacetylation on the properties of gels formed from mixtures of kappa carrageenan and konjac glucomannan. *Carbohydrate Polymers,* 59, 367-376.

PERRY, P. A. & DONALD, A. M. 2000. The role of plasticization in starch granule assembly. *Biomacromolecules,* 1, 424-432.

PETKOWICZ, C., REICHER, F. & MAZEAU, K. 1998. Conformational analysis of galactomannans: from oligomeric segments to polymeric chains. *Carbohydrate Polymers,* 37, 25-39.

PHILIPPOVA, O. E., VOLKOV, E. V., SITNIKOVA, N. L., KHOKHLOV, A. R., DESBRIERES, J. & RINAUDO, M. 2001. Two types of hydrophobic aggregates in aqueous solutions of chitosan and its hydrophobic derivative. *Biomacromolecules,* 2, 483-490.

PHILLIPS, G. O. & WILLIAMS, P. A. (eds.) 2000. *Handbook of Hydrocolloids,* Cambridge, UK: Woodhead Publishing Limited.

PICARD, C., GRUZA, J., DEROUET, C., RENARD, C., MAZEAU, K., KOCA, J., IMBERTY, A. & HERVE DU PENHOAT, C. 2000. A conformational study of the xyloglucan oligomer, XXXG, by NMR spectroscopy and molecular modeling. *Biopolymers,* 54, 11-26.

PICKARDT, C., DONGOWSKI, G. & KUNZEK, H. 2004. The influence of mechanical and enzymatic disintegration of carrots on the structure and properties of cell wall materials. *European Food Research and Technology,* 219, 229-239.

PICOUT, D. R., ROSS-MURPHY, S. B., ERRINGTON, N. & HARDING, S. E. 2003. Pressure cell assisted solubilization of xyloglucans: Tamarind seed polysaccharide and detarium gum. *Biomacromolecules,* 4, 799-807.

PILGRIM, G. W., WALTER, R. H. & OAKENFULL, D. G. 1991. Jam, jellies and preserves. *In:* H., W. R. (ed.) *The Chemistry and Technology of Pectins.* San Diego: Academic Press.

POLLARD, M. A., KELLY, R., FISCHER, P. A., WINDHAB, E. J., EDER, B. & AMADÒ, R. 2008. Investigation of molecular weight distribution of LBG galactomannan for flours prepared from individual seeds, mixtures, and commercial samples. *Food Hydrocolloids,* 22, 1596-1606.

PRAJAPATI, V. D., JANI, G. K., MORADIYA, N. G., RANDERIA, N. P., NAGAR, B. J., NAIKWADI, N. N. & VARIYA, B. C. 2013. Galactomannan: a versatile biodegradable seed polysaccharide. *International Journal of Biological Macromolecules,* 60, 83-92.

PUKANSZKY, B. 1990. Influence of interface interaction on the ultimate tensile properties of polymer composites. *Composites,* 21, 255-262.

PUTAUX, J. L. Morphology and structure of crystalline polysaccharides: Some recent studies. Macromolecular Symposia, 2005. Wiley Online Library, 66-71.

QUA, E. H., HORNSBY, P. R., SHARMA, H. S. S., LYONS, G. & MCCALL, R. D. 2009. Preparation and Characterization of Poly(vinyl alcohol) Nanocomposites Made from Cellulose Nanofibers. *Journal of Applied Polymer Science,* 113, 2238-2247.

RALET, M. C., LEROUGE, P. & QUEMENER, B. 2009. Mass spectrometry for pectin structure analysis. *Carbohydrate Research,* 344, 1798-1807.

RAMOS, L. A., MORGADO, D. L., GESSNER, F., FROLLINI, E. & EL SEOUD, O. A. 2011. A physical organic chemistry approach to dissolution of cellulose: effects of cellulose mercerization on its properties and on the kinetics of its decrystallization. *ARKIVOC: Online Journal of Organic Chemistry*.

RASSIS, D., SAGUY, I. & NUSSINOVITCH, A. 1998. Physical properties of alginate-starch cellular sponges. *Journal of Agricultural and Food Chemistry,* 46, 2981-2987.

RASSIS, D., SAGUY, I. & NUSSINOVITCH, A. 2002. Collapse, shrinkage and structural changes in dried alginate gels containing fillers. *Food Hydrocolloids,* 16, 139-151.

REGAND, A. & GOFF, H. D. 2003. Structure and ice recrystallization in frozen stabilized ice cream model systems. *Food Hydrocolloids,* 17, 95-102.

REN, Y., PICOUT, D. R., ELLIS, P. R. & ROSS-MURPHY, S. B. 2004. Solution properties of the xyloglucan polymer from Afzelia africana. *Biomacromolecules,* 5, 2384-2391.

REVOL, J., GODBOUT, J. D. L., GRAY, D. G., GODBOUT, D. L., GUDBOUT, J. D. L. & REVOL, J. F. 1995. *Forming liquid crystals of cellulose derivative comprises cellulose crystallites in a helicoidal arrangement that reflect circularly polarised visible light*.

REVOL, J. F., BRADFORD, H., GIASSON, J., MARCHESSAULT, R. H. & GRAY, D. G. 1992. Helicoidal self-ordering of cellulose microfibrils in aqueous suspension. ***International Journal of Biological Macromolecules,*** **14, 170-172.**

RICCIERI, J. E., DE CARVALHO, L. H. & VAZQUEZ, A. 1999. Interfacial properties and initial step of the water sorption in unidirectional unsaturated polyester/vegetable fiber composites. ***Polymer Composites,*** **20, 29-37.**

RICHARDSON, P. H., WILLMER, J. & FOSTER, T. J. 1998. Dilute solution properties of guar and locust bean gum in sucrose solutions. ***Food Hydrocolloids,*** **12, 339-348.**

RISICA, D., DENTINI, M. & CRESCENZI, V. 2005. Guar gum methyl ethers. Part I. Synthesis and macromolecular characterization. ***Polymer,*** **46, 12247-12255.**

ROMHÁNY, G., KARGER-KOCSIS, J. & CZIGÁNY, T. 2003. Tensile Fracture and Failure Behavior of Thermoplastic Starch with Unidirectional and Cross-Ply Flax Fiber Reinforcements. ***Macromolecular Materials and Engineering,*** **288, 699-707.**

RUDAZ, C., COURSON, R., BONNET, L., CALAS-ETIENNE, S., SALEE, H. & BUDTOVA, T. 2014. Aeropectin: fully biomass-based mechanically strong and thermal super-insulating aerogel. ***Biomacromolecules*****.**

RUSSO, D. 2008. The impact of kosmotropes and chaotropes on bulk and hydration shell water dynamics in a model peptide solution. ***Chemical Physics,*** **345, 200-211.**

SAHARI, J. & SAPUAN, S. 2011. Natural fibre reinforced biodegradable polymer composites. ***Rev. Adv. Mater. Sci,*** **30, 166-174.**

SAHEB, D. N. & JOG, J. P. 1999. Natural fiber polymer composites: A review. ***Advances in Polymer Technology,*** **18, 351-363.**

SAITÔ, H., YOKOI, M. & YAMADA, J. 1990. Hydration—dehydration-induced conformational changes of agarose, and kappa-and iota-carrageenans as studied by high-resolution solid-state ^{13}C-nuclear magnetic resonance spectroscopy. ***Carbohydrate Research,*** **199, 1-10.**

SAITO, T., KIMURA, S., NISHIYAMA, Y. & ISOGAI, A. 2007. Cellulose nanofibers prepared by TEMPO-mediated oxidation of native cellulose. ***Biomacromolecules,*** **8, 2485-2491.**

SALMEN, N. L. & BACK, E. L. 1980. Moisture-dependent thermal softening of paper, evaluated by its elastic modulus. ***Tappi,*** **63, 117-120.**

SAMIR, M., ALLOIN, F. & DUFRESNE, A. 2005. Review of recent research into cellulosic whiskers, their properties and their application in nanocomposite field. ***Biomacromolecules,*** **6, 612-626.**

SANDQUIST, D. 2013. New horizons for microfibrillated cellulose. ***Appita Journal: Journal of the Technical Association of the Australian and New Zealand Pulp and Paper Industry,*** **66, 156.**

SAVITHA PRASHANTH, M., PARVATHY, K., SUSHEELAMMA, N., HARISH PRASHANTH, K., THARANATHAN, R., CHA, A. & ANILKUMAR, G. 2006. Galactomannan esters—A simple, cost-effective method of preparation and characterization. ***Food Hydrocolloids,*** **20, 1198-1205.**

SAXENA, A., ELDER, T. J., PAN, S. & RAGAUSKAS, A. J. 2009. Novel nanocellulosic xylan composite film. ***Composites Part B-Engineering,*** **40, 727-730.**

SAXENA, A., ELDER, T. J. & RAGAUSKAS, A. J. 2011. Moisture barrier properties of xylan composite films. ***Carbohydrate Polymers,*** **84, 1371-1377.**

SAXENA, A. & RAGAUSKAS, A. J. 2009. Water transmission barrier properties of biodegradable films based on cellulosic whiskers and xylan. *Carbohydrate Polymers,* 78, 357-360.

SCHEIRS, J., CAMINO, G. & TUMIATTI, W. 2001. Overview of water evolution during the thermal degradation of cellulose. *European Polymer Journal,* 37, 933-942.

SCHELLER, H. V. & ULVSKOV, P. 2010. Hemicelluloses. *Annual Review of Plant Biology, Vol 61,* 61, 263-289.

SCHMIDT, S. J. & LAMMERT, A. M. 1996. Physical aging of maltose grasses. *Journal of Food Science,* 61, 870-875.

SCHROETER, J. & FELIX, F. 2005. Melting cellulose. *Cellulose,* 12, 159-165.

SEDDON, K. R. 1997. Ionic liquids for clean technology. *Journal of Chemical Technology and Biotechnology,* 68, 351-356.

SEN, S., MARTIN, J. D. & ARGYROPOULOS, D. S. 2013. Review of Cellulose Non-Derivatizing Solvent Interactions with Emphasis on Activity in Inorganic Molten Salt Hydrates. *ACS Sustainable Chemistry & Engineering,* 1, 858-870.

SERENO, N. M., HILL, S. E. & MITCHELL, J. R. 2007. Impact of the extrusion process on xanthan gum behaviour. *Carbohydrate Research,* 342, 1333-1342.

SHANKARACHARYA, N. B. 1998. Tamarind - Chemistry, technology and uses - A critical appraisal. *Journal of Food Science and Technology-Mysore,* 35, 193-208.

SHARMA, A., BHAT, S., VISHNOI, T., NAYAK, V. & KUMAR, A. 2013. Three-Dimensional Supermacroporous Carrageenan-Gelatin Cryogel Matrix for Tissue Engineering Applications. *Biomed Research International*.

SHARMA, R. D. 1986. Effect of fenugreek seeds and leaves on blood glucose and serum insulin responses in human subjects. *Nutrition Research,* 6, 1353-1364.

SHARMA, R. D., RAGHURAM, T. C. & RAO, N. S. 1990. Effects of fenugreek seeds on blood glucose and serum lipids in Type I diabetes. *European Journal of Clinical Nutrition,* 44, 301-306.

SHIRAKAWA, M., YAMATOYA, K. & NISHINARI, K. 1998. Tailoring of xyloglucan properties using an enzyme. *Food Hydrocolloids,* 12, 25-28.

SILVA, G. G. D., COUTURIER, M., BERRIN, J.-G., BULEON, A. & ROUAU, X. 2012. Effects of grinding processes on enzymatic degradation of wheat straw. *Bioresource Technology,* 103, 192-200.

SINGH, N., SINGH, J., KAUR, L., SINGH SODHI, N. & SINGH GILL, B. 2003. Morphological, thermal and rheological properties of starches from different botanical sources. *Food Chemistry,* 81, 219-231.

SIQUEIRA, G., BRAS, J. & DUFRESNE, A. 2009. Cellulose Whiskers versus Microfibrils: Influence of the Nature of the Nanoparticle and its Surface Functionalization on the Thermal and Mechanical Properties of Nanocomposites. *Biomacromolecules,* 10, 425-432.

SIRO, I. & PLACKETT, D. 2010. Microfibrillated cellulose and new nanocomposite materials: a review. *Cellulose,* 17, 459-494.

ŠIŠKOVÁ, M., HEJTMÁNKOVÁ, J. & BARTOVSKÁ, L. 1985. Physico-chemical properties of the ternary system urea-ammonium nitrate-water. Surface tension. *Collection of Czechoslovak Chemical Communications,* 50, 1629-1635.

SMOLE, M. S., PERSIN, Z., KREZE, T., KLEINSCHEK, K. S., RIBITSCH, V. & NEUMAYER, S. 2003. X-ray study of pre-treated regenerated cellulose fibres. *Materials Research Innovations,* 7, 275-282.

SOLOMON, O. & CIUTĂ, I. 1962. Détermination de la viscosité intrinsèque de solutions de polymères par une simple détermination de la viscosité. ***Journal of Applied Polymer Science,*** **6, 683-686.**

SOMERVILLE, C., BAUER, S., BRININSTOOL, G., FACETTE, M., HAMANN, T., MILNE, J., OSBORNE, E., PAREDEZ, A., PERSSON, S., RAAB, T., VORWERK, S. & YOUNGS, H. 2004. Toward a systems approach to understanding plant-cell walls. ***Science,*** **306, 2206-2211.**

SONG, B. K., WINTER, W. T. & TARAVEL, F. R. 1989. Crystallography of highly substituted galactomannans: fenugreek and lucerne gums. ***Macromolecules,*** **22, 2641-2644.**

SOUDAIS, Y., MOGA, L., BLAZEK, J. & LEMORT, F. 2007. Coupled DTA–TGA–FT-IR investigation of pyrolytic decomposition of EVA, PVC and cellulose. ***Journal of Analytical and Applied Pyrolysis,*** **78, 46-57.**

SPENCE, K. L., VENDITTI, R. A., ROJAS, O. J., HABIBI, Y. & PAWLAK, J. J. 2011. A comparative study of energy consumption and physical properties of microfibrillated cellulose produced by different processing methods. ***Cellulose,*** **18, 1097-1111.**

SPENCER, F. S. & MACLACHL, G. A. 1972. Changes in molecular weight of cellulose in pea epicotyl during growth ***Plant Physiology,*** **49, 58-&.**

STĂNESCU, V., OLTEANU, M., FLOREA-SPIROIU, M. & RUSU, M. 2008. Using fractal analysis to describe collagen-chitosan matrices

STARK, N. M. & ROWLANDS, R. E. 2003. Effects of wood fiber characteristics on mechanical properties of wood/polypropylene composites. ***Wood and fiber science,*** **35, 167-174.**

STOKOLS, S. & TUSZYNSKI, M. H. 2004. The fabrication and characterization of linearly oriented nerve guidance scaffolds for spinal cord injury. ***Biomaterials,*** **25, 5839-5846.**

STONE, J. E., TREIBER, E. & ABRAHAMS.B 1969. Accessibilty of regenerated cellulose to solute molecules of molecular weight of 180 to 2x10^6 ***Tappi,*** **52, 108-&.**

STUBBERUD, L., ARWIDSSON, H. G., LARSSON, A. & GRAFFNER, C. 1996. Water solid interactions .2. Effect of moisture sorption and glass transition temperature on compactibility of microcrystalline cellulose alone or in binary mixtures with polyvinyl pyrrolidone. ***International Journal of Pharmaceutics,*** **134, 79-88.**

SUN, C. C. 2008. Mechanism of moisture induced variations in true density and compaction properties of microcrystalline cellulose. ***International Journal of Pharmaceutics,*** **346, 93-101.**

SUN, J. & TAN, H. 2013. Alginate-Based Biomaterials for Regenerative Medicine Applications. ***Materials,*** **6, 1285-1309.**

SUNDARAM, J. & DURANCE, T. D. 2007. Influence of processing methods on mechanical and structural characteristics of vacuum microwave dried biopolymer foams. ***Food and Bioproducts Processing,*** **85, 264-272.**

SUNDARAM, J. & DURANCE, T. D. 2008. Water sorption and physical properties of locust bean gum-pectin-starch composite gel dried using different drying methods. ***Food Hydrocolloids,*** **22, 1352-1361.**

SURAPOLCHAI, W. & SCHIRALDI, D. A. 2010. The effects of physical and chemical interactions in the formation of cellulose aerogels. ***Polymer Bulletin,*** **65, 951-960.**

SVAGAN, A. J., JENSEN, P., DVINSKIKH, S. V., FURO, I. & BERGLUND, L. A. 2010. Towards tailored hierarchical structures in cellulose nanocomposite

biofoams prepared by freezing/freeze-drying. *Journal of Materials Chemistry,* 20, 6646-6654.

SWANSON, J. W. 1961. The science of chemical additives in papermaking. *Tappi, Vo. 44, No. 1*, 142-181.

SWATLOSKI, R. P., SPEAR, S. K., HOLBREY, J. D. & ROGERS, R. D. 2002. Dissolution of cellose with ionic liquids. *Journal of the American Chemical Society,* 124, 4974-4975.

SYMINGTON, M. C., BANKS, W. M., WEST, O. D. & PETHRICK, R. 2009. Tensile testing of cellulose based natural fibers for structural composite applications. *Journal of composite materials,* 43, 1083-1108.

SZCZESNIAK, L., RACHOCKI, A. & TRITT-GOC, J. 2008. Glass transition temperature and thermal decomposition of cellulose powder. *Cellulose,* 15, 445-451.

TAKAHASHI, M., SHIMAZAKI, M. & YAMAMOTO, J. 2001. Thermoreversible gelation and phase separation in aqueous methyl cellulose solutions. *Journal of polymer science part B: Polymer physics,* 39, 91-100.

TAMAI, N., TATSUMI, D. & MATSUMOTO, T. 2004. Rheological properties and molecular structure of tunicate cellulose in LiCl/1, 3-dimethyl-2-imidazolidinone. *Biomacromolecules,* 5, 422-432.

TANG, M. & BACON, R. 1964. Carbonization of cellulose fibers—I. Low temperature pyrolysis. *Carbon,* 2, 211-220.

TASHIRO, K. & KOBAYASHI, M. 1991. Theoretical evaluation of 3-dimensional elastic constsants of native and regenerated celluloses - role of hydrogen bonds. *Polymer,* 32, 1516-1530.

TATAROVA, I. & FOSTER, T. J. New routes towards formable cellulose. STEP-ITN End-Year Meeting, 29.09.2010 2010 Nice, France.

TATAROVA, I., MACNAUGHTAN, W., MANIAN, A. P., SIROKA, B. & BECHTOLD, T. 2012. Steam Processing of Regenerated Cellulose Fabric in Concentrated LiCl/Urea Solutions. *Macromolecular Materials and Engineering,* 297, 540-549.

TATAROVA, I., MANIAN, A. P., SIROKA, B. & BECHTOLD, T. 2010. Nonalkali swelling solutions for regenerated cellulose. *Cellulose,* 17, 913-922.

TAYLOR, I. E. & ATKINS, E. D. 1985. X-ray diffraction studies on the xyloglucan from tamarind (Tamarindus indica) seed. *FEBS letters,* 181, 300-302.

TESTER, R. F. & MORRISON, W. R. 1990. Swelling and gelatinisation of cereal starches 1 - Effects of amylopectin, amylose and lipids *Cereal Chemistry,* 67, 551-557.

TORRES, F., ARROYO, O. & GOMEZ, C. 2007. Processing and mechanical properties of natural fiber reinforced thermoplastic starch biocomposites. *Journal of Thermoplastic Composite Materials,* 20, 207-223.

TSAIH, M. L. & CHEN, R. H. 1997. Effect of molecular weight and urea on the conformation of chitosan molecules in dilute solutions. *International Journal of Biological Macromolecules,* 20, 233-240.

TURBAK, A. F., SNYDER, F. W. & SANDBERG, K. R. Microfibrillated cellulose, a new cellulose product: Properties, uses and commercial potential. *In:* SARKO, A., ed. The Ninth Cellulose Conference. Applied Polymer Symposia, 1983 New York City. Wiley, 815-827.

ULKER, Z. & ERKEY, C. 2014. An emerging platform for drug delivery: Aerogel based systems. *Journal of Controlled Release,* 177, 51-63.

UMEMURA, M. & YUGUCHI, Y. 2005. Conformational folding of xyloglucan side chains in aqueous solution from molecular dynamics simulation. *Carbohydrate Research,* 340, 2520-2532.

UMEMURA, M. & YUGUCHI, Y. 2009. Solvation of xyloglucan in water/alcohol systems by molecular dynamics simulation. *Cellulose,* 16, 361-371.

VALADEZ-GONZALEZ, A., CERVANTES-UC, J., OLAYO, R. & HERRERA-FRANCO, P. 1999. Effect of fiber surface treatment on the fiber–matrix bond strength of natural fiber reinforced composites. *Composites Part B: Engineering,* 30, 309-320.

VANDERBURGT, M. C., VANDERWOUDE, M. E. & JANSSEN, L. 1996. The influence of plasticizer on extruded thermoplastic starch. *Journal of Vinyl & Additive Technology,* 2, 170-174.

VANSOEST, J. J. G., HULLEMAN, S. H. D., DEWIT, D. & VLIEGENTHART, J. F. G. 1996. Crystallinity in starch bioplastics. *Industrial Crops and Products,* 5, 11-22.

VANZIN, G. F., MADSON, M., CARPITA, N. C., RAIKHEL, N. V., KEEGSTRA, K. & REITER, W. D. 2002. The mur2 mutant of Arabidopsis thaliana lacks fucosylated xyloglucan because of a lesion in fucosyltransferase AtFUT1. *Proceedings of the National Academy of Sciences of the United States of America,* 99, 3340-3345.

VARMA, R. S. & NAMBOODIRI, V. V. 2001. An expeditious solvent-free route to ionic liquids using microwaves. *Chemical Communications*, 643-644.

VERDEJO, R., BERNAL, M. M., ROMASANTA, L. J. & LOPEZ-MANCHADO, M. A. 2011. Graphene filled polymer nanocomposites. *Journal of Materials Chemistry,* 21, 3301-3310.

VETTER, S. & KUNZEK, H. 2002. Material properties of processed fruit and vegetables. II. Water hydration properties of cell wall materials from apples. *European Food Research and Technology,* 214, 43-51.

VISHAL GUPTA, N. & SHIVAKUMAR, H. G. 2010. Preparation and characterization of superporous hydrogels as gastroretentive drug delivery system for rosiglitazone maleate. *Daru : journal of Faculty of Pharmacy, Tehran University of Medical Sciences,* 18, 200-10.

WAMBUA, P., IVENS, J. & VERPOEST, I. 2003. Natural fibres: can they replace glass in fibre reinforced plastics? *Composites Science and Technology,* 63, 1259-1264.

WANG, C., ZHANG, Y., HUANG, H. X., CHEN, M. B. & LI, D. S. 2011. Solution conformation of konjac glucomannan single helix. *Advanced Materials Research,* 197, 96-104.

WANG, H., SUN, X. & SEIB, P. 2002. Mechanical properties of poly (lactic acid) and wheat starch blends with methylenediphenyl diisocyanate. *Journal of Applied Polymer Science,* 84, 1257-1262.

WANG, J. & SOMASUNDARAN, P. 2007. Study of galactomannose interaction with solids using AFM, IR and allied techniques. *Journal of Colloid and Interface Science,* 309, 373-383.

WANG, Q., ELLIS, P. R., ROSS-MURPHY, S. B. & BURCHARD, W. 1997. Solution characteristics of the xyloglucan extracted from Detarium senegalense Gmelin. *Carbohydrate Polymers,* 33, 115-124.

WANG, Q., LI, L., LIU, E., XU, Y. & LIU, J. 2006. Effects of SDS on the sol–gel transition of methylcellulose in water. *Polymer,* 47, 1372-1378.

WANG, Z., MCDONALD, A. G., WESTERHOF, R. J. M., KERSTEN, S. R. A., CUBA-TORRES, C. M., HA, S., PECHA, B. & GARCIA-PEREZ, M. 2013. Effect of cellulose crystallinity on the formation of a liquid intermediate and on product distribution during pyrolysis. *Journal of Analytical and Applied Pyrolysis,* 100, 56-66.

WEISSENBORN, P. K. & PUGH, R. J. 1996. Surface tension of aqueous solutions of electrolytes: relationship with ion hydration, oxygen solubility, and bubble coalescence. *Journal of Colloid and Interface Science,* 184, 550-563.

WHITNEY, S. E. C., BRIGHAM, J. E., DARKE, A. H., REID, J. S. G. & GIDLEY, M. J. 1995. In vitro assembly of cellulose/xyloglucan networks - Ultrastructural and molecular aspects. *Plant Journal,* 8, 491-504.

WHITNEY, S. E. C., BRIGHAM, J. E., DARKE, A. H., REID, J. S. G. & GIDLEY, M. J. 1998. Structural aspects of the interaction of mannan-based polysaccharides with bacterial cellulose. *Carbohydrate Research,* 307, 299-309.

WHITNEY, S. E. C., GIDLEY, M. J. & MCQUEEN-MASON, S. J. 2000. Probing expansin action using cellulose/hemicellulose composites. *Plant Journal,* 22, 327-334.

WHITNEY, S. E. C., WILSON, E., WEBSTER, J., BACIC, A., REID, J. S. G. & GIDLEY, M. J. 2006. Effects of structural variation in xyloglucan polymers on interactions with bacterial cellulose. *American Journal of Botany,* 93, 1402-1414.

WIENTJES, R., DUITS, M., BAKKER, J., JONGSCHAAP, R. & MELLEMA, J. 2001. Linear viscoelastic behavior of enzymatically modified guar gum solutions: Structure, relaxations, and gel formation. *Macromolecules,* 34, 6014-6023.

WIGGINS, P. 2002. Enzyme reactions and two-state water. *Journal of Biological Physics and Chemistry,* 2, 25-37.

WILLATS, W. G. T., MCCARTNEY, L., MACKIE, W. & KNOX, J. P. 2001. Pectin: cell biology and prospects for functional analysis. *Plant Molecular Biology,* 47, 9-27.

WILLETT, J. L. & SHOGREN, R. L. 2002. Processing and properties of extruded starch/polymer foams. *Polymer,* 43, 5935-5947.

WILLIAMS, M. A. K., FOSTER, T. J., MARTIN, D. R., NORTON, I. T., YOSHIMURA, M. & NISHINARI, K. 2000. A molecular description of the gelation mechanism of konjac mannan. *Biomacromolecules,* 1, 440-450.

WINNING, H., VIERECK, N., NORGAARD, L., LARSEN, J. & ENGELSEN, S. B. 2007. Quantification of the degree of blockiness in pectins using H-1 NMR spectroscopy and chemometrics. *Food Hydrocolloids,* 21, 256-266.

WINZOR, D. J., CARRINGTON, L. E., DESZCZYNSKI, M. & HARDING, S. E. 2004. Extent of charge screening in aqueous polysaccharide solutions. *Biomacromolecules,* 5, 2456-2460.

WOLLERDORFER, M. & BADER, H. 1998. Influence of natural fibres on the mechanical properties of biodegradable polymers. *Industrial Crops and Products,* 8, 105-112.

WORMALD, P., WICKHOLM, K., LARSSON, P. T. & IVERSEN, T. 1996. Conversions between ordered and disordered cellulose. Effects of mechanical treatment followed by cyclic wetting and drying. *Cellulose,* 3, 141-152.

WU, X., BLACK, L., SANTACANA-LAFFITTE, G. & PATRICK, C. W., JR. 2007. Preparation and assessment of glutaraldehyde-crosslinked collagen-chitosan hydrogels for adipose tissue engineering. *Journal of Biomedical Materials Research Part A,* 81A, 59-65.

WU, Y., CUI, W., ESKIN, N. & GOFF, H. 2009. An investigation of four commercial galactomannans on their emulsion and rheological properties. *Food Research International,* 42, 1141-1146.

WU, Y., LI, W., CUI, W., ESKIN, N. A. M. & GOFF, H. D. 2012. A molecular modeling approach to understand conformation-functionality relationships of galactomannans with different mannose/galactose ratios. *Food Hydrocolloids,* 26, 359-364.

XIAO, C., LU, Y., GAO, S. & ZHANG, L. 2001. Characterization of konjac glucomannan–gelatin blend films. *Journal of Applied Polymer Science,* 79, 1596-1602.

XU, Q. & CHEN, L. F. 1999. Ultraviolet spectra and structure of zinc–cellulose complexes in zinc chloride solution. *Journal of Applied Polymer Science,* 71, 1441-1446.

XU, Y. & LI, L. 2005. Thermoreversible and salt-sensitive turbidity of methylcellulose in aqueous solution. *Polymer,* 46, 7410-7417.

YAMAMURA, S., TERADA, K. & MOMOSE, Y. 1997. Change of the microstructure of microcrystalline cellulose with grinding and compression. *Journal of pharmacy and pharmacology,* 49, 1178-1181.

YAMANE, C., AOYAGI, T., AGO, M., SATO, K., OKAJIMA, K. & TAKAHASHI, T. 2006. Two different surface properties of regenerated cellulose due to structural anisotropy. *Polymer Journal,* 38, 819-826.

YAN, H. W., LINDSTROM, T. & CHRISTIERNIN, M. 2006. Some ways to decrease fibre suspension flocculation and improve sheet formation. *Nordic Pulp & Paper Research Journal,* 21, 36-43.

YILDIZ, S. Y. & ONER, E. T. 2014. Mannan as a Promising Bioactive Material for Drug Nanocarrier Systems.

YORK, W. S., VAN HALBEEK, H., DARVILL, A. G. & ALBERSHEIM, P. 1990. Structural analysis of xyloglucan oligosaccharides by 1H NMR spectroscopy and fast-atom-bombardment mass spectrometry. *Carbohydrate Research,* 200, 9-31.

YOUSSEF, M., WANG, Q., CUI, S. & BARBUT, S. 2009. Purification and partial physicochemical characteristics of protein free fenugreek gums. *Food Hydrocolloids,* 23, 2049-2053.

YUGUCHI, Y., KUMAGAI, T., WU, M., HIROTSU, T. & HOSOKAWA, J. 2004. Gelation of xyloglucan ID water/alcohol systems. *Cellulose,* 11, 203-208.

ZHAN, D. F., JANSSEN, P. & MORT, A. J. 1998. Scarcity or complete lack of single rhamnose residues interspersed within the homogalacturonan regions of citrus pectin. *Carbohydrate Research,* 308, 373-380.

ZHANG, H., WU, J., ZHANG, J. & HE, J. S. 2005. 1-Allyl-3-methylimidazolium chloride room temperature ionic liquid: A new and powerful nonderivatizing solvent for cellulose. *Macromolecules,* 38, 8272-8277.

ZHANG, H., YOSHIMURA, M., NISHINARI, K., WILLIAMS, M., FOSTER, T. & NORTON, I. 2001. Gelation behaviour of konjac glucomannan with different molecular weights. *Biopolymers,* 59, 38-50.

ZHANG, X., WU, X., GAO, D. & XIA, K. 2012. Bulk cellulose plastic materials from processing cellulose powder using back pressure-equal channel angular pressing. *Carbohydrate Polymers,* 87, 2470-2476.

ZHANG, Y. & CREMER, P. S. 2006. Interactions between macromolecules and ions: the Hofmeister series. *Current opinion in chemical biology,* 10, 658-663.

ZHENG, Y.-T., CAO, D.-R., WANG, D.-S. & CHEN, J.-J. 2007. Study on the interface modification of bagasse fibre and the mechanical properties of its composite with PVC. *Composites Part a-Applied Science and Manufacturing,* 38, 20-25.

ZHOU, Q., RUTLAND, M. W., TEERI, T. T. & BRUMER, H. 2007. Xyloglucan in cellulose modification. *Cellulose,* 14, 625-641.

ZHU, J., SABO, R. & LUO, X. 2011. Integrated production of nano-fibrillated cellulose and cellulosic biofuel (ethanol) by enzymatic fractionation of wood fibers. *Green Chemistry,* 13, 1339-1344.

ZHU, S. D., WU, Y. X., CHEN, Q. M., YU, Z. N., WANG, C. W., JIN, S. W., DING, Y. G. & WU, G. 2006. Dissolution of cellulose with ionic liquids and its application: a mini-review. *Green Chemistry,* 8, 325-327.

ZIMMERMANN, T., BORDEANU, N. & STRUB, E. 2010. Properties of nanofibrillated cellulose from different raw materials and its reinforcement potential. *Carbohydrate Polymers,* 79, 1086-1093.

ZIMMERMANN, T., PÖHLER, E. & GEIGER, T. 2004. Cellulose fibrils for polymer reinforcement. *Advanced engineering materials,* 6, 754-761.

ZOBEL, H. F. 1988. Molecules to granules - A comprehensive starch review *Starch-Starke,* 40, 44-50.

ZUGENMAIER, P. 2001. Conformation and packing of various crystalline cellulose fibers. *Progress in Polymer Science,* 26, 1341-1417.

ZULUAGA, M.-F., BAENA, Y., MORA, C.-E. & PONCE D'LEON, L.-F. 2007. Physicochemical characterization and application of yam (Dioscorea cayenensis-rotundata) starch as a pharmaceutical excipient. *Starch-Starke,* 59, 307-317.

ZYKWINSKA, A., GAILLARD, C., BULEON, A., PONTOIRE, B., GARNIER, C., THIBAULT, J.-F. & RALET, M.-C. 2007. Assessment of in vitro binding of isolated pectic domains to cellulose by adsorption isotherms, electron microscopy, and X-ray diffraction methods. *Biomacromolecules,* 8, 223-232.

ZYKWINSKA, A. W., RALET, M. C. J., GARNIER, C. D. & THIBAULT, J. F. J. 2005. Evidence for in vitro binding of pectin side chains to cellulose. *Plant Physiology,* 139, 397-407.